PHYSIK - DEPARTMENT

Inelastische Lichtstreuung an freien Ladungsträgern in Halbleiterheterostrukturen

Habilitationsschrift
von

Dr. rer. nat. Gerhard Abstreiter

TECHNISCHE UNIVERSITÄT

MÜNCHEN

INELASTISCHE LICHTSTREUUNG AN FREIEN LADUNGSTRÄGERN IN HALBLEITERHETEROSTRUKTUREN

Habilitationsschrift

von

Dr.rer.nat. Gerhard ABSTREITER

INHALT SEITE

Vorwort 2

Zusammenfassung 3

1. Einleitung 4

2. Grundlagen zur Lichtstreuung in Festkörpern 6
2.1. Ramanstreuung an Phononen 6
2.2. Lichtstreuung an freien Ladungsträgern (dreidimensional) 10
2.3. Lichtstreuung an freien Ladungsträgern (zweidimensional) 14

3. Experimentelle Aspekte 18

4. Ergebnisse und Diskussion 20
4.1. Phononen in Heterostrukturen 20
4.2. Dreidimensionale Ladungsträger in polaren Halbleitern 21
4.3. Halbleiter-Halbleiter-Grenzflächen 22
4.4. Metall-Isolator-Halbleiter-Strukturen 24
4.5. Legierungsübergitter (GaAs-$Al_xGa_{1-x}As$) 26
4.6. Periodische Dotierungsschichtstrukturen 29

5. Ausblick 32

Literaturverzeichnis 33

Anhang 1 - 12 64
(Auswahl einiger Veröffentlichungen des Autors, die im Zusammenhang mit diesem Thema stehen)

Vorwort

Die Habilitationsschrift diente dem Autor als Grundlage für eine Vortragsreihe bei der NATO-Schule über "MBE and Heterostructures" in Erice, Sizilien, 1983. Sie wird veröffentlicht in einem Buch zur Schule (Martinus Nijhoff, The Netherlands, eds. L.L. Chang and K. Ploog).

In diesem Zusammenhang sei auch auf einen ausführlichen Artikel hingewiesen, den der Autor zusammen mit A. Pinczuk und M. Cardona für ein Buch in der Springer-Serie "Topics in Applied Physics" erstellt hat. ("Light Scattering by Free Carrier Excitations in Semiconductors", G. Abstreiter, M. Cardona, and A. Pinczuk in "Light Scattering in Solids IV, Topics in Applied Physics 54, eds. M. Cardona and G. Güntherodt (1984))

Zusammenfassung

Resonante inelastische Lichtstreuung ist eine ideale Methode zur Untersuchung von elektronischen Anregungen in Halbleitern. Nach ausführlichen Untersuchungen zum Resonanzverhalten von kollektiven und Einteilchen-Anregungen in homogen dotiertem GaAs gelang im Rahmen dieser Arbeit erstmalig die Beobachtung elektronischer Ramanstreuung von einem quasi-zweidimensionalen Elektronengas in GaAs/n-$Al_xGa_{1-x}As$-Heterostrukturen. Die experimentell einfache Unterscheidungsmöglichkeit von verschiedenen Inter- und Intra-Subbandanregungen ermöglichte die Untersuchung einer Vielzahl elektronischer Eigenschaften in zweidimensionalen Ladungsträgersystemen. Insbesondere der Unterschied zwischen Einteilchen-intersubbandanregungen und entsprechenden kollektiven Anregungen erlaubte die direkte Bestimmung von Depolarisationsverschiebung und Coulomb-Matrixelementen. In polaren Halbleitern wie GaAs und InP koppeln die kollektiven elektronischen Anregungen mit den LO-Phonon-Moden. Dies führt zu einer Aufspaltung der beobachteten Linien. Voraussetzung für diese Untersuchungen ist die starke Erhöhung des Streuquerschnitts der Anregungen unter Resonanzbedingung. Diese Bedingung (Laserenergie $\simeq$ Energielücke des Halbleiters) konnte bisher für folgende Halbleitersysteme erfüllt werden: Einfach-Heterostrukturen (GaAs/n-$Al_xGa_{1-x}As$, GaAs/Ge), Legierungsvielschichtstrukturen (GaAs/$Al_xGa_{1-x}As$), Dotierungsvielschichtstrukturen (n-GaAs/p-GaAs), MIS-Strukturen (n-InP, n-InAs) und p-Kanal-Si-MOS-Strukturen. Dabei gelang es in fast allen Beispielen, sowohl Einteilchen- wie auch kollektive Intersubbandanregungen und die Wechselwirkung mit optischen Phononen zu studieren. Als besonders aufschlußreich erwiesen sich die periodischen Dotierungsvielschichtstrukturen, da es durch Variation der optischen Anregungsintensität gelungen ist, den Obergang von quasi-zweidimensionalem zu quasi-dreidimensionalem Verhalten direkt zu verfolgen.

1. Introduction

Light scattering in solids has been used extensively to study elementary excitations such as phonons, plasmons, magnons as well as interactions between them. From the measured spectra one can obtain information on the energy, the intensity, the lineshape, and the polarization properties of the excitations. The potential of Raman scattering as a tool for the investigation and characterization of various types of crystalline and amorphous solids became clear with the invention of visible lasers and especially when reliable cw dye lasers were commercially available. During the past ten years there was an enormous increase of interest in this type of work. The experimental and theoretical developments in this field have been collected and reviewed recently in four volumes of the series "Topics in Applied Physics" edited by M. Cardona and G. Güntherodt[1,2,3,4]. The present work presents in a comprehensive form special aspects of inelastic light scattering as an important and versatile tool to study semiconductor heterojunctions and multilayer systems as well as semiconductor surface and bulk properties. It is based on several extensive review articles[5,6,7,8].

In section 2 we discuss some basic concepts of light scattering. Phonon Raman scattering is presented both in a phenomenological way which describes the symmetry properties of the excitations and in a microscopic description which yields information on the coupling mechanisms. After the discussion of the phonon properties there follows a more extensive

discussion of light scattering by free carriers. The nature of collective and single particle excitations, the coupling to LO-phonons, the resonance behavior, and the characteristic differences of two- and three-dimensional electron systems is treated theoretically. Section 3 is concerned with the specific optical and electronic properties of the samples studied. It also contains some information on scattering geometries and instrumentation for Raman spectroscopy.

In the main part of this lecture (section 4) we discuss in detail experimental results which have been obtained for various different types of semiconductor structures. The usefulness of phonon Raman scattering for the characterization of single- and multilayer systems of, for example GaAs and $Al_xGa_{1-x}As$ is demonstrated. The scattering of plasmon-like excitations leads to information on carrier concentration or effective mass and electron damping. The most exciting results, however, have been obtained for quasi-two-dimensional carrier systems during the past years. Two-dimensional electrons can exist at semiconductor-semiconductor interfaces, in metal-insulator-semiconductor (MIS) structures and in semiconductor multilayer systems. Their electronic properties have been reviewed by Ando, Fowler, and Stern[9]. Here we discuss the light scattering properties of such systems which were first proposed by Burstein et al.[10] and shortly after verified experimentally[11]. Electronic excitations have been studied during the past four years for carriers confined in GaAs-$Al_xGa_{1-x}As$ single heterojunctions and multilayer structures [11 to 19], at Ge-GaAs interfaces [20], in MIS-structures

on InAs[21,22], InP[23], and Si[24,25], and in GaAs doping superlattices[26,27,28]. Light scattering by two-dimensional carrier systems has been investigated theoretically in [29]. We select a few examples of these experiments and discuss the informations which have been extracted from the measured single particle and collective carrier excitations. The section ends with the discussion of the optical and electrical properties of GaAs doping superlattices, which has been called recently an "exciting landmark in semiconductor physics"[30].

2. Fundamentals of Light Scattering in Solids

2.1. Phonon Raman Scattering

2.1.1. Phenomenological Aspects

The interaction of light with a solid is described by the electric susceptibility χ. The electric field $\vec{E}$ of the incident light wave induces an oscillating dipole moment $\vec{P}$ which is given by

$$\vec{P} = \chi(\omega, \vec{k})\ \vec{E} \tag{1}$$

χ is a tensor which in general depends on the frequency ω and the wave vector $\vec{k}$. The electric susceptibility is closely related to the dielectric function

$$\varepsilon(\omega, \vec{k}) = 1 + 4\pi\chi(\omega, \vec{k}) \tag{2}$$

The emitted power of an oscillating dipole is classically proportional to the time average of the second derivative of the dipole moment $\vec{P}$. If χ is stationary, then $\vec{P}$ oscillates

with the frequency of the incident light wave ω_i. This describes transmission and reflection of light in a solid (Fig. 1). For inelastic light scattering one has to consider the modulation of χ due to fluctuations in space and time of, for example, phonons. The lattice oscillations are given by the time dependent displacement of the atoms

$$u(\vec{r},t) = u_o e^{i(\vec{q}\vec{r} + \Omega t)} \qquad (3)$$

where u_o is the unexcited position, $\vec{q}$ is the wave-vector of the phonon with frequency Ω. In the harmonic approximation the susceptibility χ can be developed with respect to the phonon amplitudes. The higher order terms of χ lead to inelastic light scattering (Brillouin- and Raman scattering). Scattering in first order occurs with frequency $\omega_s = \omega_i \mp \Omega$ and wave vector $\vec{k}_s = \vec{k}_i \mp \vec{q}$, where $\omega_{i,s}$ and $\vec{k}_{i,s}$ are the frequencies and wave vectors of the incident and scattered light, respectively. The minus sign stands for stokes scattering, the plus for antistokes. In opaque crystals one usually has to apply back scattering geometry (Fig. 1), such that $|\vec{q}| \approx |\vec{k}_i| + |\vec{k}_s|$, which in general is much smaller than the Brillouin zone boundary. Therefore in first order phonon Raman scattering one observes only excitations with wave vector $|\vec{q}| \approx 0$.

2.1.2. Microscopic Aspects

The Raman process for phonons is described by the Fynman diagram of Fig. 2a). The incident photon ω_i creates an

electron-hole pair. In the excited state the electron (or the hole) emits a phonon Ω caused by the electron-phonon interaction H_{ep}. The scattered photon ω_s is created by the recombination of the electron-hole pair. The energy scheme for these processes is shown in Fig. 2b). If the groundstate and the excited state are real, one talks about resonant Raman scattering. For the transition susceptibility one can write

$$\chi \sim \frac{\langle f|\vec{E}_s\vec{p}|b\rangle\langle b|H_{ep}|a\rangle\langle a|\vec{p}\vec{E}_i|0\rangle}{(\omega_i - E_a)(\omega_i - \Omega - E_b)} \qquad (4)$$

where $\vec{p}$ is the momentum operator, $\vec{E}_{i,s}$ are the electric field vectors of the incident and scattered photons, $E_{a,b}$ are the energies of the excited states, respectively. H_{ep} is the Hamilton operator for electron-phonon coupling, which for the deformation potential interaction describes the periodic modulation of the electronic states due to the phonon induced lattice distortion. There are, however, also other possible interaction mechanisms like electro-optic effect or Fröhlich interaction. For the latter the macroscopic electric field of the LO-phonons in polar semiconductors is important. It is also essential for the discussion of the so-called "forbidden" Raman scattering which has been used to study surface barrier heights.

2.1.3. Selection Rules

The selection rules for allowed Raman scattering are determined by the structure and symmetry of the transition susceptibility χ, which is also called Raman tensor. These are listed for all crystal classes in [31]. For crystals with

diamond or zinc-blende type structure like GaAs there exist three irreducible components of the Raman tensor R. The optical phonons at $k \approx 0$ have Γ_{15}-symmetry. The Raman tensor component for this symmetry is

$$\Gamma_{15}: \begin{pmatrix} 0 & d & 0 \\ d & 0 & 0 \\ 0 & 0 & 0 \end{pmatrix}, \begin{pmatrix} 0 & 0 & d \\ 0 & 0 & 0 \\ d & 0 & 0 \end{pmatrix}, \begin{pmatrix} 0 & 0 & 0 \\ 0 & 0 & d \\ 0 & d & 0 \end{pmatrix}$$

The first order selection rules depend on the scattering configuration and can be evaluated by multiplying the polarization vectors of the incident and scattered light with the Raman tensor component of the corresponding phonon symmetry. In non-polar crystals like Si or Ge the TO and LO-phonons are degenerate at $k \approx 0$. In polar crystals like GaAs on the other hand, the macroscopic electric field associated with the LO-phonons leads to an LO-TO splitting. From the selection rules it follows that in backscattering geometry from (100) surfaces scattering by LO-phonons is allowed. Scattering by TO-phonons on the other hand is symmetry-forbidden. This is opposite in back-scattering from (110) surfaces. The symmetry properties of phonon Raman scattering have been used to obtain information on the crystal orientation of thin epitaxial films of GaAs[32].

2.1.4. Forbidden LO-Phonon Scattering

The selection rules just discussed can be violated by different possible symmetry-breaking mechanisms[33]:

1. Intraband scattering of electrons by LO-phonons via the Fröhlich interaction, which becomes allowed for finite q-vectors of the LO-phonons.
2. Forbidden scattering induced by the presence of impurities in the sense that the electron is scattered elastically by an impurity to provide the necessary momentum change.
3. Electric-field induced Raman scattering which can be described with a Franz-Keldysh-type theory.

All three mechanisms are especially important for LO-phonon Raman scattering under resonance condition. Forbidden LO-phonon scattering has been used for example to study surface barrier heights on clean and oxygen covered (110) cleavage surfaces of GaAs[34].

2.2. Light Scattering by Free Carriers (Three-Dimensional)

The theory of light scattering by electron plasmas in solids has been developed already in the early sixtieth[35]. The scattering cross-section was found to be related to the spectrum of density fluctuations. At higher densities, however, the one-electron excitations are modified by dynamical screening effects with the longitudinal polarization of the plasma. It has also been recognized that the band structure influences light scattering in various ways. The resonance behavior of the scattering cross-section close to optical interband energy gaps and the spin-orbit interaction of the valence bands have opened the possibility to observe excitations of single-particle

character also at high electron densities. The first observation of laser light scattering by a solid state plasma was reported by Mooradian and Wright [36] in doped n-GaAs.

2.2.1. Single-Particle Excitations

The one-electron excitation in a solid state plasma is shown schematically in Fig. 3. The necessary momentum change $\vec{q}$ is provided by the wave vectors of the incident and scattered light $\vec{k}_i$ and $\vec{k}_s$. In backscattering geometry one obtains

$$|\vec{q}| = |\vec{k}_i| + |\vec{k}_s| \approx 2\,\frac{2\pi n}{\lambda_L} \tag{5}$$

where n is the refractive index and λ_L is the wavelength of the incident and scattered light which here is taken approximately as the laser wavelength. In GaAs $|\vec{q}|$ can be varied from $\simeq 0$ cm^{-1} to $\simeq 10^6$ cm^{-1} by using different laser excitation lines. For a three-dimensional electron plasma the integration over all possible excitations with given $\vec{q}$ leads to a triangular shaped spectrum with a cut-off around $q \cdot v_F$, where $v_F = \hbar k_F/m^*$ is the Fermi velocity. This is shown schematically in Fig. 4. The triangular line shape is smeared out due to finite damping. The single-particle excitation spectrum has been found to be proportional to the imaginary part of the dielectric function Im $\varepsilon(\omega, q)$ (see [8]). To include finite damping in the calculations the Lindhard-Mermin approximation was introduced to calculate the lineshape function Im $\varepsilon(q, \omega)$ [37].

There exists a class of excitations of single-, as well as multicomponent carrier systems which carry no net fluctuation in charge density and consequently have single-particle character. These are spin-density fluctuations in which the spin of the electrons is changed via the spin orbit interaction[38]. In GaAs these excitations become dominant for photon energies close to the $E_o + \Delta_o$ energy gap. It has also been predicted that light scattering by single-particle excitations without a spin-flip is possible in the case of non-parabolic electron bands[39].

2.2.2. Collective Excitations

Electron excitations which carry a charge density fluctuation are usually dynamically screened by the electron plasma. The scattering lineshape is closely related to Im $1/\varepsilon(q,\omega)$ which peaks around the plasma frequency $\omega_p(q)$. The dispersion of ω_p is included in Fig. 4. In polar semiconductors the longitudinal plasma oscillations are coupled to the LO-phonons due to the macroscopic electric field. If we neglect damping and use a simple Drude expression for the dielectric function of the electron gas, one can write the total dielectric function[35]:

$$\varepsilon(q,\omega) = \varepsilon_\infty \left(\underbrace{\frac{\omega_{LO}^2 - \omega^2}{\omega_{TO}^2 - \omega^2}}_{\text{lattice}} - \underbrace{\frac{\omega_p^2(q)}{\omega^2}}_{\text{electrons}} \right) \qquad (6)$$

with $\omega_p^2(q) = \omega_p^2 + 3/5(qv_F)^2$ and $\omega_p^2 = 4\pi ne^2/\varepsilon_\infty m^*$. The frequencies of the resulting coupled phonon plasmon modes are determined by the zeros of eq. 6. This is illustrated in Fig. 5. In Fig. 6 we show experimental and theoretical results of the coupled modes $\omega_\pm$ as obtained in [36] for $\varepsilon(q \to 0, \omega)$. If one approaches the region of single-particle excitations and if damping is not negligible, one has to evaluate the peaks of Im $1/\varepsilon$. This has been done successfully using the Lindhard-Mermin dielectric function of the electron gas[40].

2.2.3. Resonance Behavior

Excitations by free carriers show a strong resonance enhancement close to optical gaps where carrier occupied states are involved in the transitions. In GaAs this has been studied extensively[8] for laser excitation lines close to the $E_o + \Delta_o$ energy gap. In Fig. 7a we show the transitions which are important for the spin-flip single-particle excitations. In the first step an electron is excited from the spin orbit split-off valence band to the conduction band above the Fermi energy. An electron with opposite spin can recombine with the hole in the valence band whose wave function includes both spin directions due to spin-orbit interaction. Spin-flip excitations are found to be antisymmetric, the polarizations of the incident and scattered light are crossed. The scattering cross-section of these types of excitations is strongly enhanced at the $E_o + \Delta_o$ energy gap of GaAs. As a consequence of the study of this resonance behavior it was suggested in Ref. [37]

that it should be possible to study also two-dimensional electron systems confined at semiconductor surface space charge layers.

In Fig. 7b we show transitions involved in scattering by collective excitations. The resonance condition is fulfilled for both incident and scattered photons. Therefore the resonance condition is not as sharp as for single-particle excitations. The creation of collective longitudinal excitations can be understood as the creation of single-particle electron-hole pairs by the incident photons which then emit plasmons or coupled phonon-plasmon modes. These excitations can also be observed at energy gaps which do not involve carrier occupied states via the phonon scattering mechanisms.

2.3. Light Scattering by Free Carriers (Two-Dimensional)

Two-dimensional carriers are characterized by the separation of motion perpendicular and parallel to the direction of quantization. While in the parallel direction the usual dispersion of the bands is maintained in the effective mass approximation, the carriers are bound in subbands with minimum energies E_o, E_1, E_2 ... in the direction perpendicular to the potential well. In Fig. 8a we show schematically a one-dimensional, rectangular potential well with finite height. E_o and E_1 are subbands, E_F the Fermi energy. The more realistic nature of one-dimensional potential wells at semiconductor surfaces and heterojunctions is discussed later. The dispersion

of the subbands in $k_{||}$ is shown in Fig. 8b. Depending on the scattering wavevector one can create both intra- und inter-subband excitations.

2.3.1. Intrasubband Excitations

Excitations within one subband are only possible, if there exists a component of the scattering wavevector in the $\vec{q}_{||}$ direction. Similar to the three-dimensional case one can create both single-particle and collective excitations. Because of the two-dimensional nature of the electron system there exist, however, basic differences of the excitation spectra. The integration over all possible single-particle excitations for a given $\vec{q}_{||}$ differs from the lineshape found for the three-dimensional case. This is shown schematically in Fig. 9. The collective intrasubband excitations are two-dimensional plasma oscillations of the electrons parallel to the surface or interface. The frequency of this plasmon tends to zero with decreasing $q_{||}$. So far only collective intrasubband excitations have been observed in GaAs-$Al_xGa_{1-x}As$ multilayer structures[41].

2.3.2. Single-particle Intersubband Excitations

Single-particle intersubband excitations are uncorrelated excitations of an electron below the Fermi energy in a lower subband to an empty state in the higher subband. Similar to the three-dimensional case, these unscreened excitations can

be observed when the scattering occurs via spin-density fluctuations. The measured energies directly correspond to the subband splitting, if the scattering wavevector is perpendicular to the direction of quantization. This is usually the case in backscattering geometry. An additional component of the wavevector parallel to the layers leads to a strong broadening of the spin-flip single-particle intersubband excitations. This is shown schematically in Fig. 9. Subband energies have been determined with this method for various two-dimensional carrier systems which exist in semiconductor heterostructures like GaAs, InP, Si, Ge. In these materials the resonance condition for spin-flip excitations could be fulfilled with conventional Raman spectrometers.

2.3.3. Collective Intersubband Excitations

The collective intersubband excitations of a two-dimensional plasma reflect in a way the finite extension of the carrier system in the direction of quantization. The collective excitations involve charge density fluctuations and therefore are dynamically screened by Coulomb interactions. This screening causes an upward shift with respect to the single-particle excitations. The effect is called "depolarization shift" and has been treated theoretically in [42,43,44]. It describes the dielectric response of the thin layer of carriers to the electron-hole excitation and can be written as an effective plasma frequency ω_p^* perpendicular to the layer. For a two-level model one finds

$$\omega_p^{*2} = \frac{8\pi n_s e^2}{\varepsilon\hbar}\ \omega_{01}\ f_{11} \qquad (7)$$

where f_{11} is the Coulomb integral of the wavefunctions of the two subbands involved. The measured subband excitation is then given by

$$\omega_{01}^{*2} = \omega_{01}^2 + \omega_p^{*2} \qquad (8)$$

The investigation of single-particle and collective intersubband excitations consequently leads to direct information on Coulomb matrix elements in two-dimensional carrier systems.

In polar semiconductors the collective excitations are coupled to the LO-phonons. Similar to the three-dimensional case the coupled mode frequencies can be determined from the zeros of the total dielectric function

$$\varepsilon(q,\omega) = \varepsilon_\infty \left(\frac{\omega_{LO}^2 - \omega^2}{\omega_{TO}^2 - \omega^2} + \frac{\omega_p^{*2}}{\omega_{01}^2 - \omega^2} \right) \qquad (9)$$

Damping is neglected in eq. (9). The dielectric function of the electrons is expressed in analogy to the three-dimensional case, discussed above, by a Drude-like expression where ω_p is replaced by ω_p^* and the denominator resonates at $\omega = \omega_{01}$. Eq. (9) yields two coupled modes which are plotted in Fig. 10 ($q = 0$). For $\omega_{01} \ll \omega_{LO}$ one finds $\omega_- \tilde{=} \omega_{01}^*$, while for the opposite case $\omega_{01} \gg \omega_{LO}$ the high frequency ω_+ - mode approaches ω_{01}^*. Contrary to the three-dimensional

case, the ω_--mode crosses the frequency of the transverse optical phonon ω_{TO} when $\omega_{o1} = \omega_{TO}$ and falls in the rest-strahlen region for higher subband splittings. In Fig. 10 we show both the bare subband splitting ω_{o1} and the coupled modes versus number of carriers for an electron accumulation layer on InP as calculated self-consistently[23].

3. Experimental Aspects

3.1. Sample Characteristics

In section 2.2.3. we have seen that for "electronic Raman scattering" one usually has to work under resonant conditions. In Fig. 11 the band structure with the relevant optical energy gaps is shown for the example GaAs. Transitions which involve carrier occupied states are only possible for laser excitation energies close to E_o and $E_o + \Delta_o$. In table 1 we have collected the relevant optical gaps for various semiconductors of interest.

Above the fundamental optical energy gap the semiconductors are opaque. The information depth of Raman spectroscopy is determined by the penetration depth of the laser light. Very often this is much less than 1 μm. Consequently only properties of semiconductor heterojunctions very close to the surface can be investigated using resonant inelastic light scattering techniques. The design parameters and the electrical properties of semiconductor heterostructures studied are discussed for selected examples together with the experimental results in sect. 4.

3.2. Scattering Geometries

In opaque semiconductors the most widely used scattering geometry is backscattering, where the wave vector of the incident light is normal to the surface and the scattered light is collected in backward direction. Because of the high refractive index ($n \approx 4$) of the semiconductors studied, nearly ideal backscattering conditions are fulfilled even when the incident laser beam is focussed under an angle of 45 degrees to the normal of the surface plane (see Fig. 1). In order to provide a larger component of the scattering wave vector parallel to the surface the incident light can be focussed on to the surface under glancing incidence. This opens the possibility to study also in-plane excitations of a two-dimensional electron gas.

3.3. Raman Set-up

For inelastic light scattering in semiconductors conventional Raman spectrometers can be used. The incident light is provided by cw-ion gas lasers or by cw-dye lasers. To fulfil the resonance conditions for various semiconductors photon energies covering the region from near ultraviolet to infrared have to be available. The laser beam is focussed on to the sample with a spherical or cylindrical lense. The sample is usually mounted in a temperature variable optical cryostat. The backscattered light is collected and focussed to the entrance slit of a double grating spectrometer. A polarization

analyser allows the separation of different scattering components. The scattered light is detected with a specially selected photomultiplier tube which is connected with special pulse counting electronics.

4. Experimental Results

In this section we present selected experimental results where Raman scattering has been used to investigate special properties of semiconductor heterojunctions and multilayer systems. Because of limitations in space this collection is by no means complete. So we omit the excellent work which has been carried out in high magnetic fields[45], the effect of Brillouin zone folding in superlattices on phonons[46] and the surface sensitive Raman work on cleaved GaAs under ultrahigh vacuum conditions[34].

4.1. Phonon Aspects

In section 2.1. we have learnt that under certain scattering configurations not all types of optical phonons can be observed in Raman scattering. This has been used in Ref. 32 to study the surface orientation of thin films of GaAs grown with MBE. In backscattering from (100) surfaces only scattering by LO-phonons is allowed. In the Raman spectra shown in Fig. 12 this is the case for the two upper spectra. The two lower spectra show a strong TO-mode even though obtained from thin MBE grown films with a nominally ⟨001⟩ orientation perpendicular to the surface. It could be shown that the strong "forbidden"

TO-phonon is connected with a twinning of the growing film caused by carbon contamination of the substrate surface.

In mixed crystals like $Al_xGa_{1-x}As$ phonon Raman scattering can be used to obtain information on the composition. The optical phonons in these crystals have a two-mode behavior with frequencies close to the modes of pure GaAs and pure AlAs. The frequency dependence of these modes on the molar fraction x of Al in GaAs is shown in Fig. 13. Raman spectroscopy has been used to study the depth profile of the Al-content in the $Al_xGa_{1-x}As$ films and the composition of unknown crystals and multilayer structures (see for example [32]). We want to emphasize that Raman scattering experiments can be performed on very small spots on the sample surface. Therefore it is possible to study the properties with high spatial resolution which is of the order of the focussed laser beam (a few μm^2).

4.2. Three-Dimensional Carriers in Polar Semiconductors

In polar semiconductors plasmons are coupled to LO-phonons. The frequencies of the coupled phonon-plasmon modes ω_+ and ω_- depend on the carrier concentration, the linewidth on the electron damping. Under resonance conditions one also can observe excitations with single particle character. In Fig. 14 we show resonance Raman spectra as obtained from a homogeneously doped single crystal of GaAs with $n = 7 \times 10^{17} cm^{-3}$. The spectrum $z(xy)\bar{z}$, where z and $\bar{z}$ are the propagation directions of incident and scattered light and x and y their polarization directions,

respectively, exhibits a broad spin-flip single-particle excitation band sitting on top of the hot luminescence background around the $E_o + \Delta_o$ optical energy gap. The spectrum for parallel polarizations contains the two coupled modes at frequencies ω_- and ω_+ which depend on n and q. In Ref. 32 it has been demonstrated that these modes can be used to determine directly the carrier concentration and the scattering times with high spatial resolution. This method has been applied also for the characterization of other polar semiconductors like InP and InAs.

4.3. Semiconductor Single Heterojunctions

4.3.1. The GaAs-$Al_xGa_{1-x}As$ System

The extensive study of the resonance behavior of single-particle and collective excitation by three-dimensional carriers coincided with reports of the achievement of high mobility two-dimensional systems in GaAs-$Al_xGa_{1-x}As$ heterostructures made by molecular beam epitaxy[47]. It has been realized immediately that these heterostructures are ideal candidates for electronic light scattering experiments. Shortly afterwards the first observations of light scattering by electrons confined at the interface of selectively doped GaAs-n-$Al_xGa_{1-x}As$ heterostructures was reported[11]. At these interfaces charge carriers are transferred from the donors in the $Al_xGa_{1-x}As$ layers to the energetically lower conduction band of GaAs forming a depletion layer on the $Al_xGa_{1-x}As$ side and an accumulation or inversion

layer on the GaAs side. The energy band diagram and the electric subbands are shown in Fig. 15. Raman spectra obtained from such a structure are plotted in Fig. 16. Besides the spin-flip single-particle excitations of GaAs bulk carriers one can identify single-particle intersubband excitation of the electrons confined to the interface. The energy has been compared with self-consistent calculations in Ref. 13. They are in good agreement with the subband difference E_{01}. In the work of [11] it has been demonstrated for the first time that resonant inelastic light scattering is a sensitive tool to study electronic properties of two-dimensional systems. It was also shown that with a Schottky barrier arrangement one is able to control the carrier density. This opened the possibility of fabricating high mobility field effect transistors with semiconductor heterostructures where charge transfer occurs.

In the first experiments the relatively high carrier concentration in the individual layers yielded complicated spectra especially for the collective excitations. The experiments have been repeated in the work of [18] with samples of better quality. The results are shown in Fig. 17. These spectra exhibit both higher order transitions and collective intersubband transitions which are shifted to higher energies because of the depolarization field effect. The evaluation of this shift in terms of Coulomb matrix elements is discussed in more detail together with the results obtained in multi-quantum well structures.

4.3.2. Ge on GaAs

Recently the first results of light scattering studies of electrons confined to Ge-GaAs interfaces have been reported [20]. The electronic structure of this interface has received considerable attention because of the nearly perfect lattice matching. The band gap in GaAs is larger than in Ge. Therefore charge transfer can occur from the GaAs to the Ge forming a two-dimensional carrier system at the interface. The conduction band minima in Ge are at the Brillouin zone boundary along the ⟨111⟩ direction. The resonant optical gap for electronic Raman scattering therefore is E_1 = 2.22 eV. In the work of Ref. [20] Ge-GaAs heterostructures grown by MBE have been investigated with laser excitation lines close to the E_1 gap of Ge. The samples consist of a thin Ge-layer (~ 300 Å) on top of (100) GaAs layer. The Ge-film is highly doped with As. The spectra with crossed polarizations exhibit a broad asymmetric structure which peaks around 25 meV. A theoretical fit of this spectrum indicates that it is due to interband transitions between a quasi-two-dimensional band and the continuum.

4.4. Metal-Insulator-Semiconductor Structures

Electronic light scattering by two-dimensional carriers in MIS-structures has been observed so far for electrons in InAs[21,22] and InP[23] and for holes in Si[24,25]. The work in InAs was performed with laser lines close to the E_1 and $E_1 + \Delta_1$ energy gap where no carrier-occupied states are involved

in the optical transitions. Consequently only collective intersubband excitations coupled to LO-phonons have been observed via the phonon scattering mechanisms. Only little information could be obtained from these spectra.

4.4.1. Electrons in InP

The band structure of InP is very similar to that of GaAs. The spin-orbit-split-off band gap $E_o + \Delta_o$ is about 1.6 eV at low temperature. Recently good MIS-structures with voltage tunable surface carrier concentrations have been fabricated on InP[48]. Resonant light scattering experiments have been used to investigate spectroscopically the subband structure of electron accumulation layers in such samples. Both spin-flip single-particle intersubband- as well as collective excitations have been observed (Fig. 18). The measured energies of the coupled modes and the single-particle excitations can be satisfactorily compared with self-consistent calculations for this subband system (Fig. 10). However, the increase of the subband splittings with surface carrier concentration n_s is found to be smaller than theoretically predicted. Part of this discrepancy is due to the nonparabolicity of the conduction band which has not been taken into account in the self-consistent theory.

4.4.2. Holes in Si

The most widely studied surface space-charge layers in semiconductors are accumulation and inversion layers on Si (see Ref. 9). Recently the first successful light scattering experiments on hole space-charge layers in Si (100) have been reported[24]. The resonant energy for holes is connected with the direct E_o' gap at $k \tilde{=} 0$, which is about 3.4 eV. Both collective and spin-flip subband transitions have been observed[25]. Some of the spectra exhibit very broad and asymmetric bands due to the nonparabolic dispersion of the individual subbands. Different transitions between heavy and light hole subbands could be identified. The results are in good agreement with subband calculations from Ref. [49].

4.5. Compositional Superlattices (GaAs-$Al_xGa_{1-x}As$)

4.5.1. Subband Energies and Depolarization Shifts

Electronic light scattering has been used extensively for the investigation of GaAs-$Al_xGa_{1-x}As$ quantum well structures. The first results obtained with modulation doped multilayer structures[12] appeared shortly after the successful experiments performed with single heterojunctions[11]. The electrons in multilayer structures are quantized in potential wells which are nearly rectangular due to the quantum size effect in the thin layers which, however, are modified by the space-charge potential of the transferred carriers. The subband structure for such systems was first calculated self-consistently by

Mori and Ando[50]. Spin-flip single-particle excitations have been used extensively to study the subband energies in a number of samples with different parameters[12,14,16,18]. It was realized already in the first experiments that the positions of the collective excitations observed for parallel polarizations are shifted with respect to the single-particle peaks. The differences in energies reveal in a direct way the depolarization shifts which are related to the Coulomb matrix elements (see section 2.3.3.). In GaAs the collective excitations are coupled to the LO-phonons. The coupled modes have been observed for various samples and for different subband transitions having even an odd parity[15,16]. In Fig. 19 an example is shown for a sample with d_{GaAs} = 200 Å and a two-dimensional carrier concentration $n_s \simeq 4 \times 10^{11} cm^{-2}$. Such spectra have been used for quantitative determination of ω_p^* and the Coulomb matrix elements $f_{nn'}$, which for the 0 - 1 transition are of the order 10 to 20 Å. The results are in excellent agreement with calculations using the numerical wavefunctions of the subbands.

4.5.2. Linewidth and Mobility

It had been realized that the introduction of undoped $Al_xGa_{1-x}As$ spacers at the interfaces of these compositional superlattices lead to a stronger enhancement of the electron mobilities due to the further separation of electrons from their ionized parents impurities. Pinczuk et al.[18] have studied single-particle excitations in several multi-quantum well structures with different thicknesses of the undoped

spacer layers but otherwise identical properties. The low temperature mobilities varied in these samples from 12,500 cm^2/Vs to 93,000 cm^2/Vs. The Raman results are shown in Fig. 20. The subband excitations are much sharper for the samples with higher mobilities. A striking effect was found when the widths were studied for different laser photon energies. For the samples with lower mobilities the width of the E_{01} transition has a peak for spectra obtained with photon energies close to the maximum in resonant enhancement. These results have been interpreted in terms of wave vector non-conservation due to scattering of electrons or holes by the Coulomb potential of the ionized impurities.

4.5.3. Photo-Excited Carriers

Resonant inelastic light scattering by photo-excited electrons in GaAs-$Al_xGa_{1-x}As$ multiple quantum well structures have been reported for both pure and modulation doped samples[17,19]. In undoped structures Pinczuk et al.[17] found no dependence of the subband splitting on the excitation intensity. This indicates that the creation of electrons and holes within the GaAs layers does not result in a distortion of the rectangular potential wells. No separation in space occurs for the photo-excited electron-hole pairs. Zeller et al.[19] studied modulation doped samples with high laser power densities. They found a shift of the subband splitting E_{01} to smaller energies with increasing excitation intensity. A decrease of the subband splitting is expected when the electron density in the GaAs

layers is increased more strongly than the hole concentration. This might happen due to the presence of surface depletion layers or by hole traps in the $Al_xGa_{1-x}As$ layers.

4.5.4. In-Plane Excitations

Recently the plasma frequency dispersion in a layered electron gas has been measured by inelastic light scattering[40]. A modified backscattering geometry was applied to provide the necessary wave vector component parallel to the GaAs layers of modulation doped GaAs-$Al_xGa_{1-x}As$ multi-quantum well structures. The measured dispersion of the plasmon frequency was found to be linear in the in-plane component of the wave vector. This differs from the results obtained in pure two-dimensional and pure three-dimensional plasmas. It, however, confirms basic predictions of the plasmon behavior in layered carrier systems.

4.6. Doping Superlattices

4.6.1. Electrical and Optical Properties

One of the nicest examples where resonant inelastic light scattering acts as a tool for the investigation of semiconductor heterostructures is the recent work on periodic doping multilayer structures, so-called "nipi"-crystals. This type of semiconductor superlattices has been first proposed and analyzed by Döhler[51]. It is composed of a periodic sequence of ultrathin n- and p-doped layers of GaAs and exhibits various novel and exciting electrical and optical properties which are caused by purely space-charge induced potential wells.

A doping superlattice is simply an alternation of p-n and n-p junctions of an otherwise homogeneous semiconductor. When the concentration of the donors N_D times the thickness of the n-type layers is equal to the number of the acceptors N_D times the thickness of the p-type layers the nipi-crystal is compensated. The electrons from the donors are attracted by the acceptors in the p-type layers resulting in a periodic rise and fall of the conduction and valence band. Such structures exhibit the special feature of a semiconductor with an "indirect gap in real space". Excited electrons and holes are separated in space and may have recombination lifetimes orders of magnitude longer than in homogeneous bulk crystals. The reduced effective band gap which depends on the non-equilibrium electron and hole concentrations results in a strong tunability of the optical absorption and luminescence. In Fig. 21 the modulated conduction and valence band of a nipi-crystal is given in an excited situation. The transitions of photo-luminescence and resonant Raman scattering experiments are shown schematically. The energetic position of the luminescence depends on the excitation intensity and can be used to determine the non-equilibrium carrier concentration. Indirect photoluminescence spectra are shown in Fig. 22. These experiments directly demonstrate the tunability of the effective band gap.

4.6.2. Single-Particle and Collective Excitations

To get direct information on the quantization of photoexcited carriers in doping superlattices, resonant inelastic

light scattering experiments have been performed[26,27,28]. Spin-flip single-particle intersubband excitations have been studied using different power densities of the incident laser (Fig. 23). At low excitation intensity several distinct peaks have been observed on top of a hot luminescence background (Fig. 23). These peaks could be identified as $\Delta = 1$, $\Delta = 2$, and $\Delta = 3$ intersubband transitions of photo-excited electrons in the conduction band of the doping superlattice. The subband energies obtained in this way are in excellent agreement with self-consistent calculations.

Raman spectra of collective excitations have also been observed in doping multilayer structures. Because of the occupation of several subbands already at relatively low power densities and the coupling to LO-phonons, the observed polarized spectra exhibit a complicated structure (Fig. 24). At low excitation intensities three peaks have been observed below the LO-phonon mode which represent several ω_--modes. A broad ω_+-mode can be identified above the LO-phonon. The positions of these modes are in good agreement with recent calculations performed by Ruden and Döhler[52].

4.6.3. Two- and Three-Dimensional Effects

At high power densities the subband splittings get smaller and the higher occupied states show considerable dispersion in the direction perpendicular to the layers. This can be observed by studying both the single-particle and the collective excitations in the highly excited case. While at low laser power

densities distinct subband transitions are observed, the individual peaks merge at high power densities into one broad single-particle excitation band which has a very similar lineshape as obtained for a homogeneously doped GaAs single crystal of comparable carrier concentration (see Figs 23 and 14). The spectra of the coupled modes also change with increasing power density and finally they look very similar to coupled phonon plasmon modes of homogeneously doped n-GaAs (Figs 24 and 14). The behavior with increasing power density is concomitant with the transition from a quasi-two-dimensional to a quasi-three-dimensional electron system.

5. Concluding Remarks

We have demonstrated the usefulness of inelastic light scattering for the investigation of various properties of semiconductor thin layers, -heterojunctions and -multilayer systems. We want to emphasize that Raman scattering experiments can be performed on very small spots on the surface. Thus it is possible to study all the properties discussed in this work along the whole surface with high spatial resolution. Raman spectroscopy is a powerful technique not only for the investigation of light scattering properties by itself, but it also acts as a tool to characterize and analyse electrical and optical properties of new materials.

References

1) M. Cardona (ed.): "Light Scattering in Solids", Topics in Applied Physics, Vol. 8 (Springer, Berlin, Heidelberg, New York 1975)

2) M. Cardona, G. Güntherodt (eds.): "Light Scattering in Solids II", Topics in Appl. Phys., Vol. 50 (Springer, Berlin, Heidelberg, New York 1982)

3) M. Cardona, G. Güntherodt (eds.): "Light Scattering in Solids III", Topics in Appl. Phys. Vol. 51 (Springer, Berlin, Heidelberg, New York 1982)

4) M. Cardona, G. Güntherodt (eds.): "Light Scattering in Solids IV", Topics in Appl. Phys., Vol. 54 (Springer, Berlin, Heidelberg, New York 1983)

5) A. Pinczuk and E. Burstein, in Ref. 1, p. 23

6) M.V. Klein, in Ref. 1, p. 147

7) M. Cardona, in Ref. 2, p. 19

8) G. Abstreiter, M. Cardona, and A. Pinczuk, in Ref. 4

9) T. Ando, A.B. Fowler, and F. Stern, Review of Modern Physics, Vol. 54, 437 (1982)

10) E. Burstein, A. Pinczuk, and S. Buchner, "Proc. of the 14th Int. Conf. on the Physics of Semiconductors", 1978, ed. B.L.H. Wilson (The Institute of Physics, London, 1979), p. 1231

11) G. Abstreiter and K. Ploog, Phys.Rev. Letters 42, 1308 (1979)

12) A. Pinczuk, H.L. Störmer, R. Dingle, J.M. Worlock, W. Wiegmann, and A.C. Gossard, Solid State Commun. 32, 1001 (1979)

13) G. Abstreiter, Surface Science 98, 117 (1980)

14) A. Pinczuk, J.M. Worlock, H.L. Störmer, R. Dingle, W. Wiegmann, and A.C. Gossard, Surface Science 98, 126 (1980)

15) A. Pinczuk, J.M. Worlock, H.L. Störmer, R. Dingle, W. Wiegmann, and A.C. Gossard, Solid State Commun. 36, 43 (1980)

16) G. Abstreiter, Ch. Zeller, and K. Ploog, "Proc. 8th Int. Symp. on GaAs and Related Compounds", Vienna, 1980, ed. H.W. Thim, Inst. Phys. Conf. Ser. 56 (Inst. Phys. London, 1981), p. 741

17) A. Pinczuk, J. Shah, A.C. Gossard, and W. Wiegmann, Phys. Rev. Letters 46, 1307 (1981)

18) A. Pinczuk, J.M. Worlock, Surface Science 113, 69 (1982)

19) Ch. Zeller, G. Abstreiter, and K. Ploog, Surface Science 113, 85 (1982)

20) R. Merlin, A. Pinczuk, W.T. Beard, C.E.E. Wood, J. Vac. Sci. Technol. 21, 516 (1982)

21) L.Y. Ching, E. Burstein, S. Buchner, H.H. Wieder, "Proc. of the 15th Int. Conf. on the Physics of Semiconductors" 1980, eds. S. Tanaka, Y. Toyozawa (Journal of the Physical Soc. of Japan 49 (1980), Supplement A), p. 951

22) G. Tränkle and G. Abstreiter (unpublished), G. Tränkle, Diplom-thesis (1981), Techn. Univ. München

23) G. Abstreiter, R. Huber, and G. Tränkle, Solid State Commun. (to be published)

24) G. Abstreiter, U. Claessen, and G. Tränkle, Solid State Commun. 44, 673 (1982)

25) M. Baumgartner and G. Abstreiter, to be published

26) G.H. Döhler, H. Künzel, D. Olego, K. Ploog, P. Ruden, H.J. Stolz, and G. Abstreiter, Phys.Rev. Letters 47, 864 (1981)

27) Ch. Zeller, B. Vinter, G. Abstreiter, and K. Ploog, Phys. Rev. B 26, 2124 (1982)

28) Ch. Zeller, B. Vinter, G. Abstreiter, and K. Ploog, "Proc. of the 16th Int. Conf. on the Physics of Semiconductors" Montpellier, 1982 (to be published)

29) E. Burstein, A. Pinczuk, and D.L. Mills, Surface Science 98, 451 (1980)

30) J.M. Worlock, Nature 297, 360 (1982)

31) R. Loudon, Adv. Phys. 13, 423 (1964)

32) G. Abstreiter, E. Bauser, A. Fischer, and K. Ploog, Appl. Phys. 16, 345 (1978)

33) R. Trommer, G. Abstreiter, and M. Cardona, "Proc. of the Int. Conf. on Lattice Dynamics, ed. M. Balkanski (Flammarion Sciences, Paris, 1977), p. 189

34) H.J. Stolz and G. Abstreiter, J. Vac. Sci. Technol. 19, 380 (1981)

35) See for example: D. Pines, "Elementary Excitations in Solids" (Benjamin, New York, 1963)

36) A. Mooradian, G.B. Wright, Phys. Rev. Lett. 16, 999 (1966)

37) A. Pinczuk, G. Abstreiter, R. Trommer, and M. Cardona, Solid State Commun. 30, 429 (1979)

38) D.C. Hamilton, A.L. McWhorter, "Light Scattering Spectra of Solids", ed. G.B. Wright (Springer, New York, Heidelberg, Berlin, 1969), p. 309

39) P.A. Wolf in Ref. 38, p. 273

40) G. Abstreiter, R. Trommer, M. Cardona, and A. Pinczuk, Solid State Commun. 30, 703 (1979)

41) D. Olego, A. Pinczuk, A.C. Gossard, W. Wiegmann, Phys. Rev. B 25, 7867 (1982)

42) W.P. Chen, Y.J. Chen, and E. Burstein, Surface Science 58, 263 (1976)

43) S.J. Allen Jr., D.C. Tsui, and B. Vinter, Solid State Commun. 21, 133 (1977)

44) D. Dahl and L.J. Sham, Phys. Rev. B 16, 651 (1977)

45) Z.J. Tien, J.M. Worlock, C.H. Perry, A. Pinczuk, R.L. Aggarwal, H.L. Störmer, A.C. Gossard, and W. Wiegmann, Surface Science 113, 89 (1982)

46) C. Colvard, R. Merlin, M.V. Klein, and A.C. Gossard, Phys. Rev. Letters 45, 298 (1980)

47) R. Dingle, H.L. Störmer, A.C. Gossard, and W. Wiegmann, Appl. Phys. Letters 33, 665 (1978); H.L. Störmer, J.Phys. Soc. Japan 49 Suppl. A (1980), p. 1013

48) H.C. Cheng and F. Koch, Phys. Rev. B 26, 1989 (1982)

49) E. Bangert (unpublished) (1975)

50) T. Ando and S. Mori, J. Phys. Soc. Japan 47, 1518 (1979)

51) G.H. Döhler, Phys. Status Solidi B 52, 79 and 533 (1972), J. Vac. Sci. Technol. 16, 851 (1979)

52) P. Ruden and G.H. Döhler, Phys. Rev. B, to be published

Table 1

Optical energy gaps relevant for resonant inelastic light scattering via carrier density mechanisms

GaAs	electrons	$E_o = 1.51$ eV, $E_o + \Delta_o = 1.85$ eV
GaAs	holes	$E_o = 1.51$ eV
Ge	electrons	$E_1 = 2.2$ eV, $E_1 + \Delta_1 = 2.4$ eV
Si	electrons	$E_2 = 4.35$ eV
Si	holes	$E_o' = 3.35$ eV
InP	electrons	$E_o = 1.41$ eV, $E_o + \Delta_o = 1.52$ eV

Figure Captions

Fig. 1: Schematic diagram of the geometry for reflection, transmission, and inelastic light scattering.

Fig. 2: Feynman diagram and energy level scheme for phonon Raman scattering.

Fig. 3: Single-particle excitation process of electrons in a parabolic band.

Fig. 4: Single-particle region and plasmon dispersion for electrons in a parabolic band.

Fig. 5: Dielectric function $\varepsilon(\omega)$ separated for the electronic and lattice parts.

Fig. 6: Experimental and theoretical results for the coupled modes versus carrier concentration (from [36]).

Fig. 7: Transitions involved in resonant electronic Raman scattering are shown schematically.

Fig. 8: One-dimensional rectangular potential well and dispersion of two subbands in the parallel direction. Also shown are single-particle excitation processes.

Fig. 9: $k_{||}$-dispersion of electronic excitations in two-dimensional carrier systems.

Fig. 10: Calculated and experimental results for single-particle and collective excitations of electron accumulation layers in InP (from [23]).

Fig. 11: Bandstructure of GaAs.

Fig. 12: Raman spectra of nominally ⟨100⟩ oriented thin films of GaAs (from [32]).

Fig. 13: Frequencies of the optical phonons in $Al_xGa_{1-x}As$ (from [32]).

Fig. 14: Resonance Raman spectra of homogeneously doped n-GaAs with $n = 7 \times 10^{17} cm^{-3}$.

Fig. 15: Conduction- and valence bands in a GaAs-n-$Al_xGa_{1-x}As$ heterostructure.

Fig. 16: Raman spectra of a GaAs-n-$Al_xGa_{1-x}As$ heterostructure (from [11]).

Fig. 17: Raman spectra of a high-mobility GaAs-n-$Al_xGa_{1-x}As$ heterostructure (from [18]).

Fig. 18: Raman spectra of InP-MIS structures (from [23]).

Fig. 19: Raman spectra of a GaAs-n-$Al_xGa_{1-x}As$ quantum well structure.

Fig. 20: Raman spectra of GaAs-n-$Al_xGa_{1-x}As$ multiquantum well structures with different mobilities (from [18]).

Fig. 21: Conduction and valence bands of an excited doping superlattice.

Fig. 22: Photo-luminescence spectra of a doping superlattice (from [27]).

Fig. 23: Single-particle Raman spectra of a doping superlattice (from [27]).

Fig. 24: Collective Raman spectra of a doping superlattice (from [28]).

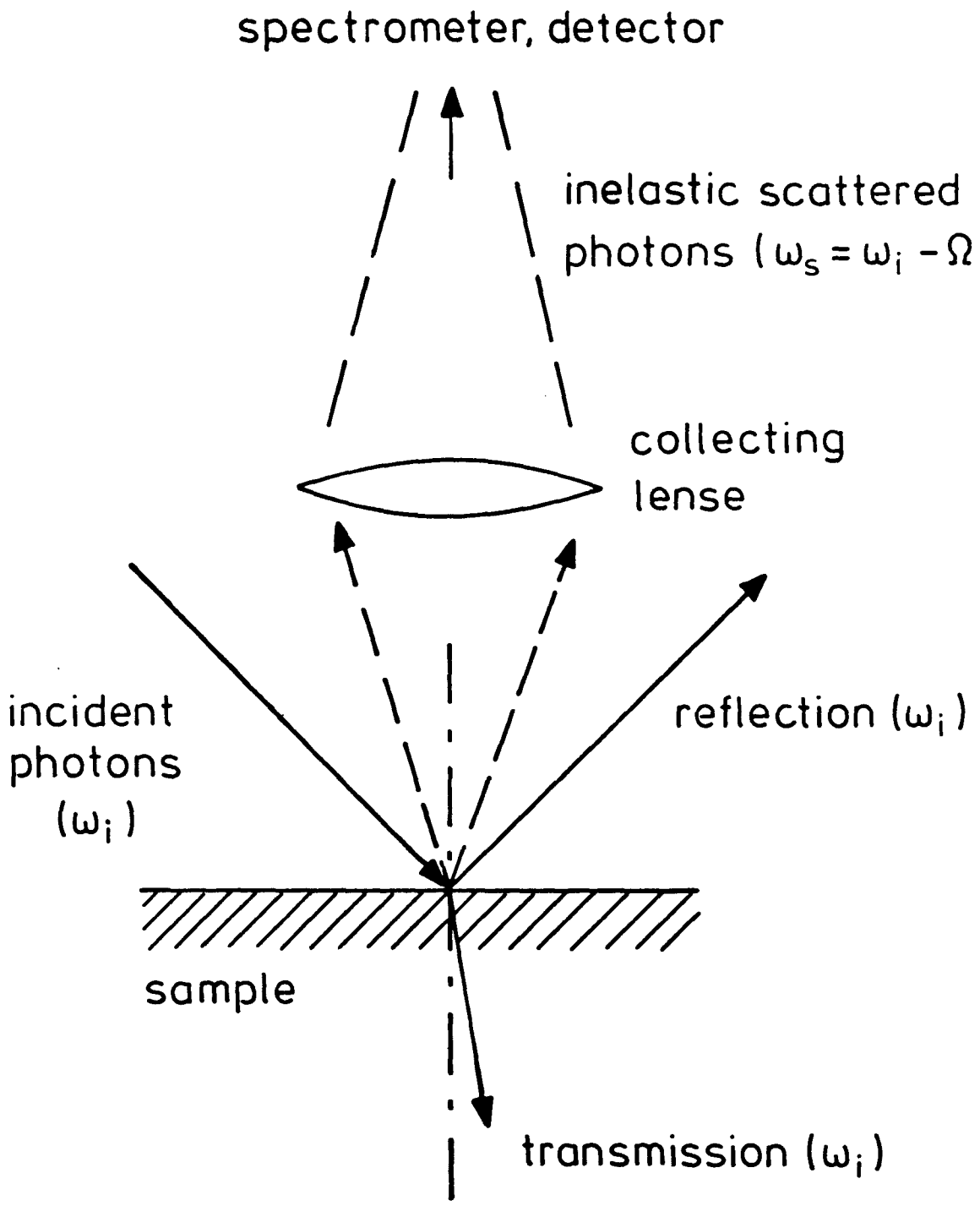
spectrometer, detector
inelastic scattered
photons ($\omega_s = \omega_i - \Omega$)
collecting
lense
incident
photons
(ω_i)
reflection (ω_i)
sample
transmission (ω_i)

Fig. 1

a.)

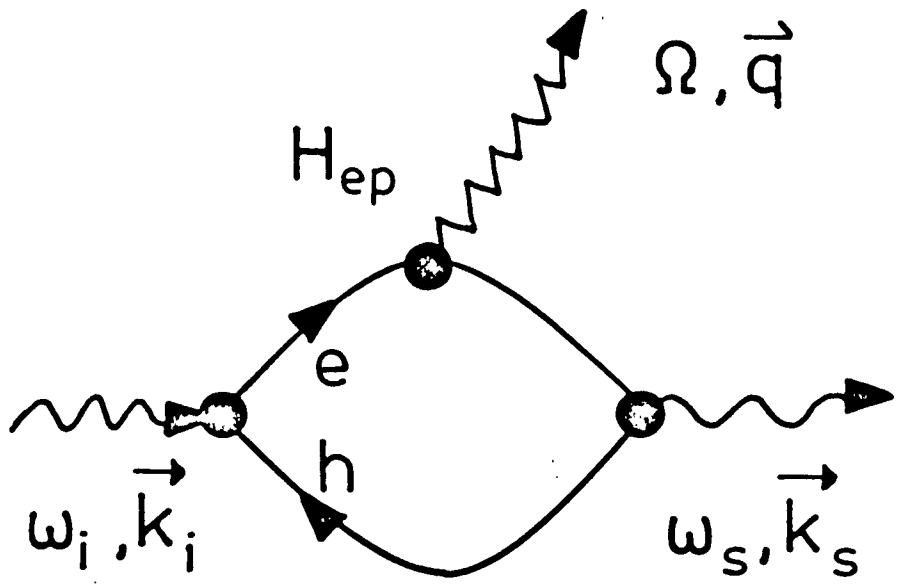

b.)

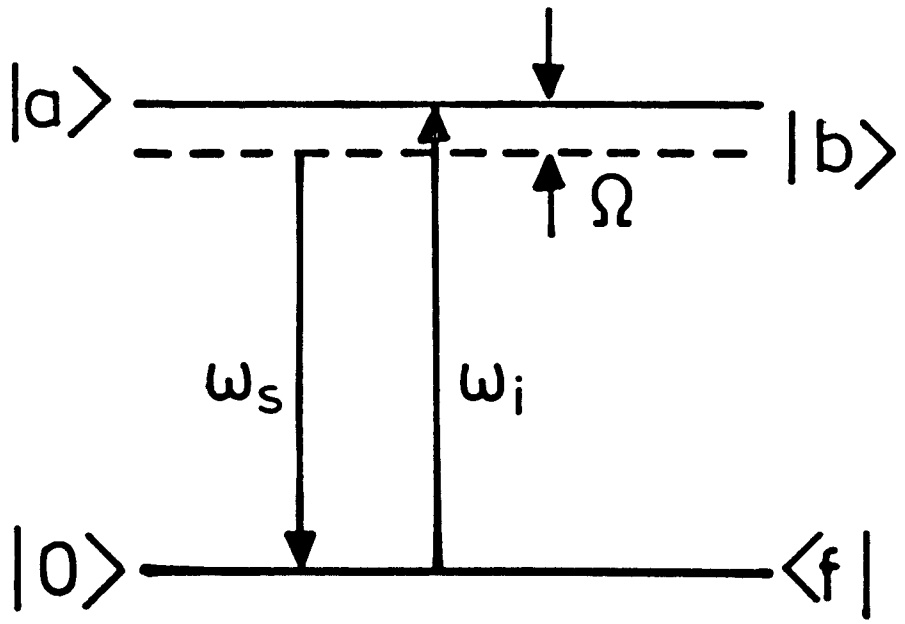

Fig. 2

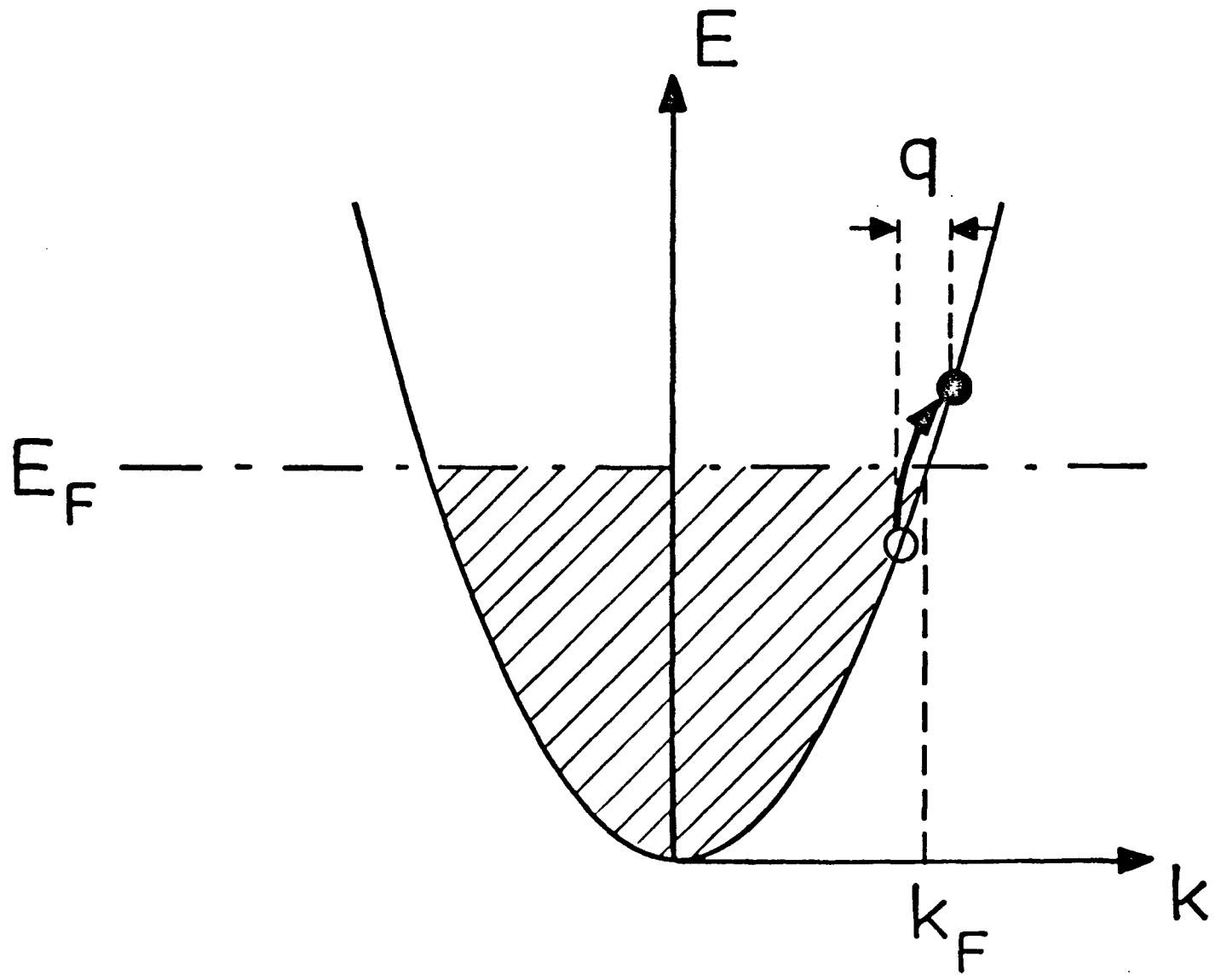

Fig. 3

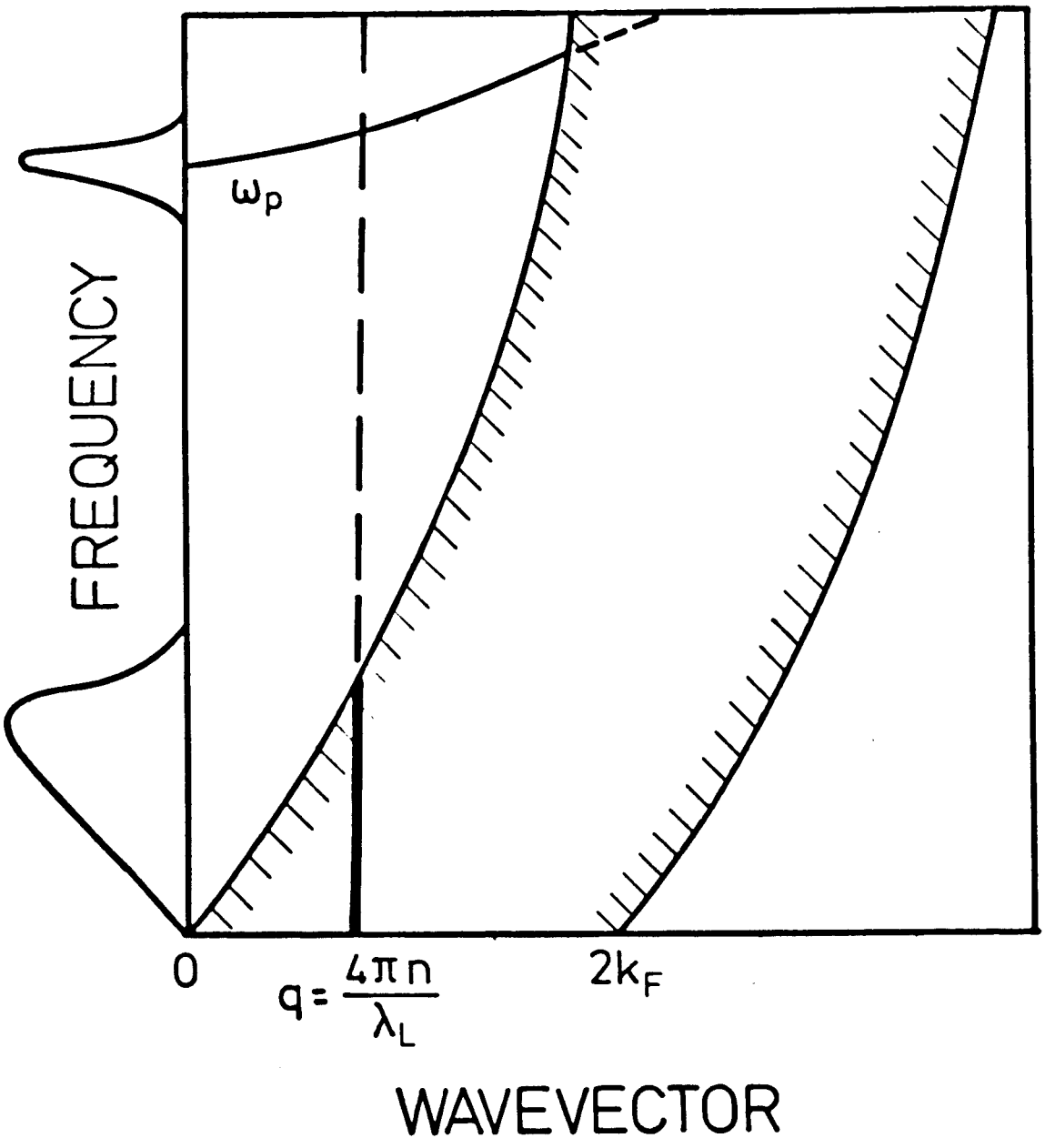

Fig. 4

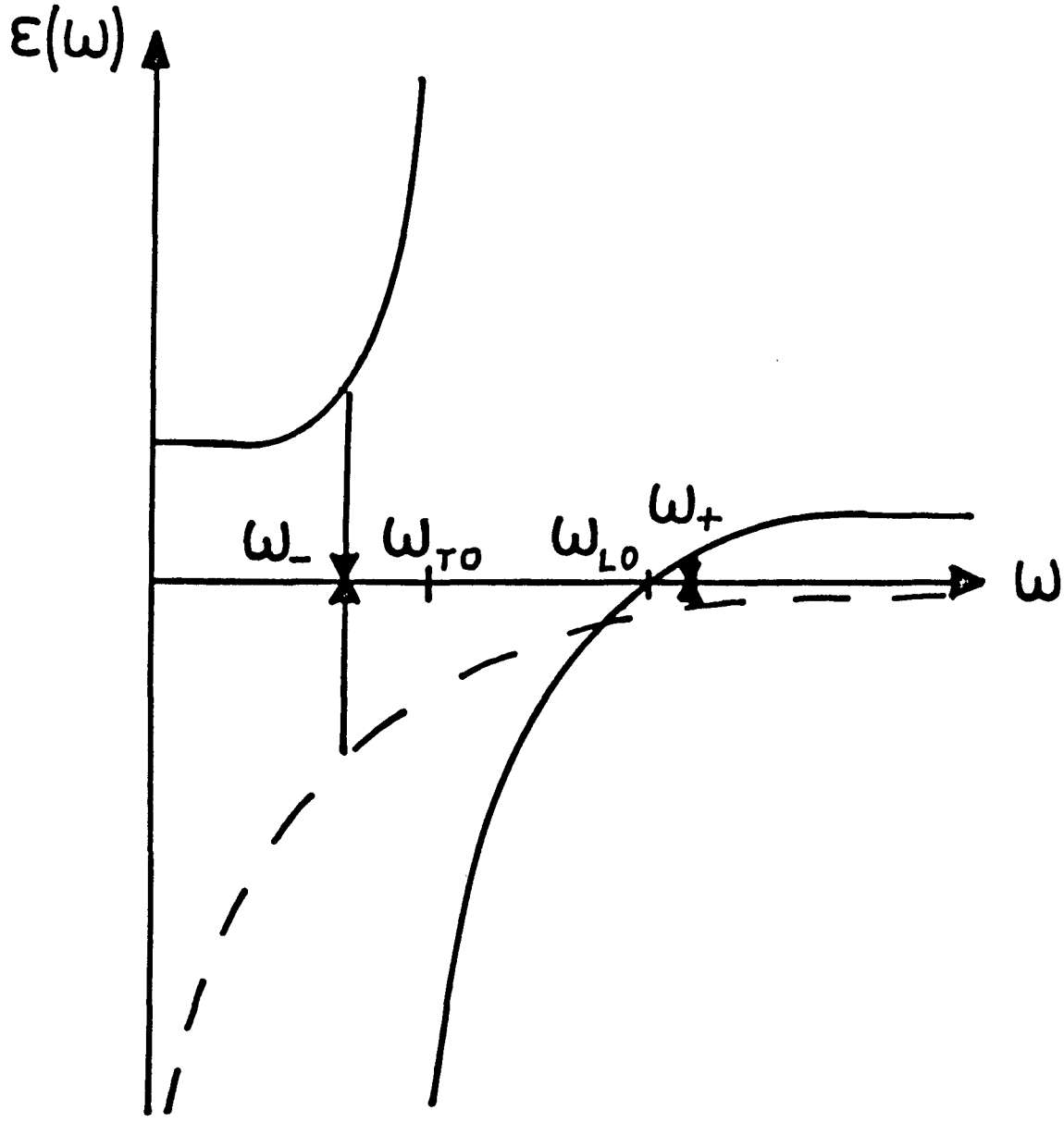

Fig.5

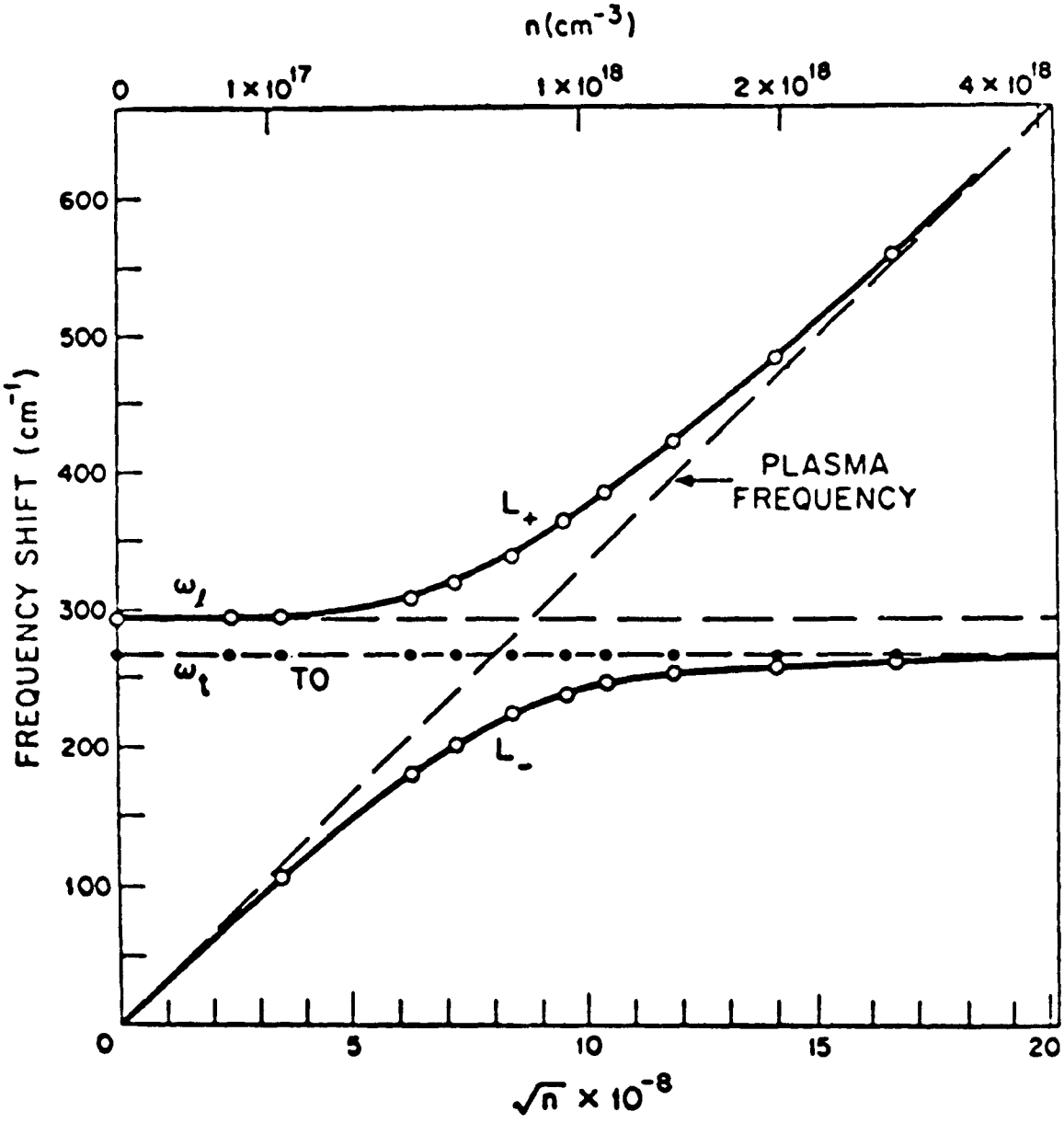
n(cm⁻³)
0
1×10¹⁷
1×10¹⁸
2×10¹⁸
4×10¹⁸
600
500
400
300
200
100
FREQUENCY SHIFT (cm⁻¹)
PLASMA
FREQUENCY
L₊
ω_l
ω_t
TO
L₋
0
5
10
15
20
√n × 10⁻⁸

Fig. 6

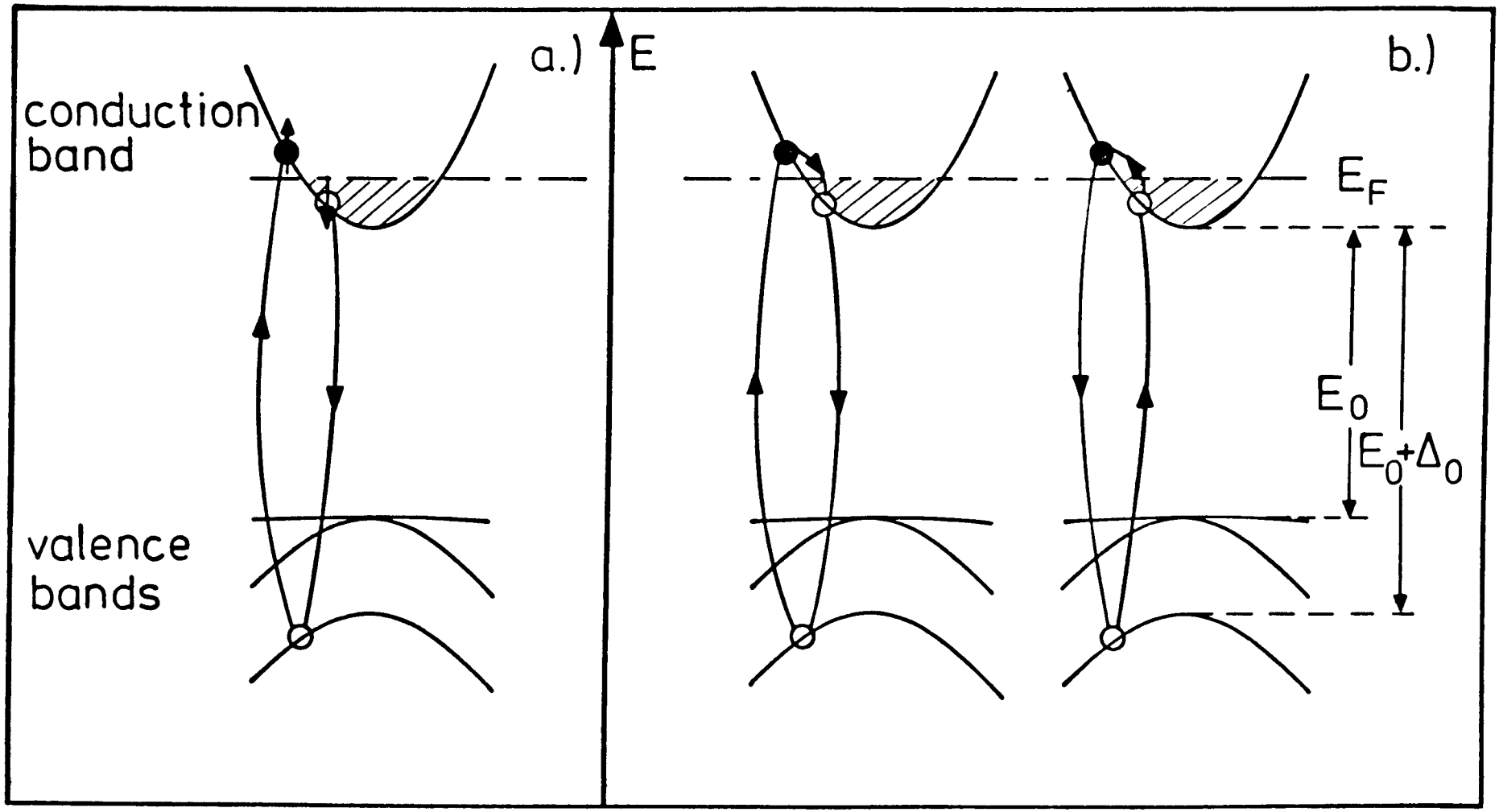

Fig. 7

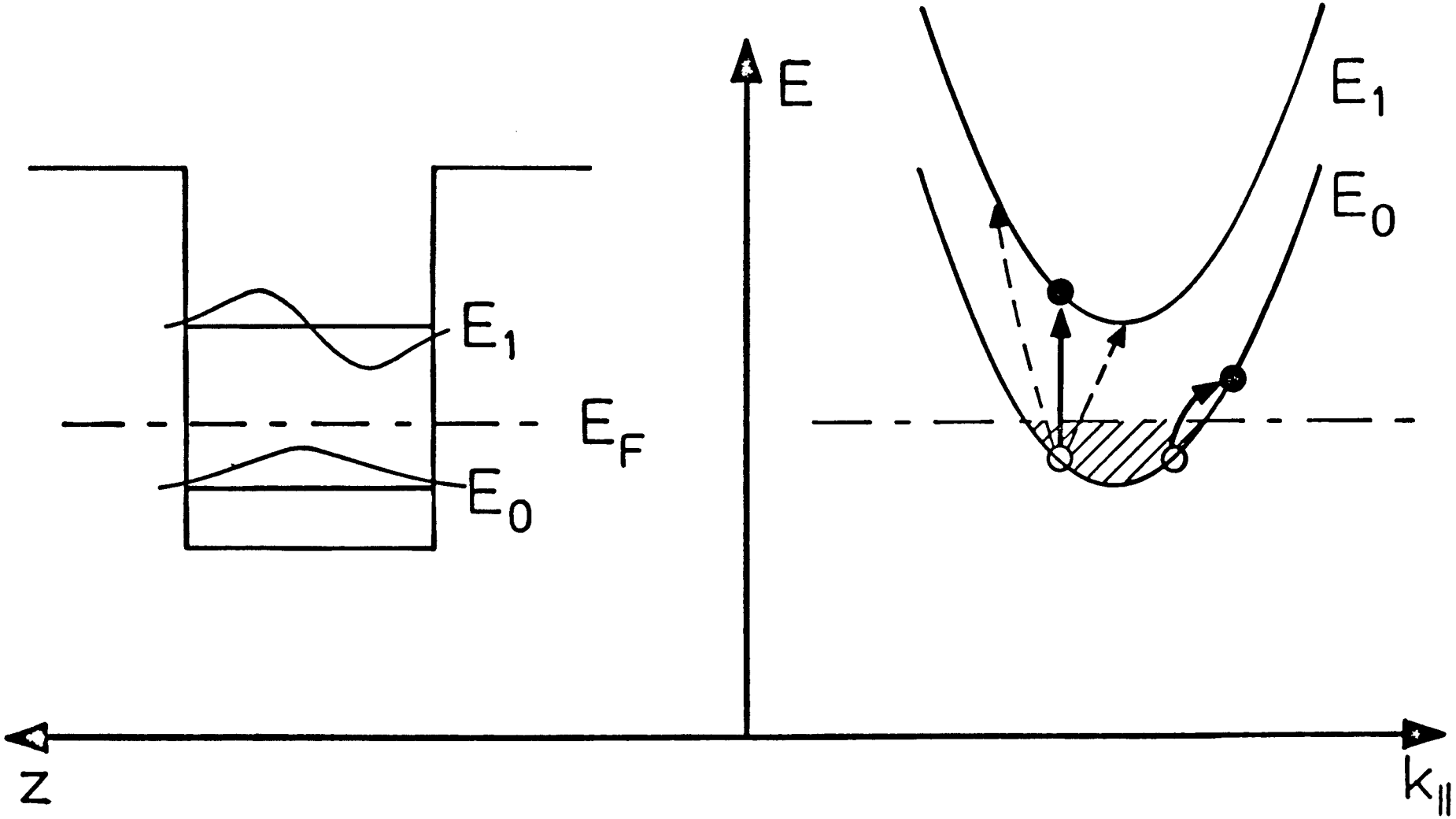

Fig. 8

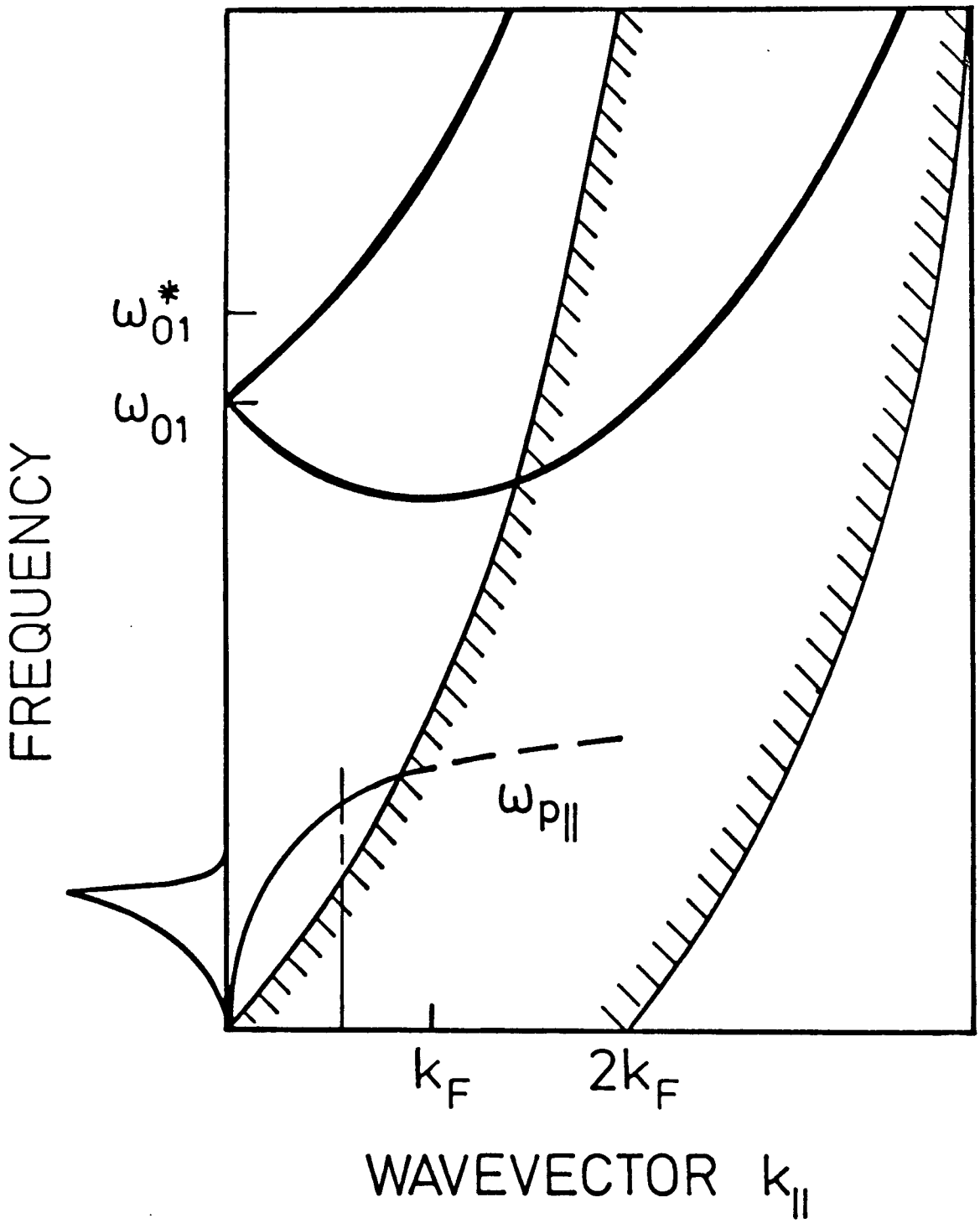
ω_{01}^{*}
ω_{01}
FREQUENCY
$\omega_{p\parallel}$
k_F
$2k_F$
WAVEVECTOR $k_\parallel$

Fig. 9

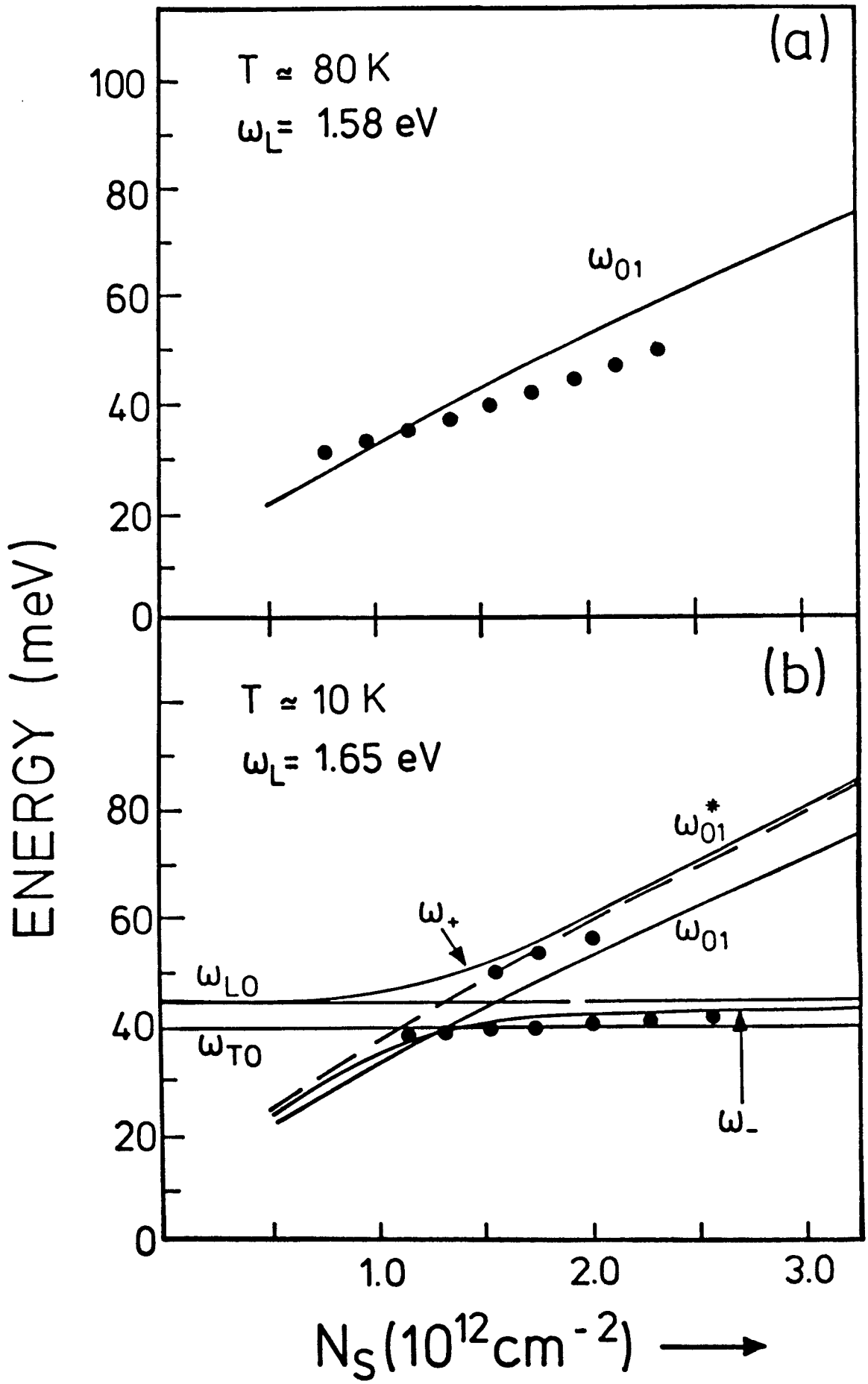
(a)
T ≃ 80 K
ω_L = 1.58 eV
ω_01
(b)
T ≃ 10 K
ω_L = 1.65 eV
ω*_01
ω_+
ω_01
ω_LO
ω_TO
ω_-
ENERGY (meV)
100
80
60
40
20
0
1.0
2.0
3.0
N_S(10^12 cm^-2) ⟶

Fig. 10

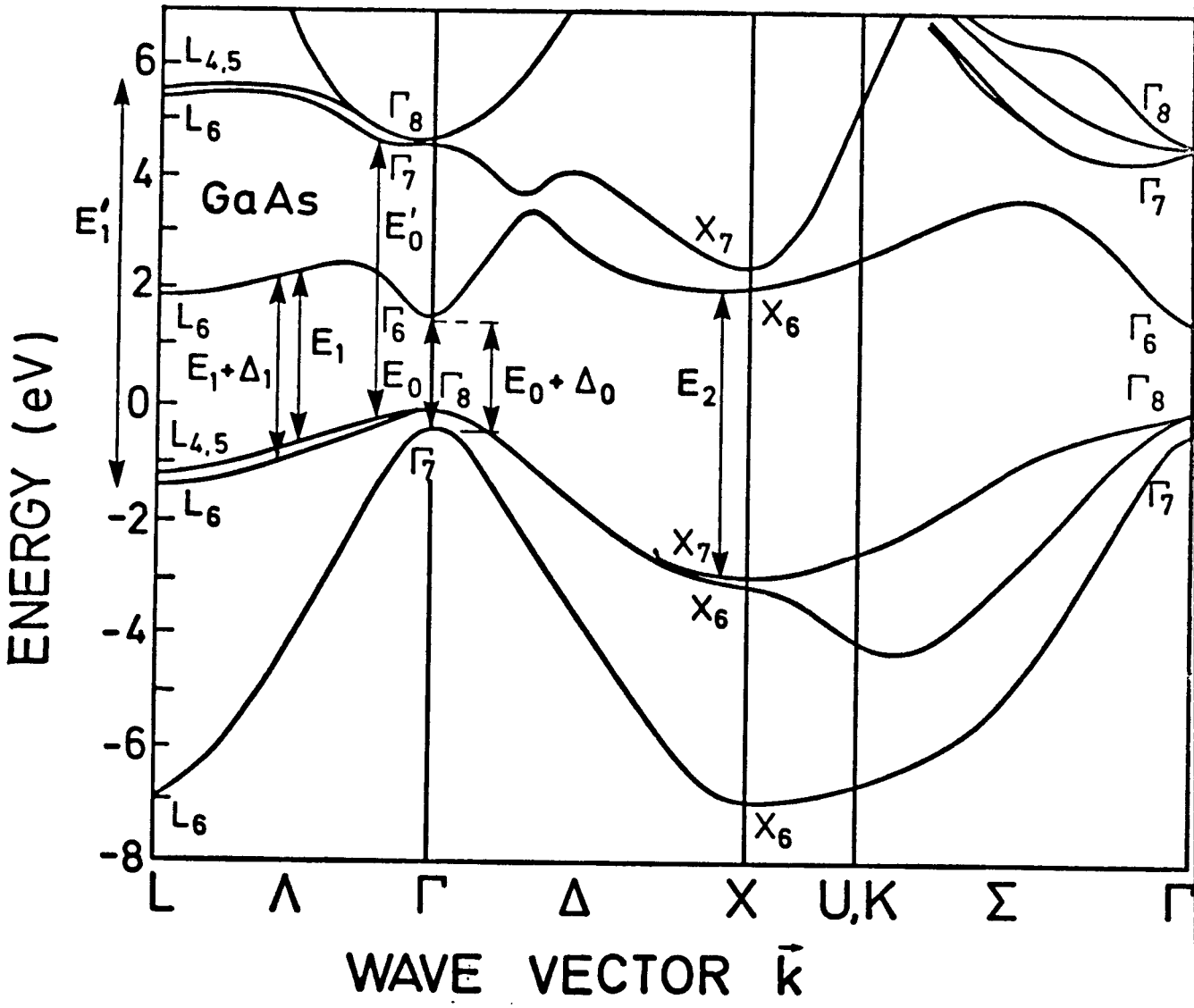
ENERGY (eV)
6
4
2
0
-2
-4
-6
-8
GaAs
$L_{4,5}$
L_6
Γ_8
Γ_7
E_1'
E_0'
E_1
$E_1+\Delta_1$
E_0
$E_0+\Delta_0$
E_2
Γ_6
X_7
X_6
L
Λ
Γ
Δ
X
U,K
Σ
Γ
WAVE VECTOR $\vec{k}$

Fig. 11

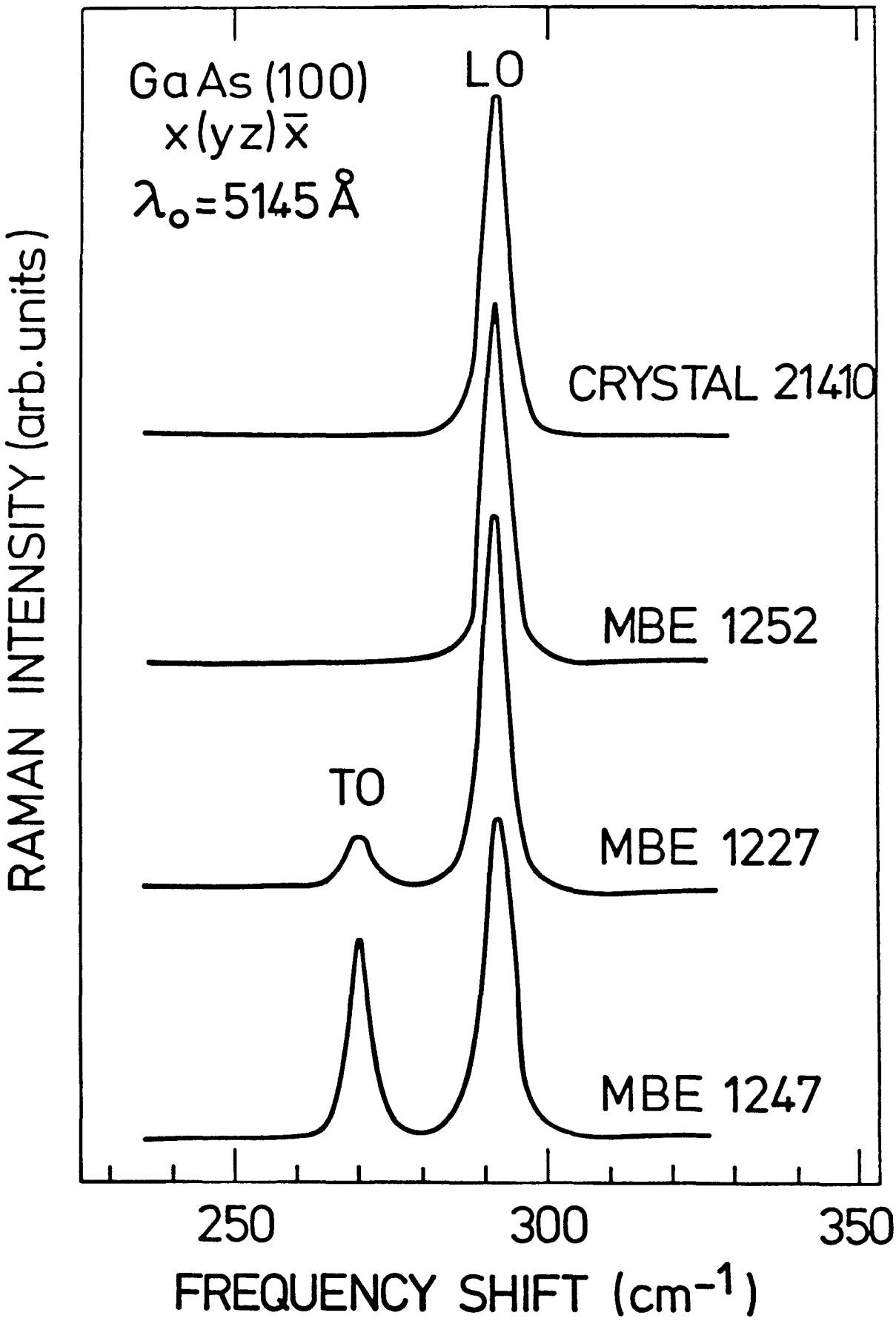
GaAs (100)
x(yz)x̄
λo=5145 Å
LO
CRYSTAL 21410
MBE 1252
TO
MBE 1227
MBE 1247
RAMAN INTENSITY (arb. units)
250
300
350
FREQUENCY SHIFT (cm⁻¹)

Fig. 12

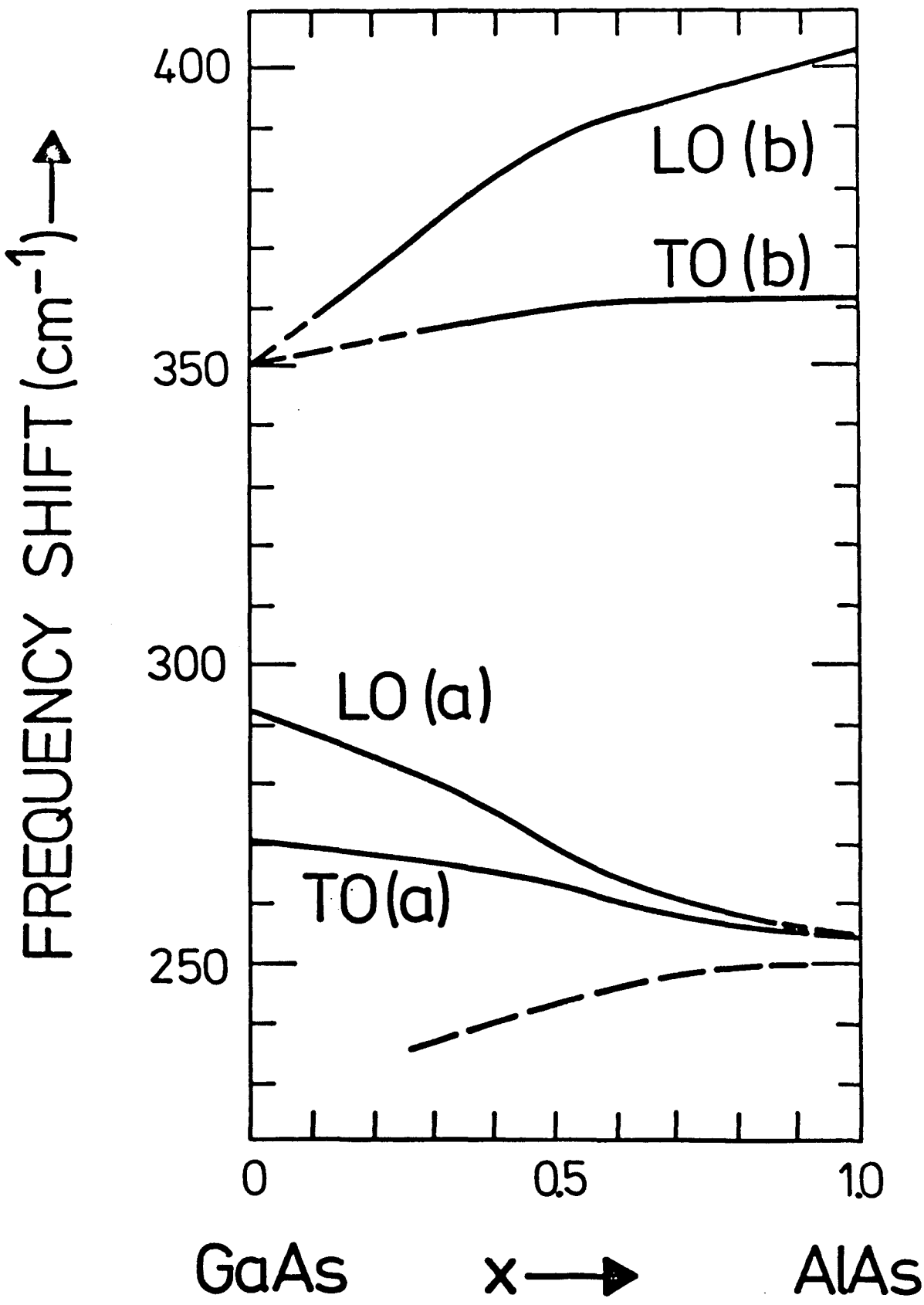
400
350
300
250
FREQUENCY SHIFT (cm^{-1}) ⟶
LO (b)
TO (b)
LO (a)
TO (a)
0
0.5
1.0
GaAs
x ⟶
AlAs

Fig. 13

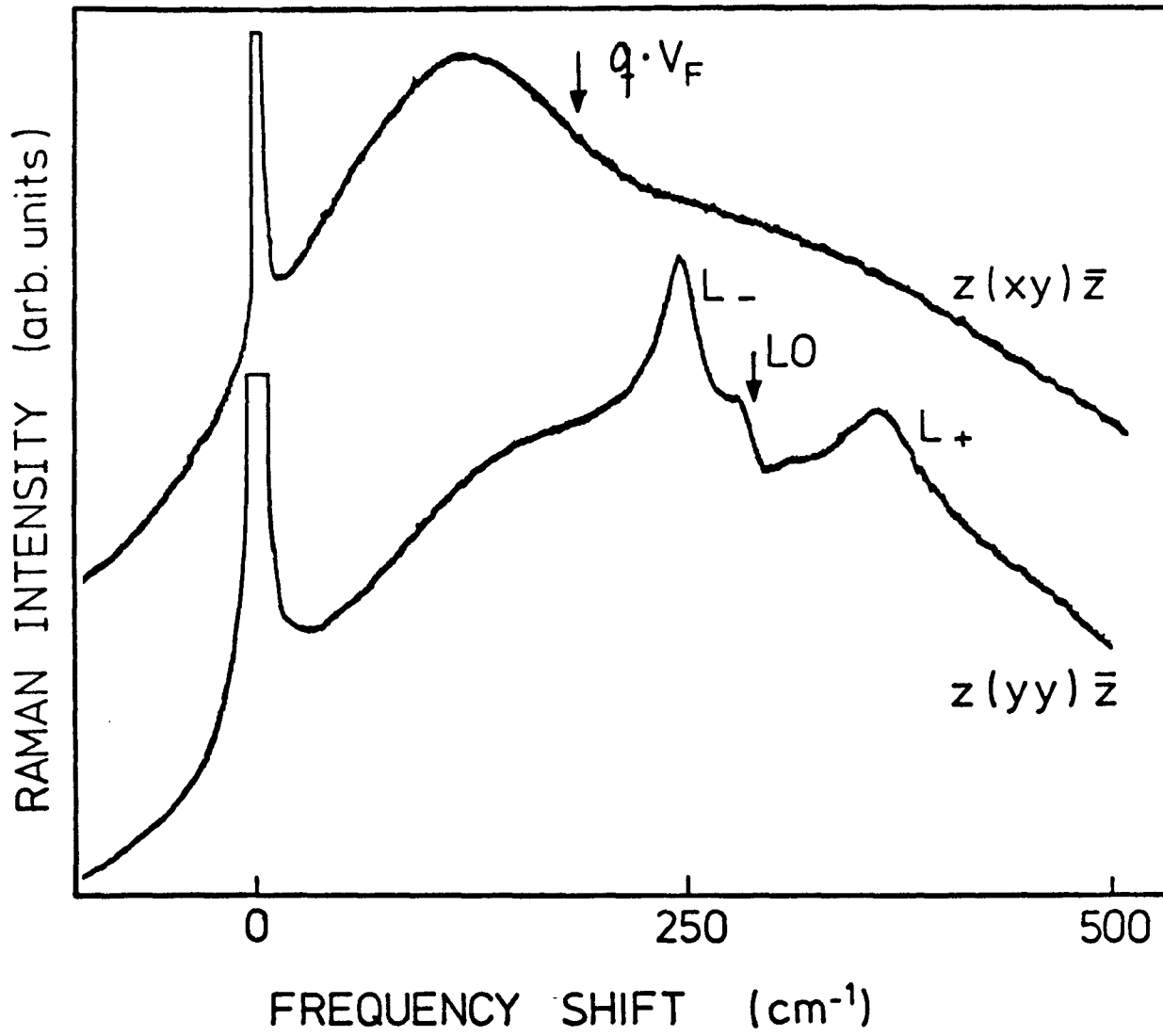
RAMAN INTENSITY (arb. units)
$q \cdot V_F$
L -
LO
L +
z(xy)z̄
z(yy)z̄
0
250
500
FREQUENCY SHIFT (cm^{-1})

Fig. 14

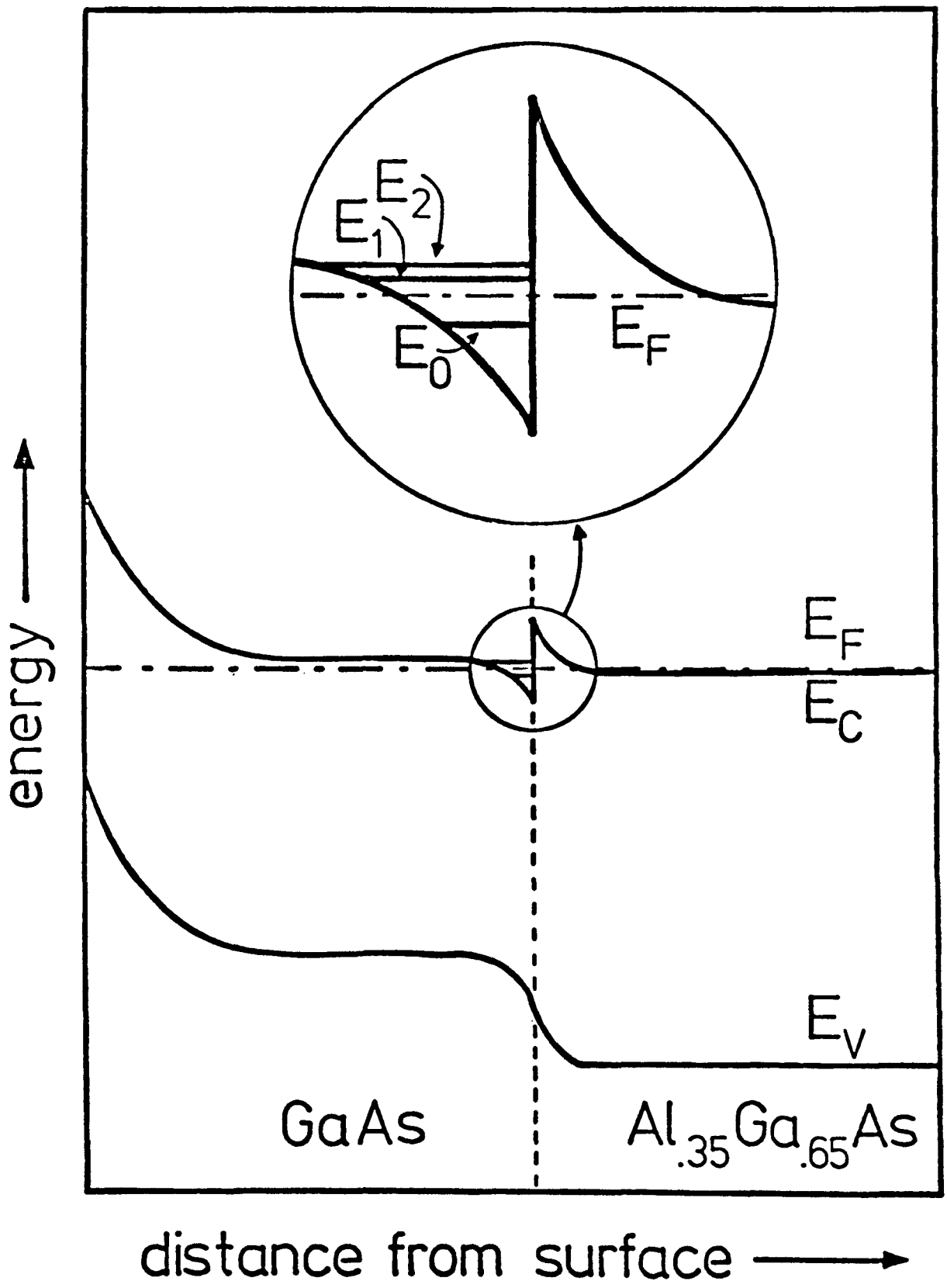
E2
E1
E0
EF
EF
EC
EV
energy
GaAs
Al.35Ga.65As
distance from surface

Fig. 15

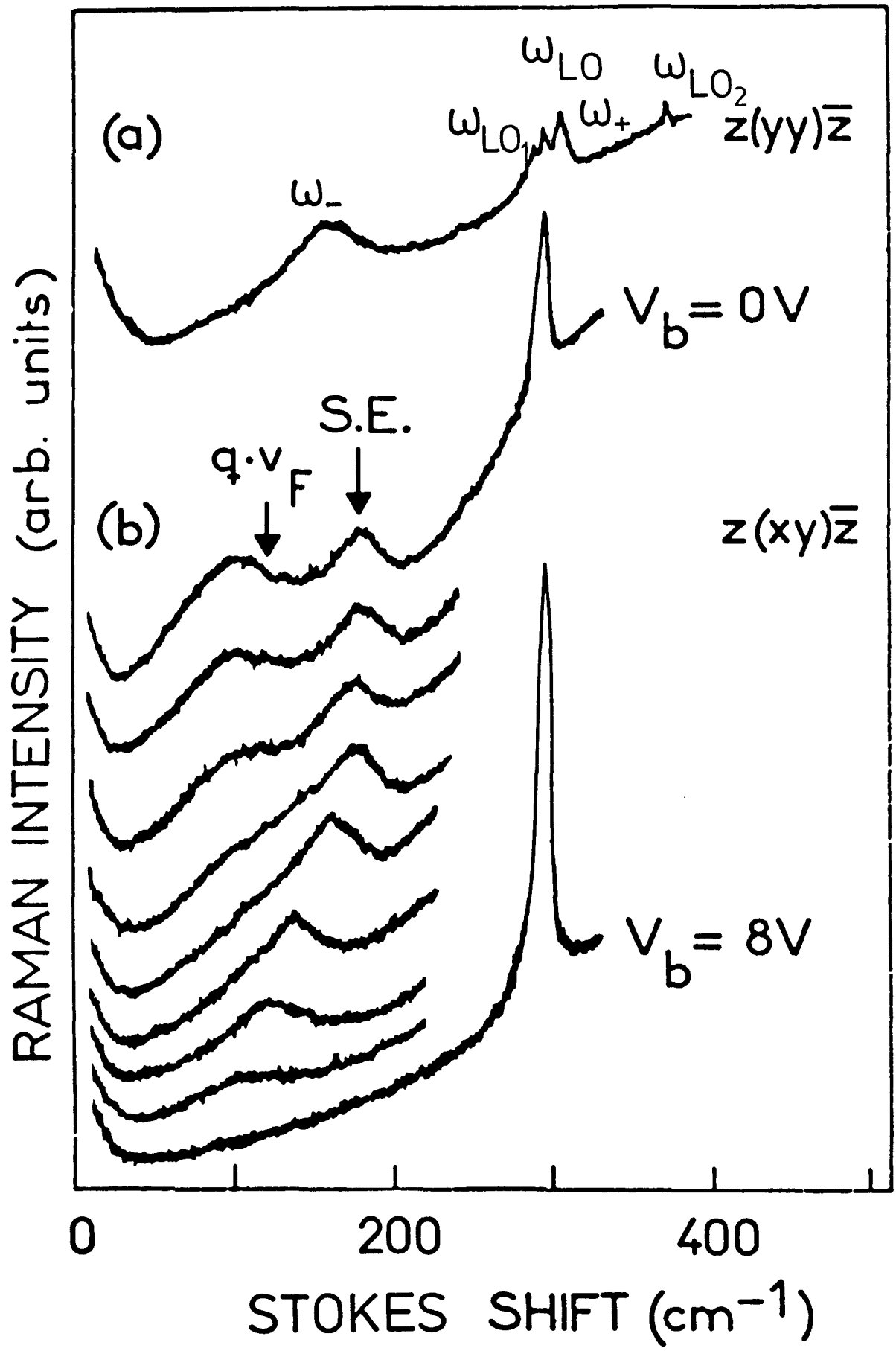
(a)
ω_{LO}
ω_{LO_2}
ω_{LO_1}
ω_+
z(yy)z̄
ω_-
V_b= 0V
S.E.
$q \cdot v_F$
(b)
z(xy)z̄
V_b= 8V
RAMAN INTENSITY (arb. units)
0
200
400
STOKES SHIFT (cm^{-1})

Fig. 16

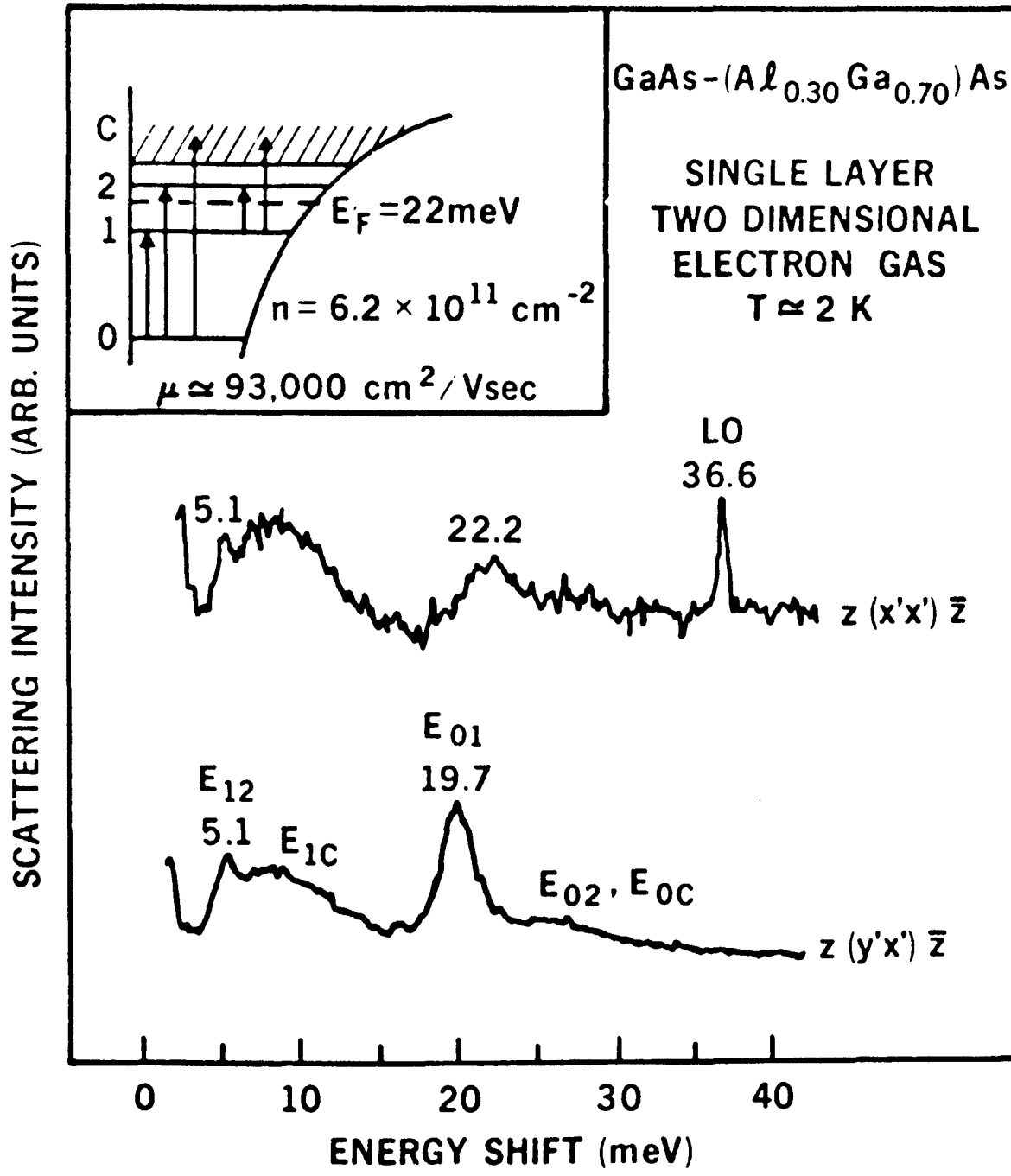
GaAs-(Aℓ0.30 Ga0.70) As
SINGLE LAYER
TWO DIMENSIONAL
ELECTRON GAS
T ≃ 2 K
C
2
1
0
E_F = 22meV
n = 6.2 × 10^11 cm^-2
μ ≃ 93,000 cm^2/Vsec
LO
36.6
5.1
22.2
z (x'x') z̄
E01
19.7
E12
5.1
E1C
E02, E0C
z (y'x') z̄
SCATTERING INTENSITY (ARB. UNITS)
0
10
20
30
40
ENERGY SHIFT (meV)

Fig. 17

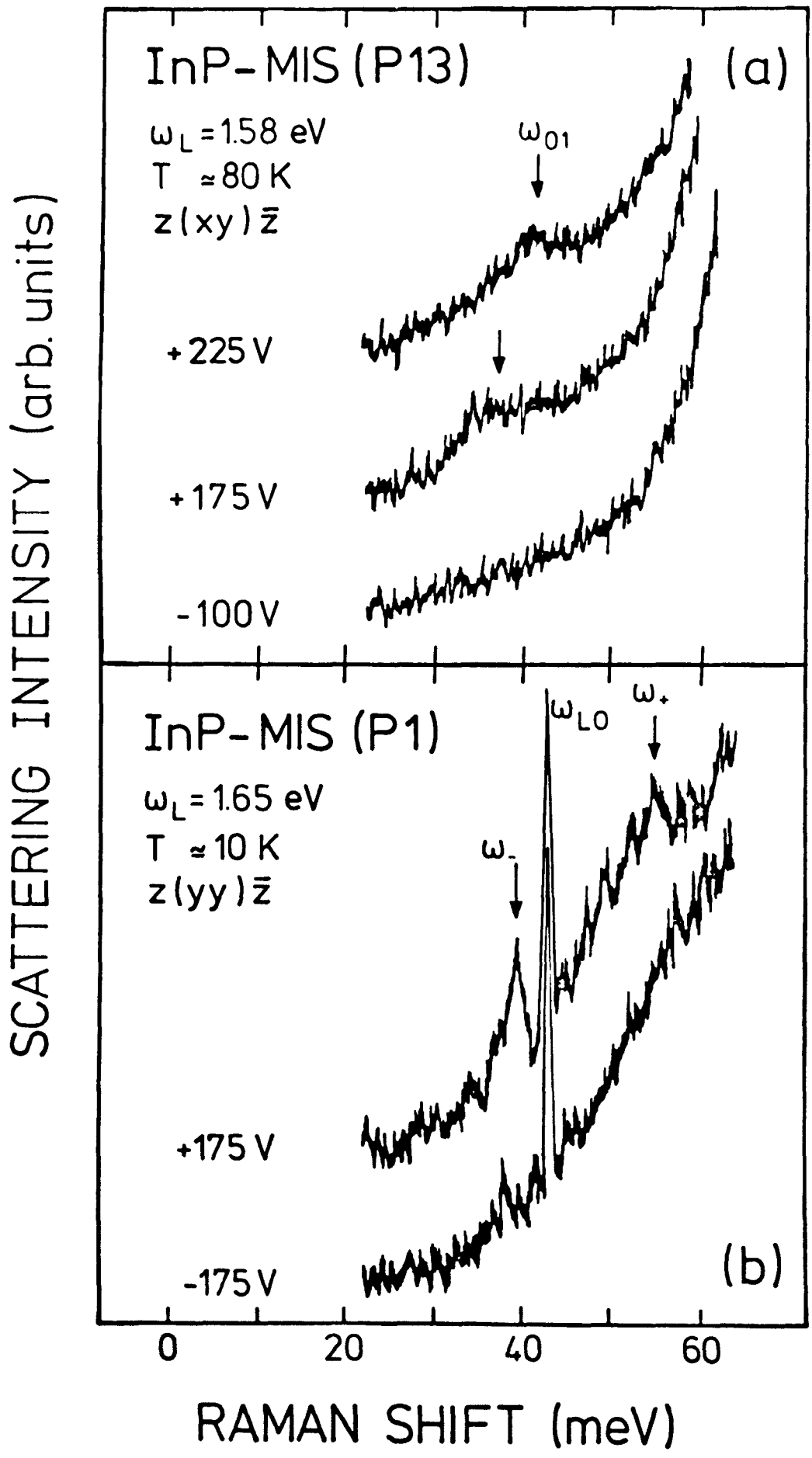
InP-MIS (P13)
(a)
ω_L = 1.58 eV
T ≈ 80 K
z(xy)z̄
ω_{01}
+225 V
+175 V
-100 V
InP-MIS (P1)
ω_L = 1.65 eV
T ≈ 10 K
z(yy)z̄
ω_{LO}
ω_+
ω_-
+175 V
-175 V
(b)
SCATTERING INTENSITY (arb. units)
0
20
40
60
RAMAN SHIFT (meV)

Fig. 18

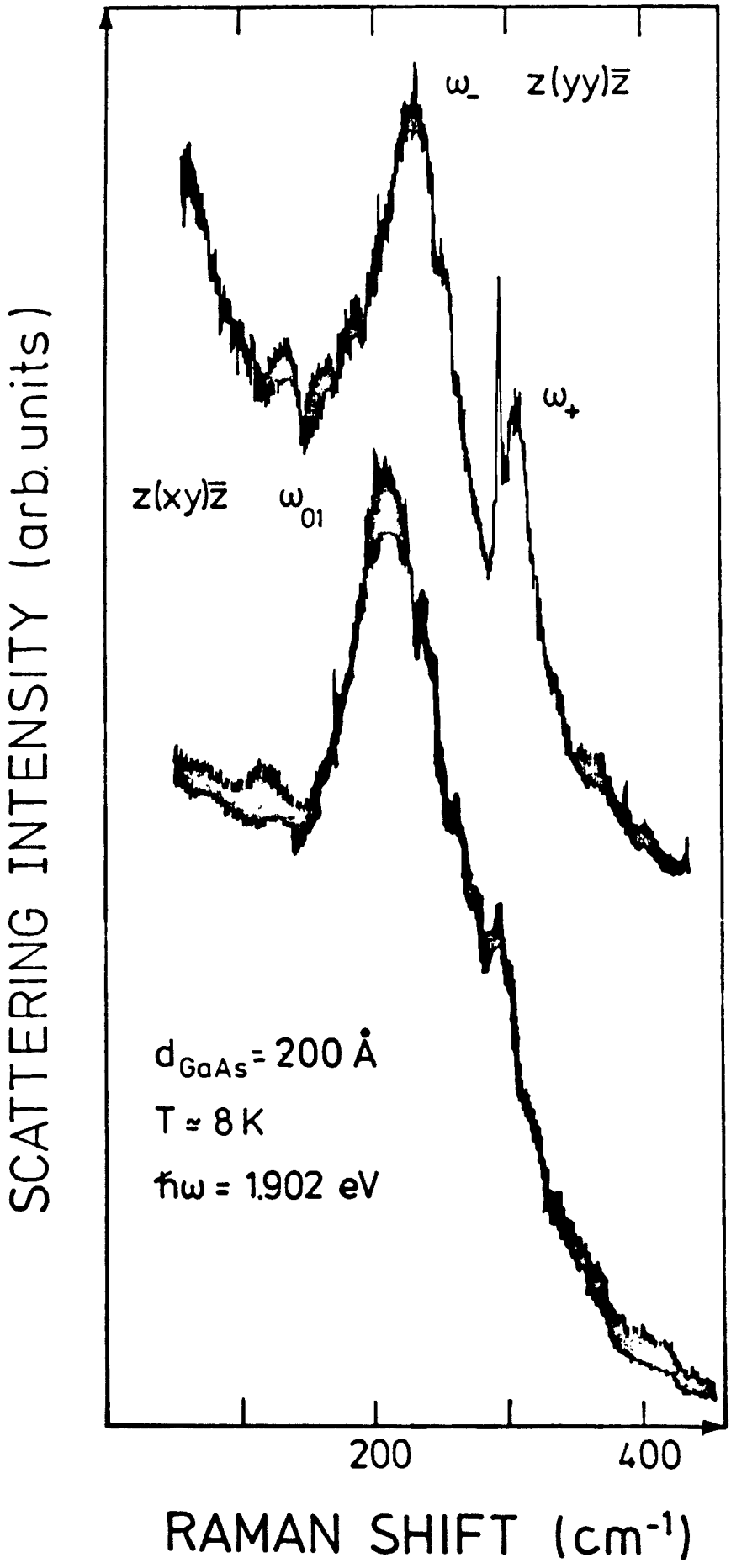
ω_ z(yy)z̄
ω+
z(xy)z̄ ω01
dGaAs = 200 Å
T ≈ 8 K
ħω = 1.902 eV
SCATTERING INTENSITY (arb. units)
200
400
RAMAN SHIFT (cm-1)

Fig. 19

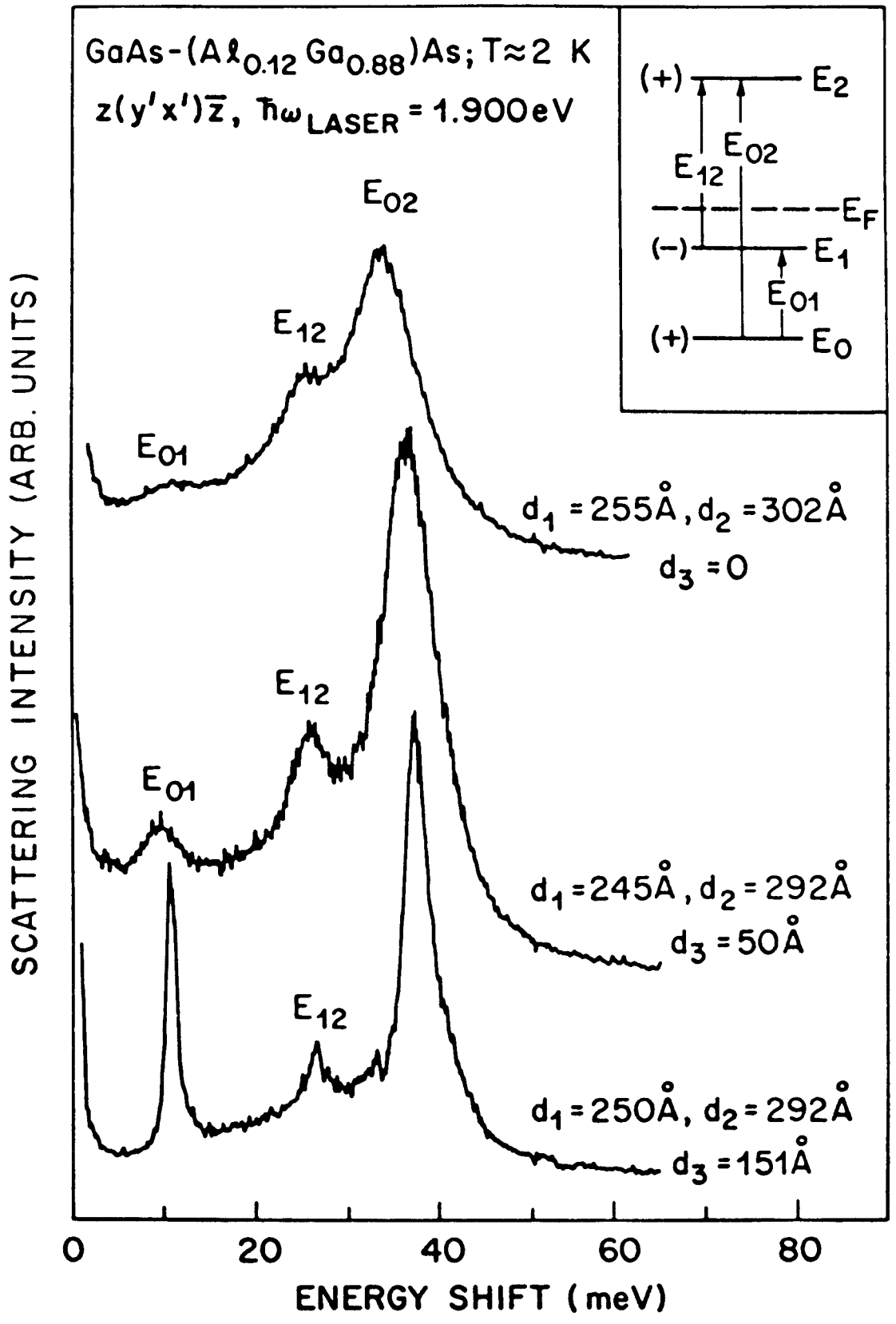
GaAs-(Al0.12 Ga0.88)As; T≈2 K
z(y'x')z̄, ħω LASER = 1.900eV
(+)
E2
E02
E12
EF
(−)
E1
E01
(+)
E0
E02
E12
E01
d1 = 255Å, d2 = 302Å
d3 = 0
E12
E01
d1 = 245Å, d2 = 292Å
d3 = 50Å
E12
d1 = 250Å, d2 = 292Å
d3 = 151Å
SCATTERING INTENSITY (ARB. UNITS)
0
20
40
60
80
ENERGY SHIFT (meV)

Fig. 20

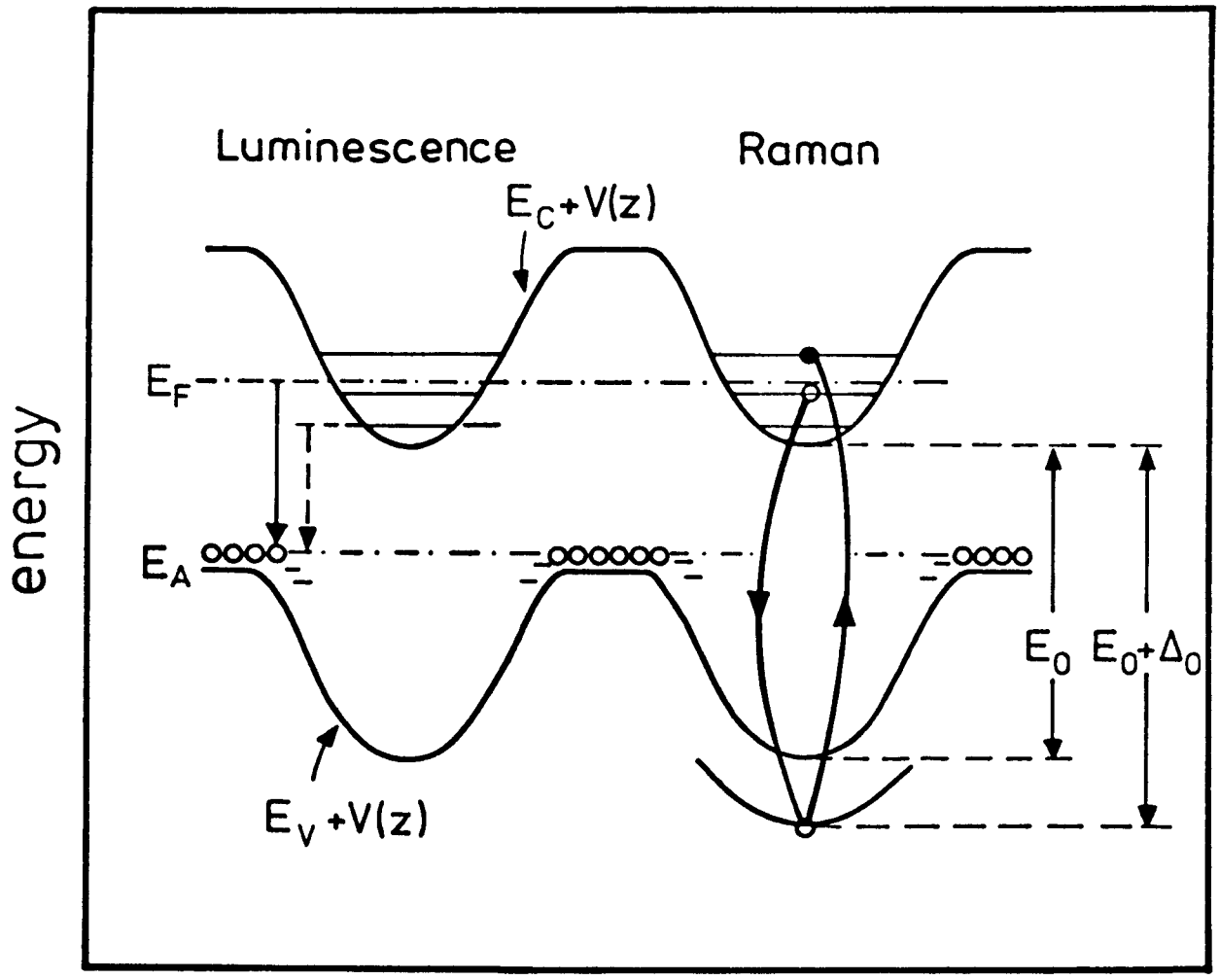
Luminescence
Raman
$E_C+V(z)$
E_F
E_A
$E_V+V(z)$
E_0
$E_0+\Delta_0$
energy
direction of periodicity z

Fig. 21

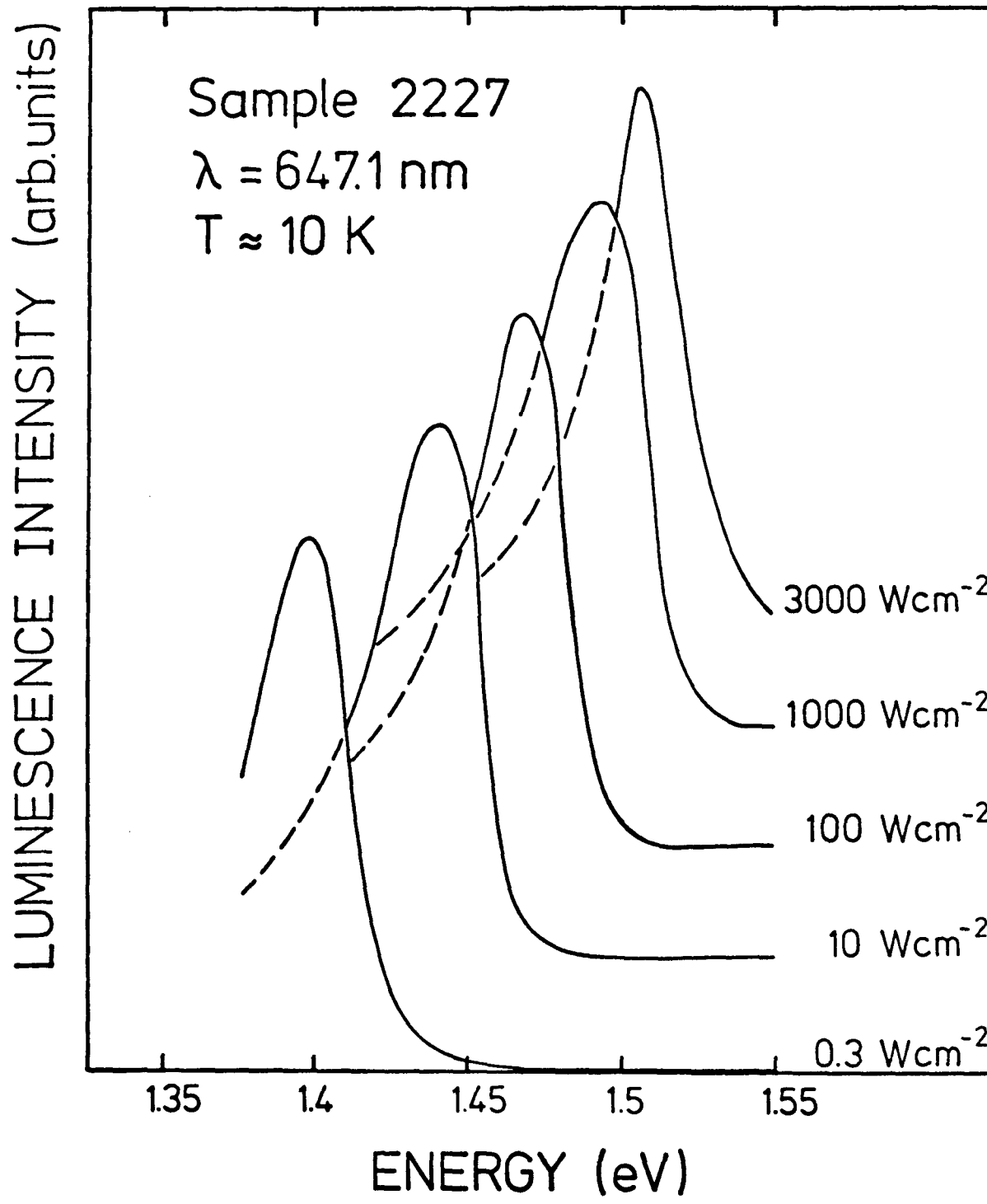
Sample 2227
λ = 647.1 nm
T ≈ 10 K
LUMINESCENCE INTENSITY (arb.units)
3000 Wcm-2
1000 Wcm-2
100 Wcm-2
10 Wcm-2
0.3 Wcm-2
1.35
1.4
1.45
1.5
1.55
ENERGY (eV)

Fig.22

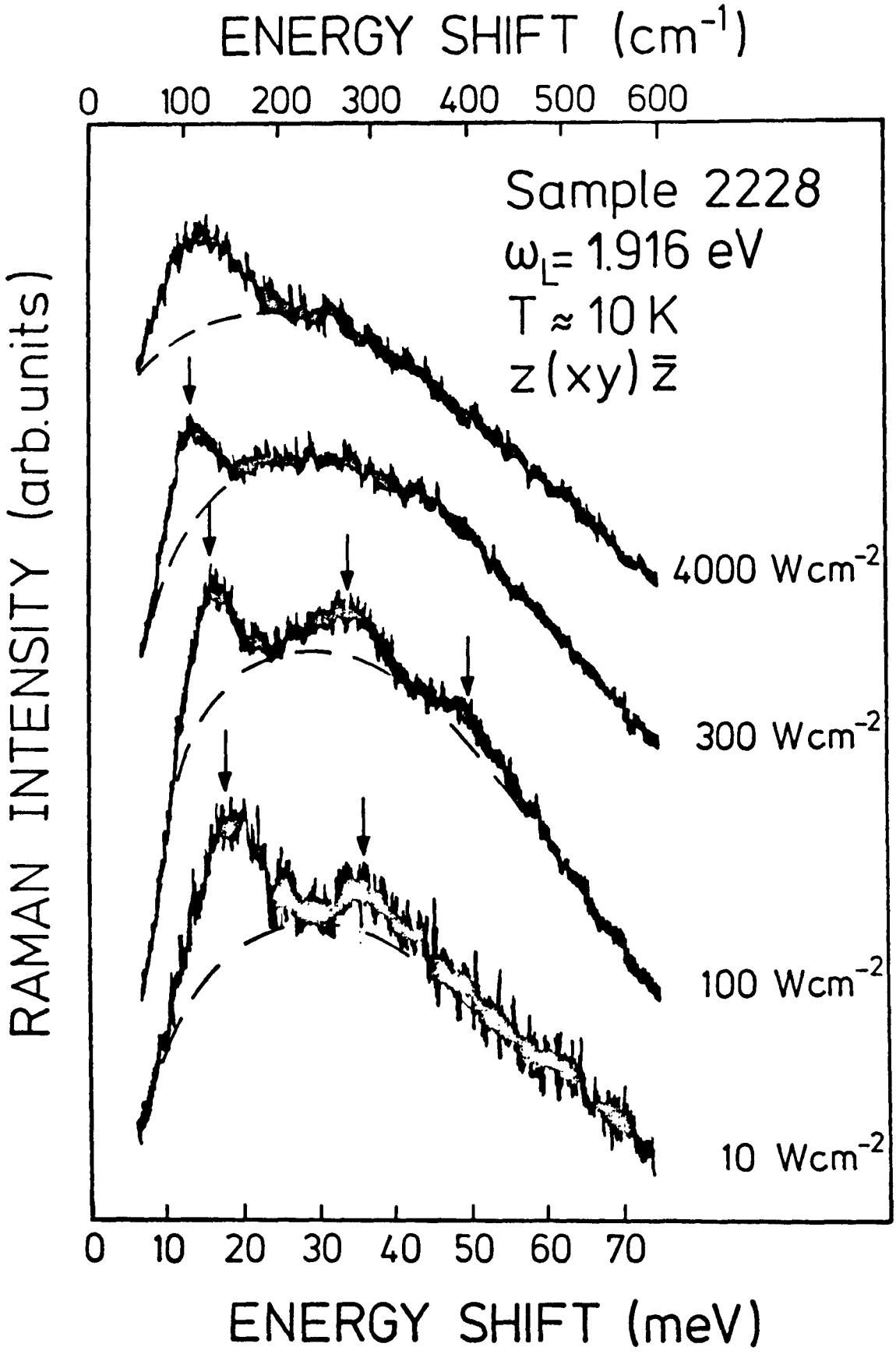
ENERGY SHIFT (cm^{-1})
0 100 200 300 400 500 600
Sample 2228
ω_L= 1.916 eV
T ≈ 10 K
z(xy)z̄
4000 Wcm^{-2}
300 Wcm^{-2}
100 Wcm^{-2}
10 Wcm^{-2}
RAMAN INTENSITY (arb.units)
0 10 20 30 40 50 60 70
ENERGY SHIFT (meV)

Fig. 23

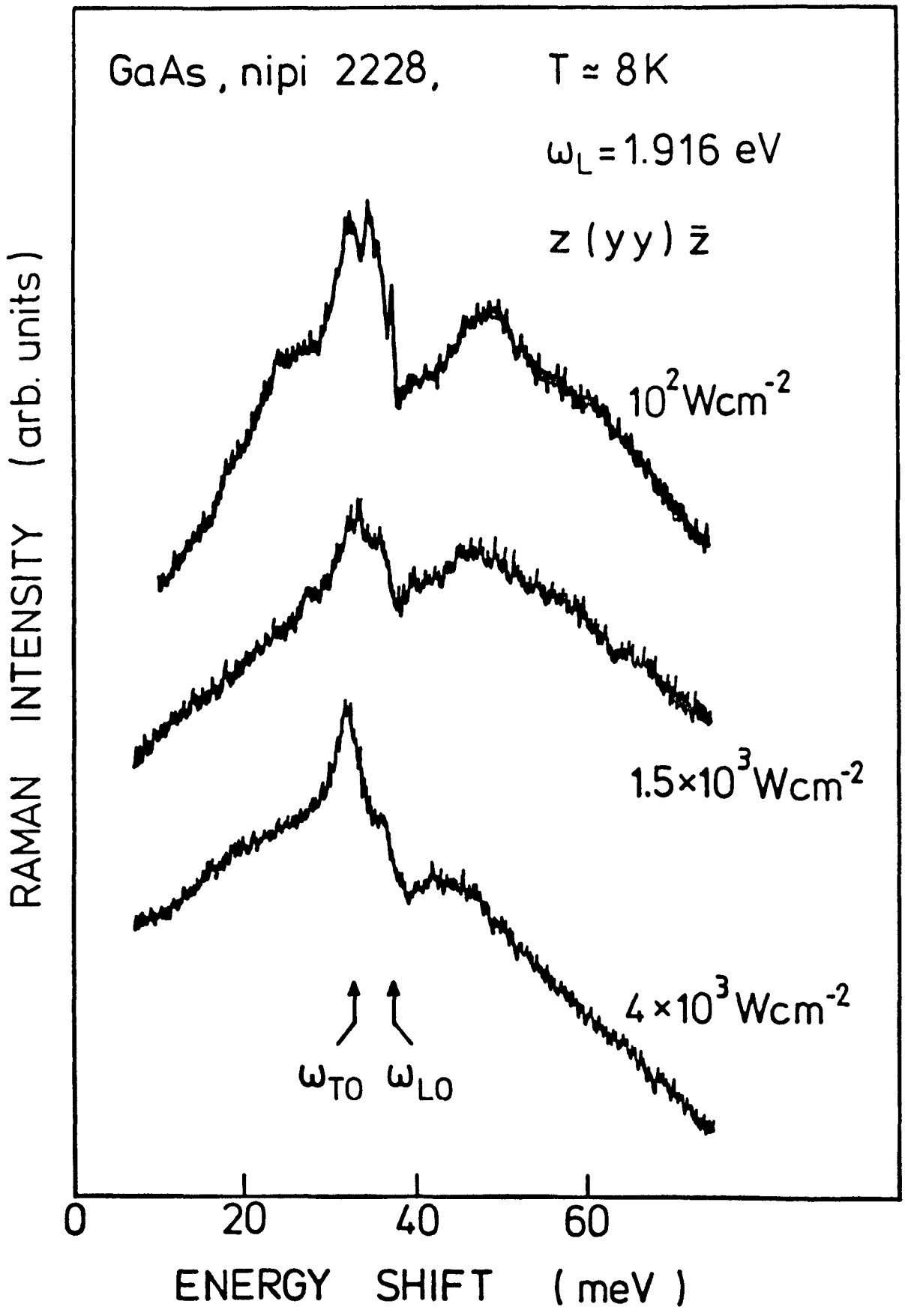
GaAs , nipi 2228,
T ≈ 8K
ω_L = 1.916 eV
z (y y) z̄
10^2 Wcm^-2
1.5×10^3 Wcm^-2
4×10^3 Wcm^-2
ω_TO ω_LO
RAMAN INTENSITY (arb. units)
0
20
40
60
ENERGY SHIFT (meV)

Fig. 24

ANHANG (1 - 12)

Appl. Phys. 16, 345–352 (1978)

Applied Physics

Raman Spectroscopy—A Versatile Tool for Characterization of Thin Films and Heterostructures of GaAs and $Al_xGa_{1-x}As$

G. Abstreiter, E. Bauser, A. Fischer,* and *K. Ploog*
Max-Planck-Institut für Festkörperforschung, D-7000 Stuttgart 80, Fed. Rep. Germany

Received 10 March 1978/Accepted 14 April 1978

Abstract. It is shown that Raman spectroscopy can provide useful information on characteristic properties of thin crystalline films of compound semiconductors. Crystal orientation, carrier concentration, scattering times of charge carriers, composition of mixed crystals and depth profiles can be studied in thin layers and heterostructures of GaAs and $Al_xGa_{1-x}As$. The advantages and disadvantages of Raman scattering compared to conventional characterization methods are discussed.

PACS: 78.30-j, 68.55+b

Thin crystalline films and heterostructures of compound semiconductors become more and more important for devices and device technology. A precise control over thickness and doping profiles of multilayer systems is necessary to achieve, for example, high quality microwave diodes or optoelectronic devices. Liquid phase epitaxy (LPE) [1] and molecular beam epitaxy (MBE) [2–4] are two methods which are used to grow such heterostructures.

Especially MBE has been developped during the past ten years in a way that nowadays one is able to control the uniformity, thickness, doping profiles and composition of thin crystalline layers ($\lesssim 100$ Å) over the whole surface of a given substrate. The relatively low growth temperature, the possibility of abruptly changing the composition, and the low growth rate make MBE a versatile technique for growing heterostructures and superlattices with alternating layers of, for example, GaAs and $Al_xGa_{1-x}As$. The thickness of the individual layers can be kept as thin as a few monolayers [5].

In order to learn something about the growth mechanisms and the characteristic properties of such thin crystalline films, many different characterization methods are employed. The MBE provides the possibility of in situ characterization of the growing and grown layers by means of, for example, reflection high energy electron diffraction (RHEED), secondary ion mass spectroscopy (SIMS) and Auger electron spectroscopy (AES) [4][1]. Many of the characteristic properties and the quality of the layer structures have to be checked and studied after growth outside the growing apparatus. Transport and magnetotransport measurements lead to information on carrier concentration, mobility and sometimes also effective masses of the carriers. But often it is not possible to separate the properties of individual layers from each other and from the substrate. Completely different information can be drawn from x-ray diffraction and electron microscopy work. Here one learns something about crystal structure, orientation, and quality. Optical methods like reflection, transmission, and luminescence experiments are employed to characterize single and multiple layers, to learn about recombination mechanisms and the role of interfaces on these mechanisms. In the case of superlattices, most of these measurements show characteristic features because of zone folding effects [5–7].

In this paper we want to show that Raman scattering experiments give additional, new and sometimes more detailed information on the properties and qualities of thin crystalline films and multilayers of GaAs and

* Present address: Max-Planck-Institut für Festkörperforschung, Hochfeld-Magnetlabor Grenoble, F-38042 Grenoble, 166 X Grenoble-Cédex, Avenue des Martyrs (C.N.R.S.).

[1] For comprehensive review of the methods see [22].

0340-3793/78/0016/0345/$01.60

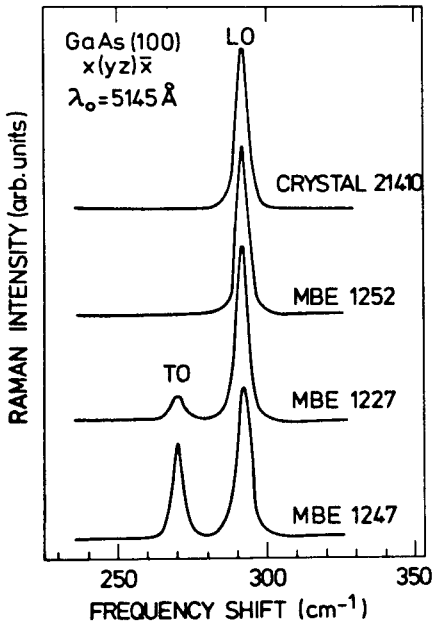

Fig. 1. Examples of Raman spectra obtained in backscattering geometry from a polished and etched (100) surface of GaAs and thin films of GaAs grown with MBE on (100) substrates. In this geometry only scattering by LO phonons is allowed. Some of the MBE grown samples show also a strong TO mode

$Al_xGa_{1-x}As$. There are two main reasons why Raman scattering is a useful tool in sample characterization and that one can learn something, where other methods fail often. First, the lattice vibrational spectra of different layers are observed as a superposition of the spectra of each layer. So it is possible to study individual layers in a nondestructive way by using different laser excitation lines with different penetration depths. The second important point is that lattice vibrations are very sensitive to the nearest neighbourhood and therefore probe the crystal structure and quality on an extremely small scale, a scale which is of the order of the lattice spacing.

In the following sections we describe various properties of thin layers which can be studied by Raman spectroscopy. Examples are shown for GaAs and $Al_xGa_{1-x}As$ crystals. At the beginning we want to mention a few experimental details.

1. Experimental Aspects

Because all of our Raman scattering experiments are performed with incident laser light in the frequency range where GaAs is opaque, we use backscattering geometry. The wavevector of the excited phonon is therefore perpendicular to the sample surface. The laser beam is focussed on to the sample with a cylindrical lense. The sample itself is mounted either at room temperature or on a cold finger of a liquid nitrogen dewar. The inelastically backscattered light is collected to the entrance slit of the spectrometer (both Jarrel Ash and Spex double monochromators are used). The collected light is analyzed and stored in a multichannel analyzer using an appropriate photomultiplier tube and conventional pulse counting electronics for signal detection. Both Ar^+ and Kr^+ ion lasers are used as light sources.

The studied samples are single crystals of GaAs with various doping concentrations (Te, Sn, Se) and thin crystalline films and multilayers of GaAs and $Al_xGa_{1-x}As$ grown with LPE and MBE. The surfaces of the bulk single crystals are polished and etched with an aqueous solution of NaCl. The MBE and LPE samples are measured as grown.

In order to get information from different depths one varies the laser frequency. The penetration depth into GaAs changes from about 1 μm at $\lambda_0 = 8000$ Å to ~ 150 Å at $\lambda_0 = 4000$ Å [8]. In the mixed crystal $Al_xGa_{1-x}As$ the direct bandgap increases with increasing Al content. At $x \sim 0.40$ the conduction bands at the Γ and X point of the Brillouin zone cross, we have a semiconductor with an indirect bandgap. Because of the shift of the bandgap to higher energies, the penetration depth into $Al_xGa_{1-x}As$ gets larger. For example at $x \sim 0.40$ the bandgap is already 2.0 eV, which means the crystal is transparent for the red Kr^+ ion laser lines while in the blue the penetration depth is still very short. Thus also in the mixed crystal system a depth profiling using different laser lines is possible.

2. Possibilities, Results, and Discussion

2.1. Crystal Orientation

From the selection rules we learn that under certain scattering configurations not all lattice vibrations can be observed in a Raman scattering experiment. Let us consider only first-order scattering (phonons at the Γ-point). Following Loudons's description of the Raman tensors [9] we find for crystals with diamond structure that for backscattering from a (100) surface, only the LO phonon can be observed. From (110) surfaces only TO phonons are allowed and for (111) surfaces both TO and LO lattice vibrations should be observable.

Figure 1 shows on the top a Raman spectrum in true backscattering geometry from a (100) surface of a slightly doped n-GaAs crystal ($n = 1.8 \times 10^{16}\,cm^{-3}$). The polarization of the incident light is along (010) and the scattered light along (001). We write this scattering configuration in the following way: $x(yz)\bar{x}$. As expected, only the LO phonon mode is observed in the Raman spectrum.

We have also studied thin films of GaAs grown with MBE and LPE on GaAs substrates with orientation ⟨100⟩ perpendicular to the surface. In Fig. 1 we show typical examples of observed Raman spectra of such layers. Some of the samples show a strong TO mode. In very thin layers it is difficult to learn something about the crystal structure from x-ray work because of the large information depth. Sometimes electron and x-ray diffraction under very small angle of incidence can provide insight into the crystal orientation and surface smoothness.

On the other hand, one can easily see deviations from the Raman scattering (Fig. 1) selection rules.

The strong TO mode which is observed in some MBE films grown on (100) GaAs substrates demonstrates that the orientation of at least parts of the films are different from the expected (100) direction. Comparing different MBE samples and the way of their fabrication we realize that the TO mode always appears when the initial substrate surface seems to be slightly contaminated by carbon, even after chemical etching in $H_2O_2/H_2SO_4/H_2O$. We have detected this contamination in situ by AES [4] prior to epitaxial growth.

It has already been pointed out previously [2] that a carbon impurity of >0.2 monolayer of the initial surface does cause surface facetting and twinning in the growing film. We have checked this phenomenon on a large number of MBE samples by Raman scattering and we always find the same result: The appearance of the "forbidden" TO phonon line depends strongly on the carbon contamination of the initial surface. There is found no TO phonon only in the case when the residual carbon on the initial surface is less than 0.1 monolayer, which is the detection sensitivity of our AES measurements. The required purity of the substrate surface can be achieved [2] by either an extremely careful chemical treatment, which might vary from sample to sample, or in a more reproducible manner by an additional Ar^+ ion sputter cleaning and annealing prior to epitaxial growth.

We have strong evidence that the strength of the TO phonon line is directly correlated with the amount of carbon on the initial surface. Starting with a contamination >0.3 monolayer carbon, a twinning of the growing GaAs film can be observed even in the RHEED pattern and the sample shows a strong "forbidden" TO phonon, with an intensity about 2/3 of that of the LO phonon (Fig. 1, spectrum at the bottom). When thin films (<200 Å) grown on these contaminated substrate surfaces are examined by scanning electron microscopy, a three-dimensional nucleation yielding irregular three-dimensional centers and discrete three-dimensional crystallographically shaped growth centers are observed. For a carbon contamination <0.2 monolayer there is no observable effect in our RHEED experiments, but there is still a small "forbidden" TO line in the Raman spectrum (Fig. 1).

The nature of the misorientation is not yet clear. It is difficult to get information on this question from Raman spectroscopy. Therefore further x-ray and electron diffraction work is necessary to get insight into the problem what actually happens during the growth. Here we just want to show that Raman scattering experiments can be used to study the crystal orientation of thin films on a microscopic scale. The effect just described has been discovered only because we are using, besides other methods, also Raman spectroscopy to characterize the MBE and LPE grown samples.

2.2. Carrier Concentration and Scattering Time in n-GaAs

Several years ago Mooradian and coworkers [10] have shown that it is possible to observe also coupled LO phonon plasmon modes in *n*-GaAs using Raman spectroscopy. The frequencies of the coupled modes are essentially given by the zeros of the real part of the following sum: the longitudinal dielectric function of the electron gas $\varepsilon_e(q,\omega)$ plus the one of the lattice vibration. The early experiments have been performed with incident laser light $\lambda_0 = 1.06\,\mu m$. In this frequency region GaAs is transparent and the scattering wavevector $k = 4\pi\,\mathrm{Re}\eta/\lambda_0$ (η is the refractive index) involved in Raman scattering is very small. The observed frequencies of the coupled modes (labelled L_+ and L_-) agree well with the calculated roots of the equation $\mathrm{Re}\{\varepsilon(q\to 0,\omega)\} = 0$.

Recently it has been demonstrated that it is also possible to study the wavevector dependence of L_+ and L_- using incident laser light in the visible ($6764 \leqq \lambda_0 \leqq 4416$ Å) [11]. Using the Drude expression for the dielectric function of the electron system the frequency of the L_+ mode can be written as [11]

$$\omega_+ = \left\{\frac{\omega_{LO}^2+\omega_p^2(q)}{2} + \left[\frac{[\omega_{LO}^2+\omega_p^2(q)]^2}{4} - \omega_p^2(q)\omega_{TO}^2\right]^{1/2}\right\}^{1/2}, \quad (1)$$

where ω_{LO} and ω_{TO} are the frequencies of the LO and TO phonons at the Γ-point, respectively, and $\omega_p(q)$ is the wavevector dependent plasma frequency [12]

$$\omega_p^2(q) = \omega_p^2 + 3/5(qv_F)^2 \quad (2)$$

with

$$\omega_p^2 = 4\pi ne^2/\varepsilon_\infty m^*; \quad (3)$$

n is the carrier concentration, v_F the Fermi velocity, and m^* is the effective mass of the carriers.

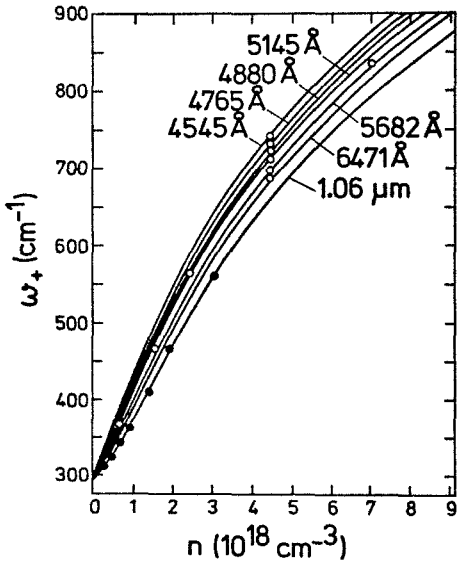

Fig. 2. The dependence of the frequency of the L_+-mode on the carrier concentration is shown for different laser lines. Experimentally obtained values of ω_+ (open circles) agree well with the theoretical curves. The closed circles are results taken from [10]

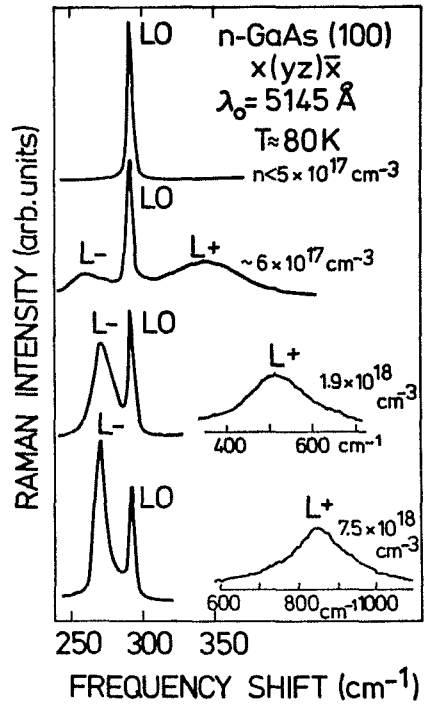

Fig. 3. Typical Raman spectra of thin MBE layers of *n*-GaAs with different donor concentrations. Both the LO phonon mode from the depletion layer and the coupled LO phonon-plasmon modes L_+ and L_- are observed

The position of the high-frequency coupled mode depends on the carrier concentration n. Therefore it can be used to determine n of highly doped crystals and thin layers. We have calculated $\omega_+(n)$ for the strongest lines of Ar^+ and Kr^+ ion lasers and for the 1.06 μm Nd^{3+} YAG laser line used in the work of [10]. This is necessary because the refractive index η of GaAs depends on the wavelength [8] so that one gets a variation of the scattering wavevector from $0.3\times10^6\,\mathrm{cm}^{-1}$ to $1.3\times10^6\,\mathrm{cm}^{-1}$ for the used laser lines ($1.06\,\mu\mathrm{m}\leqq\lambda_0\leqq4545$ Å). The results are shown in Fig. 2. One can clearly see the wavevector dependence of ω_+. At fixed n, ω_+ shifts to higher frequencies when λ_0 is changed from red to blue. This wavevector dependence was discussed extensively in [11] and [13]. We have not yet mentioned that the conduction band of GaAs is nonparabolic and therefore the effective mass m^* depends on the carrier concentration. This has to be taken into account using a mass variation of $m^*=0.070m_0$ for $n=1\times10^{17}\,\mathrm{cm}^{-3}$ to $m^*=0.096m_0$ for $n=1\times10^{19}\,\mathrm{cm}^{-3}$ [14]. The other values used in the calculations are: $\varepsilon_\infty=11.1$, $\omega_{LO}=295\,\mathrm{cm}^{-1}$, $\omega_{TO}=270\,\mathrm{cm}^{-1}$. The $\omega_+(n)$ curves shown in Fig. 2 can be used to determine the carrier concentration in the region $n>1\times10^{17}\,\mathrm{cm}^{-3}$.

So far we have discussed only the theoretical part without considering the experimental situation. At a real surface of *n*-GaAs there normally exists a depletion space charge region with a barrier height of ~1 eV. The width of this carrier free layer varies from ~3000 to ~150 Å with donor concentrations in the range $2\times10^{17}\lesssim n\lesssim5\times10^{18}\,\mathrm{cm}^{-3}$. On the other hand, using laser lines covering the range 6471–4545 Å, the penetration depth into GaAs changes from ~3000 to ~300 Å. This has been discussed already in the experimental part. Thus it is possible to observe both the coupled LO phonon-plasmon modes from the bulk and the unscreened LO phonons from the surface depletion region. The relative intensities can be used to study the surface band bending and the barrier heights of free and covered GaAs surfaces [15].

Here we concentrate on the signals from the bulk. In Fig. 3 some typical spectra are shown for different carrier concentrations. One can see that the strength of the bulk signal (L_+ and L_-) decreases compared to the surface signal (LO-phonon) with decreasing carrier concentration. This is due to the increased depletion width, while the penetration depth of ~1000 Å at $\lambda_0=5145$ Å remains unchanged. Therefore the observability of L_+ and L_- is limited to the region $n\gtrsim5\times10^{17}\,\mathrm{cm}^{-3}$. In this region the frequency of the L_- mode depends only very weakly on the carrier concentration, contrary to the L_+-mode which shifts quite strongly to higher energies if n is increased.

In Fig. 2 the experimental results of ω_+ obtained with $\lambda_0 = 5145$ Å on samples with known carrier concentration are shown (open circles). The closed circles are results taken from [10] ($\lambda_0 = 1.06\,\mu$m). For a sample with $n = 4.5 \times 10^{18}\,\text{cm}^{-3}$ we also show the results obtained with other laser lines. The agreement between theory and experiment is very good. Therefore we believe that the measurement of the L_+ mode gives a very accurate value of the carrier concentration of n-GaAs in the region $n \gtrsim 5 \times 10^{17}\,\text{cm}^{-3}$.

If one has the possibility to use a Raman spectrometer which works with infrared frequencies, one can extend this region to $n \gtrsim 1 \times 10^{16}\,\text{cm}^{-3}$ by studying the frequency of the L_--mode, which depends strongly on n in the range $1 \times 10^{16} \lesssim n \lesssim 5 \times 10^{17}\,\text{cm}^{-3}$. Then the depletion layer is no problem, because GaAs is transparent in the infrared. $\omega_-(n)$ can be taken, for example, from [10].

We have studied the ω_+ mode of various thin crystals of n-GaAs grown with MBE and LPE and could so determine the carrier concentration. The results agree well with those obtained from capacitance versus voltage and Hall effect measurements. The advantages of the Raman spectroscopy are that no contacts and no Schottky-barriers are necessary, that the substrate does not influence the results, and that the carrier concentration can be determined within very small areas (focus of the laser beam down to $4\,\mu\text{m}^2$).

If the samples are very thin, the penetration depth of the laser light can be large enough to reach the interface to the substrate. Depending on the substrate, the scattering volume with carrier density n gets smaller. In very thin samples the entire layer can be depleted. Such effects result in an increase of the intensity of the unscreened LO mode compared to the coupled modes. We have observed this behaviour on MBE layers of various thicknesses.

Apart from the position of the L_+ mode one also gets useful information from the linewidth and the lineshape. At high carrier concentration ($n > 10^{18}\,\text{cm}^{-3}$) the L_+ mode is plasmon-like and the damping should essentially be determined by the scattering time of the charge carriers. Using the electron damping $1/\tau = e/m^*\mu$ deduced from the mobility μ, we find on the other hand that the actually observed linewidth of L_+ is always larger than expected [13]. This indicates that additional damping mechanisms play an important role. Such contributions to the broadening of the plasmon-like mode may arise from an increased scattering rate caused by the presence of the surface. Sometimes one also gets an inhomogeneous broadening because of a spatial variation of the donor distribution. When the penetration depth exceeds the depletion layer only very little, we observe an asymmetric lineshape of the L_+ mode, because at the interface between the bulk and the depletion region, one always has a gradient in the carrier concentration.

If we neglect inhomogeneous broadening, which is reasonable for symmetric lineshapes, we can define a scattering rate for the electrons observed in Raman scattering

$$\frac{1}{\tau} = \frac{1}{\tau_i} + \frac{1}{\tau_p} + \frac{1}{\tau_s}. \tag{4}$$

$1/\tau_i$ is the scattering rate by impurities, $1/\tau_p$ by phonons, and $1/\tau_s$ describes surface scattering. If one measures the bulk mobility, only impurities and phonons contribute to the scattering rate and at high donor concentration $1/\tau_i$ dominates. Using, however, the width of the L_+ mode to determine $1/\tau$ or μ we have to consider also surface scattering, because only electrons close to the surface depletion layer contribute to the Raman signal. The actual surface which one should consider here, is the interface between depletion layer and bulk.

Experimentally we find for $n = 7 \times 10^{17}\,\text{cm}^{-3}$ the scattering rate deduced from the L_+ mode to be about two times larger than expected from the bulk mobility. For higher carrier concentrations the difference gets smaller and smaller. This can be explained qualitatively with surface scattering. First of all the impurity scattering rate increases with increasing donor concentration. Second, with higher carrier concentration, the depletion width gets smaller so that at a fixed laser frequency the region containing electrons which contribute to the signal gets larger. On the average the carriers are further away from the interface. Therefore surface scattering should be less important when n is very large.

Despite of these problems we believe that especially for high carrier concentrations ($n > 10^{18}\,\text{cm}^{-3}$) we can use the width of the L_+ to estimate the scattering rate and the mobility of the charge carriers in new crystals or thin layers by comparing the results with the values of known samples.

2.3. Mixed Crystals

The frequencies of the LO and TO modes of the system $Al_xGa_{1-x}As$ have been studied previously by Ilegems and Pearson [16] from a Kramers-Kronig analysis of infrared reflectance spectra and by Tsu and coworkers [17] using Raman spectroscopy. In the entire alloy composition range, the spectra show essentially two distinct bands, one at frequencies close to the modes of pure GaAs and the other close to pure AlAs. In Fig. 4 we show the dependence of the vibrational modes on the molar fraction x of Al in GaAs [16, 17]. The frequency variation of these modes can be used to

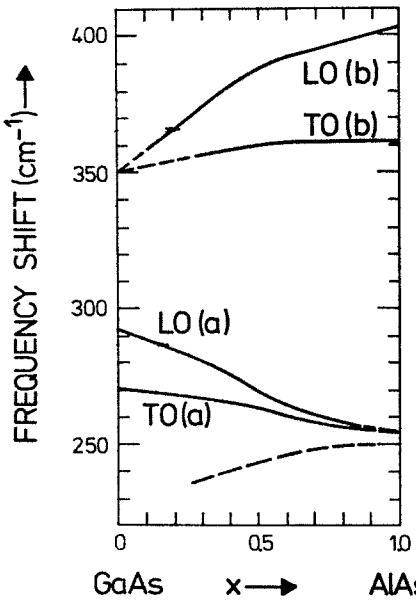

Fig. 4. The variation of the mode frequencies of $Al_xGa_{1-x}As$ with x is shown [16, 17]. This plot is used to determine x in unknown MBE and LPE layers of $Al_xGa_{1-x}As$

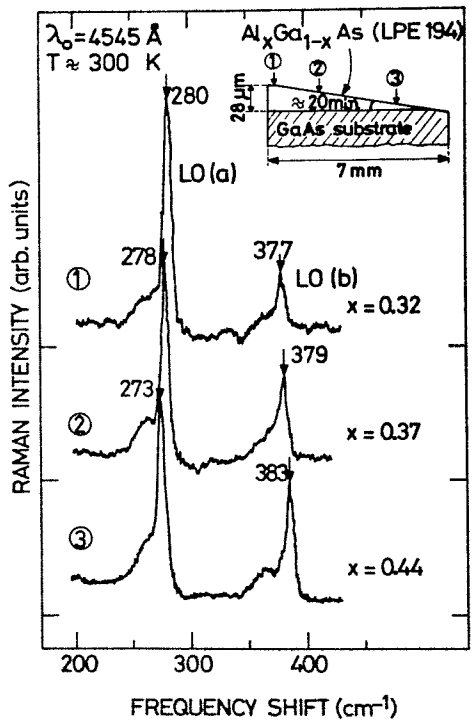

Fig. 5. Some Raman spectra of a $Al_xGa_{1-x}As$ LPE sample which has been wedged in order to study the depth profile of the Al concentration. The sample cross section is shown schematically in the insert

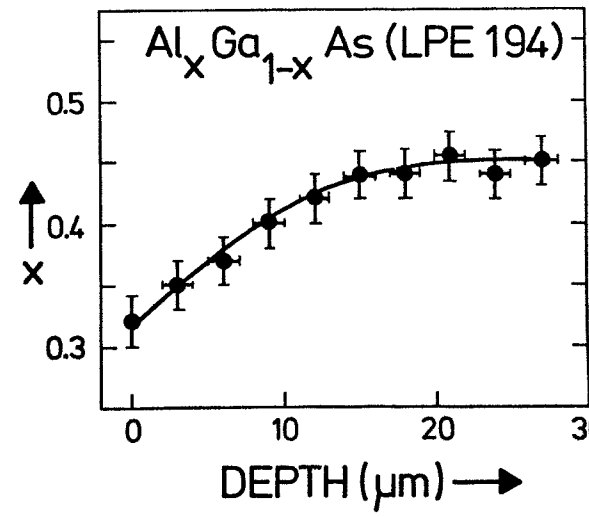

Fig. 6. Molar fraction of Al in the LPE sample described in Fig. 5 as a function of the distance from the surface

determine the value of x of unknown samples. We have used this method to characterize thin $Al_xGa_{1-x}As$ layers grown by MBE and LPE.

As discussed before, a depth profiling can be obtained, using laser excitation lines with various penetration depths. For a gradually varying Al concentration, however, this method is not very accurate. One observes only asymmetric lines caused by the slowly changing Al content (inhomogeneous broadening). Therefore we use a different method to study the Al profile of LPE layers of $Al_xGa_{1-x}As$ on GaAs substrate. The studied LPE samples have a thickness of about 30 µm. We have polished and etched the samples under an angle of ~20 min tilted with respect to the surface parallel. With a sample length of 0.7 cm we get on one side the original sample surface while on the opposite side the LPE layer is polished away. Thus when moving the laser beam over the surface, it is possible to observe Raman spectra from different depths of the grown layer. The cross section of the sample is shown schematically in Fig. 5. The experiments are performed with $\lambda_0 = 4545$ Å Ar^+ laser line, a wavelength with a very short penetration depth. In Fig. 5 we also show some spectra from different parts of the surface. One clearly observes a shift of the mode frequencies which is caused by a variation of the Al concentration towards the surface. Together with the frequency shift of the Raman lines we notice also an increasing intensity of the band originating from the pure AlAs when we measure closer to the substrate. The intensity ratio of the two different bands might also be used to determine the Al concentration. In Fig. 6 we show the dependence of the Al content on the

distance from the surface. Raman scattering experiments are accurate to about $\pm 2\%$ for determining the Al concentration in the region $x=0.05$ to 0.90.

This method of determination of the composition of mixed crystals can be extended to other systems. The mode frequencies of many III–V alloy systems have been studied during the past ten years both with Raman and infrared spectroscopy and the frequency shifts with composition can be found in the literature.

2.4. Multilayer Structures

So far we have only discussed properties of single layers of GaAs or $Al_xGa_{1-x}As$. Now we want to show that Raman spectroscopy is also a useful tool to characterize multilayer systems. During the past few years some Raman studies of periodic systems or superlattices have been performed [18–21]. These experiments show interesting features due to zone folding effects in periodic structures. We concentrate on multilayer systems which have no special periodicity so that no zone folding occurs.

In Raman scattering experiments one observes the vibrational spectra of each individual layer. This is a great advantage compared to other optical characterization methods. In reflection or transmission experiments one always gets information averaged over the studied layers, for example, the refractive index or the absorption coefficient. Raman scattering can be used to study the composition of individual layers. From the dependence of signal strength of the different layers on the thickness and on the wavelength one can also obtain information on the absorption coefficient of the different layers.

In Fig. 7 we show the Raman spectra of a three layer system consisting of 1000 Å $Al_xGa_{1-x}As$, ~200 Å GaAs, ~2000 Å $Al_xGa_{1-x}As$ on a GaAs substrate. One can clearly separate the different spectra of the layers. In the spectrum obtained with the laser excitation line $\lambda_0=4545$ Å, we see only the spectrum of the top single $Al_xGa_{1-x}As$ layer. For this layer we find $x=0.15$. The second spectrum with $\lambda_0=5682$ Å shows also the LO mode of the GaAs layer (294 cm^{-1}) and a stronger asymmetry of the $Al_xGa_{1-x}As$ lines, which indicates that the deeper $Al_xGa_{1-x}As$ layer has a higher Al concentration. The Raman lines of the two deeper layers are observed because of the larger penetration depth of the $\lambda_0=5682$ Å laser line.

If the Al content is higher, the separation of the different spectra is more clear. This can be seen in the lowest spectrum of Fig. 7, which has been obtained with a 0.5 μm thick $Al_{85}Ga_{15}As$ layer on a GaAs substrate using $\lambda_0=5145$ Å.

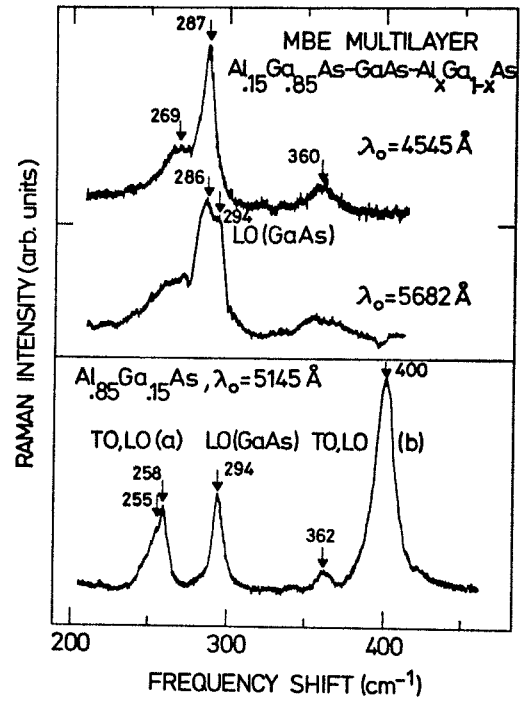

Fig. 7. Raman spectra of a three layer system $Al_xGa_{1-x}As$—GaAs—$Al_xGa_{1-x}As$ obtained with two different laser excitation lines. One clearly can separate the spectra of the different layers. As shown in the lowest trace, the frequency separation is larger for a sample with higher Al concentration. This spectrum has been obtained of a thin $Al_{0.85}Ga_{0.15}As$ layer on a GaAs substrate

Concluding Remarks

It has been shown that Raman spectroscopy can be used as a powerful technique to characterize thin films. Even depth profiling can be done in a non-destructive way. A detailed lineshape analysis might lead to further information, for example, on defects or inhomogeneous distributions of dopants and impurities.

We want to emphasize that Raman scattering experiments can be performed on very small spots on the sample surface. Thus it is also possible to study all the properties discussed in this work along the whole surface with a spatial resolution of the diameter of the focussed laser beam (a few μm^2). This might be of interest for technological applications, because it is often necessary to check the homogeneity of thin films or layered structures for devices over the whole surface area. One can also study, for example, specially grown layers for opto-electronic couplers with variations in composition, or the quality and/or carrier concentrations over large areas of samples used in semiconductor device technology. Therefore, Raman spectroscopy, a technique so far mainly used in pure research,

is also a versatile tool for sample characterization and thus a useful technique in related technological areas.

Acknowledgements. The authors would like to thank R. Tsu who initiated this work during his stay at the Max-Planck-Institut in Stuttgart. Useful discussions with R. Trommer, A. Pinczuk, M. Cardona, and H. J. Queisser are gratefully acknowledged. Part of the work has been supported by the Ministry of Research and Technology of the F.R.G.

References

1. E. Bauser, M. Frik, K. S. Loechner, L. Schmidt, R. Ulrich: J. Cryst. Growth **27**, 148 (1974)
2. A. Y. Cho, J. R. Arthur Jr.: Prog. Solid State Chem. **10**, 157 (1975)
3. L. L. Chang, L. Esaki, W. E. Howard, R. Ludeke: J. Vac. Sci. Technol. **10**, 11 (1973)
4. K. Ploog, A. Fischer: Appl. Phys. **13**, 111 (1977)
5. A. C. Gossard, P. M. Petroff, W. Wiegmann, R. Dingle, A. Savage: Appl. Phys. Lett. **29**, 323 (1976)
6. R. Tsu, L. L. Chang, G. A. Sai-Halasz, L. Esaki: Phys. Rev. Lett. **34**, 1509 (1975)
7. R. Dingle, A. C. Gossard, W. Wiegmann: Phys. Rev. Lett. **34**, 1327 (1975)
8. B. O. Seraphin, H. E. Bennett: In *Semiconductors and Semimetals*, ed. by R. K. Willardson and A. C. Beer (Academic Press, New York 1967) Vol. 3, p. 499; also: D. Aspnes (private communication)
9. R. Loudon: Adv. Phys. **13**, 423 (1964)
10. A. Mooradian, G. Wright: Phys. Rev. Lett. **16**, 999 (1966)
11. A. Pinczuk, G. Abstreiter, R. Trommer, M. Cardona: Solid State Commun. **21**, 959 (1977)
12. D. Pines: *Elementary Excitations in Solids* (Benjamin, New York 1963)
13. G. Abstreiter, A. Pinczuk, R. Trommer, M. Cardona: In: Proc. Int. Conf. on Lattice Dynamics, Paris (1977) and to be published
14. M. Cardona: Phys. Rev. 121, 752 (1961)
15. G. Abstreiter: Verh. DPG VI, **12**, 81 (1977) and to be published
16. M. Ilegems, P. L. Pearson: Phys. Rev. **1B**, 1576 (1970)
17. R. Tsu, H. Kawamura, L. Esaki: In: Proc. Int. Conf. on the Phys. of Semiconductors, Warsaw (1972) Vol. 2, p. 1135
18. J. L. Merz, A. S. Barker Jr., A. C. Gossard: Appl. Phys. Lett. **31**, 117 (1977)
19. P. Manuel, G. A. Sai-Halasz, L. L. Chang, Chin-Au Chang, L. Esaki: Phys. Rev. Lett. **37**, 1701 (1976)
20. G. A. Sai-Halasz, A. Pinczuk, P. Y. Yu, L. Esaki: Surface Sci. **73**, 232 (1978)
21. A. S. Barker Jr., J. L. Merz, A. C. Gossard: Phys. Rev. **B17**, 3181 (1978)
22. H. Ibach (Ed.): *Electron Spectroscopy for Surface Analysis*, Topics Current Phys. **4** (Springer, Berlin, Heidelberg, New York 1977)

Solid State Communications, Vol.30, pp.703-707.
Pergamon Press Ltd. 1979. Printed in Great Britain.

COUPLED PLASMON-LO PHONON MODES AND LINDHARD-MERMIN DIELECTRIC FUNCTION OF n-GaAs

G. Abstreiter[+], R. Trommer[++], M. Cardona

Max-Planck-Institut für Festkörperforschung, Heisenbergstr. 1
7000 Stuttgart 80, Federal Republic of Germany

and

A. Pinczuk*

Bell Telephone Laboratories, Holmdel, N.J. 07733, U.S.A.

Received: March 25, 1979, by M. Cardona

The wave vector dependence of coupled plasmon-LO phonon modes is studied with opaque Raman spectroscopy. The dispersion of the coupled modes is directly related to the wavevector dependence of the dielectric function of the electron gas and is influenced by finite temperatures and finite damping. The broadening of the wavevector due to absorption is also important. These effects are explained with the quantum mechanical Lindhard dielectric function for finite temperature including electron scattering in the relaxation time approximation of Mermin.

It has been suggested that Raman scattering by coupled plasmon-LO phonon modes in n-GaAs can be used to study the wave vector dependence of the longitudinal dielectric function of the electron gas $\varepsilon_e(q,\omega)$ [1,2,3,4]. For $\omega >> q v_F + \hbar q^2/2m^*$, where q is the scattering wave vector, v_F the Fermi velocity of the charge carriers and m^* the effective mass, the results are well described to lowest order in q with the Drude dielectric function including a wavevector-dependent plasma frequency. For $\omega \gtrsim q v_F + \hbar q^2/2m^*$, however, this modified Drude function does not fit the observed spectra[4,5]. In this communication we present an experimental and theoretical study of the wavevector-dependent Raman spectra covering the region $\omega \approx q v_F + \hbar q^2/2m^*$. The finite temperature quantum-mechanical expression of $\varepsilon_e(q,\omega)$ was used. The effects associated with finite electron scattering times are described within the relaxation-time approximation of Mermin[6]. We find excellent agreement between experimental and theoretical results for a wide range of wavevectors and carrier concentrations.

Raman spectra were obtained at various temperatures ($300^oK \gtrsim T \gtrsim 2^oK$) using both ion- and dye lasers in the $7525 \gtrsim \lambda_o \gtrsim 4416$ Å range. This corresponds to a range of scattering wave vectors $q = 4\pi R e n/\lambda_o$ varying from 0.6×10^6 cm^{-1} to 1.4×10^6 cm^{-1}, where n is the wavelength dependent refractive index[7]. The experiments were performed in back scattering geometry on (100) surfaces. In this geometry only longitudinal modes are allowed by the selection rules. The samples are single crystals of GaAs with various dopants (Te,Se,Sn, Si) and carrier concentrations in the range $1.8 \times 10^{16} \lesssim n \lesssim 6.7 \times 10^{18}$ cm^{-3}. Samples with $n \gtrsim 7 \times 10^{17}$ cm^{-3} were investigated most extensively. The surfaces were polished and etched with an aqueous solution of NaOCl. The experiments have been done with the polarization of the incident light along $y = (010)$ and that of the scattered light along $y = (010)$ or $z = (001)$.

The $x(yz)\bar{x}$ spectra involve coupling to fluctuations in the lattice polariza-

---

[+]Present address: Max-Planck-Institut für Festkörperforschung, Hochfeld-Magnetlabor, Avenue des Martyrs, 38042 Grenoble Cédex, FRANCE

[++]Present address: Siemens Forschungslabor, Otto-Hahn-Ring 6, 8000 München 83

*Guest scientist at the Max-Planck-Institut für Festkörperforschung during July-August, 1978

tion (deformation potential and electro-optic scattering). This mechanism is dominant away from the $E_o + \Delta_o$ energy gap ($\sim$ 1.9 eV) and does not show strong resonance behavior near the gap[8]. The $x(yy)\bar{x}$ spectra, however, are strongly resonant close to $E_o + \Delta_o$. These spectra involve the fluctuations in the charge density as discussed elsewhere[9]. The cross section of Raman scattering by the fluctuations of the lattice polarization of an opaque crystal is given by[4,10]

$$\frac{d^2\sigma}{d\Omega d\omega} \sim - \frac{(\omega_o^2 - \omega^2)^2}{(\omega_T^2 - \omega^2)^2} \times \int_{-\infty}^{+\infty} \frac{1}{(q'-q)^2 + \alpha^2} \, \mathrm{Im} \frac{1}{\varepsilon(\vec{q},\omega)} \, dq' \qquad (1)$$

where ω_T is the frequency of the TO phonon, $\omega_o^2 = \omega_T^2(1 + C)$, with C equal to the Faust-Henry coefficient, $\vec{q}$ is the wave vector of the excitation, α the absorption constant of the crystal for incident and scattered light and $\varepsilon(q,\omega)$ the total dielectric function. The integration over q' takes into account the wave vector non-conservation which is associated with the absorption of incident and scattered light in an opaque crystal

The total dielectric constant can be written in the following form:

$$\varepsilon = \varepsilon_\infty \frac{\omega_L^2 - \omega^2}{\omega_T^2 - \omega^2} + \varepsilon_e(q,\omega) \qquad (2)$$

where ω_L is the frequency of the LO-phonon and ε_∞ the high frequency dielectric constant. In the simplest case a $\vec{q}$-dependent Drude expression can be used for $\varepsilon_e(q,\omega)$. However, as shown earlier[4,5], Landau damping, especially in connection with temperature and electron collision effects play an important role. To describe these effects we use the Lindhard-Mermin dielectric function[6]

$$\varepsilon_e(\vec{q},\omega) = \frac{(1+(i\Gamma/\omega))\,\varepsilon_e^o(\vec{q},\omega+i\Gamma)}{1+(i\Gamma/\omega)\,\varepsilon_e^o(\vec{q},\omega+i\Gamma)/\varepsilon_e^o(\vec{q},o)} \qquad (3)$$

which includes the effects of finite electron collision times $\tau = (1/\Gamma)$ in the relaxation time approximation. $\varepsilon_e^o(q,\omega)$ is the Lindhard dielectric function for finite temperatures (Eq. 3.3 of Ref. 12). Equation (3) was evaluated numerically for finite temperatures.

Figure 1 shows the spectra in the $x(yz)x$ configuration for four different laser frequencies (solid lines), i.e. scattering wave vectors. In addition to the two coupled plasmon LO-phonon modes L_+ and L_- one observes also a

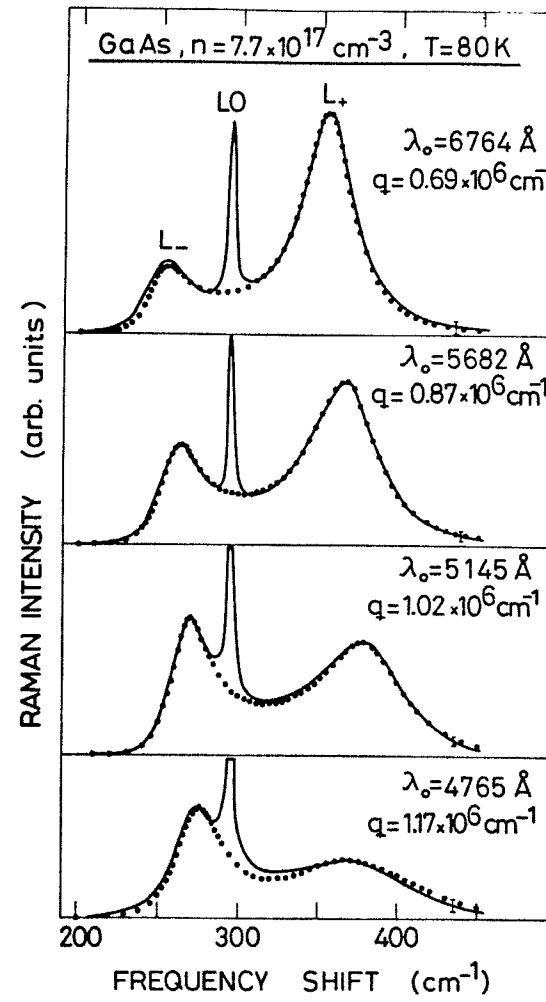

Figure 1

Raman spectra of n-GaAs in backscattering geometry from a (100) surface (solid lines) at four different laser excitation wavelengths. The dotted lines are calculations of coupled LO phonon-plasmon modes using the Lindhard-Mermin dielectric function of the electron gas.

pure LO-phonon mode at 295 cm^{-1}. This mode originates from the surface depletion layer which is present at a natural, air exposed (100) surface of GaAs. It occurs strongly in the spectra because the light penetration depth ranges between $\sim$3000 Å and $\sim$500 Å. The coupled mode spectra have been calculated using Eq. 1,2 and 3. The results are given by the dotted lines. For λ_o = 5682 Å and $\alpha = 0.55 \times 10^5$ cm^{-1} the best fit is obtained with the following parameters: Fermi energy E_F = 320 cm^{-1}, effective mass $m^* = 0.074\ m_o$, electron

damping $\Gamma = 58\ cm^{-1}$, $\omega_o = 185\ cm^{-1}$. The temperature in the experiment was ~80 K (≙ 56 cm^{-1}). Using these parameters we have also calculated the spectra for the other values of λ_o, q and α. The agreement between the calculated spectra and the experimental data is excellent. The positions, the widths and the intensity ratios of the L_+ and L_- bands are reproduced very well by the theoretical calculations. The value of Γ used in the calculations turns out to be about 50% larger than expected from the bulk mobility (3100 cm^2/Vs). This indicates either a wavevector dependence of Γ or that other damping mechanisms like surface scattering are important.

Figure 2 displays the peak positions of the L_- and L_+ bands obtained as discussed above for a wide range of scattering wave vectors. The solid lines represent the frequencies of the peaks in the calculated spectra obtained using for the absorption coefficient in Eq. (1) the same values as in Ref. 8 (typical values are $\alpha = 1.3\times10^4\ cm^{-1}$ for $\lambda_o = 7525$ Å and $\alpha = 2\times10^5\ cm^{-1}$ for $\lambda_o = 4579$ Å). The solid lines fit very well the experimental points in Fig. 2. The dashed lines in Fig. 2 were obtained from the spectra calculated with a small, wavelength independent $\alpha = 1.3\times10^4\ cm^{-1}$. They do not show the downward bending of L_+ observed experimentally and in the calculated solid line. This analysis thus shows that the bending is related to the strong absorption which allows coupling to a range of wavevectors including small ones. For these small wavevectors L_+ is stationary and the coupled modes are sharp. Thus in the limit of very strong absorption a peak appears at the frequency of $L_+(q\approx0)$. This is the origin of the observed bending in L_+ for increasing q which bears no relationship to the reentrant dispersion relation reported by Lemmens et al.[13]. In fact we find no evidence for such a dispersion relation in our calculated spectra for $\alpha << q$ (dashed line in Fig. 2).

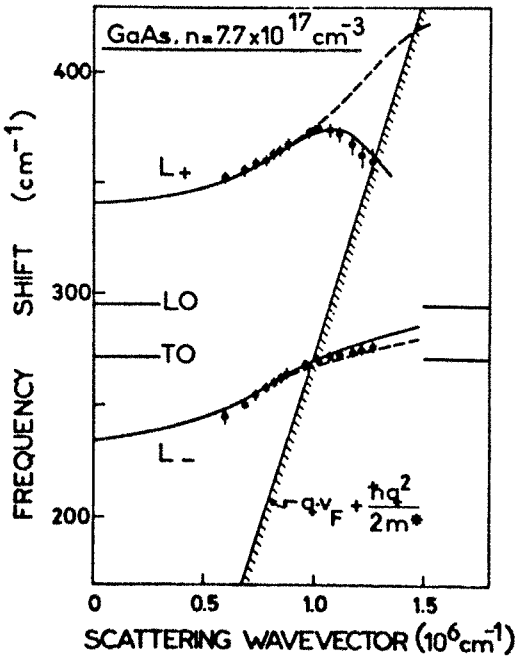

Figure 2

Dispersion of the peaks in the Raman spectra of coupled plasmon-LO phonon modes of n-GaAs. The solid and dashed lines are calculated as described in the text, the dots represent the experimental results.

We have also measured and calculated the scattering spectra in the $x(yy)\bar{x}$ configuration. The L_+ and L_- peak energies differ only slightly from those shown in Fig. 2. The difference is due to the fact that in this case ω_o must be replaced by ω_L in Eq. 1[10]. The effect is to lower the L_- band by ≈ 10 cm^{-1} and to raise that of L_+ by ~ 3 cm^{-1}.
We have also calculated the L_+ and L_- spectra for higher carrier concentrations. A comparison with the experimental results for three different samples is shown in Fig. 3. With increasing carrier concentration the depletion width becomes smaller, a fact which is reflected in the decreasing intensity of the LO phonon mode. At these high concentrations ($n > 10^{18}\ cm^{-3}$) the L_- mode is a screened LO phonon while the L_+ mode is plasmon-like. The calculated spectra are in very good agreement with the experimental data throughout the wide range of carrier concentrations. The only free parameter used in the fitting procedure is the electron damping Γ. The Fermi energy E_F and the effective mass m^* are calculated from the known carrier concentration and the band structure of GaAs (including nonparabolicity). ω_o was fixed to the value obtained from the fit of the $q = 0.87\times10^6\ cm^{-1}$ spectrum of the sample discussed above (185 cm^{-1}).

In conclusion, the Lindhard-Mermin dielectric function explains well the dispersion effects and lineshapes of the coupled mode system in n-GaAs. This function gives a better description of the experimental data than either the Drude or the simple Lindhard expression. To our knowledge this is the first time that the relaxa-

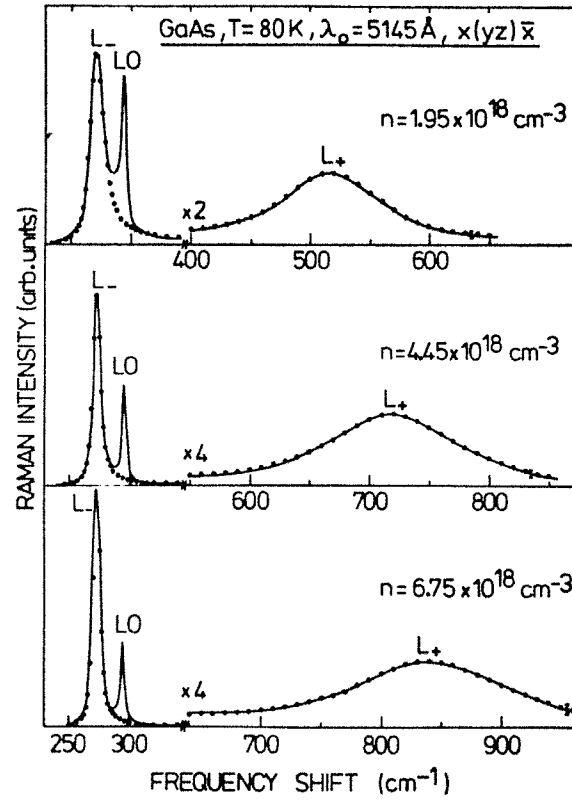

Figure 3

Raman spectra similar to Fig. 1 for three different carrier concentrations. The dotted lines are the calculated spectra.

tion approximation of Mermin has been used to describe the degenerate electron system in semiconductors. The shape of the spectra is shown to depend strongly on the absorption coefficient in the region of strong absorption. This effect obscures the possible influence of an additional surface scattering mechanism on the observed spectra.

ACKNOWLEDGEMENTS:

One of us (A.P.) would like to thank the Max Planck Institute, where he performed part of this work, for its support.

REFERENCES

1. K. MURASE, S. KATAYAMA, Y. ANDO and H. KAWAMURA, Phys. Rev. Lett. 33, 1481 (1974).
2. V.J. ZEMSKI, E.L. IVSHENKO, D.N. MIRLIN and J.J. RESHINA, Solid State Comm. 16, 221 (1975).
3. S. KATAYAMA, K. MURASE and H. KAWAMURA, Solid State Comm. 16, 945 (1975).
4. A. PINCZUK, G. ABSTREITER, R. TROMMER and M. CARDONA, Solid State Comm. 21, 959 (1977).
5. G. ABSTREITER, A. PINCZUK, R. TROMMER and M. CARDONA, Proc. of the 2nd Int. Conf. on Lattice Dynamics, ed. by M. Balkanski, Paris 1977, p. 191.
6. N.D. MERMIN, Phys. Rev. B1, 2362 (1970).
7. B.O. SERAPHIN and H.E. BENNETT in Semiconductors and Semimetals, ed. by R.K. Willardson and A.C. Beer (Academic Press, New York 1967), Vol. 3, p. 499.

8. R. TROMMER and M. CARDONA, Phys. Rev. B17, 1865 (1978).
9. A. PINCZUK, G. ABSTREITER, R. TROMMER and M. CARDONA, submitted for publication to Solid State Comm.
10. M.V. KLEIN in Light Scattering in Solids, ed. by M. Cardona (Springer Verlag, Berlin 1975), p. 147.
11. A. PINCZUK and E. BURSTEIN, same as Ref. 10, p. 23.
12. J. LINDHARD, Dan. Mat. Fys. Medd. 28, N° 8 (1954).
13. L.F. LEMMENS and J.T. DEVREESE, Solid State Comm. 14, 1339 (1974); L.F. LEMMENS, F. BROSENS, and J.T. DEVREESE, Solid State Comm. 17, 337, (1975).

Solid State Communications, Vol.30, pp.429-432.
Pergamon Press Ltd. 1979. Printed in Great Britain.

RESONANCE ENHANCEMENT OF RAMAN SCATTERING BY ELECTRON-GAS EXCITATIONS OF n-GaAs

A. Pinczuk[+]

Bell Telephone Laboratories
Holmdel, New Jersey 07733

G. Abstreiter, R. Trommer, and M. Cardona

Max-Planck-Institut für Festkörperforschung
Heisenbergstrasse 1, 7000 Stuttgart 80, F.R.G.

Received March 2, 1979 by M. Cardona

Large resonance enhancements in the inelastic light scattering intensities involving free carriers have been measured at the $E_o + \Delta_o$ energy gap of n-GaAs. Results for spin-flip single particle excitations are well described as unscreened intraband scattering involving the Γ_7 valence band as intermediate state. The resonance of the longitudinal plasmon-phonon coupled modes indicates the contribution of other so far not fully identified processes.

In this paper we report a detailed study of the resonance enhancement of Raman scattering by the single particle and collective excitations of the electron-gas of a degenerate semiconductor. These experiments made it possible to investigate the light scattering mechanisms involved. The $E_o+\Delta_o$ energy gap of n-GaAs was studied because an enhancement of mechanisms involving carrier-density fluctuations (either spin or charge) is expected in its neighborhood[1,2]. The non-degenerate character of this gap, in contrast to the E_o gap, simplifies the theoretical treatment. This energy gap is also convenient because the relatively weak luminescence does not obscure the Raman scattered light. Enhancement of the scattering by free carriers near resonance, in the qualitative fashion characteristic of the pre-dye-laser era, has also been reported by Scott et al.[3] for CdS and for GaAs by Pinczuk et al.[4].

We find that scattering by the unscreened single particle excitations is well described by the carrier-density (in this case spin-density) mechanism. On the other hand, the results for the longitudinal collective modes indicate a substantial contribution of processes other than carrier density fluctuations. In agreement with a recent estimate[2], the resonance scattering intensities are large enough to observe the excitations of carriers confined to narrow interface layers. The method could thus be used to study the two-dimensional electron-gas which exists at AlGaAs-GaAs heterostructures made by molecular beam epitaxy[5].

The n-GaAs samples investigated were Te doped in the range $1\times10^{16} \lesssim n \lesssim 6.7\times10^{18}$ cm^{-3}. Raman spectra were obtained at 80°K and 2°K with the $\sim$50 mW output of dye lasers. The penetration of the incident light in the $E_o + \Delta_o$ region is $\sim$3000 Å, which for $n \gtrsim 10^{17}$ cm^{-3} is considerably larger than the widths of the surface space charge layers[4]. We were thus observing scattering from bulk excitations. The most extensive studies were done on $x \equiv (100)$ surfaces choosing for the polarizations of the incident and scattered light $y \equiv \langle 010 \rangle$ and $z \equiv \langle 001 \rangle$ directions.

The selection rules for Raman scattering by the electron-gas have been reviewed by Mooradian[6] and Klein[7]. The $x(zy)\bar{x}$ spectra are due to the scattering by spin-flip single particle excitations (spe) described by second-order perturbation theory. The leading process near $E_o + \Delta_o$ for a zincblende type material is shown in Fig. 1a. The $x(yy)\bar{x}$ spectra are due to the L_+ and L_- coupled plasmon-LO phonon modes through third-order processes described by Figs. 1b and 1c where the dashed line represents intraband transitions via the

[+]Guest scientist at the Max-Planck-Institut für Festkörperforschung during July-August, 1978

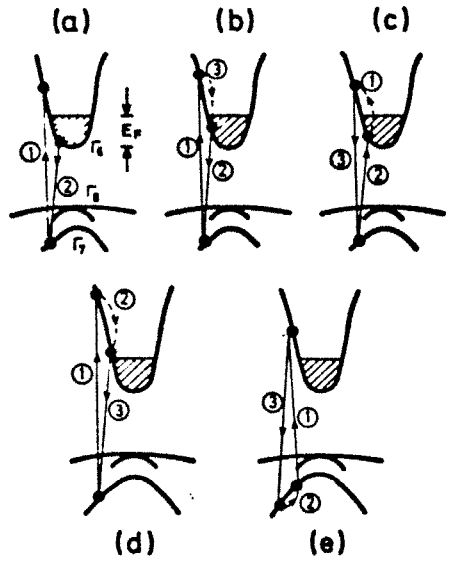

Fig. 1: Diagrams of the various Raman processes discussed in this paper. (a) single particle spin-flip scattering, (b) and (c) electron-phonon collective excitations (charge-density mechanism), (d) and (e) "Fröhlich mechanism". The dashed lines represent the Fröhlich interaction of the longitudinal collective modes. The numbers in circles give the time order of the processes.

Fröhlich interaction of the carriers with the longitudinal electric field of the coupled modes. Both types of processes just described require the presence of charge carriers and are thus referred to as carrier-density mechanisms. The coupled modes can also be excited in the x(yy)x spectra by what we shall refer to as the "Fröhlich mechanism". This is described by Figs. 1d and 1e where the dashed line involves the Fröhlich interaction. These processes do not require the presence of free carriers. If either deformation potential or interband electrooptic coupling[8,9] is used for step 2 (dashed line), the coupled modes also appear in the x(zy)x configuration.

We find that near the $E_o + \Delta_o$ resonance the x(zy)x spectra are basically the same as in Ref. 4, corresponding to scattering by spin-flip single particle excitations. The x(yy)x spectra show near resonance the coupled longitudinal modes and, at extreme resonance, also some scattering in the single particle range[4]. Away from $E_o + \Delta_o$ only scattering by the coupled modes via the phonon-like deformation potential and electro-optic mechanisms is observed[10]. The resonant x(yy)x spectra also show the additional scattering in the frequency range between the L_- and L_+ modes reported in earlier work[4]. We assign this to coupled modes of large wavevector made active by resonance Raman processes in which wavevector conservation breaks down. Unlike the case of InAs[11], the surface space charge layer is not involved here.

In Fig. 2 it is seen that the resonance enhancement of scattering by

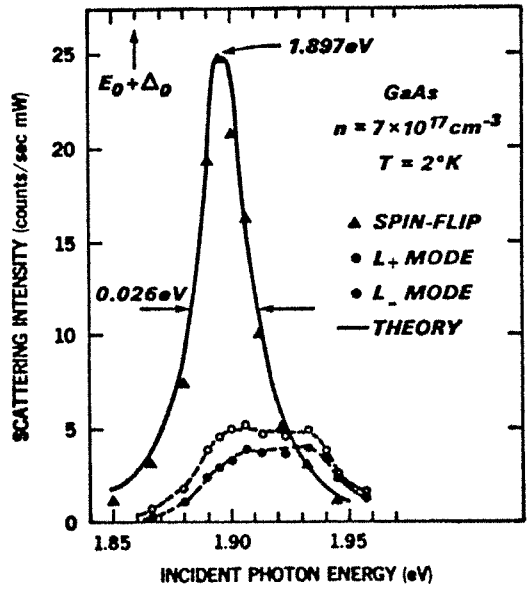

Fig. 2: Scattering intensity as function of incident photon energy of spin-flip single particle excitations at 90 cm^{-1} and the coupled modes at 245 cm^{-1} and 350 cm^{-1}. The full line is the fit with Eq. 3.

The spin-flip single particle excitations has a narrow peak at an incident photon energy $\hbar\omega_1 = 1.897$ eV. Thus, only optical interband transitions near the $E_o + \Delta_o$ energy gap need to be considered in the theory of this resonance. The scattering efficiency, due to the carrier-density mechanism, can be written as[1,12]

$$\frac{d^2R}{d\omega d\Omega} = (\hat{e}_1 x \hat{e}_2) r_o^2 \frac{\omega_2}{\omega_1} \frac{\hbar[P^2/3m_o]^2}{1-\exp(-\beta\hbar\omega)} \times$$

$$\sum_{\vec{k}} \frac{[f(\vec{k})-f(\vec{k}+\vec{q})]}{|E(\vec{k})-\hbar\omega_1-i\gamma|^2} \delta[e(\vec{k},\vec{q})-\hbar\omega] \qquad (1)$$

where ω_2 is the scattered photon frequency, $\omega=\omega_1-\omega_2$ and $e(\vec{k},\vec{q})$ are the intraband single particle excitation energies of electrons with wavevector $\vec{k}$ and wavevector transfer $\vec{q}$. $E(\vec{k})$ are the $E_o + \Delta_o$ interband energies at $\vec{k}$ and γ their damping, $P/\sqrt{3}$ the interband momentum matrix element. r_o is the classical radius of the electron and m_o the free electron mass. $f(k)$ is the Fermi di-

stribution function, $\beta=1/kT$ and $\hat{e}_1$ and $\hat{e}_2$ are the photon polarization vectors.

Because of the restrictions imposed by the Pauli principle, at T ≈ 0°K the sum in Eq. 1 runs over an interval $q=0.7\times10^6$ cm^{-1} above the Fermi wavevector which, for $n=7\times10^{17}$ cm^{-3}, is $k_F=2.75\times10^6$ cm^{-1}. Thus, because the spin-flip spe energies do not depend on spin, an approximation to Eq. 1 is[13]

$$\frac{d^2R}{d\Omega d\omega}=r_o^2\frac{q^2\hbar}{4\pi e^2}\frac{1}{|E(k_F)-\hbar\omega_1-i\gamma|^2}\times$$

$$\left[\frac{p^2}{3m_o}\right]^2 \mathrm{Im}\epsilon_e(\vec{q},\omega) \qquad (2)$$

where $\epsilon_e(\vec{q},\omega)$ is the electron-gas dielectric function and $E(k_F)$ is the interband energy at k_F. The resonance enhancement of Fig. 1 is described by

$$\Gamma=\frac{A}{(E_G-\hbar\omega_1)^2+\gamma^2} \qquad (3)$$

with A=25 (arbitrary units), $E_G=1.897$ eV and $\gamma=0.013$ eV. This is in reasonable agreement with Eq. 2: from the data of Aspnes and Studna[14] and the conduction and valence band structures of GaAs[15], we calculate $E(k_F)=1.909$ eV. We also find that, for $n=7\times10^{17}$ cm^{-3}, the integrated intensity of scattering by spin-flip spe, for $\hbar\omega_1=E_G$, is ∿ 7×10^2 times larger than TO phonon scattering i.e., $dR/d\Omega \approx 7\times10^2\times12\times10^{-6}$ cm^{-1} = 8×10^{-3} cm^{-1} [16]. This is in reasonable agreement with the value 4×10^{-3} cm^{-1} estimated using Eqs. 1 and 2 and the sum rule for $\mathrm{Im}\epsilon_e(q,\omega)$ [15]. These relatively large intensities indicate that single-particle Raman scattering from charge carriers confined to 50-100Å interface layers should be observable.

We may conclude that the carrier density mechanism gives a good description of resonant Raman scattering by spin-flip spe. However, Eq. 2 is a first-order approximation. The fact that the wavevector dependence of the interband energies E(k) was neglected in writing Eq. 2 is evidenced by the small differences found in the measured line-shapes for different incident photon energies near the peak in the resonance enhancement as shown in Fig. 3.

Figure 3 also displays a fit of the spin-flip single particle lineshape with the Lindhard-Mermin expression for $\mathrm{Im}\epsilon_e(\vec{q},\omega)$ [17]. The work of Davies and Blum[13] suggests that this expression should describe the spin-flip spectra. In the fit of Fig. 2, which is a rather good description of the experimental results, we have used a value of $\Gamma=58$ cm^{-1} for the electron-gas damping parameter. This value of Γ also yields a good fit to the line-

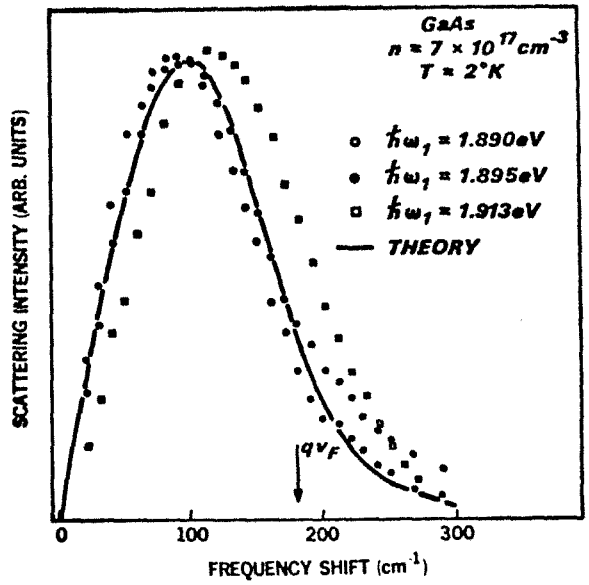

Fig. 3: Resonance Raman spectra by spin-flip single particle excitations for different incident photon energies. The full line is a fit with the Lindhard-Mermin electron-gas dielectric function

shapes of the Raman spectra of coupled longitudinal modes[18].

We can see in Fig. 2 that the resonance enhancement peak of the coupled modes has a width of 0.06 eV indicating a more complex structure than that of the spin-flip spe, possibly with two components. At $\hbar\omega_1=1.90$eV the integrated intensity of spin-flip scattering is about four times larger than that of the two coupled modes. The carrier-density mechanism predicts, at the $E_o+\Delta_o$ resonance, a value of ∿4.5. Although carrier-density scattering by the coupled modes also has a resonance at $\hbar\omega_1\approx E_G+\hbar\omega^{19}$, we estimate that its contribution is about five times smaller than the one at $\hbar\omega_1\approx E_G$. Thus, the larger width of the coupled mode resonance indicates that other processes make an important contribution.

The term due to the Fröhlich mechanism, as measured in undoped GaAs[9], is found to be too small to account for these discrepancies. However, at the $E_o+\Delta_o$ resonance of n-GaAs, the Fröhlich mechanism is enhanced by the presence of carriers which remove in part the cancellation between the contributions of the diagrams of Figs. 1d and 1e[20]. We estimate that this enhanced Fröhlich term is comparable to that of the carrier-density process of Figs. 1c and 1d.

We have seen that there is evidence of resonance processes which do not

conserve wavevector. These are likely to involve impurity-induced Raman scattering by the coupled modes similar to that proposed for LO phonons[21]. Such processes are described by fourth-order perturbation theory in which electron-impurity scattering is one of the intermediate steps. They make a substantial contribution because the damping of the intermediate optical transitions is also determined by the impurity scattering of the electrons[21].

The results obtained from samples with larger carrier concentrations are similar to those just described. The positions of the peaks in the resonance enhancements shift to higher photon energies with increasing carrier concentration. These shifts are largely explained by the change in the Fermi energy of the charge carriers[18].

In summary, we have shown that at the $E_o + \Delta_o$ resonance scattering by the spin-flip single particle electron-gas excitations of n-GaAs is well described by the carrier-density mechanism. In the case of resonance scattering by the collective longitudinal modes the contributions of additional terms, like those due to impurity-induced resonance processes and the carrier-enhanced Fröhlich mechanism, need to be further considered. The light scattering by both types of excitations is strong and the carriers in interface layers $\sim$100 Å wide should be observable.

Acknowledgement

We are grateful to Professor E. Burstein for discussions on this work. One of us (A.P.) would like to thank the Max Planck Institut, where he performed part of this work, for its support.

REFERENCES

1. D.C. HAMILTON and A.L. McWHORTER, in Light Scattering Spectra of Solids, ed. by G.B. Wright (Springer-Verlag, Berlin 1969), p. 309.
2. E. BURSTEIN, A. PINCZUK and S. BUCHNER, Physics of Semiconductors 1978 ed. by B.L.H. Wilson (The Institute of Physics, London 1979), p. 1231.
3. J.F. SCOTT, T.C. DAMEN, R.C.C. LEITE, and J. SHA, Phys. Rev. 1, 4330 (1970).
4. A. PINCZUK, L. BRILLSON, E. BURSTEIN, and E. ANASTASSAKIS, Phys. Rev. Lett. 27, 317 (1971); also Light Scattering in Solids, ed. by M. Balkanski (Flammarion Sciences, Paris 1971), p. 115.
5. H.L. STOERMER, R. DINGLE, A.C. GOSSARD, W. WIEGMAN, and M.D. STURGE, to be published in Solid State Commun.
6. A. MOORADIAN, in Advances in Solid State Physics, Vol. 9, ed. by H.J. Queisser (Pergamon-Vieweg, Oxford and Braunschweig, 1969), p. 74.
7. M.V. KLEIN, in Light Scattering in Solids, ed. by M. Cardona (Springer-Verlag, Berlin-Heidelberg, 1975), p. 147.
8. R. LOUDON, Adv. in Physics 13, 423 (1964).
9. R. TROMMER and M. CARDONA, Phys. Rev. B17, 1865 (1978).
10. A. PINCZUK, G. ABSTREITER, R. TROMMER and M. CARDONA, Solid State Commun. 21, 959 (1977).
11. S. BUCHNER and E. BURSTEIN, Phys. Rev. Lett. 33, 908 (1974).
12. S.S. JHA, Phys. Rev. 179, 764 (1969).
13. R.W. DAVIES and F.A. BLUM, Phys. Rev. B3, 3321 (1971).
14. D.E. ASPNES and A.A. STUDNA, Phys. Rev. B7, 4605 (1973).
15. M. CARDONA, in Atomic Structure and Properties of Solids, ed. by E. Burstein (Academic Press, New York, 1972), p. 514.
16. The value of the efficiency for TO scattering at $E_o + \Delta_o$, $dR/d\Omega = (12\pm1) \times 10^{-6}$ cm^{-1} has been recently determined by D. Olego, M. Grimsditch, and M. Cardona, to be published (at room temperature).
17. N.D. MERMIN, Phys. Rev. B1, 2362 (1970).
18. G. ABSTREITER, R. TROMMER, A. PINCZUK and M. CARDONA, to be published.
19. This term can be calculated from the diagram in Fig. 1c.
20. E. BURSTEIN, private communication.
21. A.A. GOGOLIN and A.E. RASHBA, in Proc. of the 13th Conf. on the Physics of Semiconductors, ed. by F.G. Fumi (Tipografia Marves, Rome, 1976), p. 284.

VOLUME 42, NUMBER 19 PHYSICAL REVIEW LETTERS 7 MAY 1979

Inelastic Light Scattering from a Quasi-Two-Dimensional Electron System in GaAs-$Al_xGa_{1-x}As$ Heterojunctions

Gerhard Abstreiter
Max-Planck-Institut für Festkörperforschung, Hochfeld-Magnetlabor, 38042 Grenoble Cédex, France

and

Klaus Ploog
Max-Planck-Institut für Festkörperforschung, 7000 Stuttgart 80, Federal Republic of Germany

(Received 21 December 1978; revised manuscript received 28 March 1979)

Resonance enhanced inelastic light scattering from a quasi-two-dimensional electron gas confined at the interface of abruptly doped GaAs/*n*-$Al_xGa_{1-x}As$ heterojunctions has been measured. The samples were fabricated using molecular-beam epitaxy with a high-contrast doping technique. The results show strong evidence for intersubband excitations in a two-dimensional electron system.

We report the observation of resonant Raman scattering from a quasi-two-dimensional electron system which is confined at the interface of GaAs/*n*-$Al_xGa_{1-x}As$ heterojunctions. The experiments were performed in backscattering geometry using an exciting laser frequency at resonance with the $E_0+\Delta_0$ energy gap of GaAs. Recently it has been shown that at this resonance one can observe free-carrier excitations with electron densities as low as about 1×10^{11} cm^{-2}.[1] It has also been suggested that the resonance enhancement of the carrier-density light-scattering mechanism

should enable one to observe electron-gas excitations at semiconductor surfaces and interfaces.[2]

The existence of two-dimensional electron-gas systems at certain GaAs/$Al_xGa_{1-x}As$ heterostructures has been demonstrated in a recent publication.[3] High mobility of electrons in heterojunction superlattices has been achieved using a modulation doping technique during growth with molecular-beam epitaxy.[4] The heterojunctions studied in the present work are fabricated by a similar technique. The samples consist of a thick $Al_xGa_{1-x}As$ layer covered by a thin GaAs layer grown successively on a nominally undoped (100) GaAs substrate. The $Al_xGa_{1-x}As$ layers, with typical values $x \simeq 0.20$, are intentionally doped either with Sn or with Ge. Doping levels of the order of $n \simeq 1 \times 10^{18}$ cm^{-3} are easily achieved. The doping source is terminated abruptly synchronous with the Al source.

Using Sn impurities, a segregation at the $Al_xGa_{1-x}As$ surface is observed,[5] which causes a smearing out of the dopant into the GaAs layer yielding heavily doped n-GaAs. Abrupt profiles are obtained with Ge impurities. However, because of a "memory effect" some Ge is incorporated in the GaAs layer. Therefore, although diffusion can be neglected at the growth temperature of 550°C, the GaAs layers of Ge-doped samples have a carrier concentration of $n \simeq 10^{17}$ cm^{-3}.

The Al concentration of the order of 20% results in a band-edge discontinuity of about 200 meV. The donor binding energy in $Al_xGa_{1-x}As$ is assumed to be much smaller than this value. The conduction-band edge of GaAs therefore lies lower than the impurity states in $Al_xGa_{1-x}As$. The electrons from the donors will move into the GaAs layer and form an accumulation layer close to the interface. The $Al_xGa_{1-x}As$ layer will be depleted towards the interface. This behavior of the conduction and valence bands is shown schematically in Fig. 1(a). At the surface of n-GaAs there exists a depletion layer which is caused by a Fermi-level pinning about 1 eV below the conduction-band edge. The width of this depletion layer depends on the carrier concentration.

At the GaAs/$Al_xGa_{1-x}As$ interface the charge carriers are confined in a one-dimensional potential well, similar to an accumulation layer in metal-oxide-semiconductor structures. The electrons are bound perpendicular to the interface. For an isotropic conduction band the energy eigenstates are given by

$$\epsilon_i(k) = \epsilon_i + \hbar^2 k_\parallel^2 / 2m^* \quad (i = 0, 1, 2, \ldots),$$

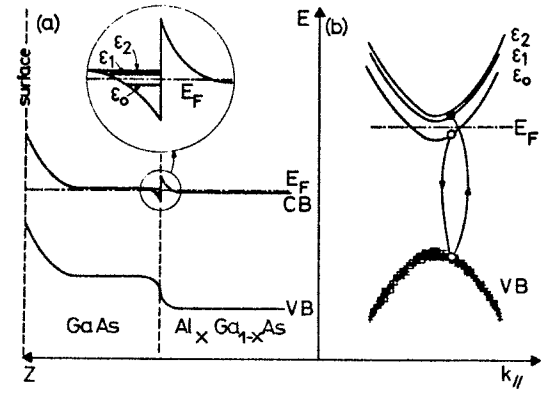

FIG. 1. (a) Energy-band disgram for abrupt GaAs/n-$Al_xGa_{1-x}As$ heterojunction. The conduction-band behavior at the interface is enlarged. ϵ_0, ϵ_1, and ϵ_2 denote the bottom of the electric subbands in the one-dimensional potential well. (b) Possible intersubband excitation process in a two-dimensional electron system. The valence band is shaded indicating the band bending towards the interface.

where the first term denotes the bottom of the electric subbands and the second one the free energy parallel to the interface. m^* is the effective mass of the electrons and $k_\parallel$ the wave vector parallel to the interface. For accumulation layers in silicon the energy values ϵ_i have been calculated self-consistently, for example, by Stern[6] and Ando.[7] Spectroscopic studies at far infrared frequencies[8] are in reasonable agreement with such calculations and demonstrate that many-body interactions play an important role.

Self-consistent calculations of the subband splitting in GaAs accumulation layers are not yet available. The energy separation $\epsilon_1 - \epsilon_0$ depends on various properties of the heterojunctions as there are the band-gap discontinuity (Al concentration), the acceptor and donor concentration in the GaAs layer, the density of the interface states, and the number of free carriers in the accumulation channel. We want to demonstrate that inelastic light scattering can be used to determine some of these parameters as well as the subband splitting in the accumulation layer itself.

Raman scattering of free carriers in GaAs has been proven to be a useful technique to study single-particle and collective excitations.[1] The selection rules and scattering mechanisms have been discussed by Mooradian.[9] The present work concentrates on single-particle excitations which involve spin flip. Spectra of this type from bulk carriers in n-GaAs have been reported, for ex-

ample, in Ref. 1. The spin-flip single-particle excitations are antisymmetric. The polarization of the scattered light is perpendicular to the polarization of the incident light. The scattering cross section is strongly enhanced at the $E_0+\Delta_0$ energy gap.[1]

Burstein, Pinczuk, and Buchner[2] have discussed the possibility of resonant inelastic light scattering by charge carriers in quasi-two-dimensional systems. The scattering process for a two-step single-particle excitation involving spin flip is shown schematically in Fig. 1(b). The valence band is smeared out indicating a band bending towards the interface. The conduction band is split into the subbands ϵ_i. In true backscattering geometry the scattering wave vector parallel to the interface is zero. The three-dimensional single-particle excitation spectrum transforms into intersubband excitations. The frequency shifts of the observed peaks directly correspond to the energy separation of the subbands.

Figure 2 displays a set of Raman spectra obtained of a GaAs/n-$Al_xGa_{1-x}As$ heterojunction. The sample consists of a highly doped n-$Al_xGa_{1-x}As$ layer and a 1500-Å-thin GaAs layer grown subsequently on a nomially undoped GaAs substrate. A semitransparent gate electrode (Ni) has been evaporated onto the thin GaAs layer. The exciting laser line was chosen to be close to the $E_0+\Delta_0$ energy gap of GaAs. At this wavelength the penetration depth in GaAs is about 3000 Å. Spectrum a is obtained in the $z(yy)\bar{z}$ backscattering configuration; the polarization of the incident and scattered light are parallel to each other. In this configuration spin-flip, single-particle excitations are not allowed. Instead we observe resonance-enhanced collective excitations (coupled plasmon–LO-phonon modes L_- and L_+ from bulk GaAs) and the pure LO-phonon modes of GaAs (LO) and $Al_xGa_{1-x}As$ (LO_1 and LO_2). This spectrum is used to characterize the sample. From the position of LO_1 and LO_2 we determine $x=0.20$.[10] The L_- and L_+ modes are sensitive to the bulk carrier concentration of the GaAs layer.[10] In the presently studied sample we find $n=2\times10^{17}$ cm^{-3}. The LO mode originates from the depletion layer at the GaAs surface, which is of the order of 800 Å wide. The results obtained in $z(xy)\bar{z}$ configuration are shown in Fig. 2, spectra b. In this configuration we observe resonance-enhanced single-particle excitations similar to the work of Ref. 1. The single-particle excitation band of bulk carriers cuts off

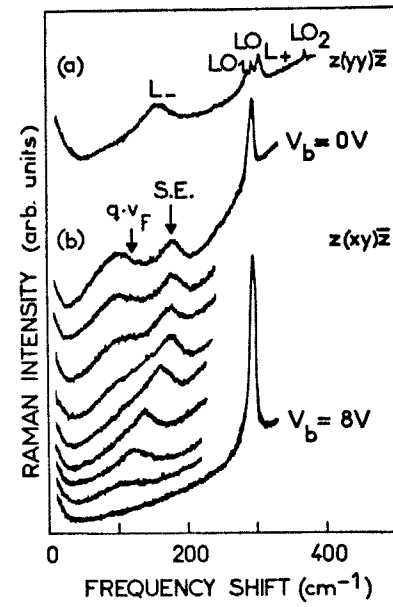

FIG. 2. Raman spectra in two scattering configurations of a GaAs/n-$Al_{0.20}Ga_{0.80}As$ heterostructure at $T=2$ K. The exciting laser frequency is $\lambda_0=6471$ Å (1.92 eV). V_b is the voltage applied across a Ni Schottky barrier in backward direction. The voltage steps in the spectra shown in b is $\Delta V=1$ V. The peak labeled S.E. is interpreted as subband excitation of the electron accumulation layer at the interface (see discussion in the text).

around $\vec{q}\cdot\vec{v}_F\simeq120$ cm^{-1}, where q is the scattering wave vector ($\simeq0.7\times10^6$ cm^{-1}) and v_F the Fermi velocity. In addition to the bulk single-particle scattering we observe the LO-phonon mode of the GaAs depletion layer (295 cm^{-1}) and a third peak at 180 cm^{-1} (labeled S.E.). We believe that this peak is caused by single-particle subband excitations (S.E.) of the two-dimensional electron gas confined at the GaAs/$Al_{0.20}Ga_{0.80}As$ interface.

This interpretation becomes more evident when one studies the voltage dependence of the spectrum (Fig. 2, spectra b). A voltage V_b applied in a backward direction across the Schottky barrier increases the depletion width. Therefore the bulk single-particle excitation peak decreases in intensity and vanishes at $V_b>3$ V. The intensity of the LO-phonon mode of the surface depletion region increases, while the subband excitation peak remains unchanged. A further increase of V_b, however, results in a shift of the band at 180 cm^{-1} to smaller wave numbers and to a decrease in intensity. It disappears completely when $V_b>7$ V.

Then the accumulation layer at the interface is also depleted. The voltage which is necessary to empty the accumulation channel depends on the power of the incident laser radiation. This is due to the screening of the depletion field by the excited photocarriers in the GaAs layer. Extrapolating the voltage to zero laser power we determine the carrier concentration in the accumulation layer $n_s \simeq 1.2 \times 10^{12}$ cm^{-2} at $V_b = 0$ V. This is in reasonable agreement with the value estimated from the doping level of the n-$Al_{0.20}Ga_{0.80}As$ layer and the barrier height at the interface ($n_s \simeq 1.5 \times 10^{12}$ cm^{-2}).

We have also studied samples with thinner GaAs layers. For $d_{GaAs} < 1000$ Å we do not observe any scattered light from bulk carriers because the natural depletion layer eliminates all except the accumulation layer electrons. The subband excitation peak disappears when $d_{GaAs} < 400$ Å. These results exclude the $Al_xGa_{1-x}As$ layer and the GaAs substrate as possible sources of the scattered light observed in thicker GaAs layers. In samples with higher Al concentration ($x = 0.36$ and 0.56) the subband excitation peak is shifted to smaller wave numbers (80–110 cm^{-1}). The lattice mismatch between GaAs and $Al_xGa_{1-x}As$ gets larger when x is increased. Therefore probably more carriers are trapped in interface states, which results in a smaller subband splitting.

Further evidence that the observed peaks are caused by the two-dimensional electron system is the resonance behavior of the scattering intensity. Plotting this intensity versus laser excitation energy, we find that the resonance enhancement peak of the subband excitations is about 10 times wider than the resonance of the single-particle excitations of bulk carriers. This is explained by the band bending of the valence band towards the interface (see Fig. 1). The half-width of the resonant subband excitation peak of the sample studied most extensively (Fig. 2) is 120 meV and the peak position is 1.91 eV.

In summary, we have demonstrated that under resonance conditions it is possible to observe inelastic light scattering from a quasi-two-dimensional electron system. This is the first observation of subband excitations using Raman spectroscopy. For a quantitative analysis of the experimental data one needs self-consistent calculations of the subband splittings which are not available so far. Effects on the line shape due to impurity-induced subband excitations with finite $k_\parallel$ should also be considered in such an analysis. The measurements reported here promise to be a useful tool in studying both single-particle and collective excitations of various space-charge layers and heterojunction superlattices which are of technological and fundamental interest.

We would like to acknowledge the expert help in sample preparation of A. Fischer and the assistance in performing the Raman scattering experiments of M. Berger and A. Köhler. One of us (G.A.) wants to mention useful and stimulating discussions with M. Cardona, G. Döhler, and A. Pinczuk. Part of the work was supported by the Bundesministerium für Forschung und Technologie of the Federal Republic of Germany.

[1]A. Pinczuk, G. Abstreiter, R. Trommer, and M. Cardona, to be published.

[2]E. Burstein, A. Pinczuk, and S. Buchner, in Proceedings of the Fourteenth International Conference on the Physics of Semiconductors, Edinburgh, 1978 (to be published).

[3]H. L. Störmer, R. Dingle, A. C. Gossard, W. Wiegmann, and M. D. Sturge, to be published.

[4]R. Dingle, H. L. Störmer, A. C. Gossard, and W. Wiegmann, Appl. Phys. Lett. 33, 665 (1978).

[5]K. Ploog and A. Fischer, J. Vac. Sci. Technol. 15, 255 (1978).

[6]F. Stern, Phys. Rev. Lett. 33, 960 (1974).

[7]T. Ando, Phys. Rev. B 13, 3468 (1976).

[8]P. Kneschaurek, A. Kamgar, and F. Koch, Phys. Rev. B 14, 1610 (1976).

[9]A. Mooradian, in *Advances in Solid State Physics, Vol. 9*, edited by H. J. Queisser (Pergamon-Vieweg, Oxford and Braunschweig, 1969), p. 74.

[10]G. Abstreiter, E. Bauser, A. Fischer, and K. Ploog, Appl. Phys. 16, 345 (1978).

Surface Science 98 (1980) 117–125

ELECTRONIC PROPERTIES OF THE TWO-DIMENSIONAL SYSTEM AT $GaAs/Al_xGa_{1-x}As$ INTERFACES

Gerhard ABSTREITER *
Max-Planck-Institut für Festkörperforschung, Hochfeldmagnetlabor, F-38042 Grenoble Cédex, France.

Received 27 July 1979; accepted for publication 16 October 1979

At the interface of GaAs/n-$Al_xGa_{1-x}As$ heterostructures charge carriers are transferred from the donors in $Al_xGa_{1-x}As$ into the conduction band of GaAs where they form a quasi-two-dimensional electron layer. The carrier confinement at the interface is demonstrated by Shubnikov–De Haas measurements. Resonant inelastic light scattering from the two-dimensional electron gas is a direct measure of the subband splitting in the space charge layer. The results are compared with recent self-consistent calculations.

1. Introduction

The large interest in the electronic properties of semiconductor surfaces and interfaces have been motivated by the development of solid state electronics. Apart from the technological importance, however, space charge layers are also very interesting physical systems. Considerable work has been done during the past ten years studying space charge layers which are created by a strong electric field applied perpendicular to the surface of semiconductors (for example using a metal–insulator–semiconductor arrangement) [1]. Natural inversion layers at the surface of certain semiconductors can also be achieved by chemical treatments [2]. The quasi-two-dimensional character and the possibility of varying the carrier density easily has attracted both experimental and theoretical physicists.

Very recently it has been shown, that one also can achieve a natural channel of charge carriers at the sharp interface of two semiconductors with different band gap energies [3–5]. The GaAs/n-$Al_xGa_{1-x}As$ system has been studied most extensively. The band gap in $Al_xGa_{1-x}As$ is larger than in GaAs. It was found that the potential barrier at the interface occurs mainly in the conduction band (~85% of the total difference of the band gap energies) [6]. Therefore it is possible that charge carriers are transferred from the donors of the $Al_xGa_{1-x}As$ layer into the energetically lower conduction band of GaAs. The $Al_xGa_{1-x}As$ layer will be depleted towards the interface, while the electrons are accumulated in the GaAs

* Now at Technische Universität München, D-8046 Garching, FRG.

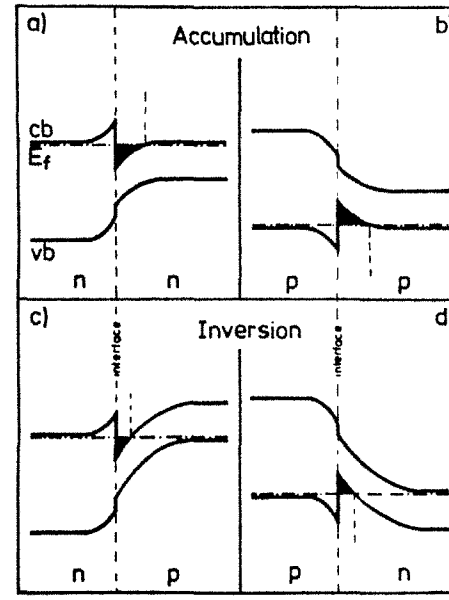

Fig. 1. Four different possible space charge layers at the interface of two semiconductors with different band gap energies: (a) n-accumulation, (b) p-accumulation, (c) n-inversion, (b) p-inversion). The carrier confinement occurs in the semiconductor with the smaller band gap.

layer. Such a charge transfer is caused by the matching of the Fermi level of the two materials at the interface.

In fig. 1, the behaviour of the conduction and valence band is shown schematically for four different types of interfaces. To achieve an n-channel, the barrier height has to be large in the conduction band – (a) and (c) in fig. 1. For p-type channels a large discontinuity of the valence band potential is necessary – (b) and (d) in fig. 1. If both materials are either n or p-type, an accumulation layer will be formed – (a) and (b). A change of the doping character from n to p at the interface results in an inversion layer – (c) and (d). The examples (a) and (c) in fig. 1 are typical for $GaAs/Al_xGa_{1-x}As$ heterojunctions. In the present work, the electronic properties of $n\text{-}GaAs/n^+\text{-}Al_xGa_{1-x}As$ will be discussed. Such systems have been studied using both magnetotransport and optical techniques.

2. Sample preparation and characterization

The samples are grown by molecular beam epitaxy [7]. They consist of a thick $Al_xGa_{1-x}As$ layer covered by thin GaAs layer grown successively on a nominally

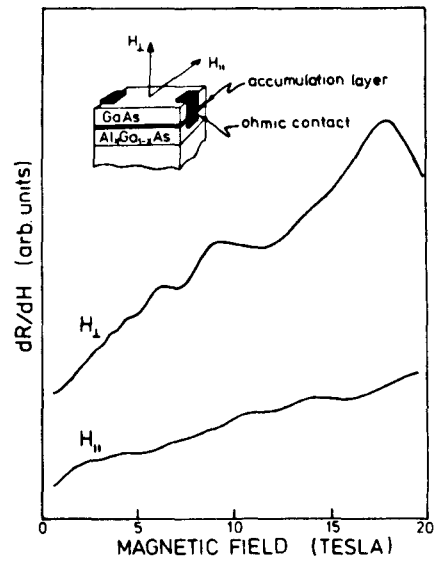

Fig. 2. First derivative of the transverse magnetoresistence a n-GaAs/n^+-$Al_xGa_{1-x}As$ heterostructure with the magnetic field parallel and perpendicular to the interface. The insert shows the sample arrangement.

undoped or Cr^+ doped (100) GaAs substrate. The $Al_xGa_{1-x}As$ layers have values of x ranging from 0.18 to 0.56 and are intentionally doped either with Sn, Ge or Si. The impurity concentrations are of the order of $\sim 1 \times 10^{18}$ cm^{-3}. The doping source is terminated abruptly together with the Al source. Sharp doping profiles at the interface could be achieved only with Ge and Si impurities. Sn impurities show a segregation at the surface and thus are smeared out into the GaAs layer. Because of a "memory" effect, however, the GaAs layer turns out to be slightly n-type even with Ge and Si dopants. The growth temperature was 550°C. Ohmic contacts to the layers have been prepared with In. The sample arrangement is shown schematically in the insert of fig. 2.

In order to prove that a two-dimensional accumulation layer exists at the interface, we have performed Shubnikov–De Haas measurements similar as reported recently by other authors [4,5]. Fig. 2 shows the first derivative of the transverse magneto-resistance of an n-GaAs/n^+-$Al_xGa_{1-x}As$ heterojunction at $T = 4.2$ K. In this sample $x = 0.18$ was determined by Raman spectroscopy [8]. The thickness d(GaAs) = 1500 Å. As shown in the insert the magnetic field H is applied perpendicular to the direction of the electric current. The top curve is the result for H perpendicular to the interface. The oscillatory behaviour observed in this configuration is periodic in $(1/H)$. With magnetic field applied parallel to the interface these oscillations disappear. This directly demonstrates the existance of a two-dimen-

sional electron gas in the system. From the oscillation period we determine the electron concentration in the accumulation channel $n_s = 0.9 \times 10^{12}$ cm^{-2}.

With H parallel to the interface, we also find a weak oscillatory behaviour of the magnetoresistance. Two periods can be extracted from the data. A careful study of these oscillations show that they are independent of the orientation of the magnetic field. Therefore they are probably caused by three-dimensional carriers in the heterostructure sample. Evaluating the period at small fields (up to 8 Tesla) with an effective mass of bulk electrons in GaAs (0.067 m_0), we find a three-dimensional carrier concentration n(GaAs) = 1.4×10^{17} cm^{-3}. From the coupled LO–phonon–plasmon modes observed with resonant Raman scattering in the GaAs layer [3,8], we determine n(GaAs) = 1.6×10^{17} cm^{-3}. This is in very good agreement with the value obtained from Shubnikov–De Haas oscillations. Therefore we believe that the oscillation period observed at low magnetic fields is caused by the three-dimensional electron gas in the top 1500 Å thick GaAs layer.

The weak oscillations observed at high fields are also independent of the direction of the magnetic field. They are only present in samples with $x \leqslant 0.30$. An interpretation of the data with $m^* = 0.067\ m_0$ leads to a carrier concentration of $n = 1.6 \times 10^{18}$ cm^{-3}. We assume that these oscillations are caused by carriers in the $Al_xGa_{1-x}As$ layer. The effective mass in $Al_xGa_{1-x}As$, however, increases with x compared to the mass in pure GaAs. Therefore the actual carrier concentration $n(Al_xGa_{1-x}As) < 1.6 \times 10^{18}$ cm^{-3} in the sample discussed. In thin $Al_xGa_{1-x}As$ layers with $x \approx 0.20$ we find that the mobility is reduced only by about 50% compared to GaAs layers with similar impurity concentrations. If the Al concentration $x > 0.30$, the mobility probably is too small to observe Shubnikov–De Haas oscillations up to 20 Tesla.

3. Inelastic light scattering

A completely different method for studying the properties of GaAs/$Al_xGa_{1-x}As$ heterostructures and space charge layers is Raman spectroscopy. Resonant Raman scattering has been used to study the single particle excitations of electrons in n-GaAs [9]. Recently it has been proposed [10], and shortly after verified [3], that the resonance enhancement of free-carrier excitations is strong enough to observe inelastic light scattering from a two-dimensional plasma confined at the surface or interface of a semiconductor. A possible scattering process is shown in fig. 3. In our experiments the exciting laser line was chosen to be in resonance with the energy difference of the conduction band and the split off valence band at the Γ-point of GaAs. Because of the band bending in the space charge region the valence band is smeared out. Therefore the resonance condition is fulfilled over a wider range of energies. The conduction band is split into electric subbands in which the carriers are bound perpendicular to the interface while they are free parallel to it. In our highly doped samples (n(GaAs) $\simeq 1 \times 10^{17}$ cm^{-3}) the Fermi level lies already a few

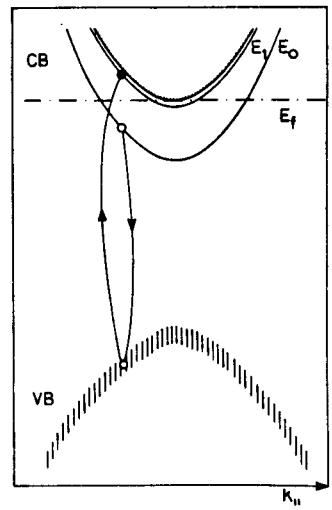

Fig. 3. Possible scattering mechanism for single particle subband excitations in the accumulation layer. The valence band is shaded indicating the band bending towards the interface. The conduction band is split into the electric subbands E_0 and E_1. The hatched curve indicates the conduction band in bulk GaAs. E_F is the Fermi energy.

meV above conduction band edge in the bulk. In fig. 3 two electric subbands E_0 and E_1 are drawn below the Fermi energy E_F. As we will discuss later, the light scattering experiments indicate the occupation of a second subband. Very recent self-consistent calculations of the subband energies in such systems also find two subbands below the Fermi energy [11].

The Raman experiments have been performed in back scattering geometry. The set-up is shown schematically in fig. 4. The subband excitations were observed in $x(yz)\bar{x}$ scattering configuration [3]. The selection rules for different scattering mechanisms are discussed in ref. [10]. The samples could be cooled to $T = 2$ K. The exciting laser light was provided by a dye-laser pumped with an Ar^+ ion laser. The back scattered light was analyzed in a double grating spectrometer together with conventional pulse counting equipment.

As shown in ref. [3] it is possible to separate the signals of bulk carriers from the scattered light of the accumulatoin layer by applying an electric field across a Schottky barrier in a way to deplete the whole GaAs layer. Here we want to present different results which also allow to separate the different contributions. In fig. 5 it is shown how the Raman spectrum of the sample, discussed extensively in ref. [3], changes with the laser excitation wavelength. For this sample, we find a carrier concentration of $n_s = 1.05 \times 10^{12}$ cm^{-2}. The single particle excitation (labelled S.P.) of bulk carriers can be observed only in a narrow region of laser wave lengths around $\lambda_0 = 6500$ Å. The subband excitation peak E_{10} is observed in a much wider range of

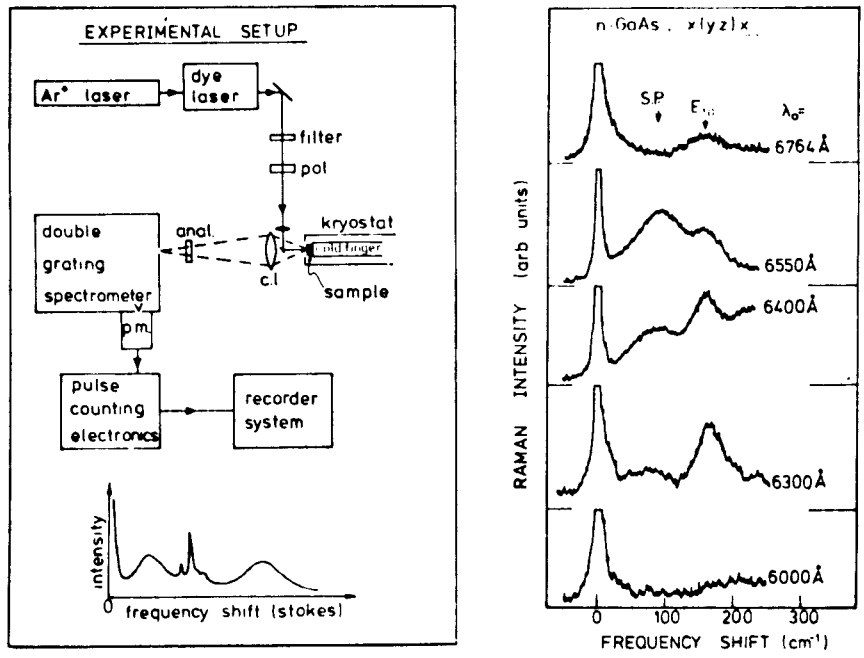

Fig. 4. Experimental set-up for inelastic light scattering in back scattering geometry. c.l. is the collecting lense and p.m. the photomultiplier.

Fig. 5. Raman spectra of a GaAs/n-$Al_xGa_{1-x}As$ heterojunction at different excitation laser wavelengths. S.P. denotes the single particle excitation of the bulk carriers, E_{10} is the subband excitation in the accumulation layer.

excitation lines. As mentioned already, this is caused by the band bending towards the interface, which smears out the valence band and thus also the resonance condition. The subband excitation E_{10} is found to be around 180 cm^{-1} in this sample.

Another possibility to separate bulk scattering from interface signals is shown in fig. 6. The Raman spectra of three essentially similar samples obtained with λ_0 = 6471 Å at T = 10 K are shown. In the $Al_xGa_{1-x}As$ layer in these samples, x is larger than 0.30, while the doping of the layers is like the samples discussed above. The GaAs layers have thickness ranging from d(GaAs) = 200–1500 Å. From Shubnikov–De Haas measurements in the samples with thicker GaAs layers we find a carrier concentration $n_s \simeq (0.4–0.5) \times 10^{12}$ cm^{-2}. The subband excitation peak lies in the region 70–100 cm^{-1}. In the sample with d(GaAs) = 1500 Å we could observe both the single particle excitations of the bulk and the subband excitation E_{10}. With d(GaAs) = 800 Å the natural depletion layer eliminates all except the accumulation layer electrons. Only the subband excitations are observed. In very thin sam-

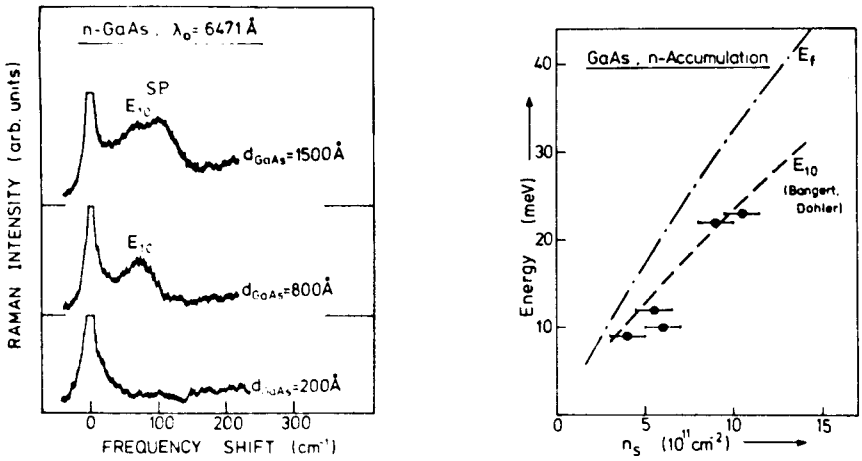

Fig. 6. Raman spectra of three heterostructures with different thickness of the top GaAs layer.

Fig. 7. Energy separation E_{10} versus carrier concentration. The points are experimentally obtained from Raman spectroscopy and Shubnikov–De Haas oscillations. The dashed curve is the theoretical subband splitting according to ref. [11]. The dash-dotted line is the Fermi energy assuming only one subband to be occupied and a non-parabolic effective mass.

ples, $d(\mathrm{GaAs}) = 200$ Å, also the accumulation layer is depleted. Thus, no free carriers could be detected.

In fig. 7 we have plotted the energy separations E_{10} of five different samples as measured with Raman spectroscopy against the carrier concentration in the accumulation channel which were determined from Shubnikov–De Haas oscillations. E_{10} increases from $\simeq 9$ meV at $n_s = 0.4 \times 10^{12}$ cm^{-2} to $\simeq 23$ meV at $n_s \simeq 1.05 \times 10^{12}$ cm^{-2}. These values are smaller than the Fermi energy E_F calculated from the carrier density n_s and the effective mass of bulk carriers in GaAs. The dash-dotted line in fig. 7 is the result for E_F assuming only one electric subband to be occupied. The effective mass was varied with n_s as estimated from the non parabolicity of the conduction band in GaAs. If only one subband is occupied, the measured value E_{10} should be about equal to E_F. The fact that the experimental points fall below the Fermi energy indicates that a second subband is occupied in the accumulation layers. Bangert and Döhler [11] recently have performed self-consistent calculations of the subband energies in such systems. They also find a second subband to be occupied. Their results for the energy separation E_{10} is given by the dashed line in fig. 7. It agrees very well with the experimental points.

This good agreement, however, might be fortuitous. The experimental results are obtained from various samples with different barrier heights at the interface ($0.18 \leq x \leq 0.56$) while in the calculations a fixed barrier height of 350 meV was

used. The second subband could not be observed in our Shubnikov–De Haas measurements. An occupation of a second subband, however, also means that the total density of carriers in the accumulation layer is larger, the experimental points have to be shifted slightly. Nevertheless there seems to be strong evidence that a second subband is occupied in the accumulation layers of GaAs even at very small electron densities.

In summary, we have shown that inelastic light scattering is a useful technique to study accumulation layers confined at the interface of $GaAs/Al_xGa_{1-x}As$ heterojunctions. The subband splitting determined with such measurements will not be obscured by effects of dielectric screening like in direct infrared absorption experiments. However, it is not yet clear to what amount excitations with finite wave vector parallel to the interface play a role in the linewidth and position of the observed peaks. Such excitations might be induced by the relatively large number of impurities present at the interface. The linewidth of the subband excitations are relatively large and do not change much with temperature up to $T = 80$ K. This indicates an inhomogeneous broadening. Not yet fully understood is the behaviour with applied electric field as discussed in ref. [3]. There is no clear correlation between the applied voltage across the Schottky barrier and the decrease of the carrier density in the accumulation channel. The shift of E_{10} to smaller energies also needs further consideration. Another discrepancy is found in the actually observed carrier concentration n_s and the number expected from the barrier height and the doping level in $Al_xGa_{1-x}As$. Some of the missing carriers probably occupy a second subband. This, however, does not account for all, especially when the Al concentration in the sample is large. We assume that interface states also play an important role.

The few experiments discussed above show that it is possible to create a two-dimensional electron system at the interface of two semiconductors and that such systems can be studied with resonant inelastic light scattering. The obtained results promise that this type of measurements will be applied to study electronic properties of various space-charge layers confined at semiconductor surfaces and interfaces.

Acknowledgements

This work is the result of a collaborative effort during the past year at the Max-Planck-Institut für Festkörperforschung, Stuttgart, and the Hochfeldmagnetlabor in Grenoble. In particular I wish to thank K. Ploog and A. Fischer who have produced and characterized the excellent samples with their molecular beam epitaxy apparatus. My thanks also go to G. Döhler and E. Bangert for their valuable theoretical contributions which they provided to me prior to publication, M. Berger, A. Köhler and G. Siegle for their technical assistance, and D.C. Tsui for a critical reading of the manuscript.

References

[1] See, for example, Surface Sci. 73 (1978).
[2] Natural accumulation layers in ZnO have been reported, for example by D. Eger, A. Many and Y. Goldstein, Surface Sci. 58 (1976) 18.
[3] G. Abstreiter and K. Ploog, Phys. Rev. Letters 42 (1979) 1308.
[4] H.L. Störmer, R. Dingle, A.C. Gossard, W. Wiegmann and M.D. Sturge, Solid State Commun. 29 (1979) 705.
[5] D.C. Tsui and R.A. Logan, Appl. Phys. Letters (July 1979).
[6] R. Dingle, in: Festkörperprobleme, Vol. 15, Ed. H.J. Queisser (Pergamon–Vieweg, Braunschweig, 1975) p. 21.
[7] The samples were prepared by K. Ploog and A. Fischer at the Max-Planck-Institut für Festkörperforschung in Stuttgart. This work is sponsored by the Bundesministerium für Forschung and Technologie.
[8] G. Abstreiter, E. Bauser, A. Fischer and K. Ploog. Appl. Phys. 16 (1978) 345.
[9] A. Pinczuk, G. Abstreiter, R. Trommer and M. Cardona, Solid State Commun. 30 (1979) 429.
[10] E. Burstein, A. Pinczuk and S. Buchner, in: Physics of Semiconductors, 1978, Ed. B.L.H. Wilson (The Institute of Physics, London 1979) p. 1231.
[11] E. Bangert and G.H. Döhler, private communication;
E. Bangert and G.H. Döhler, to be published.

VOLUME 47, NUMBER 12 PHYSICAL REVIEW LETTERS 21 SEPTEMBER 1981

Observation of Tunable Band Gap and Two-Dimensional Subbands in a Novel GaAs Superlattice

G. H. Döhler, H. Künzel, D. Olego, K. Ploog, P. Ruden, and H. J. Stolz
Max-Planck-Institut für Festkörperforschung, D-7000 Stuttgart 80, Federal Republic of Germany

and

G. Abstreiter
Physik Department, Technische Universität München, 8046 Garching, Federal Republic of Germany
(Received 16 June 1981)

Luminescence and Raman measurements on a new type of superlattice consisting of n- and p-type doped GaAs layers grown by molecular-beam epitaxy confirm crucial predictions of theory. A strongly tunable energy gap is found in luminescence. Raman experiments provide the first observation of electronic subbands in purely space-charge-induced quantum wells. A combined analysis of the luminescence and Raman data yields excellent agreement with self-consistent subband calculations based only on the design parameters of the sample.

PACS numbers: 73.40.Lq, 78.55.Ds, 78.30.Gt

In this Letter we provide definite experimental evidence for the validity and applicability of basic ideas of a new type of artificial semiconductor superlattice which consists of ultrathin n- and p-type doped layers, possibly separated by intrinsic layers, of the same semiconducting material ("n-i-p-i" crystals).[1] Compared with the well-known compositional superlattices AlAs-GaAs[2] or InAs-GaSb[3] these doped superlattices exhibit novel electronic properties which result from a very efficient spatial separation between electron and hole subbands (indirect gap in real space) by the periodic space-charge potential. This separation implies recombination lifetimes which may be increased by many orders of magnitude over those of bulk material. Consequently, large deviations of the electron and hole concentration from thermal equilibrium are metastable under weak excitation conditions. In addition, the space-charge-induced superlattice potential itself is strongly affected by a variation of the electron and hole concentration, e.g., by photoexcitation or carrier injection. The effective energy gap of a n-i-p-i crystal as well as the structure of the two-dimensional (2D) subbands should thus no longer be fixed material parameters but tunable quantities.

The n-i-p-i superlattice configuration used for the present investigations was grown by molecular-beam epitaxy.[4] It consists of twenty n (Si) and p (Be) doped GaAs layers with equal doping concentrations $n_D = n_A = 1 \times 10^{18}$ cm^{-3} deposited on a (100) semi-insulating substrate. The individual layer thickness is $d_n = d_p = 40$ nm.

The concept of a tunable energy gap in this n-i-p-i superlattice was first examined by photoluminescence (PL) measurements with the sample cooled to 4.2 K. Various laser lines of a Kr^+-gas laser with either slit or point focus on the (100) surface of the sample were used as excitation source. Four PL spectra for $\lambda_L = 676.4$ nm as a function of the excitation intensity I^{exc} are shown in Fig. 1. For high I^{exc} the asymmetric PL spectrum approaches the direct-band-gap energy of GaAs. A strong redshift of about 200 meV is found with stepwise reduction of I^{exc} down to values of a few watts per square centimeter, where we reached the detectability limit of our experimental setup.

In order to obtain direct information on the expected quantization and subband structure in this GaAs n-i-p-i superlattice we additionally performed resonant inelastic light scattering experiments in backscattering geometry from the (100) surface of the sample. This technique has been

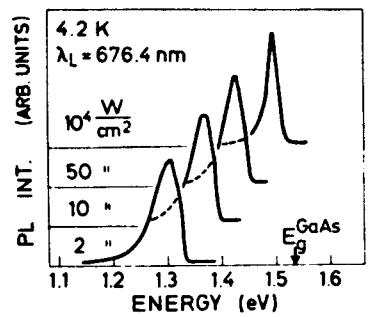

FIG. 1. Photoluminescence spectra of a GaAs n-i-p-i superlattice with $n_D = n_A = 10^{18}$ cm^{-3} and $d_n = d_p = 40$ nm as a function of the laser excitation intensity.

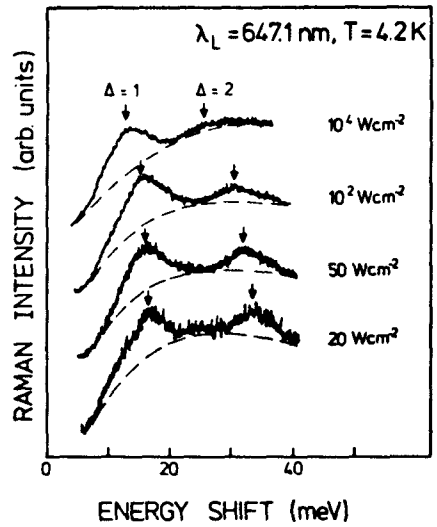

FIG. 2. Single-particle excitation spectra of the studied GaAs n-i-p-i superlattice observed with resonant Raman scattering for different laser excitation intensities.

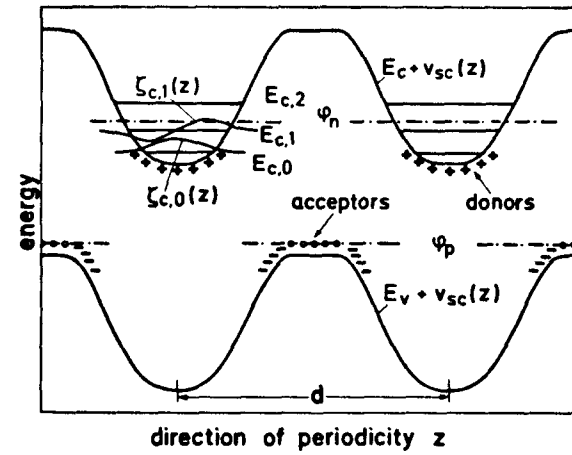

FIG. 3. Schematic real-space energy diagram of an n-i-p-i crystal. See text for explanation.

successfully applied to study the 2D subband structure in selectively doped n-$Al_xGa_{1-x}As$/GaAs single heterojunction[5] and multi-quantum-well structures.[6] The bare single-particle intersubband excitation energies are measured by the spin-flip scattering signal which is polarized perpendicular to the exciting beam.[7] The laser excitation line ($\lambda_L = 647.1$ nm) was chosen close to the $E_0 + \Delta_0$ gap of GaAs. The resonance condition is fulfilled for electrons in the conduction band but not for holes in the valence band. In Fig. 2 four Raman spectra obtained for different I^{exc} are shown. Two peaks sitting on top of the $E_0 + \Delta_0$ luminescence are clearly observed. These peaks are interpreted as single-particle intersubband transitions of the photoexcited electrons in the GaAs n-i-p-i superlattice. With decreasing I^{exc} the peaks shift to higher energies.

We now show that the observed shift of the PL and the energetic position of the intersubband transitions, both as a function of I^{exc}, are in perfect quantitative agreement with theory. The only input data for our calculations are the design parameters n_D, n_A, d_n, and d_p of the GaAs n-i-p-i superlattice investigated. The self-consistent potential $v_{sc}(z)$ seen by a carrier moving in the direction of periodic n- and p-type doping (z direction in Fig. 3) is the sum[8] of a contribution $v_0(z)$ due to the bare ionized impurities, the Hartree term $v_H(z)$ of the mobile carriers, and an exchange and correlation contribution $v_{xc}(z)$ which is treated in the local density approximation of the density functional formalism. At a given 2D electron concentration per layer $n^{(2)}$, the electron distribution $n(z)$ is obtained from $n(z) = \sum_\mu n_\mu^{(2)} \times |\zeta_{c,\mu}(z)|^2$. The subband wave functions $\zeta_{c,\mu}(z)$ are the self-consistent solutions of the effective-mass one-particle Schrödinger equation for conduction-band electrons in the potential $v_{sc}(z)$. The 2D-carrier concentration $n_\mu^{(2)}$ in the μth subband is derived from the requirement of equal Fermi level φ_n in occupied subbands together with the condition $n^{(2)} = \sum_\mu n_\mu^{(2)}$. The hole distribution $p(z)$ is obtained to a good approximation by assuming that the holes populate a narrow impurity band above the valence subbands. This assumption corresponds to a cancellation of the acceptor space charge $-en_A(z)$ by holes within the central part of the p-type layers and vanishing $p(z)$ outside. The band edges modulated by the self-consistent potential $v_{sc}(z)$, the quasi Fermi levels φ_n and φ_p, the subband energies $E_{c,\mu}$, and the wave functions $\zeta_{c,\mu}(z)$ for the lower electron subbands in a n-i-p-i superlattice are shown schematically in Fig. 3. The situation shown corresponds to an excited state of the crystal with $\varphi_n > \varphi_p$.

The results of the calculated electronic structure of the studied sample are summarized in Fig. 4 and compared with experiments. Figure 4(a) displays the calculated subband energies $E_{c,\mu}$ and the electron quasi Fermi level φ_n as a function of carrier concentration in the range $n^{(2)} = (1.5\text{–}4.0) \times 10^{12}$ cm^{-2}. The hole quasi Fermi level φ_p is assumed to lie in the center of the

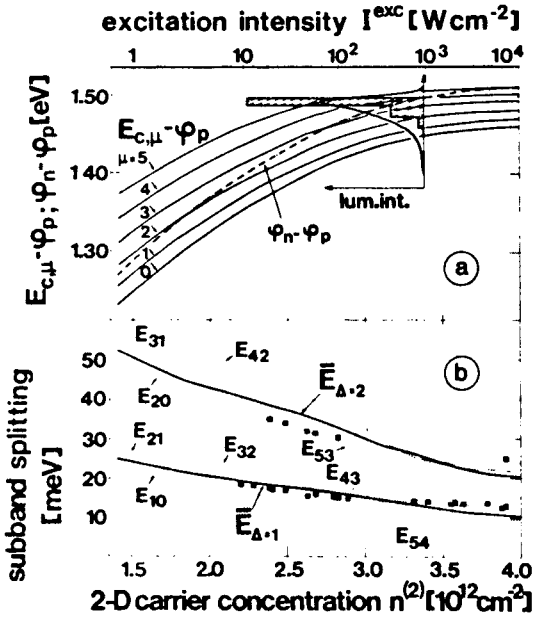

FIG. 4. Variation of the energy gaps $E_{c,\mu}-\varphi_p$ and of $\varphi_n-\varphi_p$ (top part) and of subband spacings $E_{\mu\nu}=E_{c,\mu}-E_{c,\nu}$ (dotted lines in bottom part) vs carrier density per layer as calculated self-consistently for the sample investigated. Inset in top part: Comparison of calculated spectrum (shaded area) with the observed one (λ_L = 799.9 nm) (full line). Bottom part: squares, single-particle intersubband energies as determined by Raman spectroscopy; heavy lines, calculated average subband spacings.

narrow acceptor impurity band and is taken as the origin of the energy scale. The strong increase of the energy gap $E_{c,0}-\varphi_p$ reflects the decrease of the amplitude of the self-consistent space-charge potential $v_{sc}(z)$ due to increasing compensation of the bare impurity space-charge potential $v_0(z)$ by the mobile carrier potential $v_H(z)+v_{xc}(z)$.

The luminescence of the GaAs *n-i-p-i* superlattice arises from recombination of electrons in the occupied conduction subbands with the holes in the impurity band. The spectral range of photon energies is $E_{c,0}-\varphi_p<\hbar\omega<\varphi_n-\varphi_p$. The relative intensities of the contributions of different subbands, however, increases strongly with the index μ because of exponentially increasing overlap between electron and acceptor band wave functions. Therefore, an asymmetric, stair-shaped luminescence spectrum is expected. As an example the calculated spectrum is shown for $n=3.4\times10^{12}$ cm^{-2} as an inset in Fig. 4(a).

The total PL is expected to increase with $n^{(2)}$, also on an exponential scale, because of the increasing overlap between electron and hole states when $v_{sc}(z)$ flattens (see Fig. 3). Together with the stationarity condition it follows that the steady-state PL exhibits a roughly logarithmic blue shift as a function of increasing I^{exc}. The high-energy edge of the experimental PL spectrum $\hbar\omega_{max}$ at a given I^{exc} yields the value of $\varphi_n-\varphi_p$. In terms of our calculated results of Fig. 4(a) the observed shift of the high-energy edge of the PL between $\hbar\omega_{max}=1.28$ and 1.51 eV corresponds to a variation of the steady-state 2D carrier concentration between $n^{(2)}=1.46\times10^{12}$ and 3.80×10^{12} cm^{-2}. The relation between I^{exc}, PL frequencies, and steady-state carrier concentration was used to calibrate the carrier-concentration scale with the experimental I^{exc} scale (see top scale in Fig. 4). Indeed, a roughly logarithmic relation between those two scales is found.

For a comparison between the shape of the experimentally observed and the theoretical spectra the experimental PL spectrum obtained with the 799.9 nm laser line is shown in the inset of Fig. 4(a). The theoretically expected steplike structure is not observed, but the width and the asymmetric shape agree quite well with the theory. The lack of the steplike structure is easily understood as a consequence of inhomogeneous excitation of different *n-i-p-i* layers caused by the limited penetration depth of the laser light. The excitation intensity decreases by about a factor of 2 within the *n-i-p-i* structure. Therefore, the steady-state carrier concentration and, hence, the PL energies decrease slightly from layer to layer. In the total spectrum, which is the superposition of all these contributions, the steplike structure can no longer be detected.

For the detection of quantization effects in a *n-i-p-i* crystal inelastic light scattering experiments are particularly suitable for several reasons. Inspection of Fig. 4(b) shows that the intersubband spacing $E_{c,\mu+\Delta}-E_{c,\mu}$ for $\Delta=1$ and 2 is much less sensitive to changes of $n^{(2)}$, and thus to inhomogeneous excitation, than the gap energies $E_{c,\mu}-\varphi_p$. In addition, the contributions of only a few *n*-type layers near the surface are heavily weighted because the scattered light is strongly absorbed if the photon energy is close to the $E_0+\Delta_0$ gap of GaAs. Finally, the (nearly) momentum-independent energy differences $E_{c,\mu+\Delta}-E_{c,\mu}$ causing a (broadened) line spectrum are more easily detected than a steplike structure in the luminescence.

In Fig. 4(b) we have plotted the observed subband splitting as a function of steady-state carrier concentration which was determined from the simultaneously measured PL signal. The full lines in Fig. 4(b) correspond to the average subband spacing $\bar{E}_{\Delta=1}$ and $\bar{E}_{\Delta=2}$ obtained by weighting with the number of states participating in the respective $E_{c,\mu+\Delta}-E_{c,\mu}$ processes. The excellent quantitative agreement between the measured and the calculated intersubband spacing, even over a wide range of carrier concentration, leads unambiguously to the conclusion that the photoexcited electrons in the GaAs n-i-p-i superlattice are populating 2D subbands.

The results of the photoluminescence and the Raman measurements confirm the most crucial predictions of the theory of n-i-p-i superlattices.[1] The observation of a strong shift of the luminescence as a function of excitation intensity demonstrates that introducing the concept of a tunable indirect energy gap in real space is sound and that even large nonequilibrium carrier concentrations are metastable. Inelastic light scattering definitely shows single-particle intersubband excitations. This result is of special significance as it represents the first observation of quantization and 2D-subband formation in purely space-charge–induced potential wells. It proves, in particular, that the statistical impurity potential fluctuations are so effectively screened by the mobile electrons that they do not prevent the formation of 2D subbands. Excellent quantitative agreement of the observed variation of effective energy gap and corresponding subband spacing with self-consistent calculations of the n-i-p-i subband structure is found over the full range of carrier concentrations studied. The agreement between theory and experiment demonstrates not only that our theoretical approach is correct, but it also proves a high standard of controlled doping with sharp profiles accomplished by molecular-beam epitaxy.

We would like to acknowledge the expert help in sample preparation of A. Fischer and the technical assistance of H. Hirt and M. Siemers. This work was supported in part by the Bundesministerium für Forschung und Technologie of the Federal Republic of Germany.

[1]G. H. Döhler, Phys. Status Solidi (b) 52, 79, 533 (1972), and J. Vac. Sci. Technol. 16, 851 (1979).

[2]See, for example, R. Dingle, in *Festkörperprobleme: Advances in Solid State Physics*, edited by H. J. Queisser (Vieweg, Braunschweig, 1975), Vol. XV, p. 21; L. Esaki and L. L. Chang, Thin Solid Films 36, 285 (1976).

[3]L. L. Chang and L. Esaki, Surf. Sci. 98, 70 (1980).

[4]K. Ploog, A. Fischer, G. H. Döhler, and H. Künzel, in *Gallium Arsenide and Related Compounds 1980*, Institute of Physics Conference Series No. 56, edited by H. W. Thim (Institute of Physics, London, 1981), p. 721.

[5]G. Abstreiter and K. Ploog, Phys. Rev. Lett. 42, 1308 (1979).

[6]A. Pinczuk, H. L. Störmer, R. Dingle, J. M. Worlock, W. Wiegmann, and A. C. Gossard, Solid State Commun. 32, 1001 (1979).

[7]E. Burstein, A. Pinczuk, and D. L. Mills, Surf. Sci. 98, 451 (1980).

[8]G. H. Döhler, Surf. Sci. 73, 97 (1978).

Inst. Phys. Conf. Ser. No. 56: Chapter 9 741

STUDY OF GaAs-$Al_xGa_{1-x}As$ MULTILAYER SYSTEMS BY RESONANT INELASTIC LIGHT SCATTERING TECHNIQUES

G Abstreiter and Ch Zeller

Physik-Department E 16, Technische Universität München
8046 Garching, Federal Republic of Germany

K Ploog

Max-Planck-Institut für Festkörperforschung
7000 Stuttgart, Federal Republic of Germany

Abstract

Resonant inelastic light scattering spectroscopy has been used to study selectively doped GaAs-$Al_xGa_{1-x}As$ multilayers. Electronic single particle and collective intersubband excitations have been observed in the quasi two-dimensional systems. The collective excitations are coupled to the longitudinal optical phonon modes of GaAs. The results allow a quantitative separation of effects of dielectric screening on the electric subband splitting.

1. Introduction

Light scattering spectroscopy has developped to a versatile technique in studying various properties of compound semiconductor heterojunctions and multilayer systems. The electron and phonon spectra, measured in a non-destructive way with high spatial resolution, provide information on crystal orientation, carrier concentration, scattering times and composition of mixed crystals (see for example Abstreiter et al. 1978). In superlattices successful attempts have been performed to look for zone folding effects on the phonon spectrum (Colvard et al. 1980). Electronic excitations in selectively doped GaAs-$Al_xGa_{1-x}As$ heterojunctions and multilayer systems have been observed for the first time by Abstreiter and Ploog (1979) and by Pinczuk et al. (1979a). Such experiments can be used to get information on the electric subband energies and the effects of depolarization fields in two-dimensional electron systems. The present publication contains additional experimental work on these questions and focusses on the differences of single particle and collective excitations in multilayer structures.

2. Background

In heterojunctions and multilayer systems which consist of two different semiconductors with different band-gap energies, one can achieve two-dimensional electron systems with very high mobilities at the interface or in the layers of the semiconductor with the smaller band-gap

0305-2346/81/0056-0741$01.50

energy. In such systems the large band gap semiconductor is doped selectively. In the GaAs-$Al_xGa_{1-x}As$ system the energy gap increases with increasing Al concentration. The potential barrier at the interface occurs mainly in the conduction band (Dingle 1975). Therefore charge carriers are transferred from the donors of the $Al_xGa_{1-x}As$ layers into the energetically lower conduction band of the GaAs layers. The $Al_xGa_{1-x}As$ is depleted towards the interface, while the electrons are accumulated in the GaAs. The two-dimensional character and the high mobility in such systems has been demonstrated by Störmer et al. (1979) and Tsui and Logan (1979) using Shubnikov-de Haas experiments.

In figure 1 the behaviour of the bottom of the conduction band and the top of the valence band is shown schematically for both a single interface and a multilayer system.

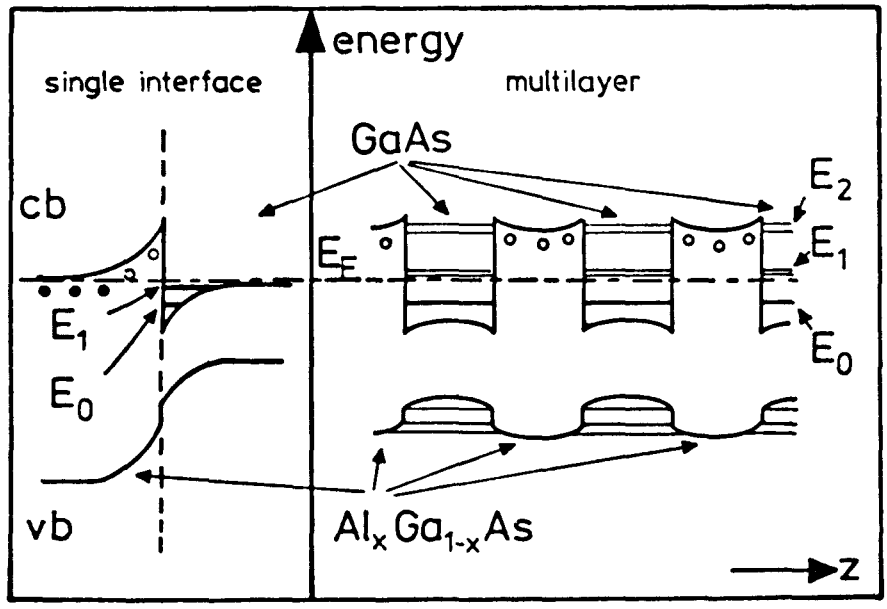

Fig. 1: The variation of the conduction band (cb) and the valence band (vb) perpendicular to the layers is shown schematically. E_o, E_1, E_2 are electric subbands.

The accumulation layer at the single interface is similar to space charge layers in metal-insulator-semiconductor systems. The subband energies E_o, E_1, ... are determined essentially by the number of carriers n_s in the space charge layer and have been calculated self-consistently by Bangert and Döhler (1979). The results agree well with

subband splittings determined from light scattering experiments (Abstreiter 1980).

In the multilayer system the potential well depends also on the width of the GaAs layers. For layer thicknesses of order or less than 100 Å, the quantum well structure plays the dominant role. The subband energies are determined by the rectangular potential well and the coupling between the wells when a superlattice is formed. With increasing layer thickness the band bending gets more pronounced, and the subband splitting depends stronger on the carrier concentration in the layers. Mori and Ando (1979) have performed extensive calculations of the subband energies for an intermediate case where the layer width d_{GaAs} = 200 Å and the barrier height V_o = 300 meV.

Subband splittings in two-dimensional systems, especially in semiconductor space charge layers, have been studied extensively using direct infrared absorption techniques (see for example Koch 1979). The measured energy separation is known to be shifted away from the bare energy splitting by two different mechanisms. There is an upward shift caused by the screening of the excitation. This effect is called the depolarization field effect and has been pointed out by Chen et al. (1976) and Allen et al. (1976). It describes the dielectric response of the thin space charge layer to the electron hole excitation and can be written as an effective plasma frequency ω_p^* perpendicular to the layer. If we assume that only the lowest subband is occupied and consider only the 0 → 1 transition, the effective plasma frequency is then given by

$$\omega_p^{*2} = \frac{8\pi n_s e^2}{\varepsilon_\infty \hbar}\, \omega_{01}\, f_{11} \qquad (1)$$

where ω_{01} is the bare subband splitting, ε_∞ = 11.1, and f_{11} is a Coulomb integral of the wavefunctions of the two lowest subbands. The measured subband resonance is then given by

$$\omega_{01}^{*2} = \omega_{01}^2 + \omega_p^{*2} \qquad (2)$$

The second effect which shifts the excitation energy down is due to final state interactions of the excited electron hole pair and is called exciton-like shift (Ando 1977). As Mori and Ando (1979) pointed out, this effect should be small in GaAs multilayer systems.

In the present work we want to demonstrate how resonant inelastic light scattering experiments can be used to determine the depolarization shift ω_p^*. Inelastic light scattering in two-dimensional electron systems has been discussed theoretically by Burstein et al. (1979).

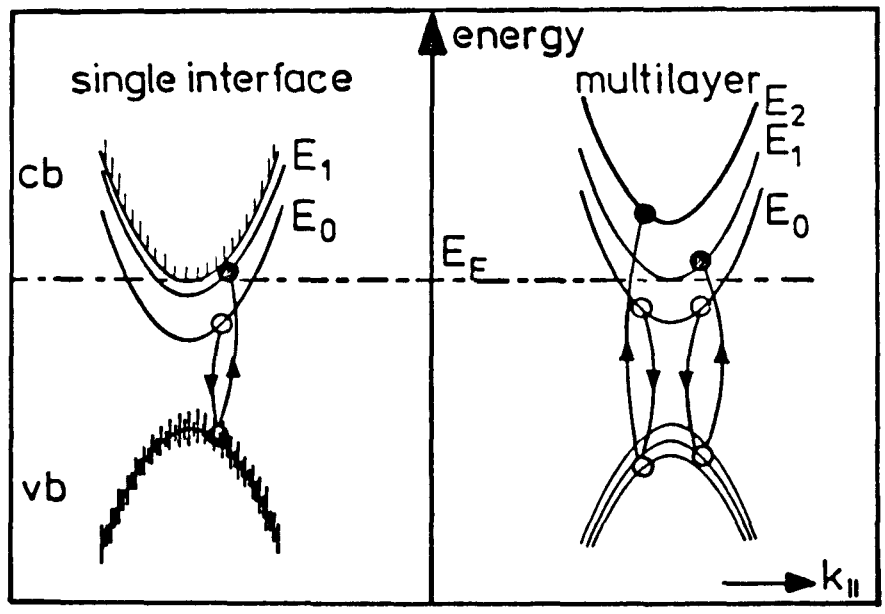

Fig. 2: Single particle scattering processes in two-dimensional electron systems. The bands are assumed to have parabolic dispersion in the direction $k_{||}$ parallel to the layers.

In figure 2 single particle scattering processes are shown for single interface and multilayer structures. An electron may be excited from the valence band to an empty subband in the conduction band, while an electron from the occupied ground subband E_o recombines with the hole in the valence band.

This type of excitation can be observed in a Raman experiment as spin-flip single particle excitation. The two electrons involved have opposite spin. The scattering occurs via spin-density fluctuations which are not sensitive to Coulomb interactions responsible for the depolarization shift. Thus the measured excitation energy is equal to the subband splitting ω_{o1} or ω_{o2}. Spin-flip single particle excitations are observed in backscattering from (100) surfaces in crossed polarizations $x(yz)\bar{x}$. The incoming light is polarized along y = (100) and the scattered light along z = (001).

From figure 2 it is also evident that the resonance condition is much sharper for the multilayer system, where the valence band states are quantized, too. At the single

interface the valence band is smeared out towards the interface, which broadens the resonance enhancement.

Similar to light scattering experiments in a three-dimensional solid state plasma, where both resonance enhanced single particle and collective excitations are observed (Pinczuk et al. 1979b), one also can excite collective intersubband transitions in the two-dimensional systems using $x(yy)\bar{x}$ geometry. The collective excitations involve charge-density fluctuations and therefore are shifted by the depolarization field effect. The measured frequency is ω_{01}^{*}. Thus it is possible to separate the depolarization shift by measuring both spin-flip single particle excitations and collective intersubband excitations in two-dimensional electron systems.

In polar semiconductors, like GaAs, the collective excitations, however, are coupled to the LO phonon modes (Burstein 1979). The frequencies of the coupled intersubband-LO phonon modes are determined by the zeros of the real part of the dielectric function. Considering only the two lowest subbands, the dielectric function may be written in the following form:

$$\varepsilon = \varepsilon_{\infty}\left(\frac{\omega_L^2 - \omega^2}{\omega_T^2 - \omega^2} + \frac{\omega_p^{*2}}{\omega_{01}^2 - \omega^2}\right) \tag{3}$$

where ω_L and ω_T are the LO and TO phonon frequencies in GaAs. For the coupled modes we obtain

$$\omega_{\pm}^2 = \frac{1}{2}\left(\omega_{01}^2 + \omega_L^2 + \omega_p^{*2}\right) \pm \frac{1}{2}\left[\left(\omega_{01}^2 + \omega_L^2 + \omega_p^{*2}\right)^2 - 4\left(\omega_{01}^2\omega_L^2 + \omega_T^2\omega_p^{*2}\right)\right]^{1/2} \tag{4}$$

The measurement of the coupled modes ω_- and ω_+ contains the information on ω_p^{*}. The two limiting cases $\omega_{01} \ll \omega_L$ and $\omega_{01} \gg \omega_L$ give the expected results $\omega_- = \omega_{01}^{*}$ and $\omega_+ = \omega_{01}^{*}$, respectively.

3. Experimental

In the present work we have studied two GaAs/n-$Al_xGa_{1-x}As$ multilayer structures which were grown using molecular beam epitaxy. They consist of twenty alternating layers grown successively on a semi-insulating (100) GaAs substrate. Sample 1 has layer thicknesses of $d_{GaAs} = d_{AlGaAs} = 200$ Å. The $Al_xGa_{1-x}As$ layers have an Al concentration $x = 0.15$ and are intentionally doped with Si. The doping source was terminated abruptly but slightly earlier than the Al source and turned on slightly after the $Al_xGa_{1-x}As$

growth had started. The doping level in the $Al_xGa_{1-x}As$ layers $(N_D - N_A) = 2 \times 10^{17} cm^{-3}$, while the GaAs layers are kept as pure as possible ($(N_D - N_A) \simeq 5 \times 10^{15} cm^{-3}$). Sample 2 is very similar to sample 1 with the only difference that $d_{GaAs} = d_{AlGaAs} = 300$ Å.

The light scattering experiments were performed in backscattering geometry. The samples were mounted in the exchange gas chamber of a temperature variable cryostat allowing a temperature variation between T = 4 K and 300 K. For excitation of the electric subband systems, laser emission lines of a Rhodamin 6 G and a Rhodamin 101 dye laser were used. The energies of these laser lines are close to the $E_o + \Delta_o$ energy gap of GaAs and fulfill the resonance condition. The scattered light was collected and focussed to the entrance slit of a Jarrel Ash double monochromator with holographic gratings. The light was detected using conventional photon counting techniques.

4. Results

In figure 3 spectra are shown as obtained close to the $E_o + \Delta_o$ resonance with sample 1. The spectrum $x(yz)\bar{x}$ shows one main peak at 212 cm^{-1} which is labelled ω_{01}. This peak is ascribed to the 0 → 1 spin-flip single particle intersubband excitation in the GaAs layers. The

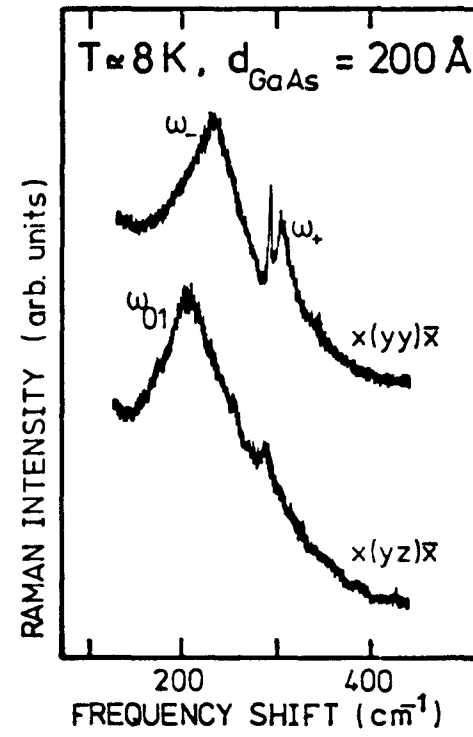

Fig. 3:
Raman spectra of a GaAs/n-$Al_xGa_{1-x}As$ multilayer structure with $d_{GaAs} = d_{AlGaAs} = 200$ Å. The laser excitation line was $\lambda_L = 6517$ Å. The peaks labelled ω_{01}, ω_- and ω_+ are caused by electronic intersubband excitations in the multilayers.

scattering intensity of this peak shows a sharp resonance behaviour close to the $E_0 + \Delta_0$ energy gap of GaAs. The excitation energy agrees well with the subband splitting calculated by Mori and Ando (1979).

The spectrum $x(yy)\bar{x}$ shows two bands $\omega_- = 229$ cm^{-1} and $\omega_+ = 308$ cm^{-1} and a sharp peak in between. The sharp peak is identified as LO phonon mode of the $Al_xGa_{1-x}As$ layers and is used to determine the Al concentration $x = 0.15$. The ω_- and ω_+ bands show the same resonance behaviour as the ω_{01} peak. We ascribe the two peaks to coupled intersubband-LO phonon modes of the GaAs layers. From the position of ω_- and ω_+ we can deduce the effective plasma frequency ω_p^*. The best value which fits both frequencies is $\omega_p^* = 120$ cm^{-1}. For the evaluation of ω_p^* we use equation (4) and the bare subband splitting $\omega_{01} = 212$ cm^{-1} as measured in the $x(yz)\bar{x}$ configuration. This value of ω_p^* is a little smaller than the results of Pinczuk et al. (1980), who performed similar experiments on a multilayer system with somewhat higher carrier concentration and somewhat smaller subband splitting.

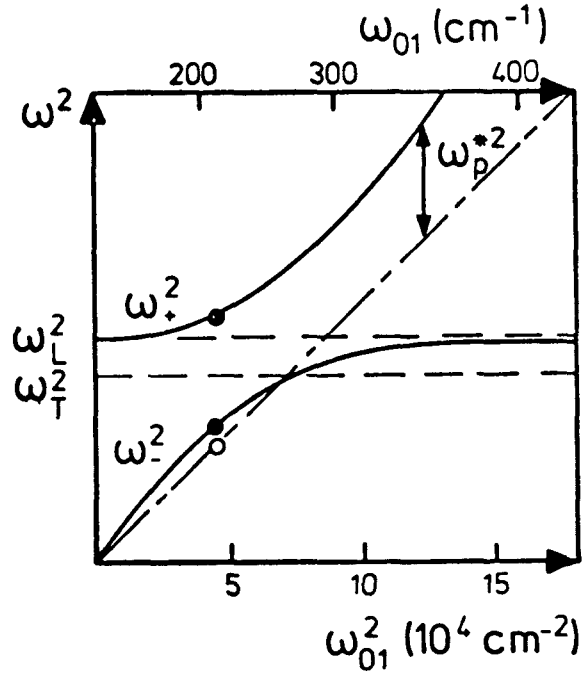

Fig. 4: The dependence of the ω_+ and ω_- modes on the subband splitting ω_{01}.

In figure 4 the dependence of the ω_- and ω_+ mode on the subband splitting ω_{01} is shown. The carrier concentration n_s and the overlap integral f_{11} are assumed to be constant.

At small values of ω_{01} the ω_- mode approaches $\omega_{01}^* = (\omega_{01}^2 + \omega_p^{*2})^{1/2}$. The ω_+ mode is equal to the LO phonon frequency. With increasing subband splitting ω_- bends downwards and crosses the ω_{01} value at the TO phonon frequency, while the ω_+ mode bends upwards and approaches ω_{01}^*. The points at $\omega_{01} = 212$ cm^{-1} mark the experimental results of sample 1.

In sample 2 the results are somewhat different. The widths of the potential barriers are 300 Å. Therefore the subband splitting ω_{01} is smaller than in sample 1. Actually in the observed spectra it is difficult to detect the 0 → 1 transition because of a strong luminescence and Rayleigh background at small frequency shifts. The nature of the observed luminescence is not yet completely understood. In sample 2, however, one clearly observes the ω_{02} transition in $x(yz)\bar{x}$ configuration. The frequency shift for this excitation lies around 265 cm^{-1}. The linewidth and the resonance behaviour is similar as for the ω_{01} band observed in sample 1. The $x(yy)\bar{x}$ spectra show two coupled modes $\omega_- = 263$ cm^{-1} and $\omega_+ = 320$ cm^{-1}. An interpretation of these modes as coupled 0 → 2 intersubband LO-phonon modes leads to an effective plasma frequency $\omega_p^*(0 \rightarrow 2) = 111$ cm^{-1}.

In all the above evaluations we have neglected effects of final state interactions (exciton effects), which is reasonable, if they are much smaller than the depolarization field effects. If we assume, however, that the exciton shifts are the same for single particle and collective excitations, then the above analysis is still meaningful even with sizeable exciton effects.

In summary, we have demonstrated that resonant inelastic light scattering is a useful technique to study the subband structure in space charge layers and multilayer systems and to evaluate depolarization field effects in subband spectroscopy. Therefore it has some advantages compared with conventional infrared subband spectroscopy. At present we are working on various multilayer systems with different well widths d_{GaAs}, depths V_0, and carrier concentrations n_s to get a more complete picture on the depolarization shifts and their dependence on the subband splittings and Fermi energies. We also hope to apply the light scattering technique successfully to metal-insulator-semiconductor systems in order to compare the results with infrared absorption and to shine light on the size of depolarization shifts in various semiconductor space charge layers.

Acknowledements

We would like to thank A. Fischer for the expert help in growing the samples with molecular beam epitaxy which is supported by the Bundesministerium für Forschung und

Technologie of the Federal Republic of Germany. The financial support of the Deutsche Forschungsgemeinschaft (SFB 128 B) is gratefully acknowledged.

References

Abstreiter G, Bauser E, Fischer A, and Ploog K, 1978 Appl. Phys. 16, 345-52.

Abstreiter G and Ploog K, 1979 Phys. Rev. Letters 42, 1308-11.

Abstreiter G, 1980 Surface Science 98

Allen S J, Tsui D C, and Vinter B, 1976 Solid State Commun. 20, 425-28.

Ando T, 1977 Solid State Commun. 21, 133-36.

Bangert E and Döhler G, 1979 private communication and to be published.

Burstein E, Pinczuk A, and Mills D L, 1979 Physics of Semiconductors, ed. by Wilson B L H (The Institute of Physics, London), 1231-34 and 1980 Surface Science 98

Chen W P, Chen Y J, and Burstein E, 1976 Surface Science 58, 263-65.

Colvard C, Merlin R, Klein M V, and Gossard A C, 1980 Phys. Rev. Letters 45, 298-301.

Dingle R, 1975 Festkörperprobleme XV, ed. Queisser H J (Pergamon-Vieweg, Braunschweig), 21-48.

Koch F, 1977 Surface Science 80, 110-24.

Mori S and Ando T, 1979 J. Phys. Soc. Japan 47, 1518-27.

Pinczuk A, Worlock J M, Störmer H L, Dingle R, Wiegmann W, and Gossard A C, 1979a Solid State Commun. 32, 1001-03, and 1980 Surface Science 98

Pinczuk A, Abstreiter G, Trommer R, Cardona M, 1979b Solid State Commun. 30, 429-32.

Pinczuk A, Worlock J M, Störmer H L, Dingle R, Wiegmann W, and Gossard A C, 1980 preprint

Störmer H L, Dingle R, Gossard A C, Wiegmann W, and Sturge M D, 1979 Solid State Commun. 29, 705-09.

Tsui D C and Logan R A, 1979 Appl. Phys. Letters 35, 99-101.

PHYSICAL REVIEW B VOLUME 26, NUMBER 4 15 AUGUST 1982

Quasi-two-dimensional photoexcited carriers in GaAs doping superlattices

Ch. Zeller, B. Vinter, and G. Abstreiter
Physik-Department, Technische Universität München, D-8046 Garching, Federal Republic of Germany

K. Ploog
Max-Planck-Institut für Festkörperforschung, D-7000 Stuttgart 80, Federal Republic of Germany

(Received 30 March 1982)

Periodic multilayer structures of GaAs exhibit new semiconductor properties such as tunable effective band gap, long lifetime of photoexcited carriers, and quantization of carriers in space-charge-induced potential wells. We present a more careful treatment of the high excitation regime, where the subbands broaden into minibands, than earlier self-consistent calculations. Experimentally we have used photoluminescence and resonant inelastic light scattering measurements to study the subband structure. The luminescence peak is found to shift with decreasing photoexcitation intensity far below the band gap of GaAs. By comparing the peak position with the theory we determine the carrier concentration. Resonant spin-flip single-particle excitations directly give the subband splittings which are in good agreement with the theoretical results. At high excitation intensities, the subbands merge and a quasi-three-dimensional behavior is found.

I. INTRODUCTION

In recent years extensive theoretical and experimental studies of artificial semiconductor superlattices have been performed. Most of the work was focused on the electrical and optical properties of the compositional multilayer structures $Al_xGa_{1-x}As$-GaAs (Ref. 1) and InAs-GaSb (Ref. 2). The introduction of the modulation-doping technique[3] has opened new possibilities, especially in connection with the strongly enhanced mobilities[4] of transferred electrons in such structures. The progress achieved is due to the further development of molecular-beam epitaxy as an excellent crystal-growth technique used for the preparation of ultrathin semiconducting films of different composition and/or doping.

Apart from these successful achievements in the field of compositional multi-quantum well structures, extensive theoretical studies of a different type of artificial semiconductor superlattice composed of ultrathin n- and p-doped semiconductor layers have been performed already by Döhler ten years ago.[5] More recently,[6] Döhler has shown that these new types of superlattices should have a number of new properties such as tunable effective band gap, long lifetime of photoexcited carriers, quantization of carriers in space-charge induced-potential wells, and tunable absorption coefficients. The development of abrupt doping techniques in combination with molecular-beam epitaxy recently made feasible the growth of GaAs-doping superlattices.[7] In these so-called n-i-p-i crystals the electrons of the donor impurities in the n-type layers are transferred in space to the acceptor sites in the p-type layers. This results in space-charge potentials perpendicular to the layers caused by the ionized impurities. It is easy to calculate the space-charge potential and the subband splitting in this situation. The potential-well depth and the subband energies depend only on the layer thickness d_n and d_p and on the impurity concentration N_D and N_A.

The first experimental evidence for the validity of the basic theoretical ideas was the observation of strong-absorption tails extending far into the gap of the pure material.[7] The direct observation of a tunable effective band gap and the quantization of photoexcited carriers in space-charge potential wells has been reported recently.[8]

In this work we present more extensive studies of both photoluminescence and resonant inelastic light scattering experiments of different GaAs-doping superlattice structures. In Sec. II we discuss the concept and theoretical calculations of subband energies in such n-i-p-i crystals. We treat more carefully than previous calculations[8] the highly excited regime where effects associated with

the finite-miniband width of the subbands became noticeable. In Sec. III the sample characterization and the experimental techniques are described. The experimental results are discussed in Sec. IV followed by some concluding remarks.

II. MINIBAND THEORY

The theory of the electronic structure of *n-i-p-i* superlattices has been developed by Döhler[5,6] and by Döhler and co-workers.[8-10] When the superlattice potential is deep, the electrons are strongly bound to one layer and the superlattice potential can be treated as a series of independent potential wells in which the electrons behave quasi-two-dimensionally. It is well known that the binding of the electrons leads to quantization into subbands with dispersion,

$$\epsilon_n(\vec{k}_{||})=E_n+\frac{\hbar^2 k_{||}^2}{2m} , \tag{1}$$

where $\vec{k}_{||}$ is the wave vector parallel to the layers, m is the electron effective mass, and the subband bottom energies E_n are eigenvalues of the one-dimensional Schrödinger equation

$$-\frac{\hbar^2}{2m}\frac{d^2}{dz^2}\zeta_n(z)+V(z)\zeta_n(z)=E_n\zeta_n(z) , \tag{2}$$

where $V(z)$ is the superlattice potential in one layer. The potential consists of the potential from ionized impurities and of the direct Hartree potential from the electrons themselves. Inclusion of exchange and correlation effects through the local-density-functional formalism does not change the results much.[10] It was shown in Ref. 8 that the calculated subband-energy separations agree well with resonant Raman scattering measurements.

In this work we present a more careful treatment of the highly excited case in which so many electrons are created that states with energy near or even above the top of the superlattice potentials are occupied. In that case the two-dimensional nature of the system is less pronounced, since electrons can easily tunnel between the wells. We mention that for the $Al_xGa_{1-x}As$-GaAs superlattice such states have been investigated by Ando and Mori.[11] Our method of solution is quite different from theirs, however, so we describe it in some detail here.

The potential $V(z)$ is a periodic function of z, $V(z+d)=V(z)$, $-\infty<z<\infty$, where $d=d_n+d_p$ is the superlattice period, and we chose $z=0$ in the middle of an n-type layer so that the potential is also even $V(z)=V(-z)$. For such a potential the stationary states are a product of plane waves parallel and Bloch waves perpendicular to the layers. The Bloch waves $\psi_{nk}(z)$ have the form

$$\psi_{nk}(z)=u_{nk}(z)e^{ikz} , \tag{3}$$

where n is a miniband index, k a wave vector in the first Brillouin zone

$$-\frac{\pi}{d}<k<\frac{\pi}{d} ,$$

and $u_{nk}(z)$ is periodic

$$u_{nk}(z)=u_{nk}(z+d) .$$

The Bloch function satisfies the Schrödinger equation

$$\left[-\frac{\hbar^2}{2m}\frac{d^2}{dz^2}+V(z)\right]\psi_{nk}(z)=E_n(k)\psi_{nk}(z) . \tag{4}$$

Instead of solving this eigenvalue equation for a given k we go the opposite way and choose the energy E. By direct integration starting from $z=0$ we construct two real solutions, $\psi_1(z)$ and $\psi_2(z)$, to the Schrödinger equation in the interval

$$-\frac{d}{2}<z<\frac{d}{2} .$$

We choose initial conditions $\psi_1(0)=0,\psi_1'(0)=1$ and $\psi_2(0)=1,\psi_2'(0)=0$.

Because of symmetry around $z=0$ we have

$$\psi_1(z)=-\psi_1(-z)$$

and

$$\psi_2(z)=\psi_2(-z) ,$$

so at the end points we have

$$\begin{aligned} p_1&\equiv\psi_1\left[\frac{d}{2}\right]=-\psi_1\left[-\frac{d}{2}\right] ,\\ p_1'&\equiv\psi_1'\left[\frac{d}{2}\right]=\psi_1'\left[-\frac{d}{2}\right] ,\\ p_2&\equiv\psi_2\left[\frac{d}{2}\right]=\psi_2\left[-\frac{d}{2}\right] ,\\ p_2'&\equiv\psi_2'\left[\frac{d}{2}\right]=-\psi_2'\left[-\frac{d}{2}\right] . \end{aligned} \tag{5}$$

We then try to find a Bloch solution as a linear combination of these two solutions:

$$u_{nk}(z)e^{ikz}=a_1\psi_1(z)+a_2\psi_2(z) . \tag{6}$$

The periodicity of $u_{nk}(z)$ applied at $\pm d/2$ leads to

a homogeneous system of linear equations for a_1 and a_2,

$$p_1(1+e^{ikd})a_1+p_2(1-e^{ikd})a_2=0\,,$$
$$p_1'(1-e^{ikd})a_1+p_2'(1+e^{ikd})a_2=0\,, \tag{7}$$

which has a nonzero solution only if

$$e^{2ikd}-e^{ikd}(p_1p_2'+p_2p_1')+1=0\,, \tag{8}$$

where we have made use of the fact that the Wronskian

$$\psi_1(z)\psi_2'(z)-\psi_2(z)\psi_1'(z)=-1\,.$$

For $|p_1p_2'+p_2p_1'|>2$ this equation has purely imaginary solutions for k, so that the chosen energy lies in a gap. For

$$|p_1p_2'+p_2p_1'|\leq 2$$

we have two symmetric real k values in the first Brillouin zone, and from Eqs. (6) and (7) we can find the corresponding two Bloch solutions $u_{nk}e^{ikz}$ and $u_{n_1-k}e^{-ikz}$.

If we normalize so that

$$\int_{-d/2}^{d/2}|u_{nk}(z)|^2dz=1\,, \tag{9}$$

the electron density is given by (for temperature $T=0$ K)

$$\rho(z)=\frac{md}{\pi\hbar^2}\sum_n\int_{-\pi/d}^{\pi/d}\frac{dk}{2\pi}[E_F-E_n(k)]\Theta(E_F-E_n(k))\,|u_{nk}(z)|^2\,, \tag{10}$$

where the Fermi energy E_F is determined by the condition

$$N=\frac{md}{\pi\hbar^2}\sum_n\int_{-\pi/d}^{\pi/d}\frac{dk}{2\pi}[E_F-E_n(k)]\Theta(E_F-E_n(k))\,, \tag{11}$$

and N is the areal density of electrons per lattice period.

Having shown how we solve the Schrödinger equation (4), we make the Hartree approximation in the standard way, i.e., the lattice potential is determined by solving Poisson's equation

$$\frac{d^2V}{dz^2}=-\frac{e^2}{\epsilon}[\rho(z)-N_D(z)+N_A(z)]\,, \tag{12}$$

where $N_D(z)$ and $N_A(z)$ are the distributions of ionized donors and acceptors and ϵ is the permittivity of GaAs. The Poisson and the Schrödinger equations are calculated self-consistently. Because of macroscopic charge neutrality, acceptors in a sufficiently broad region around the top of the potential well will be neutralized to compensate for the charge of the free electrons. The charge-neutrality condition and symmetry secure that the whole periodic lattice potential can be found by integrating Poisson's equation in one lattice period with the initial condition $dV/dz=0$ for $z=0$. Compared with the method of Ando and Mori[11] the advantages of this method are that all calculations are done in one well and that diagonalization of matrices of high rank is avoided.

It should be mentioned that in practice we first determine the miniband edges $E_n(k=0)$ and $E_n(k=\pi/d)$ by iteration. $\epsilon=12.53\epsilon_0$ and $m=0.067m_0$ have been used in the calculations.

In Fig. 1 we show some characteristic results in a highly excited case. Contrary to the weakly excited case, where the potential well is almost parabolic and the subbands almost equidistant, we have here a much shallower and more rectangular potential. Consequently, the subband separation between the lowest two subbands is smaller than be-

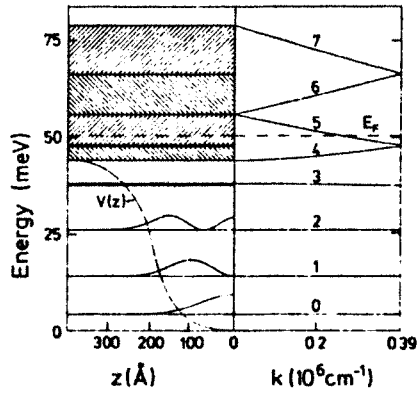

FIG. 1. Results of theoretical calculations for a sample with $d_n=d_p=40$ nm and $N_D=N_A=10^{18}$ cm^{-3} in a highly excited case with a two-dimensional concentration of 3.75×10^{12} cm^{-2}. Left side: self-consistent potential $V(z)$ and energy levels. The square of the electron wave function is shown for the lowest three subbands. The widths of the minibands are indicated by hatches. Right side: dispersion $E_n(k)$ in the direction perpendicular to the layers.

tween the next two subbands. Near the top of the potential the wave function between neighboring wells overlaps strongly and therefore the subbands broaden to minibands with considerable dispersion in $E_n(k)$ shown in the right part of the figure. For energies sufficiently high above the top of the potential the gaps become small and the electrons are almost free in the direction perpendicular to the superlattice layers also, so that we have a three-dimensional almost-free-electron gas. The results of this theory are compared with the experiments described in Sec. IV.

III. EXPERIMENTAL TECHNIQUES

The GaAs *n-i-p-i* structures used in the present experiments have been prepared by molecular-beam epitaxy. Twenty alternative *n*(Si)- and *p*(Be)-doped GaAs layers were grown on a semi-insulating or n^+-GaAs (100) substrate. The doping concentration $N_D = N_A = 1 \times 10^{18}$ cm^{-3} was the same for all layers. The individual layer thickness (d_n and d_p) varies from 20 nm in sample 2227 to 60 nm in sample 2229. In the ground state we have $N_D d_n = N_A d_p$ which is the situation of the compensated *n-i-p-i* crystal. The ground-state parameters of the samples studied are summarized in Table I.

In the ground state the periodic potential well is parabolic, which results in an equidistant spacing of the subbands. The effective-energy gap E_g^{eff}, approximately given by $E_g - 2V_0$ with $E_g \simeq 1.52$ eV, is the low-energy limit of the tunability of the optical properties of these structures.

In *n-i-p-i* crystals photoexcited electron-hole pairs are separated in space and collected in the respective doped layers. The Hartree potential of free carriers is then added to the space-charge potential of the ionized impurities which results in an increased effective-energy gap E_g^{eff} and, consequently, in a decreased well depth and subband splitting. In order to study these effects, we have performed photoluminescence and inelastic light scattering experiments as shown schematically in Fig. 2. The samples were mounted in the exchange gas chamber of a temperature-variable cryostat and cooled to $T \simeq 10$ K. The photoexcitation was produced by the 647.1-nm emission line of the Kr^+ ion laser. The power density was varied by several orders of magnitude using attenuators and point and line focus. The backscattered light was collected and focused on the entrance slit of a Jarrel-Ash double monochromator and analyzed and detected with a GaAs photomultiplier tube and conventional pulse-counting electronics. In the used setup spectra could be obtained down to 1.35 eV where both our spectrometer and the photomultiplier have their cutoff.

TABLE I. Parameters of the studied *n-i-p-i* crystals in the ground state. $2V_0$ is the depth of the potential wells.

Sample	$d_n = d_p$ (nm)	$N_D = N_A$ (cm^{-3})	$2V_0$ (meV)	$N_D d_n$ (cm^{-2})
2227	20	1×10^{18}	144	2×10^{12}
2228	40	1×10^{18}	578	4×10^{12}
2229	60	1×10^{18}	1300	6×10^{12}

IV. RESULTS AND DISCUSSIONS

In order to obtain information on the tunability of the effective energy gap and on the photoexcited quasistable carrier concentration per layer, we have studied the photoluminescence spectra of the three samples using different excitation intensities. The luminescence in excited GaAs-doping superlattices arises from the recombination of electrons in the occupied subbands with the holes which are assumed to occupy a narrow impurity band centered around the position of the acceptor levels in the *p*-type layers. This assumption is reasonable in view of the large difference of the effective mass of holes and electrons. Also we find experimentally

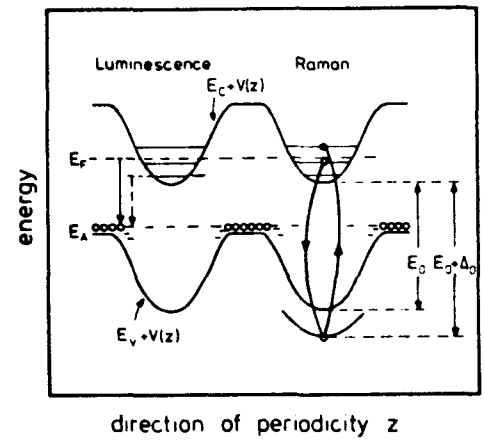

FIG. 2. Real-space energy diagram of an excited *n-i-p-i* crystal. E_c and E_v are the conduction- and valence-band edges, respectively, E_F is the Fermi energy in the conduction band, E_A is the acceptor level, and $V(z)$ is the superlattice potential. The Raman and luminescence processes are shown schematically.

that in homogeneously doped p-type GaAs (Be) the low temperature luminescence remains relatively sharp up to concentrations of 1×10^{19} cm^{-3} and is mainly due to transitions from the conduction band to the Be-acceptor levels.[12] In homogeneously doped n-type GaAs (Si), on the other hand, the system is already degenerate at donor concentrations $N_D \gtrsim 1\times10^{17}$ cm^{-3}.

In n-i-p-i crystals the excited electrons and holes are separated in space. The recombination is due to the overlap of the wave functions of the electrons in the subbands or minibands with the acceptor-band wave functions. At low excitation intensities, this overlap is extremely small. However, it increases exponentially with increasing carrier concentration. In addition, the strongest overlap occurs for the highest occupied subband. In the quasi-two-dimensional case the density of states is constant in each subband. Consequently, we expect a staircaselike luminescence line shape with the high energy onset at $E_F - E_A$, where E_F is the Fermi energy in the conduction band and E_A is the energy of the acceptor impurity band. As discussed already in Ref. 8, the steplike character of the luminescence has not been observed, which is caused by the inhomogeneous excitation of the individual layers due to the limited penetration depth of the laser light.

In Fig. 3 we show some photoluminescence spectra of sample 2227 obtained with different excitation intensities. The observed peaks are asymmetric with a relatively sharp onset on the high-energy side and a tail on the low-energy side. The peak position shifts to higher energies with increasing excitation intensity. At very high laser excitation the peak approaches the band gap of GaAs and the line is more symmetric. Similar results have been obtained for the other samples. The red shift of the luminescence peak for low-excitation intensities is much stronger in the n-i-p-i crystals 2228 and 2229 which have a larger width of the layers and, consequently, much deeper potential wells at a fixed carrier concentration.

On the left-hand side of Fig. 4 we show the shift of the luminescence peak for the three samples versus excitation intensity. The experimental points mark the inflection points on the high-energy side of the luminescence lines. These values correspond to the energy difference $E_F - E_A$. Using the calculations described in Sec. II, we can now convert the laser-excitation scale to a carrier-density scale N per layer. The theoretical results for $E_F - E_A$ for the three samples are shown on the right-hand side of Fig. 4. This figure is used to

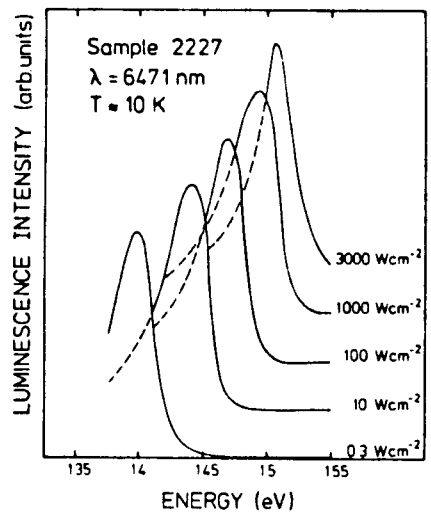

FIG. 3. Photoluminescence spectra of a GaAs n-i-p-i superlattice with $d_n = d_p = 20$ nm and $N_A = N_D = 10^{18}$ cm^{-3} at different laser-excitation intensities.

determine the two-dimensional carrier concentration from the luminescence peaks. It should be mentioned that at very high excitation intensities, when the lines are more symmetric and approach the GaAs energy gap, this method gives only a lower limit of N.

In order to get direct information on the subband splitting, we have performed resonant inelastic light scattering experiments. This technique has been successfully applied to study the subband splitting of two-dimensional electron systems in $Al_xGa_{1-x}As$-GaAs single heterojunctions[13] and multiquantum well structures.[14] The relevant light scattering processes in two-dimensional plasmas have been discussed theoretically by Burstein *et al.*[15] based on the theory of light scattering by three-dimensional carrier systems. There have also been some successful attempts made to observe light scattering by photoexcited carriers in undoped quantum well structures,[16] as well as in pure, homogeneous GaAs.[17,18] Compared with n-i-p-i crystals, however, the situation there is different because the electron-hole pairs are not separated in space. Consequently, their recombination lifetime is much shorter. The photoexcited plasma in a homogeneously doped or pure semiconductor is a multicomponent carrier system which gives rise to acoustic-plasma modes which have been observed recently.[18]

To observe light scattering signals of a quasi-two-dimensional electron system it is necessary to work under resonance conditions where the scatter-

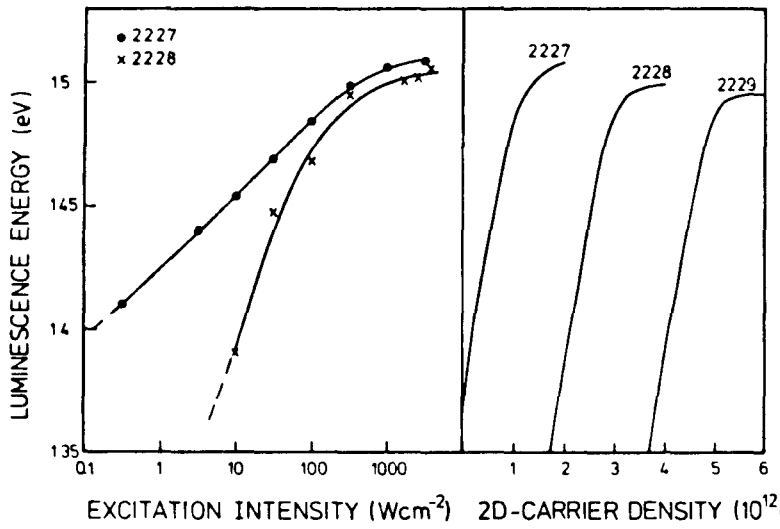

FIG. 4. Left side: measured high-energy cutoff of photoluminescence as a function of excitation intensity for the samples 2227 and 2228. The behavior of sample 2229 is similar to that of sample 2228. Right side: theoretical dependence of $E_F - E_1$ on the two-dimensional carrier density.

ing cross-section is strongly enhanced. The 647.1-nm laser line used in our experiments is close to the $E_0 + \Delta_0$ gap of GaAs. At this energy gap the resonance condition is only fulfilled for electrons in the conduction band, but not for holes in the valence band. It has been shown that at this resonance both the spin-flip single particle and the collective excitations of the carrier system can be observed. Spin-flip single-particle excitations give direct information on the subband splitting, while the collective excitations have been used to study the depolarization shift and the Coulomb matrix elements in $Al_xGa_{1-x}As$-GaAs multiquantum well structures.[19,20]

In Ref. 8 it was shown that spin-flip single-particle excitations can be used to study subband splittings in *n-i-p-i* crystals. The scattering process is shown schematically in Fig. 2. For the Raman experiments the inhomogeneous excitation due to the limited penetration depth of the incident laser light is not so important as for luminescence experiments for two reasons: (i) the subband splitting is less sensitive to the excitation intensity than the effective-energy gap, (ii) the scattered light is strongly reabsorbed, and consequently, signals from the constituent *n-i-p-i* layers close to the surface are heavily weighted in the spectra.

In Figs. 5–7 we show the experimental results for the three studied *n-i-p-i* crystals. Spectra are shown for several excitation intensities. The dashed lines indicate the $E_0 + \Delta_0$ hot-luminescence background which is always observed in *n* GaAs. On top of this background distinct peaks are seen (marked by the arrows). In all samples these peaks shift to smaller energies with increasing excitation

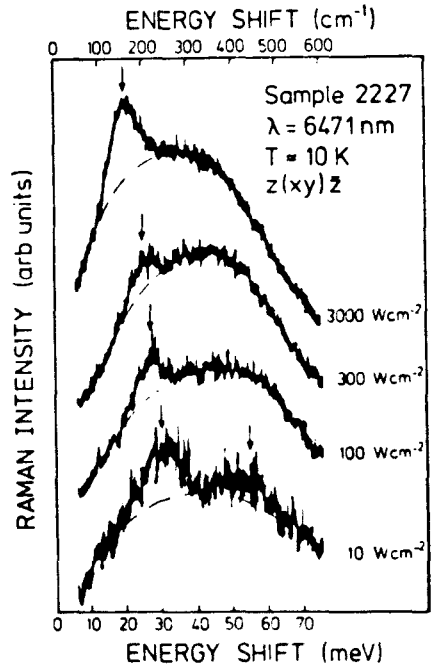

FIG. 5. Single-particle light scattering spectra at different excitation intensities. The subband transitions are marked by arrows. The dashed lines indicate the $E_0 + \Delta_0$ hot-luminescence background.

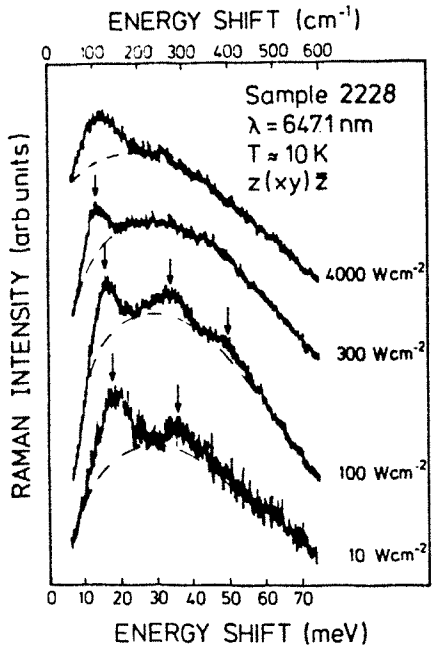

FIG. 6. Single-particle spectra at different excitation intensities for sample 2228.

intensity. In some cases three peaks with approximately equidistant energies are observed. These excitation lines are identified as $\Delta=1$, $\Delta=2$, and $\Delta=3$ intersubband transitions in the *n-i-p-i* layers.

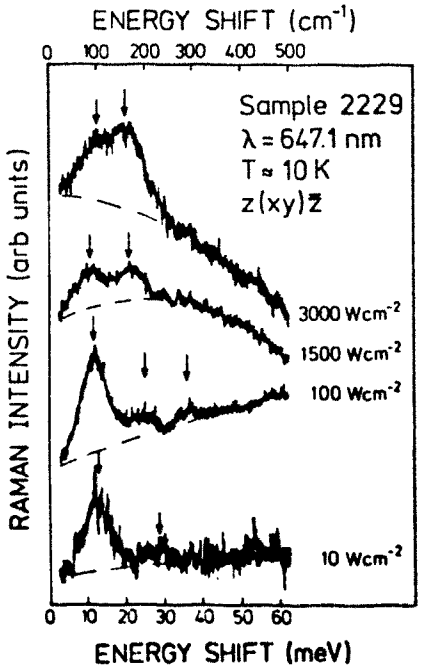

FIG. 7. Single-particle spectra at different excitation intensities for sample 2229.

In Fig. 8 the positions of the subband excitations are compared with the calculated splittings. The full points mark the experimental results. The crosses are the results of Ref. 8 obtained for sample 2228. With the use of the procedure discussed above, the two-dimensional carrier density has been derived from the luminescence experiments carried out simultaneously with the Raman measurements. The potential well is only an ideal harmonic oscillator for extremely low excitation. For higher N the subband splittings are not exactly equal. Therefore, the solid lines in Fig. 8 show the theoretical results for the average subband splittings $\Delta=1$, 2, and 3. These have been obtained by weighting the excitation energies by the number of electrons which can make the transitions. The energies calculated in this way are in excellent agreement with the experimental results for all three samples.

The arrows in Fig. 8 mark the carrier density at which the Fermi energy according to the calculations reaches the top of the potential wells in the conduction band. At higher electron concentrations part of the carriers occupy states for which the overlap of the electron wave functions between neighboring wells is strong enough to broaden the subbands into minibands with considerable dispersion perpendicular to the layers. At the same time the mean subband distance gets smaller. This is observed in the spectra at high excitation intensities. In sample 2229 (Fig. 7) the subband excita-

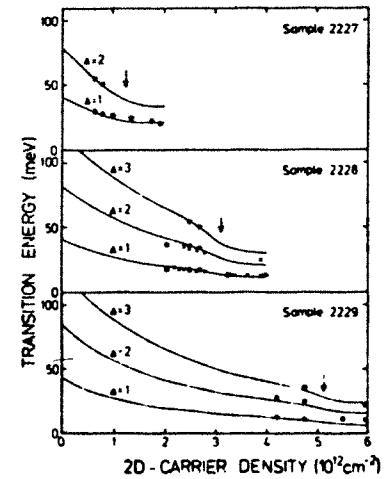

FIG. 8. Comparison of experimental subband transition energies with the results of self-consistent calculations. The dots mark our own experimental values, the crosses are from Ref. 8. For carrier densities higher than those marked by arrows the Fermi energy lies above the top of the potential wells.

tions merge at 3000 Wcm^{-2} resulting in a broad single-particle excitation band which is already very similar to the results obtained for the free-electron system in GaAs.[21] A similar broadening and change in line shape is observed for the other samples. At high-excitation intensities the photoexcited electrons in *n-i-p-i* crystals are therefore quasi-three-dimensional rather than two dimensional. This is also the reason that the luminescence line is more symmetric at high carrier concentrations.

V. CONCLUDING REMARKS

In summary, we have shown that new types of GaAs-doping superlattices definitely show the predicted properties such as tunable effective band gap and quantization of electrons in purely space-charge-induced potential wells. The experimental results obtained with three different types of compensated GaAs *n-i-p-i* crystals are in very good agreement with self-consistent subband calculations which are only based on the design parameters of the samples. In the calculation the effect of the finite miniband width of the subbands was treated more carefully. The spin-flip single-particle spectra clearly show this broadening at high-excitation intensities. The spectral line shapes change and become very similar to single-particle excitations of a three-dimensional electron gas.

We have also measured Raman spectra of collective excitations (coupled with LO-phonon modes) which, in principle, allow the quantitative determination of the effect of resonant screening in the electron system. With increasing excitation intensity, however, more and more subbands are occupied and the spectral line shapes become complicated. At very high density, again a quasi-three-dimensional coupled plasmon-LO-phonon spectrum is observed. Thus the *n-i-p-i* system makes it possible to study the effects on resonant screening concomitant with the continuous change from a two-dimensional to a thee-dimensional system. The coupled-mode frequencies have been calculated recently.[10] For a quantitative interpretation of the collective coupled-mode spectra, however, more theoretical work is necessary.

ACKNOWLEDGMENTS

We would like to thank G. H. Döhler and P. Ruden for detailed discussions concerning the theory and A. Fischer for the expert help in sample preparation. The work was supported by the Deutsche Forschungsgemeinschaft via SFB 128 and by the Bundesministerium für Forschung und Technologie of the Federal Republic of Germany.

[1]See, for example, R. Dingle, in *Festkörperprobleme, Advances in Solid State Physics*, edited by H. J. Queisser (Vieweg, Braunschweig, 1975), Vol. XV, p. 21; L. Esaki and L. L. Chang, Thin Solid Films 36, 285 (1976).

[2]L. L. Chang and L. Esaki, Surf. Sci. 98, 70 (1980).

[3]R. Dingle, H. L. Störmer, A. C. Gossard, and W. Wiegmann, Appl. Phys. Lett. 33, 665 (1978).

[4]See, for example, H. L. Störmer, J. Phys. Soc. Jpn. 49, 1013 (1980).

[5]G. H. Döhler, Phys. Status Solidi B 52, 79 (1972); 52, 533 (1972).

[6]G. H. Döhler, J. Vac. Sci. Technol. 16, 851 (1979).

[7]K. Ploog, A. Fischer, and H. Künzel, J. Electrochem. Soc. 128, 400 (1981).

[8]G. H. Döhler, H. Künzel, D. Olego, K. Ploog, P. Ruden, H. J. Stolz, and G. Abstreiter, Phys. Rev. Lett. 47, 864 (1981).

[9]G. H. Döhler and K. Ploog, Prog. Cryst. Growth Charact. 2, 145 (1979).

[10]P. Ruden and G. H. Döhler, Phys. Rev. B (in press).

[11]T. Ando and S. Mori, J. Phys. Soc. Jpn. 47, 1518 (1979).

[12]Even at room temperature the photoluminescence line remains relatively sharp [M. Ilegems, J. Appl. Phys. 48, 1278 (1977)].

[13]G. Abstreiter and K. Ploog, Phys. Rev. Lett. 42, 1308 (1979).

[14]A. Pinczuk, H. L. Störmer, R. Dingle, J. M. Worlock, W. Wiegmann, and A. C. Gossard, Solid State Commun. 32, 1001 (1979).

[15]E. Burstein, A. Pinczuk, and D. L. Mills, Surf. Sci. 98, 451 (1980).

[16]A. Pinczuk, J. Shah, A. C. Gossard, and W. Wiegmann, Phys. Rev. Lett. 46, 1341 (1981).

[17]K. M. Romanek, H. Nather, and E. O. Göbel, Solid State Commun. 39, 23 (1981).

[18]A. Pinczuk, J. Shah, and P. Wolff, Phys. Rev. Lett. 47, 1487 (1981).

[19]A. Pinczuk, J. M. Worlock, H. L. Störmer, R. Dingle,

W. Wiegmann, and A. C. Gossard, Solid State Commun. 36, 43 (1980).
[20]G. Abstreiter, Ch. Zeller, and K. Ploog, *Gallium Arsenide and Related Compounds, 1980,* edited by H. W. Thim (IOP, London, 1981), Vol. 56, p. 741.
[21]A. Pinczuk, G. Abstreiter, R. Trommer, and M. Cardona, Solid State Commun. 30, 429 (1979).

Solid State Communications, Vol. 44, No. 5, pp. 673–676, 1982.
Printed in Great Britain.

0038–1098/82/410673–04$03.00/0
Pergamon Press Ltd.

INELASTIC LIGHT SCATTERING IN HOLE-ACCUMULATION LAYERS ON SILICON

G. Abstreiter, U. Claessen and G. Tränkle

Physik-Department, Technische Universität München, D-8046 Garching, Fed. Rep. Germany

(*Received* 8 *March* 1982; *in revised form* 15 *May* 1982 *by E. Mollwo*)

Hole-accumulation layers on silicon (100) are studied using resonant inelastic light scattering techniques. The observed intersubband transitions are in good agreement with Hartree calculations of Bangert and with recent infrared absorption experiments. The width of the spectra can be explained qualitatively using the nonparabolic $k_{\parallel}$ dispersion of the individual subbands.

IN RECENT YEARS electric subbands in silicon space charge layers have been studied extensively using spectroscopic methods [1]. Compared to parabolic electronic subbands the structure of hole subbands is considerably more complicated. In the effective-mass-approximation the subband energies are derived from the Luttinger–Kohn–Hamiltonian taking spin–orbit interaction into account. The six p-like valence bands are mixed by the surface electric field. As a result of the interaction of electric field and spin coupled to the orbital angular momentum each subband splits into two branches for finite $k_{\parallel}$ (see Fig. 1). The dispersion of each branch is nonparabolic and depends on the direction in $k_{\parallel}$-space. Because of these complications only a small number of spectroscopic studies on hole subbands have been carried out so far.

Inter-subband transitions of holes on (100) surfaces have been observed already several years ago using far-infrared (FIR) absorption techniques [2, 3]. The subband structure was calculated by Bangert *et al.* [4, 5] and independently by Ohkawa and Uemura [6]: The calculations have been performed in Hartree approximation up to a hole density of $10^{13}\,cm^{-2}$. The Hartree energies of both groups do not agree very well.

The FIR absorption experiments of [3] were restricted to densities below $10^{12}\,cm^{-2}$ where they are in surprisingly good agreement with calculations of Ohkawa [7], which include many-body effects. In both theories, however, depolarization shifts are not taken into account. For higher densities recent absorption experiments [8] support the Hartree calculations of Bangert [5].

In the IR absorption experiments mentioned above [2, 3, 8] the excitation energy was fixed. To match the resonance condition the subband splitting had to be changed. This was done by changing the surface carrier density n_s via the gate voltage using a metal–oxide–semiconductor capacitor arrangement. The resulting absorption spectrum is a complicated function of n_s. Consequently it is difficult to obtain exact information on lineshapes and linewidths.

In general more direct spectroscopic information can be extracted from excitation spectra as a function of energy. Recently inelastic light scattering has proven to be a useful tool for the investigation of electric subbands in various semiconductor structures [9–11]. The relevant light scattering processes in two-dimensional carrier systems have been discussed theoretically by Burstein *et al.* [12]. In order to observe light scattering signals of a two-dimensional plasma, it is necessary to work under resonance conditions where the scattering cross-section is strongly enhanced. In GaAs the $E_0 + \Delta_0$ direct optical gap has been used to study both single particle and collective intersubband excitations [13, 14]. For holes in silicon, the resonant energy is connected with the direct E_0' gap at $k \simeq 0$, which is about 3.4 eV.

In the schematic diagram of Fig. 1, the transitions involved in a resonant two step scattering process are shown. The $k_{\parallel}$ dispersion of the hole subbands indicates the non-parabolic behaviour (schematically according to calculations by Bangert [5]).

In the present communication we report on the observation of hole intersubband transitions on Si(100) surfaces using a laser excitation line close to the E_0' gap. The samples studied are large-gate-area MOS capacitors fabricated on oxidized n-type Si wafers. The doping concentration is $1 \times 10^{15}\,cm^{-3}$ and the oxide thickness approximately 2000 Å. A semi-transparent NiCr gate electrode has been evaporated on the oxide.

The 356.4 nm (3.48 eV) emission line of a Kr^+ ion laser has been used as excitation line. The experiments were done in back-scattering geometry. The scattered light is collected and focussed on the entrance slit of a Jarrel–Ash double grating monochromator and detected using conventional photon counting techniques. The polarization of the scattered light has not been specially

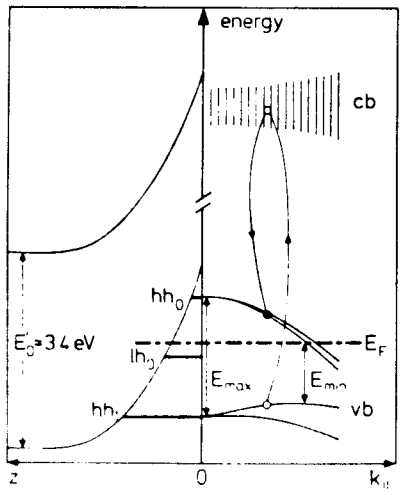

Fig. 1. Schematic diagram of subband structure and inelastic light scattering process for holes in silicon. E_0' is the direct gap at $k = 0$. hh_0, lh_0, and hh_1 denote the lowest heavy hole and light hole subbands which are filled up to the Fermi energy E_F. On the right the non-parabolic heavy hole subband dispersion in $k_{\parallel} = (k_x k_y)$ space is shown schematically.

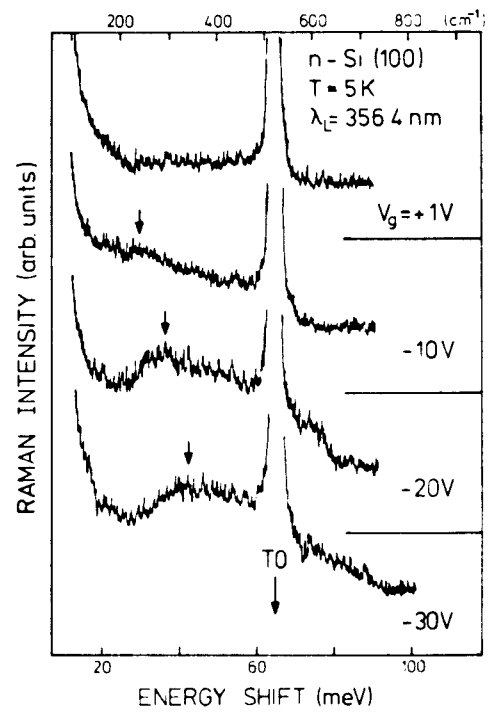

Fig. 2. Raman spectra of hole quasi-accumulation layers observed for different gate voltages V_g. $V_g = -10$ V corresponds to $n_s \simeq 1 \times 10^{12}$ cm^{-2}.

analyzed. However, the grating efficiency is such that we observe mainly polarized ($z(yy)\bar{z}$) spectra (collective excitations) [14]. Spectra have been obtained for various gate voltages V_g which determine the surface hole concentration.

For the case of hole inversion layers an additional contribution to the total surface charge comes from the depletion of the donor states. In light scattering experiments this field is partly screened by photoexcited carriers. The decrease in depletion field results in an apparent shift of the threshold voltage. This effect has been studied by means of low temperature capacitance measurements similar as described in [3]. For the intense laser radiation used in our experiments we find an increase in carrier concentration by as much as the total depletion charge. Consequently we study quasi-accumulation layers.

In Fig. 2 spectra are shown as obtained for different gate voltages V_g, i.e. different hole concentrations. $V_g = +1$ V corresponds to flat band in the presently studied sample. No hole signal is detected in this spectrum. Below 15 meV there is an increase in background signal due to Rayleigh scattered light. At about 64 meV we observe a strong mode caused by the ($k \approx 0$) optical phonons of silicon. In the other regions the background signal is flat and structureless, which means that signals from the metal gate and from the oxide as well as second order scattering in silicon are not important.

Applying a negative gate voltage results in additional scattering intensity in a relatively wide energy region. The peak value of this broad excitation line shifts to higher energies with increase gate voltage (marked by the arrows in Fig. 2). For $V_g > -30$ V ($n_s > 3 \times 10^{12}$ cm^{-2}, (not shown in the figure) the width of the excitation band increases drastically. For gate voltages larger than -50 V ($n_s > 5 \times 10^{12}$ cm^{-2}) the peak disappears and we observe a continuum up to more than 100 meV. We also note that with the appearance of the broad surface hole excitation band the intensity of the optical phonon mode at $\simeq 64$ meV decreases by as much as 10%.

The excitation lineshape is shown more clearly in the difference spectrum of Fig. 3, where the spectra at $V_g = -25$ V ($n_s = 2.5 \times 10^{12}$ cm^{-2}) and +1 V ($n_s = 0$) have been subtracted. The difference corresponds directly to the surface hole excitations. We observe a peak at about 39 meV and a long tail to the high-energy side. Similar lineshapes are observed throughout the whole range of gate voltages.

In Fig. 4 we have plotted the peak values of the difference spectra vs. carrier concentration. The dashed vertical lines indicate the width at half maximum of each spectrum. The asymmetry of the excitation bands for $n_s \lesssim 3 \times 10^{12}$ cm^{-2} is evident. At larger n_s a strong broadening occurs. We also show the infrared absorption results of [8]. In those experiments two fixed infrared

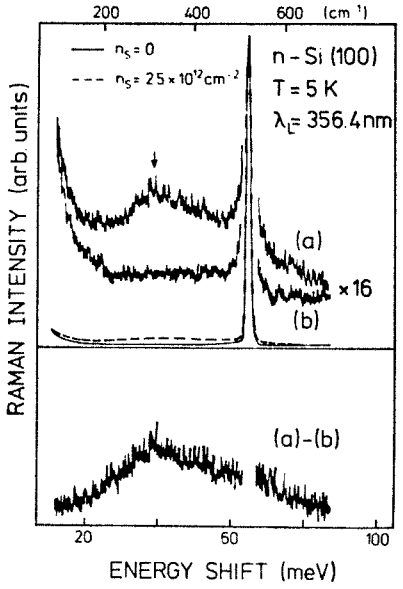

Fig. 3. Top: Raman spectra obtained for $n_s = 2.5 \times 10^{12}$ cm^{-2} (a) and for zero density (b). Bottom: The difference between (a) and (b) is shown. It corresponds directly to the hole excitation lineshape.

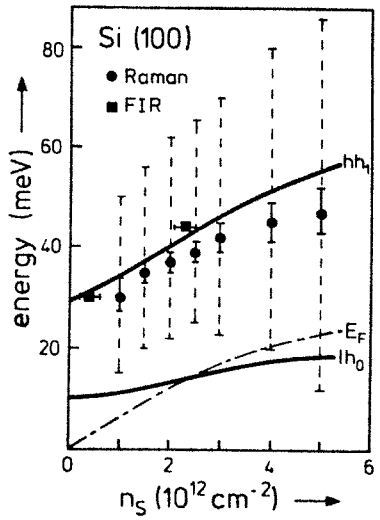

Fig. 4. Subband energies ($k_\parallel = 0$) vs. n_s are shown for the lower subbands. The zero point on the energy axis corresponds to the heavy hole ground state hh_0. The solid lines lh_0 and hh_1 are taken from [5]. Squares correspond to infrared absorption peaks, circles mark maxima in Raman scattering intensity (see text).

laser frequencies have been used. The radiation was polarized parallel to the surface, so that the resonance positions are not affected by depolarization. Full squares mark the absorption peak positions obtained in a sweep of carrier density n_s (inversion layer, depletion charge 2.8×10^{11} cm^{-2}) using 30.2 and 44.4 meV laser energies. For comparison, the bottom of the three lowest subbands as calculated by Bangert [5] for (100) hole inversion layers are shown, the depletion charge being 1.2×10^{11} cm^{-2}. As explained above the Raman scattering data correspond to depletion charge zero, i.e. to quasi-accumulation. Unfortunately no calculation for accumulation layers is available. However, for high surface charge density the contribution of depletion field becomes less important. For a qualitative explanation of the spectra we therefore will neglect the depletion field.

It is possible to relate the lower subbands to the heavy hole or light hole valence band by analyzing the Bloch part of the total wavefunction. This identification has been made by Bangert for the lowest three subbands as indicated in Figs. 1 and 4. In Fig. 4 the zero point of the energy axis is chosen to be the heavy hole ground state energy (hh_0) at $k_\parallel = 0$. The diagram suggests that the observed hole excitation lines are mainly transitions between the heavy hole ground state and the first excited heavy hole subband (hh_1). It should be noted, however, that the calculations do not include many-body corrections as well as depolarization shifts present in the Raman experiments.

As mentioned already in the introduction the dispersion of each branch of subband is nonparabolic and depends on the direction of $k_\parallel$. This gives rise to a continuum of transition energies. In Fig. 1 we have marked the range (E_{min}, E_{max}) for one branch of the heavy hole subbands. If we neglect the dispersion of hh_1, the width of the hole excitation bands is expected to be proportional to the Fermi energy. Since the band splitting is more pronounced for higher carrier densities a further broadening of the lines with increasing n_s is expected. At $n_s \simeq 2 \times 10^{12}$ cm^{-2} the light hole subband begins to get occupied adding scattering intensity especially on the low energy side. This is in qualitative agreement with the experimental results, which show relatively narrow, but asymmetric excitation lines at small n_s and an extreme broadening of the bands for $n_s > 4 \times 10^{12}$ cm^{-2}. In order to make a quantitative comparison, however, the dispersion and splitting of the different subbands in the whole two-dimensional $k_\parallel$-space up to k_F has to be included. Such calculations are not yet available.

In conclusion, we have demonstrated that resonant inelastic light scattering can be used to get information about subband splittings and $k_\parallel$ dispersion of hole subbands on silicon surfaces. A more extensive study of the hole subbands has to include the investigation of the low energy regime where we expect light hole–heavy hole transitions. In addition the polarization properties of the scattered light should give information on resonant screening.

Acknowledgements – We thank E. Bangert for useful discussions concerning the theory of hole subbands and for providing unpublished results. The work has been supported by the Deutsche Forschungsgemeinschaft via SFB 128.

REFERENCES

1. See for example, *Proc. Conf. on Electronic Properties of Two-Dimensional Systems*, published in *Surf. Sci.* **58** (1976); **73** (1978); **98** (1980); **113** (1982).
2. A. Kamgar, P. Kneschaurek, W. Beinvogl & J.F. Koch, *Proc. 12th Int. Conf. Phys. Semicond.* (Edited by M.H. Pilkuhn), p. 709. Stuttgart (1974).
3. P. Kneschaurek, A. Kamgar & J.F. Koch, *Phys. Rev.* **B14**, 1610 (1976).
4. E. Bangert, K. von Klitzing & G. Landwehr, *Proc. 12th Int. Conf. Phys. Semicond.* (Edited by M.H. Pilkuhn), p. 714. Stuttgart (1974).
5. E. Bangert (unpublished) (1975).
6. F.J. Ohkawa & Y. Uemura, *Suppl. Progr. Theoret. Phys.* **57**, 164 (1975).
7. F.J. Ohkawa, *J. Phys. Soc. Japan* **41**, 122 (1976).
8. U. Claessen, Diplomarbeit, TU München (1981) (unpublished).
9. G. Abstreiter & K. Ploog, *Phys. Rev. Lett.* **42**, 1308 (1979).
10. A. Pinczuk, J.M. Worlock, H.L. Störmer, R. Dingle, W. Wiegmann & A.C. Gossard, *Solid State Commun.* **32**, 1001 (1979).
11. L.Y. Ching, E. Burstein, S. Buchner & H.H. Wieder, *J. Phys. Soc. Japan* **49**, Suppl. A, 951 (1980).
12. E. Burstein, A. Pinczuk & D.L. Mills, *Surf. Sci.* **98**, 1231 (1980).
13. A. Pinczuk, J.M. Worlock, H.L. Störmer, R. Dingle, W. Wiegmann & A.C. Gossard, *Solid State Commun.* **36**, 43 (1980).
14. G. Abstreiter, Ch. Zeller & K. Ploog, *Inst. Phys. Conf. Ser.* **56** (Edited by H.W. Thim), p. 741. Bristol and London (1981).

Solid State Communications, Vol. 47, No. 8, pp. 651–654, 1983.
Printed in Great Britain.

0038–1098/83 $3.00 + .00
Pergamon Press Ltd.

SUBBAND ENERGIES IN ACCUMULATION LAYERS ON InP

G. Abstreiter, R. Huber, G. Tränkle and B. Vinter*

Physik-Department, Technische Universität München, 8046 Garching, Federal Republic of Germany

(*Received* 7 *March* 1983 *by M. Cardona*)

Resonant inelastic light scattering with incident photon energies close to the $E_0 + \Delta_0$ optical gap in InP is used to study spin–flip single-particle and collective intersubband excitations in surface accumulation layers. The determined subband splittings and the depolarization shifts are compared with self-consistent calculations. From the obtained results it is concluded that the non-parabolicity of the conduction band cannot be neglected in the evaluation of the subband energies especially at high carrier concentrations.

THE FABRICATION of electrically tunable metal–insulator–semiconductor (MIS) structures using the direct band gap material InP has attracted some interest in connection with high-speed devices and optoelectronic applications [1, 2]. Experimental results of the low temperature electronic properties of space-charge layers on InP have been published recently [3, 4]. Magneto-transport measurements were used to study the mobility and the occupation of electric subbands in surface accumulation layers. The subband energies have been calculated self-consistently by various groups [3, 5, 6]. Cheng and Koch [4] estimated the subband splitting by analyzing carefully the occupation of two subbands as observed by Shubnikov–de Haas oscillations. Their results agree well with self-consistent Hartree calculations. So far, however, no spectroscopical investigation of the energy separations has been reported.

In the present communication we present reasonant inelastic light scattering data which yield direct information on the electron energy levels as well as depolarization shifts. The experimental results are compared with self-consistent subband calculations which include exchange and correlation effects in the density functional formalism. The depolarization shift [7, 8] is calculated explicitly using a two-level model. The coupling of the subband system with longitudinal optical (LO)-phonons in the polar semiconductor InP is also taken into account.

Resonant inelastic light scattering has been used successfully to study single-particle and collective intersubband excitations of quasi-two-dimensional electron systems in GaAs heterostructures and doping superlattices [9–12]. Recently this technique also has been applied to investigate surface accumulation layers in Si- and InAs–MIS structures [13, 14]. The selection rules relevant for the scattering processes involved have been discussed by Burstein *et al.* [15]. In order to observe light scattering signals of a two-dimensional plasma one has to work under resonance conditions where the scattering cross-section is strongly enhanced. In GaAs and InP it turns out that the $E_0 + \Delta_0$ energy gap is the most convenient optical gap for these conditions. At this resonance direct optical interband transitions involve carrier occupied states in the conduction band. Consequently the carrier density scattering mechanisms are dominant. Because of the mixed spin nature of the corresponding valence band both, scattering via charge-density as well as spin-density fluctuations are allowed. They can be separated experimentally (depolarized and polarized spectra) and are used to determine quantitatively Coulomb matrix elements.

The InP samples studied in this work were prepared in a similar way as described in [4]. After the polishing-etching procedure the fresh (100) surfaces of the p- and n-type InP wafers were coated directly with an insulating lacquer layer of thickness $d_l \simeq 2\,\mu$m. A semi-transparent Ti or NiCr gate electrode has been evaporated on top of this insulator. The MIS-capacitor arrangement was completed by putting electrical contacts to the backside of the InP wafer and to the gate electrode. The samples were then mounted in the exchange gas chamber of a temperature variable cryostat and have been characterized using both capacitance- and magneto-transport measurements. The electrical properties of our samples were found to be very similar to those discussed by Cheng and Koch [4]. In order to fulfill the resonance conditions, inelastic light scattering experiments have been performed using the 1.55 eV and 1.64 eV emission lines of a Kr^+-ion laser as well as the continuously tunable lines of an oxazine-dye laser. The laser beam of power less than 100 mW was focussed on the sample

* Present address: Thomson–CSF, F-91401 Orsay, France.

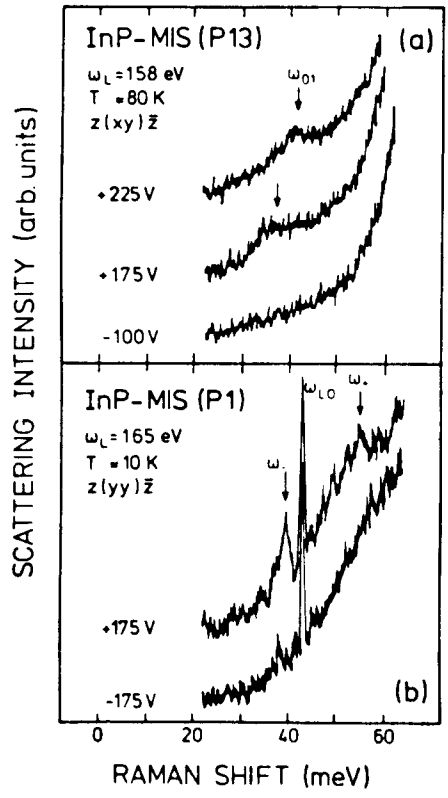

Fig. 1. Resonant inelastic light scattering spectra of InP–MIS structures. $z(x,y)\bar{z}$ denotes the scattering configuration in which spin–flip single-particle intersubband excitations are observed. The arrows mark the deduced subband splitting ω_{01}. The collective excitations ω_- and ω_+ as well as the LO phonons are observed in the parallel scattering configuration $z(yy)\bar{z}$.

with a cylindrical lens. The back-scattered light was collected and analyzed using a double grating spectrometer with conventional pulse counting equipment.

From the analysis of Shubnikov–de Haas oscillations Cheng and Koch [4] find that the surface electrons in InP are in accumulation subbands, even in p-type samples. They conclude that the surface layer is always n-type, which may be caused by the preparation method used. In our samples we find the same behavior. In light scattering experiments in addition one always studies accumulation or quasi-accumulation layers because of the screening of possible depletion charges due to the photoexcited carriers. The experimental results therefore must be compared with calculations using negligible depletion charge.

In Fig. 1 we show resonant Raman spectra as obtained from InP–MIS–structures. z and $\bar{z}$ denote the propagation directions of the incident and scattered light normal to the surface. x and y are $\langle 110\rangle$ and $\langle 1\bar{1}0\rangle$ polarization directions of the light in the surface plane.

We first discuss the crossed polarized spectra $(z(xy)\bar{z})$ shown in Fig. 1(a). With positive gate voltage a relatively broad single peak is observed on top of a luminescence background which shifts to higher energies with increasing voltage or increasing surface carrier concentration. The structure is absent below the threshold voltage. In analogy to the results obtained in GaAs heterojunctions [9, 10], this peak is assigned to the lowest spin–flip intersubband excitation ω_{01}, which represents the single-particle energy separation.

In order to compare the measured subband splittings with self-consistent calculations a careful determination of the carrier concentration n_s at each gate voltage is necessary. To avoid shifts in the threshold voltage, which are likely to occur in samples with lacquer insulators under illumination, the positive bias voltage was switched after each measurement for the same period of time to negative voltages. Under similar conditions we performed Shubnikov–de Haas experiments which have been used to determine the carrier concentrations.

The subband energies have been calculated self-consistently in the Hartree-approximation as in [6]. Contrary to the case of Si and to the calculation in [5], we find only a small shift of the subband splittings to higher energies when exchange and correlation effects are included in the local density functional formalism. The finite temperature has been taken into account using the Fermi distribution function of the electrons. This method has been applied in [16] to study temperature dependent effects in Si space-charge layers.

In Fig. 2(a) the calculated subband splitting ω_{01} is compared with the results obtained from the resonant inelastic light scattering experiments. The energy difference deduced from Shubnikov–de Haas oscillations in [4] is also plotted in the figure. There is good agreement in the absolute values. The increase of the subband splitting with increasing carrier concentration, however, is found to be smaller for the spectroscopical values than predicted in the theory. This is somewhat contrary to the excellent agreement between the subband splittings obtained from the occupation of the subbands and the calculations. One has, however, to consider that in both the theory as well as in the evaluation of the subband splitting from the measured occupancies of two subbands a constant effective mass $m^* = 0.08m_0$ has been used for the surface electrons. Including nonparabolicity of the conduction band in the analysis of [4] and in the calculations, one obtains a smaller subband splitting especially at high carrier concentration. The re-examination of the Shubnikov–de Haas data with an increasing effective mass due to non-parabolicity yields good agreement also in the slope of the subband splitting vs n_s between the spectroscopical light scattering results and the magneto-transport experiments. The necessary

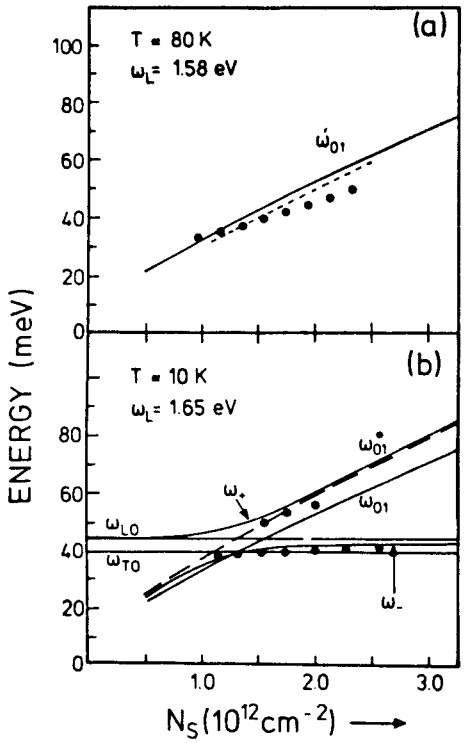

Fig. 2. Comparison of the experimental results of subband splitting and collective coupled modes with self-consistent calculations. The points mark the spectroscopical Raman results, the solid lines represent the theory. The dashed line in (a) shows the results obtained from magneto-transport measurements according to [4]. The relative error of the experimental values is given approximately by the size of the points. The absolute error may be larger by a factor of three both with respect to N_s and to the energy.

increase of the effective mass is in reasonable agreement with the theoretical non-parabolicity of the conduction band.

Measurements of the type just discussed in principle allow the determination of final state interactions (exciton-like shifts) which should be present in the optical excitation spectra, but should be absent in the determination of subband differences from transport experiments. It causes a shift of single-particle excitations to smaller energies. The effect, however, is expected to be small in GaAs and InP. Due to the uncertainties in the non-parabolic effective mass and in n_s this exciton-like shift could not be determined quantitatively.

We consider now the collective intersubband excitations which are observed in the scattering configuration $z(yy)\bar{z}$ [Fig. 1(b)]. The measured subband splitting is known to be shifted upwards from the bare energy splitting due to the so-called depolarization shift which describes the resonant screening of the excitation [7, 8]. If only two subbands are considered, the resonance is given by $\omega_{01}^{*2} = \omega_{01}^2 + \omega_p^{*2}$, where $\omega_p^* = (8\pi n_s e^2/\epsilon_{00}\hbar) \times \omega_{01} f_{11}$ is an effective plasma frequency perpendicular to the surface layer and f_{11} is the Coulomb overlap integral of the subband wave functions involved. In polar semiconductors the collective excitations are coupled to the LO-phonon modes resulting in two modes with energies $\omega_\pm$ [15]. These coupled modes have been observed in n-accumulation layers of InP as shown in Fig. 1(b).

The measured energies ω_+ and ω_- are compared with calculations based on the numerical wave functions of the two subbands obtained from the self-consistent calculations discussed above. In Fig. 2(b) the calculated bare subband splitting ω_{01} is shown for comparison. We note that the ω_--mode is close to ω_{01}^* for small values of n_s, while the ω_+-mode approaches the depolarization shifted energy ω_{01}^* at high n_s, when $\omega_{01} > \omega_{LO}$. ω_- crosses the bare subband splitting when $\omega_{01} = \omega_{TO}$ and falls in between ω_{LO} and ω_{TO} for higher n_s. This behavior is also observed experimentally. From the measured energy values of ω_{01}, ω_+, and ω_- one directly determines the effective plasma frequency ω_p^* and the Coulomb matrix element f_{11} which can be expressed in terms of a length. For $n_s = (1.55 \pm 0.10) \times 10^{12}\,cm^{-2}$ we find $\omega_p^* = (21 \pm 1)$ meV and $f_{11} = (3 \pm 0.5)$ Å. This compares best with the theory using $n_s = 1.3 \times 10^{12}\,cm^{-2}$, where $\omega_p^* = 20.2$ meV and $f_{11} = 3.8$ Å. The agreement between the calculations and the experimental results is satisfactory taking into account that the surface accumulation layer is approximated by a two-subband system.

In conclusion we have demonstrated that reasonant inelastic light scattering is an ideal method to study the subband structure of surface space-charge layers in InP. These are the first experiments where both spin-flip single-particle excitations and collective intersubband excitations could be studied in one system with a wide range of tunability in n_s and ω_{01}. The depolarization shift and the Coulomb matrix elements could be determined quantitatively.

Acknowledgements – Helpful discussions with Prof. F. Koch are gratefully acknowledged. The work was financially supported by the Deutsche Forschungsgemeinschaft via the Sonderforschungsbereich 128.

REFERENCES

1. D.L. Lile, D.A. Collins, L.G. Meiners & L. Messick, *Electron Lett.* 24, 657 (1978).
2. D. Fritzsche, *Insulating Films on Semiconductors, 1979*, (Edited by G.G. Roberts & M.J. Morant), p. 258. Institute of Physics, Bristol (1980).

3. K.v. Klitzing, Th. Englert & D. Fritzsche, *J. Appl. Phys.* **51**, 5893 (1980); K.v. Klitzing, Th. Englert, E. Bangert & D. Fritzsche, *Proc. 15th Int. Conf. Phys. Semicond.* Kyoto (1980) [*J. Phys. Soc. Japan* **49**, Suppl. A, 979 (1980)].
4. H.C. Cheng & F. Koch, *Solid State Commun.* **37**, 911 (1981); *Phys. Rev.* **B26**, 1989 (1982).
5. G.H. Kawamoto, J.J. Quinn & W.L. Bloss, *Phys. Rev.* **B23**, 1875 (1981).
6. S. Das Sarma, *Solid State Commun.* **41**, 483 (1982).
7. W.P. Chen, Y.J. Chen, & E. Burstein, *Surf. Sci.* **58**, 263 (1976).
8. S.J. Allen Jr., D.C. Tsui & B. Vintner, *Solid State Commun.* **21**, 425 (1976).
9. G. Abstreiter & K. Ploog, *Phys. Rev. Lett.* **42**, 1308 (1979); G. Abstreiter, Ch. Zeller & K. Ploog, *Inst. Phys. Conf. Ser.* **56** (Edited by H.W. Thim), p. 741. Britstol and London (1981).
10. A. Pinczuk, J.M. Worlock, H.L. Störmer, R. Dingle, W. Wiegmann & A.C. Gossard, *Solid State Commun.* **32**, 1001 (1979); **36**, 43 (1980).
11. G.H. Döhler, H. Künzel, D. Olego, K. Ploog, P. Ruden, H.J. Stolz & G. Abstreiter, *Phys. Rev. Lett.* **47**, 864 (1981).
12. Ch. Zeller, B. Vinter, G. Abstreiter & K. Ploog, *Phys. Rev.* **B26**, 2124 (1982); *Proc. 16th Int. Conf. Phys. Semicond.* Montpellier (1982) (to be published).
13. G. Abstreiter, U. Claessen & G. Tränkle, *Solid State Commun.* **44**, 673 (1982).
14. L.Y. Ching, E. Burstein, S. Buchner & H.H. Wieder, *J. Phys. Soc. Japan* **49**, Suppl. A, p. 951 (1980).
15. E. Burstein, A. Pinczuk & D.L. Mills, *Surf. Sci.* **98**, 451 (1980).
16. S. Das Sarma & B. Vinter, *Phys. Rev.* **B23**, 6822 (1981).

J. Phys. C (in press)

Hole Subbands on Silicon Surfaces

M. Baumgartner and G. Abstreiter
Physik-Department, Technische Universität München
D-8046 Garching, Fed. Rep. of Germany
and
E. Bangert
Physikalisches Institut der Universität Würzburg
D-8700 Würzburg, Fed. Rep. of Germany

Abstract

The subband structure of hole space charge layers in Si is investigated both theoretically and experimentally. The subband energies and the $k_{\parallel}$-dispersion are calculated self-consistently in the Hartree approximation. The results are compared with measured subband excitations as obtained with resonant inelastic light scattering techniques. Various transitions are observed in a wide range of carrier concentrations on (100) as well as on (110) and (111) Si surfaces. From the lineshapes and linewidths information on the $k_{\parallel}$-dispersion of the individual subbands is obtained. By analyzing the polarization of the scattered light we were able to separate collective and single-particle excitations.

1. Introduction

During the past ten years many investigations have been performed to study the electric subband structure of surface space charge layers on various different semiconductors. Most of the work is concerned with n-type accumulation or inversion layers in Si (for a review see: Ando et al. 1982). Compared to the more or less parabolic electronic subbands the structure of hole subbands is considerably more complicated. The first calculations of subbands in the case of degenerate valence bands have been performed by Bangert and coworkers (Bangert et al. 1974) and independently by Ohkawa and Uemura (Ohkawa and Uemura 1975, Ohkawa 1976). Spectroscopic information has been obtained using far-infrared spectroscopy (Kneschaurek et al. 1976, Kamgar 1977). Those early laser absorption experiments were, however, restricted to energies below 20 meV where they were found to be in good agreement with calculations which include many-body effects (Ohkawa 1976). Recently, there has been made some effort to extend the FIR absorption experiments to higher energies (Claessen 1981, Martelli et al. 1983). The new results obtained for higher carrier densities are in surprisingly good agreement with Hartree calculations. In the absorption experiments the excitation energy was fixed, while the surface carrier density N_s was changed via the applied gate voltage using a metal-oxide-semiconductor capacitor arrangement. The resulting absorption spectrum is usually a complicated function of N_s. In general more direct spectroscopic information can be extracted from excitation spectra as a function of energy. Recently

resonant inelastic light scattering has proven to be a useful tool for the investigation of subbands in various semiconductor structures (for a review see: Abstreiter et al. 1983). The light scattering signals of two-dimensional plasmas are, however, only observable when one fulfills resonance conditions. For holes in Si it has been shown (Abstreiter et al. 1982) that, close to the direct E_0'-gap at $k \tilde{=} 0$, the resonance enhancement is strong enough to measure subband excitations.

In the present work we discuss results obtained in a wide energy region for (100) as well as (110) and (111) surfaces of Si. The measured subband separations are compared with self-consistent Hartree calculations. In section 2 we discuss the concept of these calculations. After the description of experimental details in section 3 the results are discussed on the basis of our calculations.

2. Theory

Our calculation of the hole subband structure for inversion layers is based on the description of the degenerate valence bands by Luttinger's (Luttinger and Kohn 1965) second-order k·p-matrix. Although spin-orbit coupling in Si is weak, it cannot be neglected, because the separation of 44 meV between the upper two degenerate bands and the spin-orbit split-off band is of the same magnitude as the electric subband separations. Further, the lack of inversion symmetry caused by the surface electric field lifts the spin-degeneracy of the individual subbands, and a modification of the subband dispersions goes along with this. Experimental evidence for this spin-splitting

was recently found in p-GaAs space charge layers (Störmer et al., 1983). Therefore the following 6x6-Luttinger matrix represents the valence-band structure appropriately:

$$H=\begin{pmatrix} E_1 & R+i\Delta & S & 0 & 0 & \Delta \\ R-i\Delta & E_2 & T & 0 & 0 & i\Delta \\ S & T & E_3 & -\Delta & -i\Delta & 0 \\ 0 & 0 & -\Delta & E_1 & R-i\Delta & S \\ 0 & 0 & i\Delta & R+i\Delta & E_2 & T \\ \Delta & -i\Delta & 0 & S & T & E_3 \end{pmatrix} \qquad \begin{aligned} E_1 &= Lk_x^2 + M(k_y^2 + k_z^2) \\ E_2 &= Lk_y^2 + M(k_z^2 + k_x^2) \\ E_3 &= Lk_z^2 + M(k_x^2 + k_y^2) \\ R &= Nk_xk_y \\ S &= Nk_xk_z \\ T &= Nk_yk_z \end{aligned} \qquad (1)$$

with coordinates parallel to the [100] crystallographic directions. The subband states are then determined by the following equations:

$$\left\{H\left(k_x, k_y, -i\frac{\partial}{\partial z}\right) + V(z)\right\} \varphi_{i,k_x,k_y}(r) = E_i(k_x,k_y)\,\varphi_{i,k_x,k_y}(r) \qquad (2)$$

$$V(z) = V_1(z) + V_2(z) \qquad (3)$$

$$V_1(z) = \frac{e^2}{\varepsilon\varepsilon_0}\int_\infty^z dz' \int_\infty^{z'} dz'' \left\{ \sum_{\text{occupied}} \left| \varphi_{i,k_x,k_y}(z'') \right|^2 \right\}$$

$$V_2(z) = \begin{cases} \frac{\ell^2}{2\ell\varepsilon_0}(N_D - N_A)(z-\ell)^2 & z \leq \ell \\ 0 & z \geq \ell \end{cases}$$

$$\varphi_{i,k_x,k_y}(z=0) = \varphi_{i,k_x,k_y}(z=\infty) = 0 \qquad (4)$$

The z-axis is perpendicular to the silicon surface. H is the matrix (1), where k_z is replaced by $-i\partial/\partial z$. Therefore (2) is

appropriate only for the (100) surface orientation. For the two other cases H is transformed to new coordinate systems to have the z-axis parallel to the (110) or (111) direction. The wavefunction φ labelled with the subband index i depends also on the wavevector components k_x, k_y. For the band-bending V(z) in (3) there are two contributions. The first is the Hartree potential from all charges of the occupied subband states, and the second gives the contribution of $N_D - N_A$ ionized donors in the depletion layer of thickness ℓ. The boundary conditions are given in (4). The calculation of the subband states $E_i(k_x,k_y)$, φ_{i,k_x,k_y} from (2), (3), (4) is straightforward.

To get a matrix formulation for Schrödinger's equation, an expansion in terms of orthogonal basis functions is applied:

$$\varphi_{i,k_x,k_y}(r) = e^{i(k_x x + k_y y)} \sum_{l=1}^{6} \sum_{j=1}^{n} a_{jl}\, v_j(z)\, u_l \qquad (5)$$

The u_ℓ are the Bloch functions at the zone center, and

$$v_j(z) = \frac{\sqrt{\alpha}}{|Ai'(-Y_j)|}\, Ai(\alpha z - Y_j) \qquad (6)$$

is the normalized Airy function equipped with a stretching parameter α. With help of this variational parameter the extension of the basis function can be related to that of the potential to give a rapid convergence of series (5). Y_i are the zeros of the Airy function, such that the boundary conditions of (4) are realized. During the calculation it turned out

that six basis functions (n = 6) are sufficient, if no more than two subbands are occupied. Thus eigenvalues and eigenvectors of 36-dimensional matrices had to be computed. According to the k·p-perturbation theory the operators $\partial/\partial z$, z, $\partial^2/\partial z^2$ act only on the $v_j(z)$, and the quantities:

$$\langle j|\partial/\partial z|k\rangle \quad , \quad \langle j|z|k\rangle \quad , \quad \langle j|\partial^2/\partial z^2|k\rangle = \alpha^3\langle j|z|k\rangle - \alpha^2\gamma_j\delta_{jk} \tag{7}$$

are easily found by numerical integration. The calculation of the matrix elements of the potential $V_1(z)$ is more lengthy:

$$V_1(z) = \frac{e}{\varepsilon\varepsilon_0}\int_{\infty}^{z} dz' \int_{\infty}^{z'} dz'' \varrho(z'') = \frac{e^2}{\varepsilon\varepsilon_0}\int_{\infty}^{z} dz' (z-z') \sum_{\text{occupied}} \left|\varphi_{i,k_x,k_y}(z')\right|^2 . \tag{8}$$

We insert the ansatz (5) and make use of the orthogonality of the u_ℓ:

$$V_1(z) = \frac{e^2}{\varepsilon\varepsilon_0} \sum_{r=1}^{n} \sum_{s=1}^{n} P_{rs} \int_{\infty}^{z} dz' (z-z') v_r(z') v_s(z') \tag{9}$$

$$P_{rs} = \sum_{\text{occupied}} \sum_{\ell=1}^{6} a_{r\ell}(k_x,k_y)\, a^*_{s\ell}(k_x,k_y) \tag{10}$$

$$= \sum_i \sum_\sigma \frac{1}{(2\pi)^2} \int_{E_i(k_x,k_y) \geq E_F} dk_x\, dk_y \sum_{\ell=1}^{6} a_{r\ell}(k_x,k_y)\, a^*_{s\ell}(k_x,k_y)$$

which contains a sum over the occupied subbands ($\sum_i$), a sum over both spin-components ($\sum_\sigma$) and an integration on that part of the 2-dimensional k-space, where $E_i(k) \geq E_F$. The components $a_{j\ell}$ of the eigenvectors are slowly varying functions of k_x and k_y, such that only one point per $\Delta k_x \cdot \Delta k_y = 0.1 \times 10^{12}\,\text{cm}^{-2}$ had to be calculated to realize an adequate

interpolation. Furthermore, symmetry arguments permit to restrict the computation to only 1/4 of the k-space in the case of (110) surface orientation, to 1/8 for the (100) case, and to 1/12 for the (111) case.

The carrier concentration N_s determines the Fermi energy and the occupied areas in the two-dimensional k-space by:

$$N_s = \sum_{\text{occupied}} 1 = \sum_i \sum_\sigma \frac{1}{(2\pi)^2} \int_{E_i(k_x,k_y) \geq E_F} dk_x dk_y \qquad (11)$$

Since the $v_j(z)$ are a fixed set of functions, $V_1(z)$ is determined by the quantities P_{rs}. Thus our calculation was done by starting with an arbitrary set of these quantities, solving (2) by matrix diagonalization for appropriate pairs of k_x, k_y to get the subband energies $E_i(k_x,k_y)$ and the eigenvectors $a_{r\ell}(k_x,k_y)$, then E_F is obtained from (11) and a new set of P_{rs} from (10). After about 10 loops the ingoing and the outcoming P_{rs} differ less than 0.1%.

The numerical calculations are performed for the case of an inversion layer with $N_D - N_A = 10^{15}\text{cm}^{-3}$ ionized donors in the depletion layer. At high carrier concentrations this gives only a small contribution to the surface potential with negligible influence on the subband energies. It, however, is an important effect at low carrier concentration. The valence band parameters used for the explicit calculation are (Dexter and Lax 1954): $L = -6.5\ \hbar^2/2m_o$, $M = -2.7\ \hbar^2/2m_o$, $N = -7.3\ \hbar^2/2m_o$, $3\Delta = 44$ meV, and $\varepsilon = 11.9$ as dielectric constant of Si. In Fig. 1 the self-consistent potential is plotted versus z for a carrier concentration of $N_s = 4.5 \times 10^{12}\text{cm}^{-2}$ and the (100) orientation.

Six subbands are indicated, two of which lie above the Fermi energy and are populated by holes. By inspection of the eigenvectors of these states, we tried to associate the subbands with the valence-band branches. For the highest, the third, and the lowest state it was possible to factor the wave-functions into the same Bloch part and the envelope functions ψ, shown in the insert of Fig. 1. The form of the Bloch part indicates that the states belong to the heavy-hole band. The envelope functions represent a ground state and two excited states. For the other three subbands such a factorization was not possible. The composition by the Bloch functions of the second level shows that this state belongs to the light-hole band. For the fourth and fifth subbands the inspection of the eigenvectors gives no definite relations to the valence band branches. However, we will see later the experiments suggest that the fourth level is related to the spin-orbit split-off band. The subband energies as a function of carrier concentration will be discussed in connection with the experimental results in section 4.

In Fig. 2 we show the $k_{//}$-dispersion of three subbands in the direction [010]. In bulk-Si all states are at least two-fold spin-degenerate, due to the inversion symmetry of the lattice. Since this symmetry is lost, if the surface electric field is applied, the spin-degeneracy is lifted within the subbands. This can be seen for a special case in Fig. 2. Although spin-orbit coupling is weak, a considerable splitting results. From time reversal it follows that the states $|k,s\rangle$ and $|-k, -s\rangle$ are Kramers degenerate (s denotes the spin-variable). Thus each branch of a subband is composed of an equal amount of both

spin-orientations. From Fig. 2 it becomes also clear that the dispersion is quite different for the individual subbands. In addition we find that it also depends on the direction of $k_{//}$. As we will see later, these properties of the surface valence bands lead to extremely broad subband excitation lines for most of the transitions, especially at high carrier concentrations.

3. Experiment

The samples studied are large-gate-area Si-MOS-capacitors fabricated on oxidized n- and p-type Si-wafers. Three different surface orientations have been used. The gate electrodes consist of thin ($\sim$ 50 Å) semi-transparent NiCr-films of an approximate area of 7 mm^2. The MOS-capacitor arrangement is completed by putting electrical contacts to the backside of the Si-wafer and to the gate electrode. The essential sample parameters are given in table 1. V_h is the threshold voltage for hole conductivity. The gate voltage V_g is defined as $(V_a - V_h)$, where V_a is the externally applied voltage. The induced surface carrier concentration is obtained from V_g and the oxide thickness d_{ox}. For the inelastic light scattering experiments the samples were mounted in the exchange gas chamber of a liquid He flow-through cryostat or on the cold finger of a liquid N_2 dewar. The laser beam was focussed onto the sample using a spherical lense. The backscattered light is collected and analyzed in a Jarrel-Ash double grating spectrometer. The experimental arrangement is shown schematically in Fig. 3. For the detection of the scattered light we used a GaAs-photomultiplier with conventional pulse counting electronics.

Both parallel polarized $z(yy)\bar{z}$ and, by rotating the polarization direction of the incoming light by 90 degrees, also perpendicular polarized $z(xy)\bar{z}$ spectra have been obtained. According to the selection rules (Burstein et al. 1980) the $z(yy)\bar{z}$ spectra reflect the collective excitations of the carrier system, while for the crossed polarized case one may detect spin-flip single-particle excitation. In order to observe light scattering signals of a two-dimensional plasma, it is necessary to work under resonance conditions, such that the scattering cross-section is strongly enhanced. The first experiments of this type have been performed with excitations close to the $E_0 + \Delta_0$ direct optical gap of GaAs (Abstreiter and Ploog 1979, Pinczuk et al. 1979). Carrier occupied states are involved in the relevant transitions. For holes in Si, the resonant energy is connected with the direct E_0' gap at $k = 0$, which is about 3.4 eV. In the schematic diagram of Fig. 4, the transitions involved in a resonant two-step scattering process are shown. The $k_{||}$-dispersion of the hole subbands is also indicated. We used the 356.4 nm (3.48 eV) emission line of a Kr^+ ion laser as excitation line. This energy is close enough to the E_0' gap of Si in order to fulfill the resonance condition (Abstreiter et al. 1982).

In light scattering experiments the depletion field is partly screened due to the photoexcited carriers. The decrease of the depletion field results in an apparent shift of the threshold voltage. We have studied this effect by low temperature capacitance measurements. For the intensive laser radiation used in

our experiments, an increase in carrier concentration by as much as the total depletion charge is found. Therefore we always study hole accumulation layers even in n-type samples. This has to be kept in mind when comparing the experimental results with the calculations.

4. Results and Discussion

In this section the various experimental results are discussed and compared with theory for each of the three surface orientations studied.

4.1 (100)-Surface

In Fig. 5 a series of spectra is shown as obtained in the $z(yy)\bar{z}$ geometry for different gate voltages V_g. The sample temperature was approximately 10 K. At V_g = +2 V, when no holes are present at the surface, the Raman spectrum is quite flat and structureless except for the increase at small energies due to Rayleigh scattered light and the strong signal at about 65 meV caused by the optical phonons of Si. This top spectrum shows that signals from the metal gate electrode and from the oxide as well as second-order phonon scattering in Si are negligible in the present series. Inducing a hole space charge layer at the interface by applying a negative gate voltage results in the appearance of additional structures in the spectra. A relatively broad peak with its maximum at about 35 meV is observed for V_g = -8 V. With increasing negative gate voltage this peak shifts to higher energies while it broadens drastically. For V_g more than -30 V a more or less

structureless continuum up to energies higher than 100 meV is observed. These excitations have been observed already earlier (Abstreiter et al. 1982) and have been interpreted as transitions between the two lowest lying heavy-hole-like subbands. Not observed previously was the very sharp line at about 10 meV which shows up in the spectra for V_g more than -18 V. This narrow peak also shifts to higher energies with increasing V_g, concomitant with a slight broadening.

In Fig. 6 we show a series of spectra obtained with the same (100) sample but for the $z(xy)\bar{z}$ configuration, where the incoming light is polarized perpendicular to the scattered light. Due to the mixed spin nature of the valence band wavefunctions one should be able to observe spin-flip single-particle excitations in this geometry. Both the broad structure and the narrow peak, similar as for the parallel polarized spectra, are observed. The arrows in the experimental figures mark the maxima of the peaks after subtracting the trace obtained without holes (dashed lines). Here the narrow peak at about 10 meV appears much weaker compared with the experiments shown in Fig. 5.

The marked energies are plotted versus surface carrier concentration N_s in Fig. 7. The solid lines represent energy differences between individual subbands at $k_{\parallel} = 0$, obtained from calculations as described in section 2. The sharp low energy peak lies close to the energy separation of the lowest heavy- and light-hole-like subbands ℓ_o and h_o. For low carrier densities the experimental values deviate from the theory

towards the low energy side. This is expected because the calculations are performed for an inversion layer. The experiments on the other hand are done for accumulation layers, where the subband splitting vanishes with $N_s \rightarrow 0$.

The energy peaks of the broad structure are close to the separation of the heavy-hole-like subbands in agreement with the earlier interpretation (Abstreiter et al. 1982). We have studied the behavior of this broad excitation line to very small carrier concentrations and find that the peak position does not go to zero as expected for accumulation layers. Therefore, we believe that at least part of the transitions are excitations from the spin-orbit split-off subband system (s.o.) to the heavy-hole ground state h_o. In our calculations there exists an unidentified subband close to the first excited heavy-hole subband h_1 (see Fig. 1). We have plotted the N_s-dependence of this level in Fig. 7 and tentatively ascribe it to the difference between the spin-orbit split-off subband and h_o. It is found to be in fair agreement with the experiment and it also lies close to the bulk spin-orbit splitting of 44 meV.

The depolarization shift ω_p^* can be extracted from the observed differences in the spectra obtained with different polarizations. The collective excitations are shifted with respect to the spin-flip single-particle excitations to higher energies. Considering only two levels this shift is given by (Allen et al. 1976) $\omega_{01}^{*\,2} = \omega_{01}^{\,2} + \omega_p^{*2}$. The depolarization shift is directly related to the Coulomb matrix-element, to the bare energy separation ω_{01}, and to the occupation difference of the

two levels ($N_s^0 - N_s^1$). The experiments for (100)-surfaces clearly show this shift. The analysis leads to a value of $\omega_p^* \tilde{\sim}$ 20 meV. Because of the large width of the transitions the exact determination of the depolarization shift is, however, not possible.

As already mentioned, the lineshape and linewidth depend not only on lifetime effects but are strongly influenced by the different $k_{\parallel}$-dispersions of the individual subbands. Therefore it is rather surprising that the light-hole heavy-hole transitions give rise to very sharp peaks with a half width as narrow as 2 meV. Because of this small linewidth one has to conclude that the two subbands involved have nearly the same $k_{\parallel}$-dispersion. Inspection of Fig. 2, where the $k_{\parallel}$-dispersion is calculated for one direction and one N_s, shows that the lower branch of the ℓ_o subband is nearly parallel to the h_o subband. We believe that transitions between these two branches are involved in the sharp line observed at low energies. To observe such sharp lines it is, however, necessary that the dispersion in all $k_{\parallel}$-directions is the same and that this behavior holds for different N_s-values. The broad structure on the other hand is composed of different transitions like $h_1 - h_o$ and s.o.-h_o which all exhibit strongly different $k_{\parallel}$-dispersions.

4.2 (110)-Surface

Compared with (100)-surfaces the situation is more complicated for (110)-surfaces, because more subbands are involved in the same energy region. Figs 8 and 9 display low-

temperature spectra obtained in $z(yy)\bar{z}$ scattering configuration. Again the Raman spectra with no holes at the surface are indicated by the dashed lines. At low carrier concentrations structures appear, one relatively narrow peak in the energy region between 20 and 30 meV (marked by the arrows in Fig. 8) and a relatively weak and broad signal extending to energies higher than the optical phonon line. With increasing negative gate voltage the low energy peak shifts and broadens and finally merges with the broad structure. A more or less continuous background signal is observed further. These quasi-continuous electronic excitations interact with the optical phonons, which manifests itself in an asymmetric broadening of the one-phonon line at about 65 meV. The effect is understood as a quantum-mechanical interference of the continuum states with the discrete energy state and has been analyzed recently in terms of electron-phonon matrix elements (Baumgartner and Abstreiter 1983). At even higher negative gate voltages a pronounced difference occurs between the low and high energy wings of the one-phonon line (Fig. 9). Apart from this quasi-continuum a new weak structure appears at about 20 meV at high carrier concentrations. This peak is marked by the arrows in Fig. 9 and shows only a weak dependence on the gate voltage.

In Fig. 10 the peak positions of the observed excitation lines are plotted versus carrier concentration. The solid lines represent the calculated subband separations. Experimental results for crossed polarizations and for higher temperatures are also included in this figure. For low carrier concentrations

the broad band (see Fig. 8) at higher energies coincides with the subband separation of the heavy-hole-like ground subband and the spin-orbit split-off subband, which could be identified theoretically in this case. The sharper peak at lower energies on the other hand agrees well with the calculated energy separation $h_1 - h_o$. The deviations at small N_s again are explained by the vanishing subband separation for accumulation layers. In both cases, however, there are other possible transitions close by like $\ell_o - h_o$ for the low energy and $h_2 - h_o$ for the high energy peak. Such transitions may contribute to the shape and width of the observed structures. The additional peak observed at high N_s ($N_s > 4 \times 10^{12} cm^{-2}$ at T = 10 K) lies close but somewhat higher than the $h_1 - \ell_o$ calculated energy difference. Such transitions are only possible when ℓ_o is occupied with holes. According to our calculations the occupation of ℓ_o occurs at $N_s \approx 3.5 \times 10^{12} cm^{-2}$ for T = 0 K, in excellent agreement with the experiment.

We have also studied spin-flip single-particle excitations using crossed polarizations. Only the two low energy peaks have been detected. Within the experimental error there is no measurable depolarization shift. This behavior, which is different compared to the (100)-surface, is not yet understood. It might be related to the fact that on (110)-surfaces more subbands are involved in the observed spectra.

The crosses in Fig. 10 mark the peak positions deduced from spectra taken at higher temperatures ($T \approx 80$ K). Two peaks are observed which are slightly higher in energy than at low

temperatures. A shift to higher energies is expected from the thermal occupation of higher bands. The redistribution of charge leads to a different potential with increased subband separation. Similar temperature effects have been studied for electron space charge layers (Schäffler and Koch 1981). We also find that the low energy peak, which is attributed to transitions $h_1 - \ell_o$, shows up already at smaller N_s, which is caused by the earlier thermal occupation of ℓ_o.

4.3 (111)-Surface

A series of Raman spectra obtained from a (111)-Si-MOS sample at $T \tilde{-} 8$ K is shown in Fig. 11. In this geometry the reference spectrum without holes at the surface (V_g = + 1 V) exhibits already some structure below the optical phonon line. It is due to weak second-order phonon scattering in Si. Surface hole induced spectra can be obtained by subtracting this background signal. At $T \tilde{-} 80$ K only one relatively broad peak is observed which shifts quite strongly to higher energies with increasing negative gate voltage. The peak maxima are marked by arrows. In Fig. 12 the measured energies are plotted versus carrier concentration. The crosses represent the $T \tilde{-} 80$ K data. Also included are the deduced results from $T \tilde{-} 10$ K data. The two solid lines are calculated $\ell_o - h_o$ and $h_1 - h_o$ subband separations which are theoretically the only ones in this energy region for the (111)-surface. For the parallel polarized spectra one broad peak is observed which follows more or less the $h_1 - h_o$ energy difference. From the width we conclude, however, that also $\ell_o - h_o$ transitions contribute to the

observed structures. The spin-flip single-particle spectra $(z(xy)\bar{z})$ also exhibit quite broad structures. In those data, however, a splitting of the lines is observable, especially at low carrier concentrations. This clearly demonstrates that different transitions contribute to the observed spectra. The agreement of the energetic positions with the calculated $h_1 - h_o$ and $\ell_o - h_o$ subband separations is as good as for the other surface orientations. Similar as for the (100)-surface we find a slight shift between the parallel and perpendicular polarized spectra. Considering the experimental uncertainty, however, no quantitative determination of the depolarization shift is possible.

5. Concluding Remarks

We have demonstrated that resonant inelastic light scattering experiments can be used to obtain various spectroscopic information about the subband structure of hole accumulation layers in Si. The good agreement between experimental results and self-consistent Hartree calculations based on the Luttinger-Kohn Hamiltonian shows that many-body corrections are negligible in a wide region of N_s. The splitting of the individual subbands predicted from the theory for finite $k_{\parallel}$ is experimentally supported by the observation of the extremely sharp subband transition on (100)-surfaces and its interpretation. Most of the other excitations exhibit very broad and partly asymmetric lineshapes which can be understood by strongly different $k_{\parallel}$-dispersions of the various subbands involved. A complete understanding of the lineshapes requires the calculation of the transition

matrix elements in the whole two-dimensional $k_{\parallel}$-space. Such calculations have not been performed so far.

Acknowledgements

Part of this work has been supported by the Deutsche Forschungsgemeinschaft via SFB 128.

References

Abstreiter G, Ploog K, 1979 Phys. Rev. Letters 42, 1308 - 1311

Abstreiter G, Claessen U. Tränkle G 1982 Solid State Communications 44, 673-676

Abstreiter G, Cardona M, Pinczuk A 1983 in Topics in Applied Physics 54 (Heidelberg: Springer, in press)

Allen Jr S J, Tsui D C, Vinter B 1976 Solid State Communications 20, 425-428

Ando T, Fowler A B, Stern F 1982 Reviews of Modern Phys. 54, 437-672

Bangert E, v Klitzing K, Landwehr G 1974 Proceedings of the 12th Int. Conf. on the Physics of Semiconductors (Stuttgart: Teubner) 714-718

Baumgartner M, Abstreiter G 1983 Proceedings of the 5th Int. Conf. on the Electronic Properties of Two-Dimensional Systems (Oxford, to be published in Surface Science)

Burstein E, Pinczuk A, Mills D L 1980 Surface Science 98, 451-468

Claessen U 1981 (Thesis Techn. Univ. Munich, unpublished)

Dexter R N, Lax B 1954 Phys. Rev. 96, 223-224

Kamgar A 1977 Solid State Communications 21, 823-826

Kneschaurek P, Kamgar A, Koch J F 1976 Phys. Rev. B 14, 1610-1622

Luttinger J M, Kohn W 1955 Phys. Rev. 97, 869-883

Martelli F, Koch F (to be published)

Ohkawa F J, Uemura J 1975 Suppl. Progr. Theor. Phys. 57, 164-175

Ohkawa F J 1976 J. Phys. Soc. Japan 41, 122-129

Pinczuk A, Störmer H L, Dingle R, Worlock J M, Wiegmann W, Gossard A C 1979 Solid State Communications 32, 1001-1003

Schäffler F, Koch F 1981 Solid State Communications 37, 365-368

Störmer H L, Schlesinger Z, Chang A, Tsui D C, Gossard A C, Wiegmann W 1983 Phys. Rev. Letters 51, 126-129

Table 1

Sample characteristics

Surface	Substrate	d_{ox} (nm)	V_h (Volts)
(100)	p-type	212	- 2
(110)	n-type	130	- 4
(111)	n-type	95	- 2

Figure Captions

Fig. 1: Self-consistent potential of a hole inversion layer on (100)-Si versus distance from the surface. The energies for $k_{\parallel} = 0$ of six subbands are shown. The insert gives the envelope functions ψ of three heavy-hole subbands.

Fig. 2: $k_{\parallel}$-dispersion with surface electric field induced spin-splitting of three subbands for a (100)-surface of Si. h_0 and h_1 denote heavy-hole subbands, ℓ_0 is the ground state of the light-hole subband system.

Fig. 3: Sample and light scattering assembly.

Fig. 4: Schematic diagram of the subband structure and the inelastic light scattering process for holes. E_0' is the direct energy gap of Si at $k \tilde{\approx} 0$. The $k_{\parallel}$-dispersion is shown on the right-hand side. The relevant conduction band energy is smeared out due to upward bending of the bands.

Fig. 5: Raman spectra of hole accumulation layers on (100)-Si observed for different gate voltages in parallel polarization. For positive gate voltages no holes are present at the surface. The spectrum for $V_g = +2$ V is indicated by the dashed lines in the other spectra. The differences reflect directly the hole excitations in the surface accumulation layers.

Fig. 6: Raman spectra similar as shown on Fig. 5 except for perpendicular polarization.

Fig. 7: Measured and calculated subband energy separations for the (100)-surface of Si.

Fig. 8: Raman spectra of collective excitations in hole accumulation layers on (110)-surfaces in the low gate voltage regime.

Fig. 9: Spectra like those of Fig. 8 but for higher carrier concentrations.

Fig.10: Measured and calculated subband energy separations for the (110)-surface of Si.

Fig.11: Raman spectra of hole excitations on (111)-surfaces at $T \stackrel{\sim}{-} 80$ K.

Fig.12: Measured and calculated subband energy separations for the (111)-surface of Si.

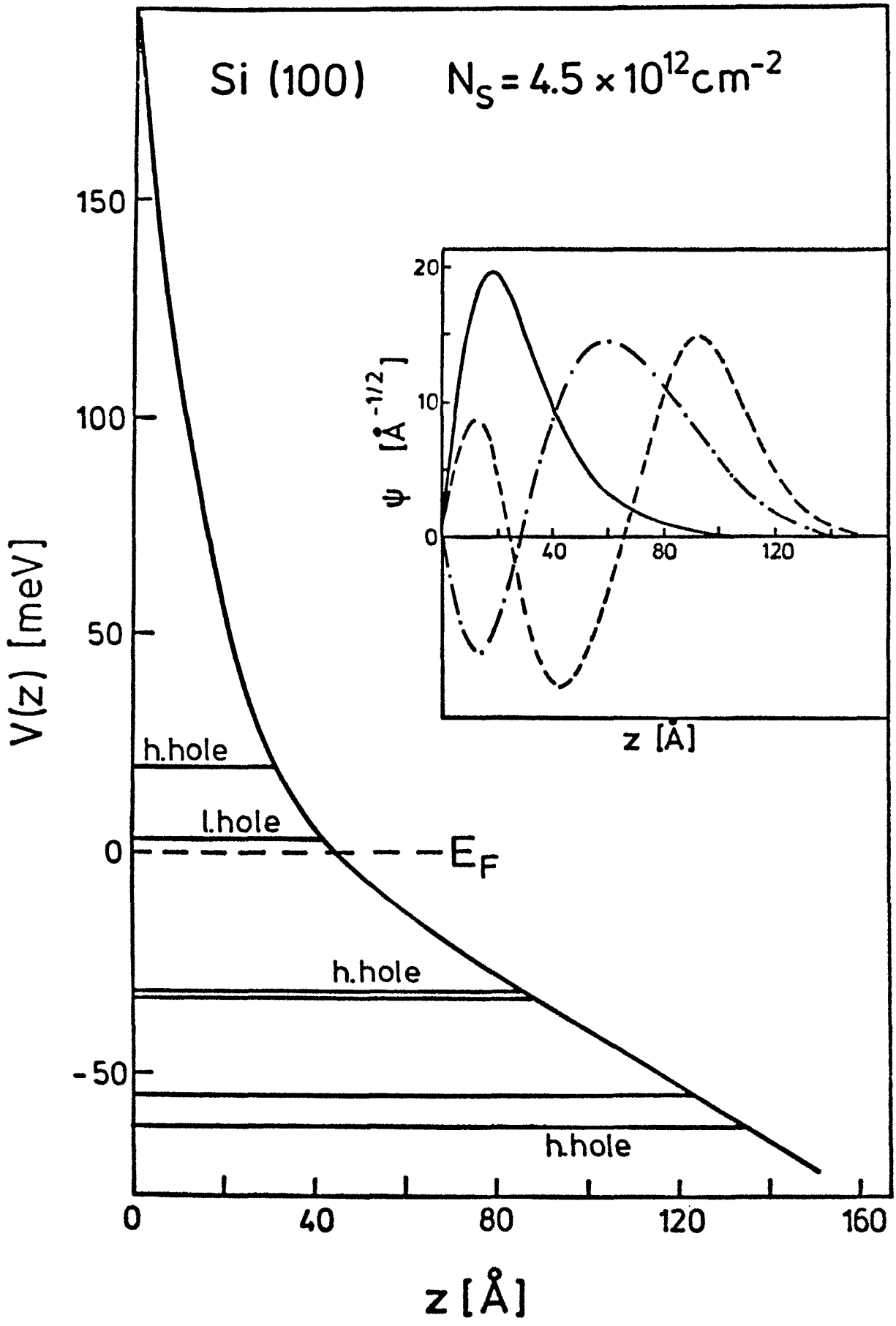
Si (100) $N_S = 4.5 \times 10^{12} cm^{-2}$
150
100
50
0
-50
V(z) [meV]
h.hole
l.hole
E_F
h.hole
h.hole
0
40
80
120
160
z [Å]
20
10
0
ψ [$Å^{-1/2}$]
40
80
120
z [Å]

Fig. 1

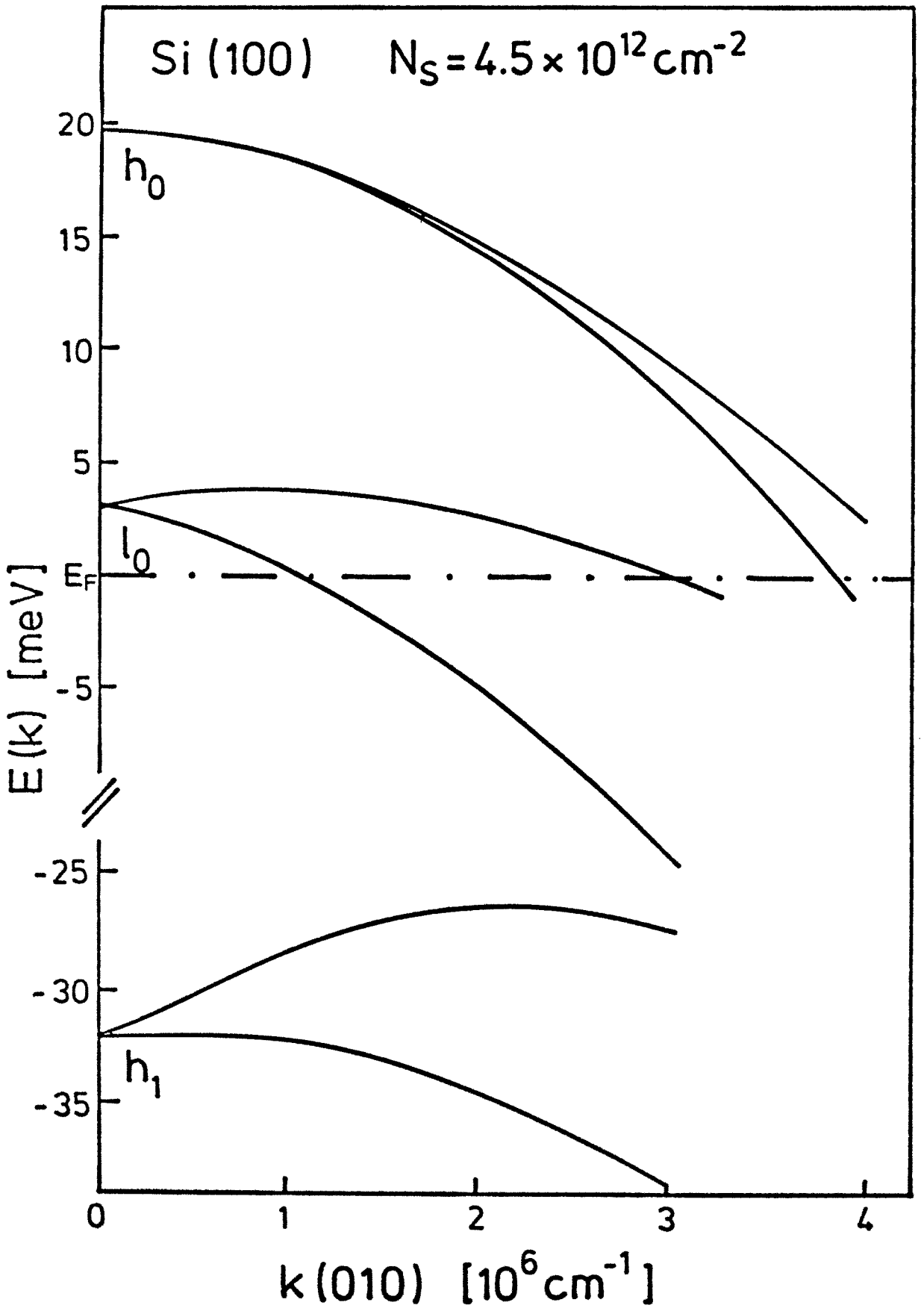
Si (100) $N_S = 4.5 \times 10^{12} cm^{-2}$
20
15
10
5
E_F
-5
-25
-30
-35
h_0
l_0
h_1
E(k) [meV]
0
1
2
3
4
k (010) [$10^6 cm^{-1}$]

Fig. 2

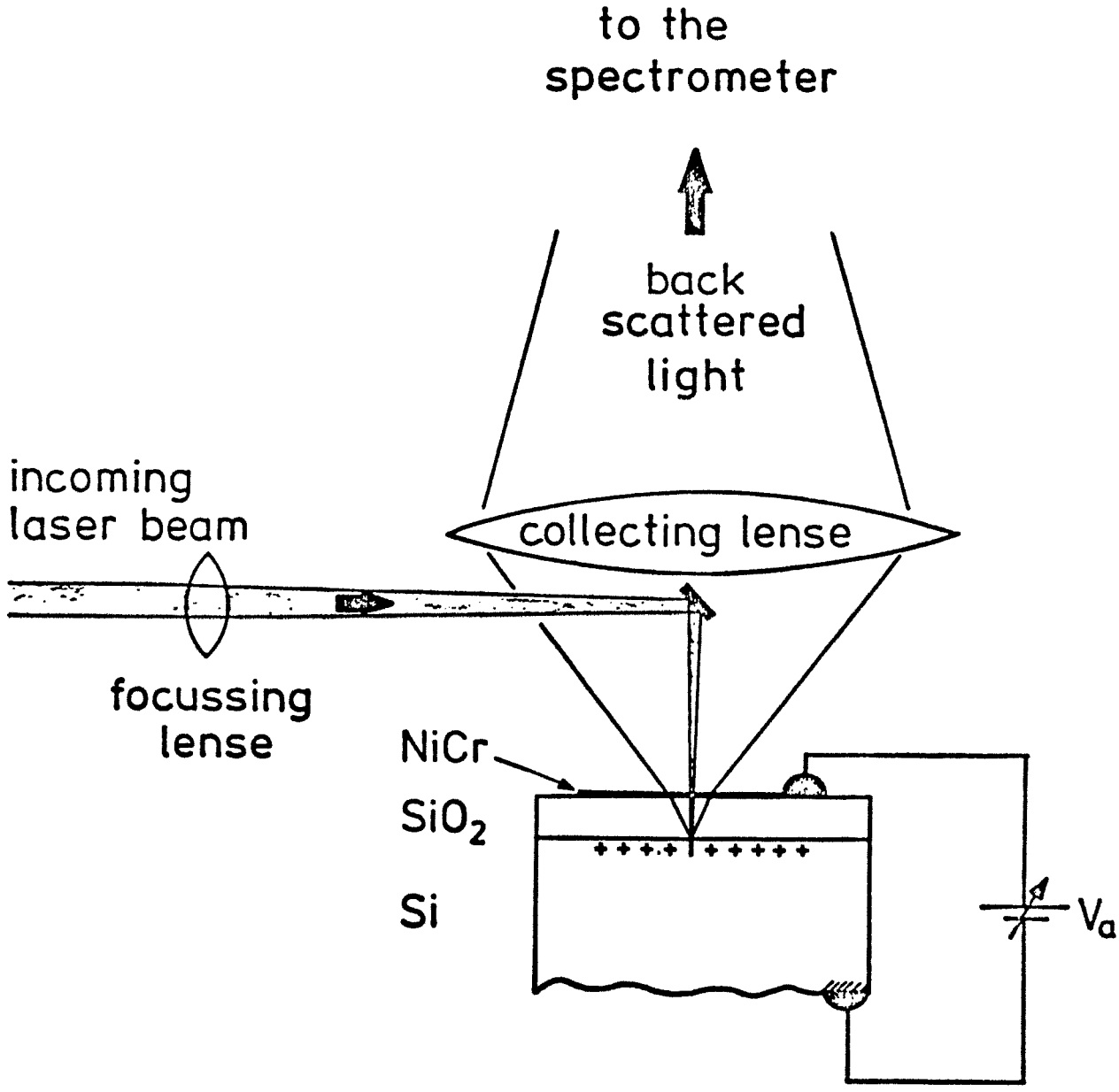
to the
spectrometer
back
scattered
light
incoming
laser beam
collecting lense
focussing
lense
NiCr
SiO_2
Si
V_a

Fig. 3

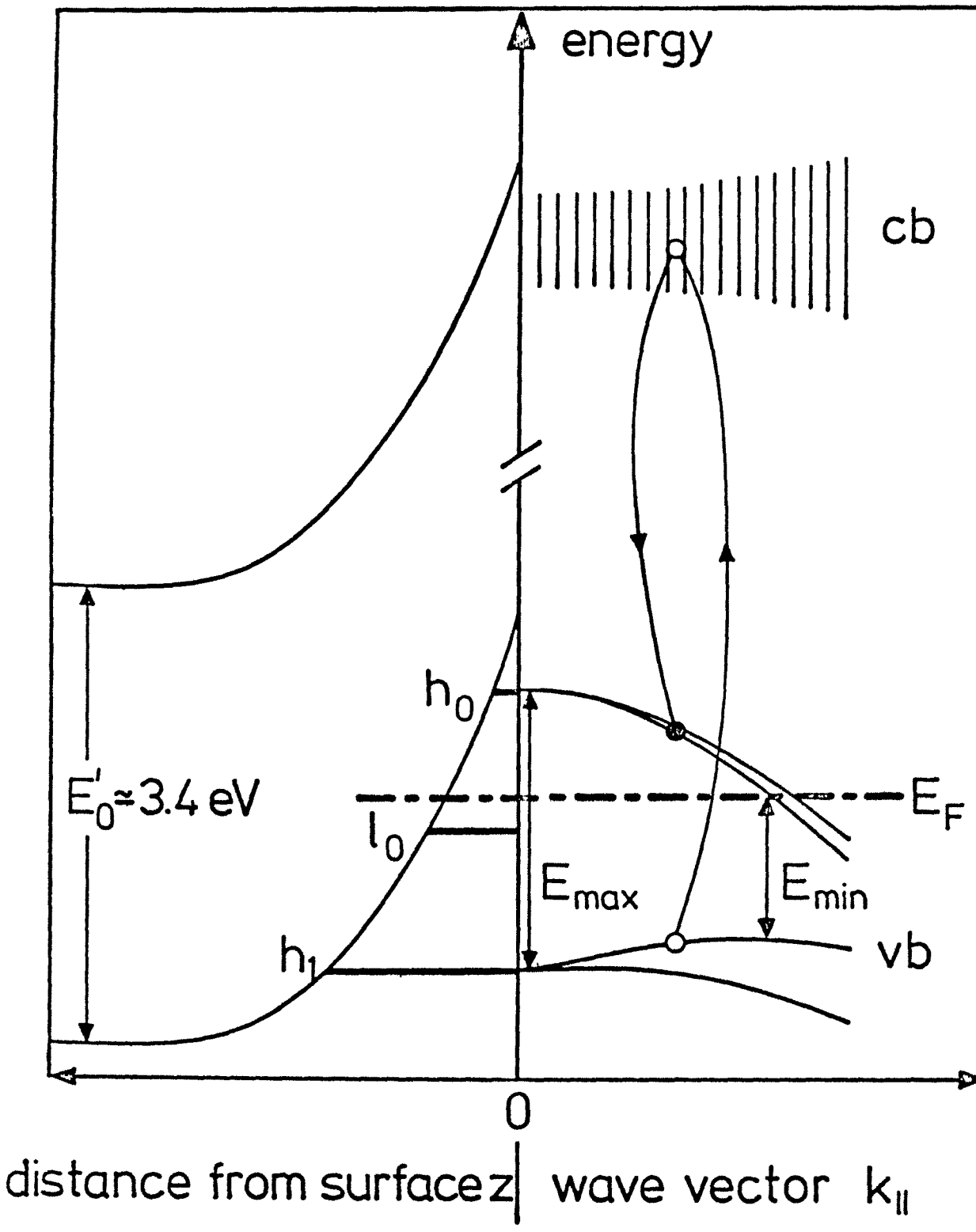
energy
cb
h_0
$E_0' \approx 3.4$ eV
E_F
l_0
E_{max}
E_{min}
h_1
vb
0
distance from surface z
wave vector $k_{||}$

Fig. 4

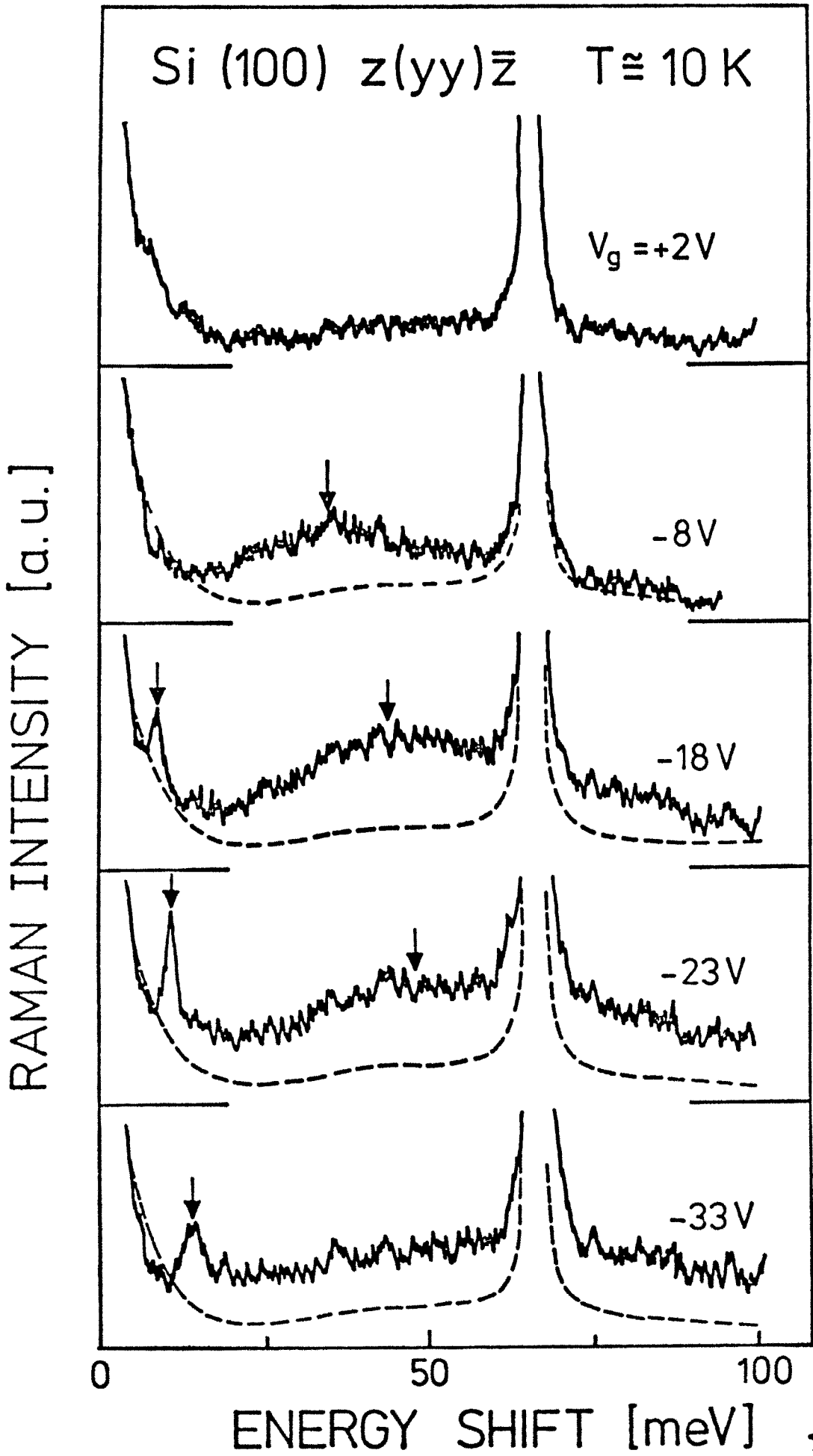
Si (100) z(yy)z̄ T≅ 10 K
V_g =+2V
-8V
-18V
-23V
-33V
RAMAN INTENSITY [a.u.]
0
50
100
ENERGY SHIFT [meV]

Fig. 5

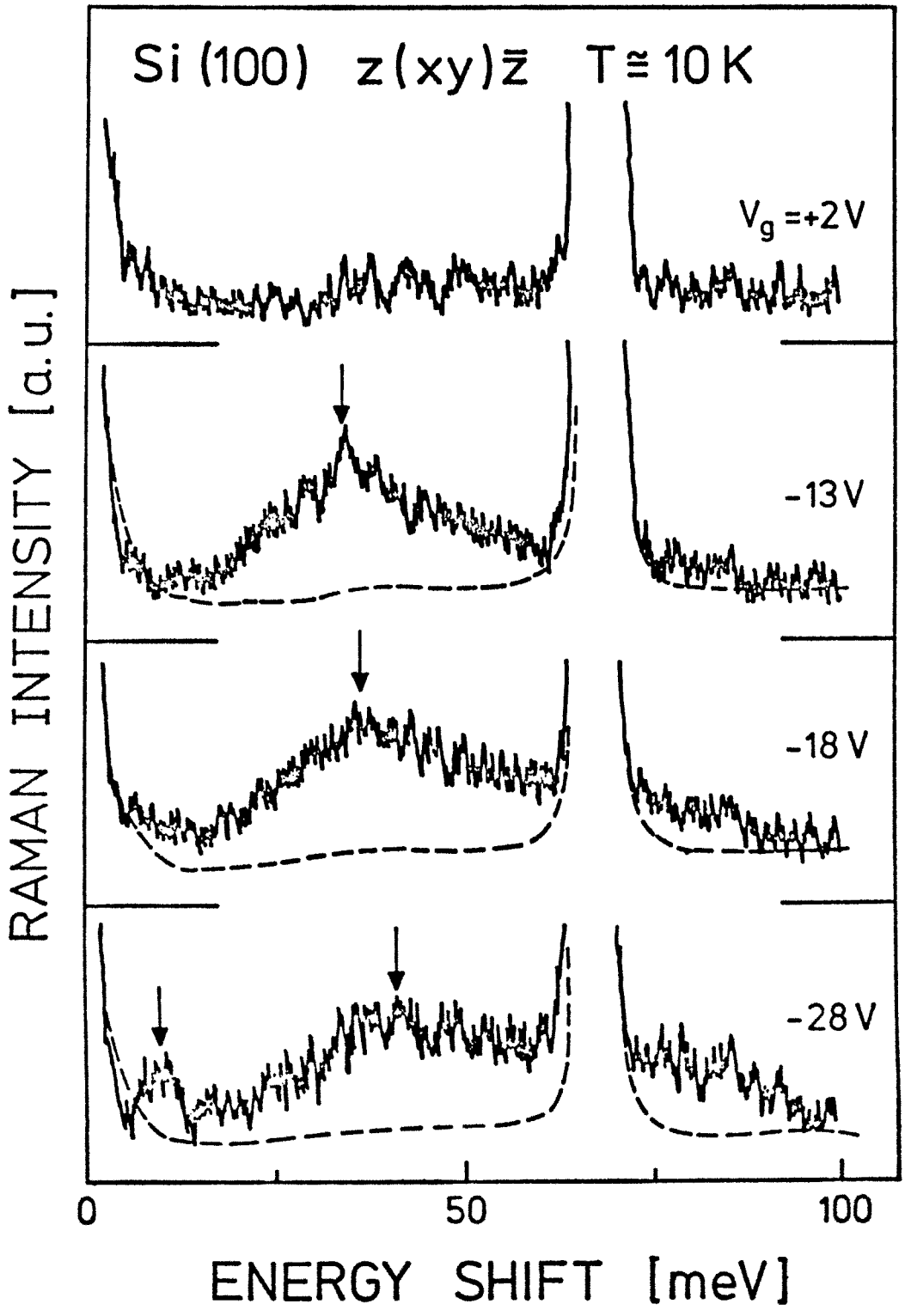
Si (100) z(xy)z̄ T≅10 K
V_g =+2 V
-13 V
-18 V
-28 V
RAMAN INTENSITY [a.u.]
0
50
100
ENERGY SHIFT [meV]

Fig. 6

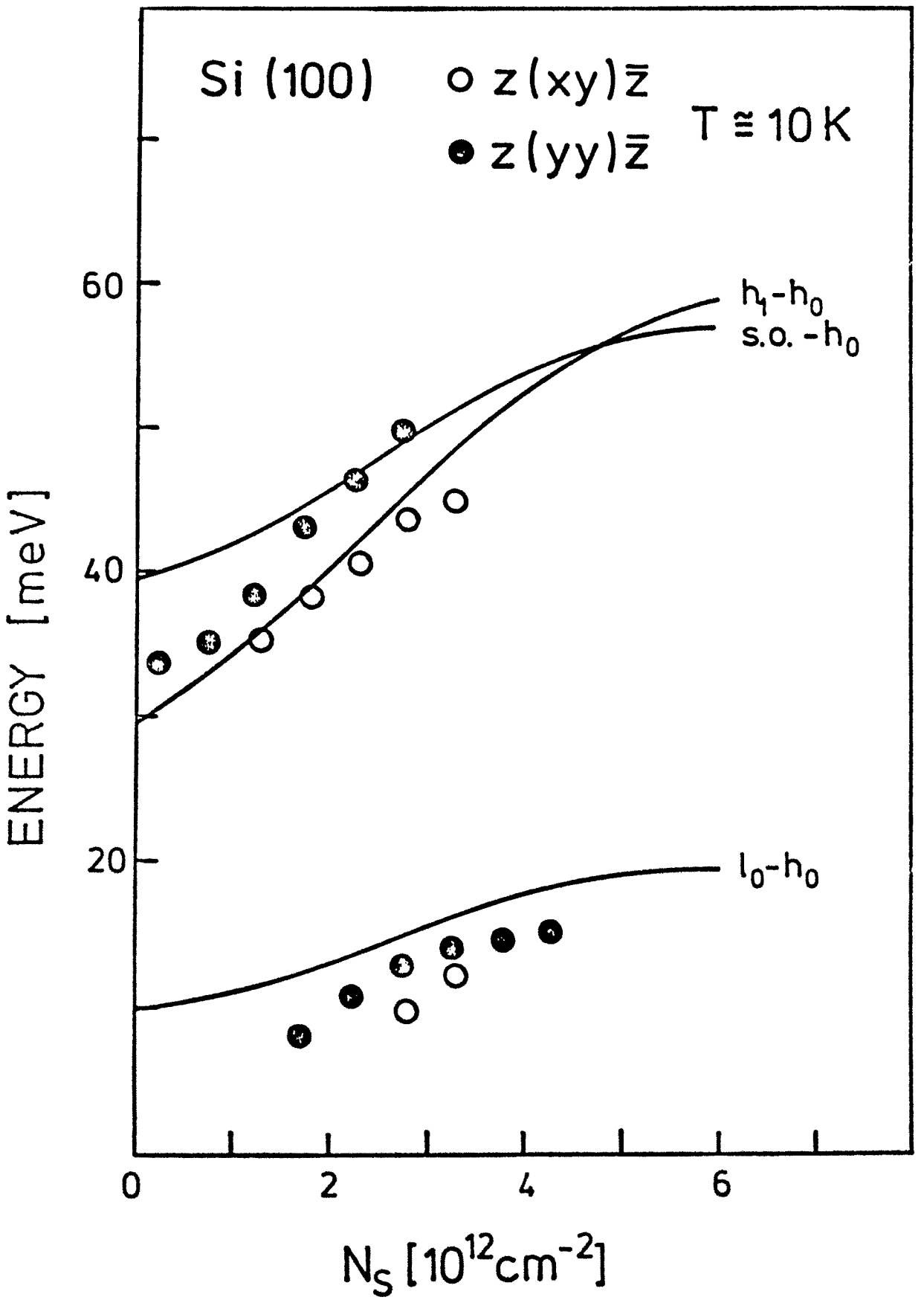
Si (100)
o z(xy)z̄
● z(yy)z̄
T ≅ 10 K
60
40
20
ENERGY [meV]
h1-h0
s.o. -h0
l0-h0
0
2
4
6
Ns [10^12 cm^-2]

Fig. 7

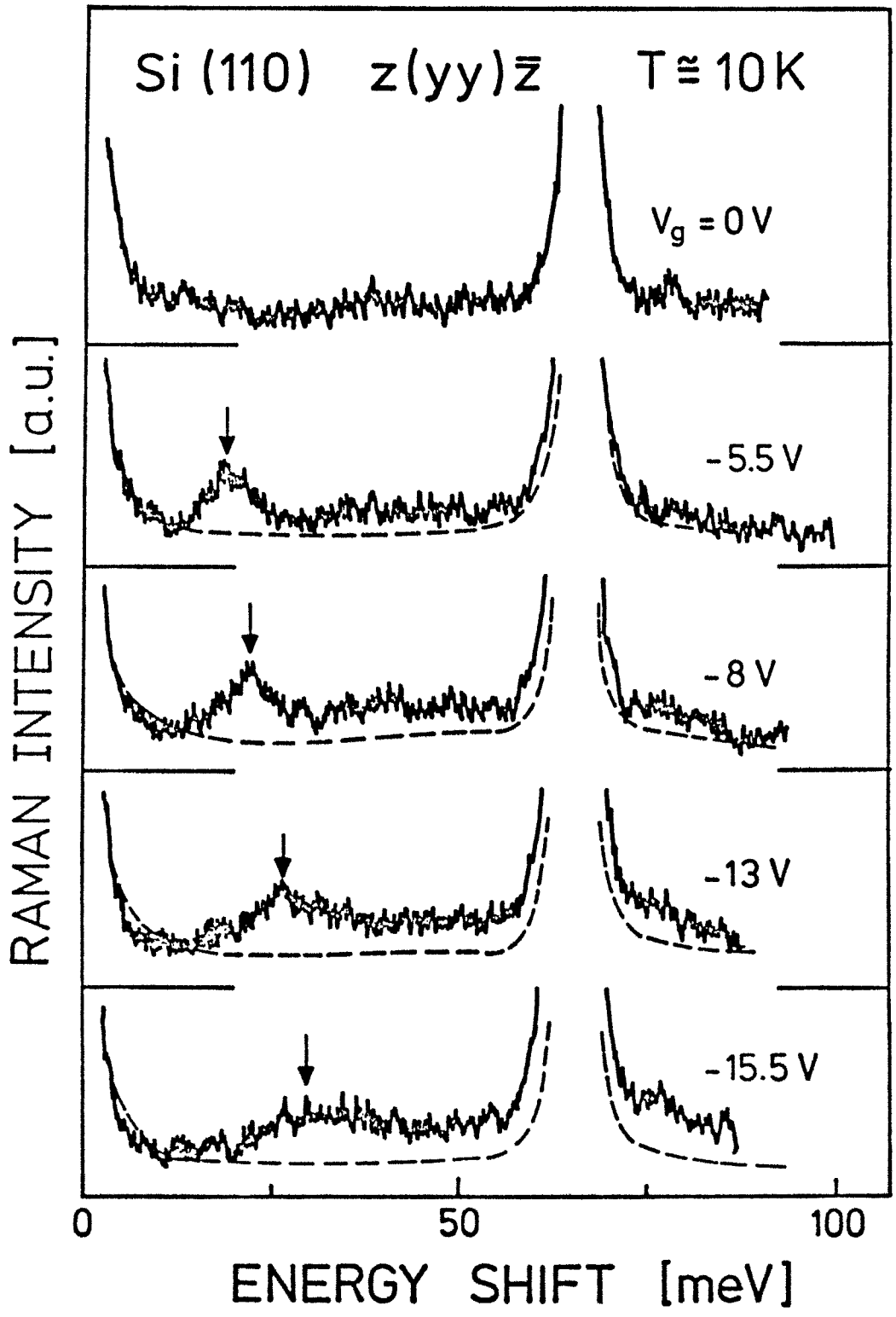
Si (110) z(yy)z̄ T≅10K
V_g = 0 V
-5.5 V
-8 V
-13 V
-15.5 V
RAMAN INTENSITY [a.u.]
0
50
100
ENERGY SHIFT [meV]

Fig. 8

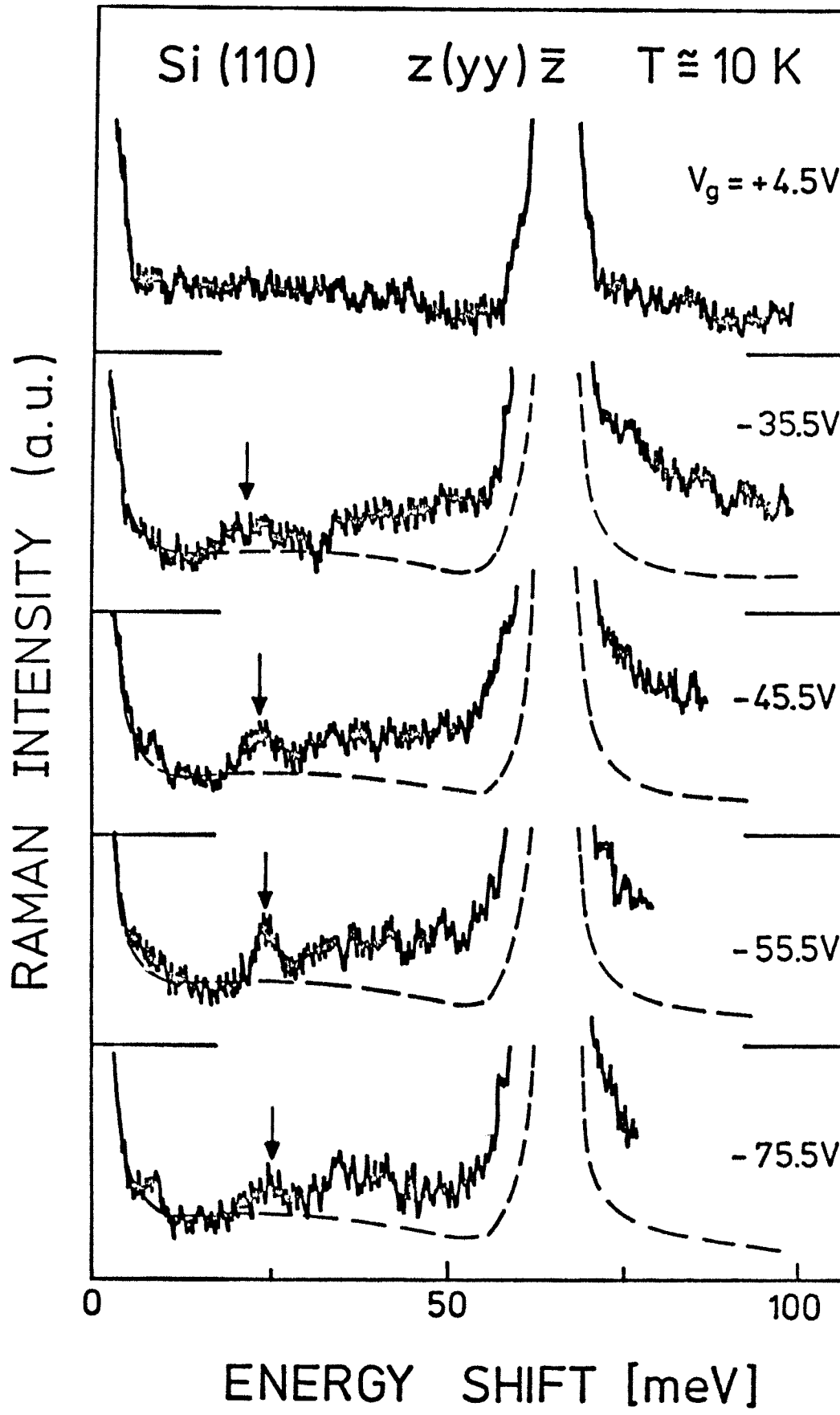
Si (110) z(yy)z̄ T ≅ 10 K
V_g = +4.5V
-35.5V
-45.5V
-55.5V
-75.5V
RAMAN INTENSITY (a.u.)
0
50
100
ENERGY SHIFT [meV]

Fig.

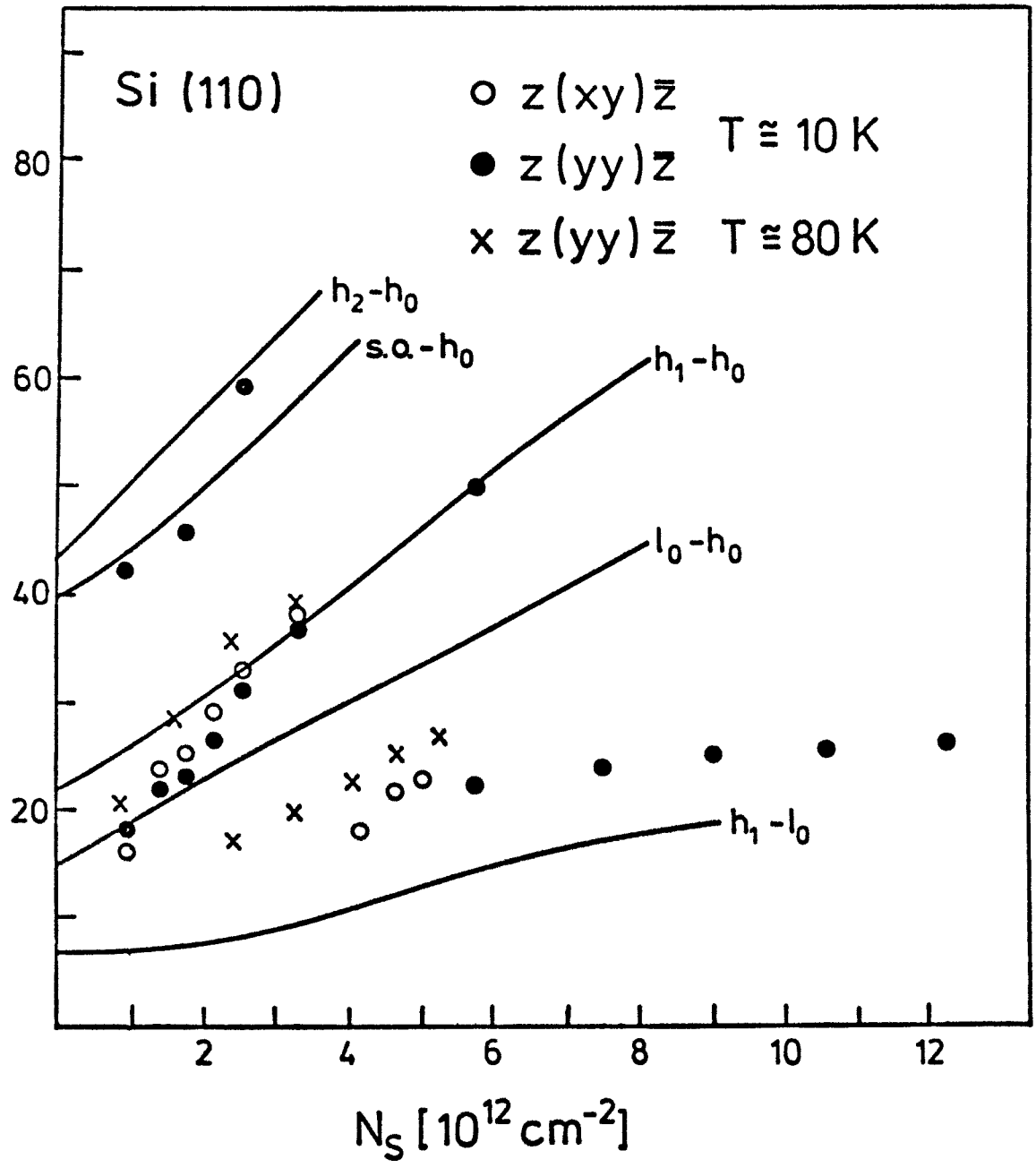
Si (110)
o z(xy)z̄
● z(yy)z
T ≅ 10 K
x z(yy)z̄ T ≅ 80 K
h2-h0
s.o.-h0
h1-h0
l0-h0
h1-l0
80
60
40
20
2
4
6
8
10
12
NS [10^12 cm^-2]

Fig. 10

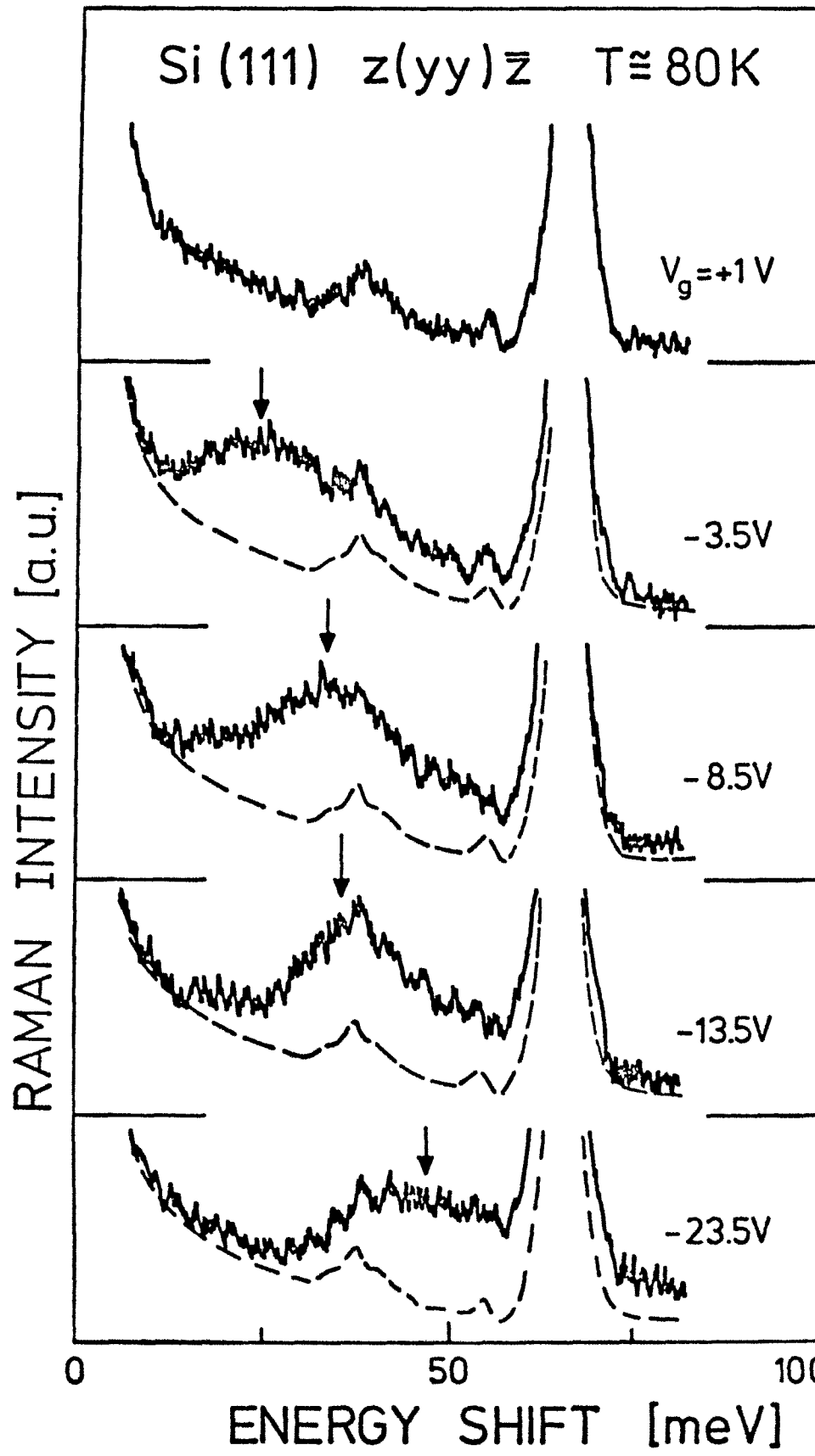
Si (111) z(yy)z̄ T≅80K
V_g=+1V
-3.5V
-8.5V
-13.5V
-23.5V
RAMAN INTENSITY [a.u.]
0
50
100
ENERGY SHIFT [meV]

Fig.

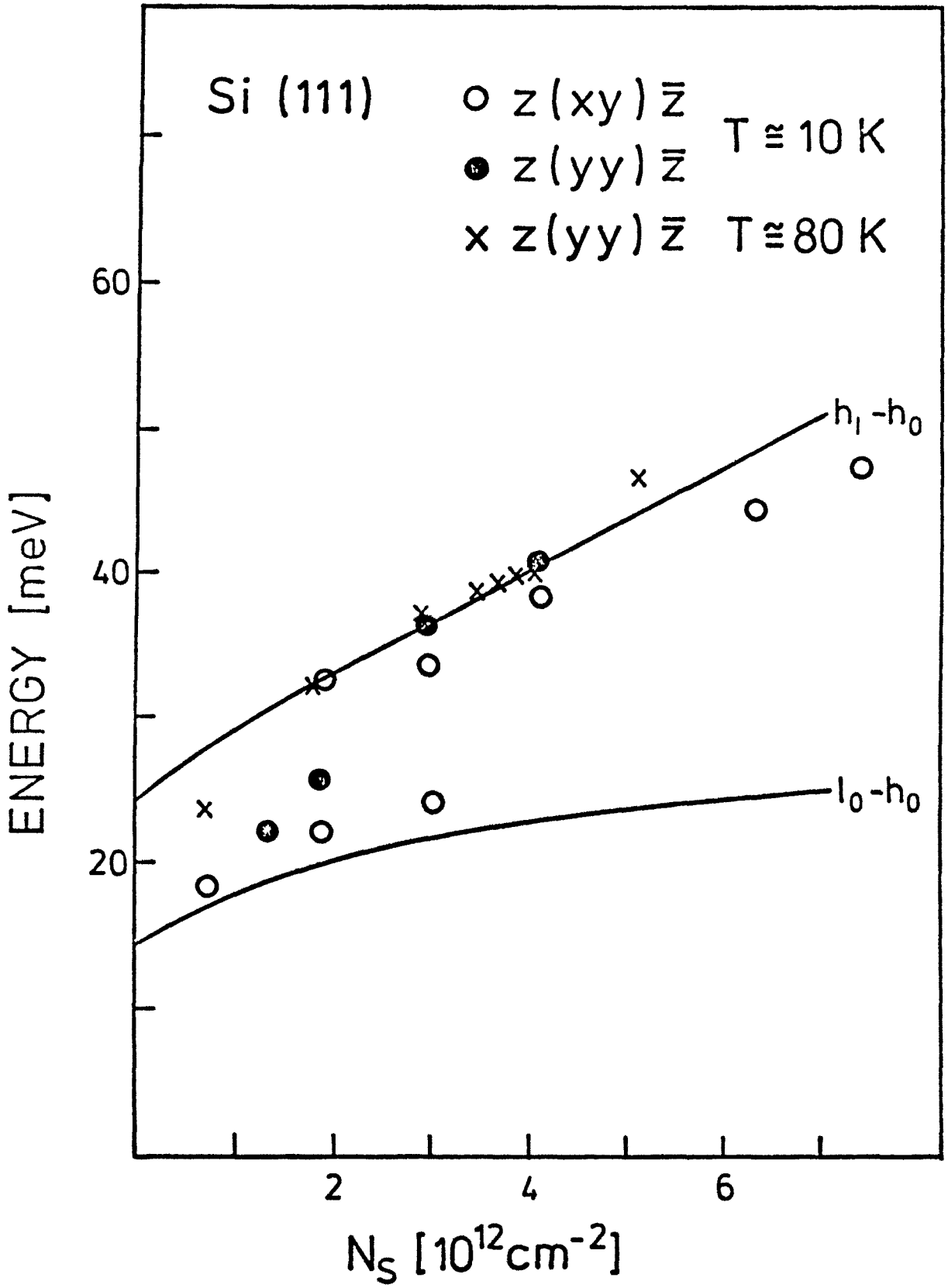
Si (111)
o z(xy)z̄
● z(yy)z̄
x z(yy)z̄
T ≅ 10 K
T ≅ 80 K
60
40
20
ENERGY [meV]
h1 -h0
l0 -h0
2
4
6
Ns [10^12 cm^-2]

Fig. 12

VOLUME 52, NUMBER 2 PHYSICAL REVIEW LETTERS 9 JANUARY 1984

In Situ Investigation of Band Bending during Formation of GaAs-Ge Heterostructures

H. Brugger, F. Schäffler, and G. Abstreiter
Physik-Department, Technische Universität München, 8046 Garching, Federal Republic of Germany
(Received 18 October 1983)

Symmetry-forbidden phonon Raman scattering is used to investigate *in situ* the formation of GaAs-Ge heterojunctions. Under epitaxial growth conditions the band bending in GaAs induced by the first monolayers of Ge decreases strongly for thicker overlayers. For amorphous overlayers the Fermi level remains pinned around midgap. A simple model is presented which explains the observed behavior. The development of the Ge phonons demonstrates crystalline growth for substrate temperatures $T_s \geq 300$ K and amorphous growth for $T_s \sim 100$ K.

PACS numbers: 73.20.-r, 73.40.Lq, 78.30.Gt

The GaAs-Ge system has received considerable attention for a long time, a fact which is caused primarily by the different nature of the band gaps of the two materials concomitant with a nearly perfect lattice matching.[1] The valence-band discontinuity ΔE_v is determined most reliably from photoemission experiments. Results of several groups have been summarized recently,[2] giving an average value of $\Delta E_v = 0.33$ eV. A second important feature is the potential variation across the interface. Mönch and co-workers performed detailed studies of these properties[3-5] using photoemission and work-function measurements. They find a Fermi-level pinning on UHV-cleaved GaAs (110) surfaces at around midgap for Ge coverages of less than one monolayer. They conclude that Fermi-level pinning is governed by chemisorption-induced defects (e.g., vacancies or antisite defects), as has been discussed for metal and oxygen overlayers before.[6] Attempts to trace the band-bending behavior of the interface to a Ge overlayer thickness larger than the electron escape depth of about 6 Å[5] seems questionable: Strong Ga and As core-level signals from atoms segregated near the free Ge surface prevent a probing of the interface.[5] In Fig. 1(a) we show the profile of valence- and conduction-band edges around the GaAs-Ge interface, as expected from a defect model. Both layers are assumed to be *n* type, with the Ge free surface being depleted naturally. The fixed valence-band discontinuity together with the Fermi-level pinning at the interface results in depletion regions on the GaAs as well as on the Ge side of the junction.

This is in contradiction to the recent work of Merlin *et al.*[7] who studied *n*-GaAs/*n*-Ge heterostructures grown by molecular-beam epitaxy. In their resonant inelastic light scattering experiments they have observed electronic excitations of a two-dimensional carrier system in the Ge layer. It is believed that the measured broad and asymmetric excitation line is due to intersubband transitions of electrons confined at the GaAs-Ge interface. Thus it seems possible to achieve interfaces with a negligible amount of interface states. A two-dimensional electron system is formed by the charge transfer from the donor states in GaAs to the conduction band in Ge. The resulting band scheme for such heterostructures is shown in Fig. 1(b).

In the present work we report on *in situ* investigations of band bending in GaAs during the formation of GaAs-Ge heterostructures. The barrier height has been measured from submonolayer coverages on clean UHV-cleaved GaAs (110) sur-

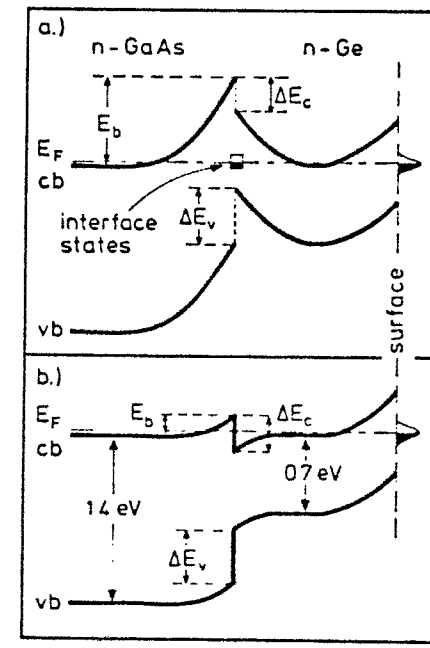

FIG. 1. Real-space energy diagram of a GaAs-Ge interface (schematically) (a) Fermi-level pinning at interface states and (b) potential variation in the absence of interface states.

faces up to Ge overlayers of about a hundred monolayers (~200 Å). The surface band bending in polar semiconductors can be determined from the Raman intensity of the resonantly excited symmetry-forbidden LO phonon, which depends strongly on the surface electric field.[8] This has been shown quantitatively by use of a Schottky-barrier arrangement on (110) surfaces of GaAs.[9] Raman scattering by LO phonons is not allowed in backscattering from those surfaces. Close to resonance, however, symmetry-breaking mechanisms are responsible for the observation of "forbidden" LO-phonon scattering.[9] Electric-field-induced scattering is dominant in most cases. It agrees qualitatively with a Franz-Keldish-type theory which gives, in the limit of weak electric fields E, an E^2 behavior for the LO-phonon intensity. As the barrier height E_b is also proportional to E^2 (Schottky model), the LO-phonon intensity reflects directly E_b, provided that the light penetration depth is smaller than the depletion width. The usefulness of this method in determining the Fermi-level pinning on clean and covered GaAs (110) surfaces has been demonstrated recently[10-12] and will be discussed for Ge on GaAs in the following.

The samples were prepared by cleaving single crystals of nominally 7×10^{17} cm^{-3} Te-doped GaAs bars in an UHV chamber with base pressure $<10^{-10}$ mbar. The sample temperature could be varied from 100 to 700 K. High-purity Ge was evaporated from an effusion cell. During evaporation with a maximum growth rate of 0.05 Å/s the pressure did not exceed 1×10^{-9} mbar. The film thickness has been controlled by a crystal quartz monitor. The Raman measurements were performed *in situ*. In order to fulfill the resonance condition for forbidden LO-phonon scattering and to keep the light penetration depth small we used the laser lines of a Kr^+-ion laser and a Stilben dye laser in the energy range around 3 eV, close to the E_1 gap of GaAs. The backscattered light [polarized (110)(110)] was collected and analyzed with a double-grating spectrometer and conventional pulse counting electronics.

Figure 2 shows three series of Raman spectra of TO and forbidden LO phonons in GaAs at various Ge coverages and different growth temperatures T_g. Each spectrum ranges from 30 to 40 meV. Ge thicknesses are given in monolayers (ML), where one ML corresponds to the distance of neighboring (110) planes, i.e., 2.0 Å. All spectra are normalized to the intensity of the TO-phonon mode, which does not depend on the surface electric field. The measuring temperature T_m was 300 K with the exception of the uppermost series, where $T_m = T_g = 100$ K, to avoid annealing effects.

In Fig. 3 the intensity ratio I_{LO}/I_{TO} for each series has been evaluated in terms of surface-

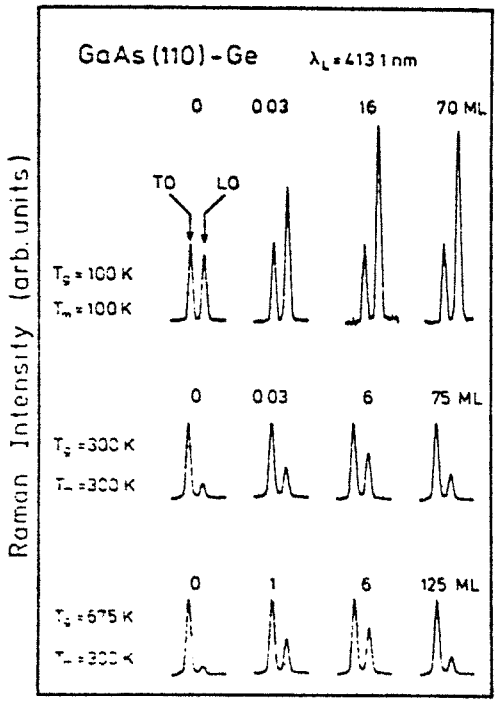

FIG. 2. Raman spectra of TO- and forbidden LO-phonon scattering in GaAs at various Ge coverages. T_g is the growth temperature, and T_m the sample temperature during the measurements.

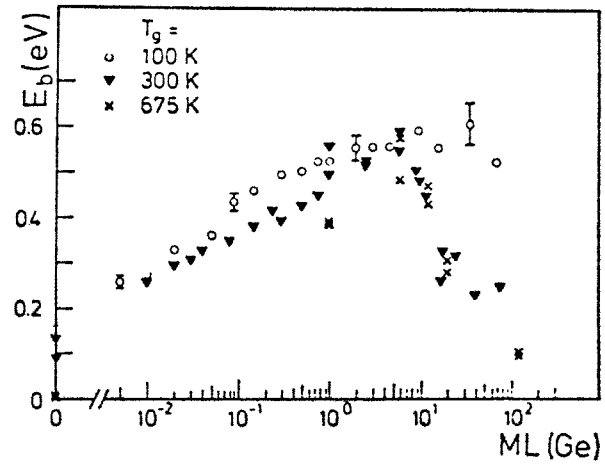

FIG. 3. Barrier height E_b as a function of Ge deposition.

barrier heights E_b: As I_{LO}/I_{TO} is in good approximation proportional to E_b,[9] the energy scale is fixed by two values. I_{LO}/I_{TO} corresponding to $E_b = 0$ eV (flat band) is determined from the freshly cleaved GaAs surface. To assure flat-band behavior, we measured the coupled phonon-plasmon modes close to the surface at low temperatures.[11] To get a second calibration point we attribute I_{LO}/I_{TO} of semitransparent metal Schottky barriers to the literature value $E_b \approx 0.65$ eV.[6] These samples have been prepared under the same conditions as the heterojunctions. As the absolute value of I_{LO} depends strongly on T_m (see Fig. 2), the scaling procedure has to be performed for each temperature separately. From this calibration we find the following for the GaAs band bending at the interface: The barrier height increases initially with Ge coverage for all growth temperatures investigated (100 K $\leq T_m \leq$ 675 K). For T_m = 100 K the band bending reaches a saturation value of ~0.6 eV at about 1 ML of Ge and remains constant within experimental error up to the thickest Ge layers grown. This is in contrast to the measurements at $T_m \geq 300$ K, where the barrier height drops drastically when the Ge coverage exceeds about 6 ML. The lowest measured value is $E_b \approx 0.1$ eV for a 250-Å-thick Ge film deposited at T_s = 675 K.

We have also investigated the nature of the grown Ge films by analyzing Raman spectra obtained with $\hbar\omega_L = 2.41$ eV which is close to the $E_1 + \Delta_1$ resonance of Ge. Examples are shown in Fig. 4. Films grown at low temperature (T_s = 100 K) do not exhibit any sharp phonon structure. Their Raman spectra are typical for amorphous Ge[13] (top curve in Fig. 4). This spectrum has been obtained for a 140-Å-thick Ge film with use of a scattering configuration for which both first-order LO- and TO-phonon Raman scattering in GaAs are forbidden. Otherwise the weak structure of the amorphous film is dominated by the strong TO-phonon mode of GaAs at 33.4 meV. For Ge films grown at higher temperatures ($T_s \geq$ 300 K) the optical-phonon line of crystalline Ge develops nicely. The first hints of the Ge phonons are observed already for films as thin as 3 to 4 ML. As shown in the lower part of Fig. 4 the intensity of the Ge phonon line increases strongly with film thickness, while the TO-phonon line of GaAs decreases as a result of absorption of light in the Ge film. Note the different energy scales used in Fig. 4. The phonon Raman spectra demonstrate directly that Ge films grown with a low evaporation rate at room temperature already

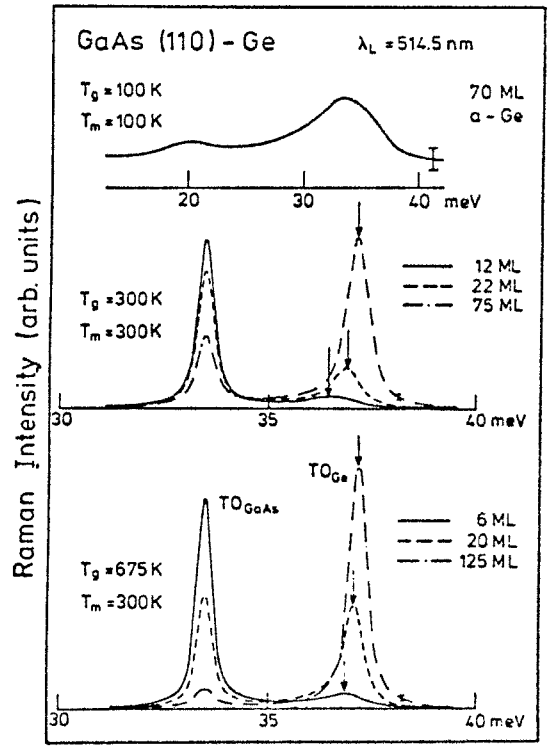

FIG. 4. Raman spectra of thin GaAs-Ge heterostructures grown at different temperatures. The arrows mark the phonon peaks of the thin crystalline Ge layers. Note the shift to smaller energies with decreasing film thickness which reflects the lattice dynamics of a thin Ge slab.

have a crystalline nature. Comparing the line shapes and intensities of the phonon modes with published data[13] shows, however, that room-temperature–grown films are polycrystalline with a grain size of the order of 10 μm. Overlayers of similar thickness grown at T_s = 675 K exhibit sharper, more symmetric and more intense phonon lines, indicating a much higher quality of the epitaxial films.

A simple model is proposed to explain our results. It does not involve any chemisorption-induced defects: The free, ideally cleaved GaAs (110) surface minimizes its energy by reconstruction. Dangling-bond energy states are swept out of the direct energy gap. Consequently, no band bending occurs.[14] Chemisorption of Ge atoms can lift the surface reconstruction, giving rise to dangling-bond states (both Ga and As unpaired bonds). The energy of these states is expected to lie within the band gap,[14] causing surface band bending. On the other hand, neither Ge-Ga nor Ge-As bonds create electron states inside the fundamental gap.[15,16] Thus, if we as-

sume perfect epitaxial Ge growth, all interface states will be removed after the deposition of one monolayer of Ge. E_F, however, is further pinned at probably slightly different energy at the free Ge surface. Consequently, for thin Ge films, there exists still considerable band bending at the interface. With increasing Ge thickness, E_b at the interface decreases resulting finally in a band scheme as shown in Fig. 1(b). For the amorphous films on the other hand there remain enough unpaired dangling-bond states to cause Fermi-level pinning at the GaAs side of the interface.

In conclusion, we have used resonant Raman scattering to investigate the interface barrier height between Ge and GaAs from the lowest coverages, where photoemission is believed to give reliable results, up to Ge overlayers of more than 250 Å thickness where real heterojunction life starts. We find strong evidence that the band bending in GaAs induced by low coverages of Ge is drastically reduced when epitaxial growth occurs. The idea that Fermi-level pinning on GaAs (110) is due to chemisorption-induced defects seems not to be generally applicable, because it is unlikely that such defects are annealed during epitaxial growth. This, however, would be necessary to explain the small interface barrier observed for thick epitaxial overlayers.

We want to thank K. Ploog and his group for providing the effusion cells, and E. Umbach for useful discussions concerning photoemission experiments. The work has been supported by the Deutsche Forschungsgemeinschaft via Sonderforschungsbereich 128.

[1]See for example, A. G. Milnes and D. L. Feucht, *Heterojunctions and Metal-Semiconductor Junctions* (Academic, New York, 1972).

[2]A. D. Katnani and G. Margaritondo, Phys. Rev. B 28, 1944 (1983), and references therein.

[3]W. Mönch and H. Gant, J. Vac. Sci. Technol. 17, 1094 (1980).

[4]W. Mönch and H. Gant, Phys. Rev. Lett. 48, 512 (1982).

[5]W. Mönch, R. S. Bauer, H. Gant, and R. Murschall, J. Vac. Sci. Technol. 21, 498 (1982).

[6]W. E. Spicer, P. W. Chye, P. Skeath, C. Y. Su, and I. Lindau, J. Vac. Sci. Technol. 16, 1422 (1979); W. E. Spicer, I. Lindau, P. Skeath, and C. Y. Su, J. Vac. Sci. Technol. 17, 1019 (1980).

[7]R. Merlin, A. Pinczuk, W. T. Beard, and C. E. E. Wood, J. Vac. Sci. Technol. 21, 516 (1982).

[8]A. Pinczuk and E. Burstein, Phys. Rev. Lett. 21, 1073 (1968).

[9]R. Trommer, G. Abstreiter, and M. Cardona, in *Proceedings of the International Conference on Lattice Dynamics*, edited by M. Balkanski (Flammarion, Paris, 1977), p. 189.

[10]H. J. Stolz and G. Abstreiter, Solid State Commun. 36, 857 (1980), and J. Phys. Soc. Jpn. 49, 1101 (1980).

[11]H. J. Stolz and G. Abstreiter, J. Vac. Sci. Technol. 19, 380 (1981).

[12]F. Schäffler and G. Abstreiter, *Surface Studies with Lasers*, Springer Series in Chemical Physics Vol. 33 (Springer-Verlag, New York, 1983), p. 131.

[13]R. P. Salathe, H. P. Weber, and G. Badertscher, Phys. Lett. 80A, 65 (1980).

[14]See for example, E. J. Mele and J. D. Joannopoulos, Phys. Rev. B 17, 1816 (1978).

[15]W. E. Pickett, S. G. Louie, and M. L. Cohen, Phys. Rev. B 17, 815 (1978).

[16]J. Pollmann and S. T. Pantelides, Phys. Rev. B 21, 709 (1980).

An dieser Stelle möchte ich allen herzlich danken, die zum Gelingen dieser Arbeit beigetragen haben.

Besonders erwähnen möchte ich:

M. Baumgartner, H. Brugger, R. Huber, W. Einberger, H. Kirchstetter, F. Schäffler, G. Tränkle und Ch. Zeller, die aktiv und engagiert im Rahmen ihrer Diplom- bzw. Promotionsarbeiten mitgearbeitet haben;

Dr. K. Ploog und seine Mitarbeiter am Max-Planck-Institut in Stuttgart, die einen Großteil der hochwertigen Halbleiterschichtstrukturen hergestellt haben und auf viele unserer Sonderwünsche eingegangen sind;

Alle Mitarbeiter von E 16, die in kollegialer Weise durch vielseitige Unterstützung die Durchführung unserer Forschungsarbeiten ermöglichten;

Herrn Prof.Dr. F. Koch und Herrn Prof.Dr. M. Cardona, die es mir ermöglichten, in diesem Forschungsgebiet tätig zu sein und die mit vielen Anregungen zu dieser Arbeit beigesteuert haben.

Die Deutsche Forschungsgemeinschaft hat im Rahmen des SFB 128 diese Arbeit finanziell unterstützt.